SAMPLING METHODS (REACTORS, CONTAMINATION)

M.P. NANDAKUMAR
H. HÅKANSON
B. MATTIASSON
Lund University
Lund, Sweden

KEY WORDS

Biosensors
Coaxial catheter
Expanded bed
Flow injection analysis
On-line analysis
On-line cell disintegration
Sample handling
Sampling
Sampling probes

OUTLINE

INTRODUCTION

To optimize fermentation processes, that is, to ensure maximum growth and/or productivity, the fermentation conditions should be controlled and maintained at their optimum values. However, the media for fermentations and other bioprocesses are very complex in nature. These are often multiphase systems. The liquid phase contains soluble nutrients (e.g., sugar, proteins, vitamins, salts, and products of metabolism such as amino acids, alcohols, and organic acids). Furthermore, there may be a solid phase of suspended material (insoluble substrate/product, carrier materials, etc.). The gas phase is in equilibrium with dissolved gases in the medium. Analysis of any of these compounds by traditional techniques is tedious and time-consuming and cannot provide on-line information of the process. Recently, the increasing demand of high-value products has focused interest on well-controlled, optimized processes. This has initiated the development of new on-line measurement techniques (1–3). The ideal situation would be to have specific probes that can operate in situ during the fermentation. However, at present there is only a limited number of such probes available for measuring pH, dissolved oxygen, and carbon dioxide. There is still no suitable technology for operating biosensors containing a biological macromolecule. In the last few years research on biosensors for bioprocess control has been growing. These sensors offer the ability to measure concentrations of various biomolecules, as well as biological parameters, very specifically using immobilized enzymes or cells or other biochemical/biological entities. Unfortunately, these sensors are inactivated by steam sterilization (4). Because sensor technology is not yet sufficiently advanced to permit this type of monitoring, the majority of analysis is still carried out outside of the bioreactor, a process requiring sampling and sample-handling strategies. This review highlights the importance of sampling and sample handling and the techniques used.

STRATEGIES FOR SAMPLING

For analysis of any bioprocess, off-line or on-line sampling is a prerequisite and is the basis for the final analytical result. The following strategies/criteria are important when designing a sampling device (5).

1. The sterility of the process must be maintained during sampling.
2. The delay between sampling and analysis may result in changes in the composition of the sample. Precautions must be taken to prevent or compensate for that.
3. The analysis must be accurate and reproducible.
4. When constructing the sampling and sample treatment unit, the selection of material must be governed by compatibility criteria such that the process being monitored is not negatively influenced.
5. Protein adsorption and cell colonization on the sampling and sample-handling device may lead to an imparted mass transport and formation of unwanted immobilized catalytic activities that may severely influence the composition of the sample before analysis can be carried out.

Considering these parameters, a sampling system for on-line monitoring of fermentation processes must meet the following criteria.

1. The system can take representative samples from fermenter but should not disturb the fermentation process.
2. The system should be sterilizable and provide a sterile barrier to avoid contamination.
3. Separation of cells, solids, or macromolecules should be carried out with as short a delay as possible within the sampling devices (6).

There are many different types of sampling units available to achieve these goals (7). This review highlights a detailed description of some of the sampling devices used for on-line monitoring of bioprocesses, especially when biosensors are used in the analytical step. It should, however, be stressed that the sampling and sample handling as described here will be applicable when setting up any kind of analysis to monitor a bioprocess. Figure 1 presents a schematic description of different sampling modes.

NATURE OF THE SAMPLE

The character of the reaction mixture to be sampled determines the choice of sampling method. Different kinds of analytes require different sampling protocols.

Volatile Compounds and Compounds Present in Gaseous Phase

Volatile compounds may be present in the head space of a fermentation or be dissolved in the liquid medium. At equilibrium, the concentration in the head space reflects that in the liquid. The composition of the gas phase is usually less complex than that of the aqueous phase; therefore, when the metabolites are volatile, it is probably simpler to monitor the concentration in the gas phase. The risks of infection of the fermentation are lower when sampling from the gas phase. This has made it attractive to use analysis of the gas phase when monitoring industrial fermentations.

There are two main modes described in the literature for the sampling of gases and volatile compounds:

1. Analysis of the outlet gases or of the headspace gases.
2. Analysis of the volatile gaseous compounds dissolved in the culture medium.

A sampling method is applied that is based on a technology for supplying oxygen to bioprocesses that are disturbed by bubbling oxygen. Oxygen is supplied in a tubing made of hydrophobic material. The oxygen penetrates the walls of the tubing and is released to the cultivation broth. Similar phenomena can take place for gaseous compounds with an opposite concentration gradient (8). Tubings made from materials that are permeable to organic solvent molecules are immersed in the fermentation broth, and an inert gas that flows through the lumen of the tubings transports the solvent molecules to an analyzer (e.g., a gas-sensitive semiconductor sensor placed downstream of the tubing) (9,10).

Recently a new approach for monitoring carbon dioxide during fermentation was reported based on a piezoelectric crystal (11). A change in the oscillation frequency of the crystal occurs due to selective sorption of a gaseous compound to the surface, and the change in frequency is directly proportional to the mass deposited. Fast response, simple use, and low cost may lead to a more extensive use of this technique. More details on sampling of gases during fermentations are described in the literature (12,13).

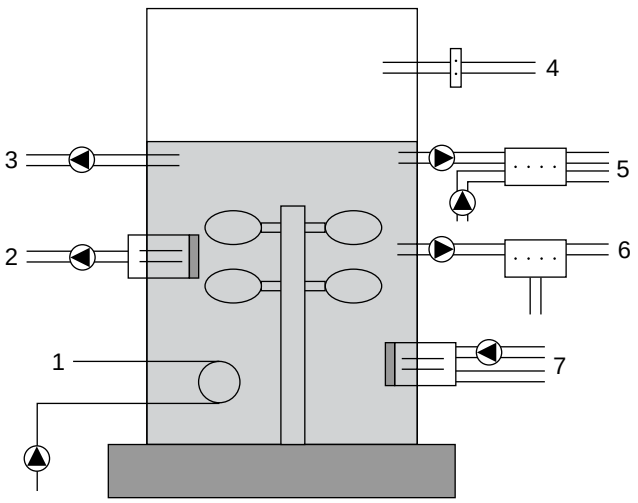

Figure 1. Schematic presentation of different modes of sampling from a bioreactor. The different concepts are (1) dialysis, (2) a membrane unit for removing a particulate-free sample from the turbulent liquid around the impeller, (3) direct sampling, (4) sampling of headspace, (5) sampling and filtering the sample outside the fermenter using a receiving buffer to catch the permeate, (6) sampling with filtering where the permeate is collected, (7) a membrane dialysis probe with the receiving buffer being pumped through the unit.

Analysis of Nonvolatile Compounds

Analytes Dissolved in the Liquid Medium. Automatic sampling, either continuously or by a frequently repeated procedure, is a prerequisite for on-line or "at-line" monitoring. The sampling system normally serves also as a sterile barrier between the bioreactor and the analytical system. Different analytical systems can be used. Flow injection analysis (FIA) is a common and convenient way to carry out the analysis (14). The samples are heterogeneous, with compounds dissolved in the medium, some forming complexes with other constituents, some not fully soluble, some particulate, and so forth. Manual sampling and off-line analysis are still in practice; however, they result in delays in analysis, risks of infection, and less reproducible sample handling (15). Sampling can be done using sampling units mounted either inside or outside the bioreactor. Several systems of both kinds have been reported recently (16,17). The advantages and disadvantages of internal and external sampling modules are presented in Table 1.

Table 1. Advantages and Disadvantages of Internal and External Sampling Modes

Mode of sampling	Advantages	Disadvantages
In situ modules	Short answering time, simple design, less contamination, suited for coupling on on-line analyzers	Problem of long-term stability, not exchangeable, adhesion of microorganisms and fouling, positioning is crucial, size limitation
External modes	Exchangeable, suited for coupling of on-line analysers	Complex design, longer answering time, fouling, shear stress

Direct Sampling. Direct sampling from a bioreactor is possible through a catheter with a small inner diameter. It is possible to connect this sample stream directly to a FIA system or any other analytical device. However, for precise measurements, the metabolic activity in the sample must be stopped immediately after sampling, otherwise unwanted reactions may take place during the period after sampling but before analysis. If a deactivation is carried out with addition of an inhibitory agent (18), one has to examine the possibility of interference from the reagent on the analysis (19).

One device that addresses these challenges is the coaxial catheter unit (20,21), which is connected to the bioreactor for direct sample withdrawal. It consists of two concentrically placed tubings, an inner and an outer (Fig. 2); the outer protrudes beyond the inner a few millimeters. The sampling is done via the inner tubing. An inhibitor is fed into the space between the tubings, and the broth plus the inhibitor are mixed in the small mixing zone at the tip of the catheter. Inhibition thus takes place at the moment of sampling. A major advantage of the direct sampling system is that a complete sample is obtained, and it is therefore possible to measure the biomass concentration on-line (22) and even perform analysis on intracellular compounds (23,24). The coaxial catheter has not yet been used for sample withdrawal from cultures of filamentous fungi and highly viscous fluids. This method is so far limited to studies of unicellular organisms.

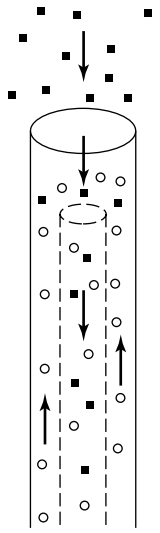

Figure 2. The coaxial catheter. The unit consists of two concentrically placed catheters, the inner being a few millimeters shorter that the outer. Sample is sucked into the inner and is transported away for analysis. The space between the two catheters is used to transport an inhibitor solution toward the tip of the coaxial catheter, where it is mixed with the sample and then withdrawn. If the inner catheter sucks at, for example, double the rate of the inhibitor feed, one volume inhibitor is mixed with one volume of sample and then transported to analysis.

Membrane-Based Sampling Techniques. The sampling system acts as an aseptic barrier between the bioreactor and the analytical equipment. The basic idea behind this type of sampling device is to utilize a membrane for separation during the sampling process. In most cases separations based on differences in size are carried out. The membrane-based sampling techniques can also be applied to cultures of filamentous fungi and in other viscous media. The major disadvantage of the membrane module is clogging of the membrane, mainly due to deposition of proteins on the membrane surface. Reviews on membrane modules are present in the literature (3,25,26).

When using a membrane sampling module, there are three types of separation forces that can be utilized: pressure-driven difference, concentration difference, and electrical potential difference. Applying any of these forces, transport over the membrane will occur and may serve several purposes:

1. Cells are removed from the sample, thus stopping the metabolic activity.
2. Compounds that may interfere with the analysis are retained.
3. Membrane sampling acts as a barrier between the analytical system and the bioreactor.

The details of four major types of membrane separation processes, used in combination with FIA, are presented in Table 2.

Membrane modules can be categorized into two groups: those placed in a recycle loop connected to the bioreactor (filtration outside the reactor), and those placed in situ (as with dialysis filtration). When the membrane unit is placed outside the reactor, fermentation broth is usually pumped through the membrane unit and then recycled to the fermentor. Some characteristics both pro and con of such a device are listed in Table 3.

What is special with the external loop membrane unit is that upon passage of the fermentation broth through the loop, special conditions may prevail. Thus, oxygen limitations may be severe, and, damaging shear forces may appear. This type of device is thus less suited to dealing with high-cell-density fermentations of aerobic cells or with

Table 2. Membrane Separation Procedures Used for Sampling

Mode of separation	Particles separated	Driving force
Filtration	Water and dissolved species	Gravity
Microfiltration	Water and dissolved species (possible to separate unicellular organisms)	Pressure difference
Ultrafiltration	Water and salts (separates biologicals, colloids, and macromolecules)	Pressure difference
Electrodialysis	Charged molecules and ions	Electrical potential
Dialysis	Low molecular weight species	Concentration difference

Table 3. Advantages and Disadvantages in Using a Membrane Unit Placed Outside the Bioreactor

Pro	Con
Replacement of membrane possible	Oxygen depletion may appear in the external loop
Quick response	Shear forces
	Risk of infection

shear-stress-sensitive cells. The great advantage to using an external membrane is the greater flexibility. Thus, a membrane may be easily replaced when needed.

There are two basic modes of operation: the permeate may be collected and used for analysis, or alternatively, a receiving buffer is pumped through the unit on the collection side of the membrane to collect substances passing the membrane. It is important that analyte collection is carried out under sterile conditions. This is usually secured by intermittent sterilization (27–29).

The membranes used for external filtration are made of a variety of materials (e.g., nylon, polypropylene, acrylnitril copolymer, cellulose acetate, cellulose nitrate, polyvinylpyrroliden fluoride) and are available in different pore sizes. Normally, membranes with pore sizes of 0.2 μm are preferred because they guarantee the separation of medium from the biomass and other suspended material (30). Sampling units with external filters are available commercially. The Bio-Pem (B. Braun, Melsungen, Germany) consists of a chamber (vol. 175 mL) containing a magnetically stirred rod. The stirrer ensures a tangential flow across the membrane, which is placed in the bottom of the chamber (31). This unit was successfully used for sample withdrawal during a cultivation process involving unicellular microorganisms but was found unsuitable for sampling cultures of fungi. A major draw back of the Bio-Pem is the large dead volume in the membrane module, which may cause substrate depletion in the loop as well as high response times. An alternative method involves a cross-flow filtration module in which the dead volume is less, resulting in a much shorter response time ($<$10 s). This module is applied efficiently in fed-batch penicillin fermentations on complex media (32) and for wastewater treatment (33).

There is still another unit based on a planar membrane (Fig. 3). The membrane is clamped between two metal blocks, which are then screwed together. During filtration, the incoming broth (feed) is pumped into grooves in the upper block, and the filtrate is collected in the lower chamber. The broth is separated into two streams: the particular-free filtrate (permeate), which passes the membrane, and the particulate-enriched retentate, which is returned to the fermentor. The filtrate is then led to an injection loop for later injection into the analytical system. After passing the loop, two possibilities arise: the filtrate is either returned to the bioreactor or sent to the waste collector. The latter would quickly empty a small fermentor. To avoid this, the filtrate can be recycled to the fermentor, but this increases the risk of contamination. Placing a sterile barrier (e.g., a microfilter) between the injection loop and the bioreactor reduces the risk (34). This may be acceptable in microbial fermentations, but in certain types of processes, such as human cell line production, such a strategy cannot be applied because such cells are very slowly growing and must be cultivated during long time periods and at the same time have a high value. An alternative approach is called discontinuous filtration. The filtrate line is closed between injections and opened shortly before the injection to flush the tubings and the loop (35).

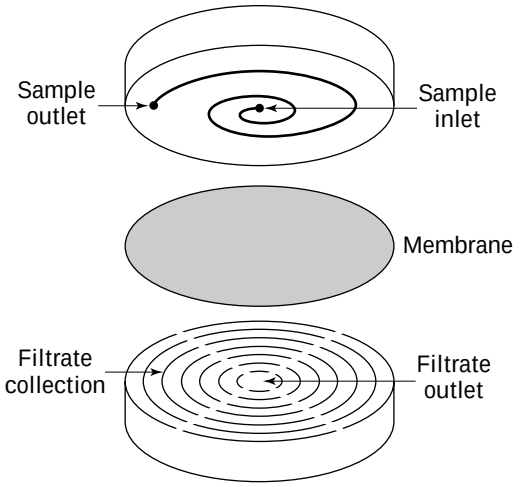

Figure 3. Schematic presentation of the flux membrane dialysis module. The membrane is mounted between the two holders, and sample is introduced on one side. The filtrate is collected and transported for future analysis.

There are several units with planar membranes available on the market. These units have been used for different applications. The A-SEP TM module (Applicon, Schiedam, The Netherlands) has been used for monitoring acetate and phosphate during *Escherichia coli* fermentations (36), utilizing a standard 47-mm-wide 0.45-μm MF membrane. The Minitan TM system (Millipore, Bedford, Mass.), using two membranes, has been employed for the determination of glucose in *Candida rugosa* cultivations

(37), followed by several others for the determination of glucose, diols, and ethanol (38,39).

Membrane filters may also be available in the form of hollow fibers of different diameter and porosity (Fig. 4). Depending on the intended application, the cartridge contains different numbers of hollow fibers. In accordance with the cross-flow filtration principle, the medium is pumped at high velocity (1 m s^{-1}) through the fiber. A pressure is applied, and the filtrate is collected on the outer side of the fibers. It is also possible to pump the broth on the outer side of the fiber(s) and collect the filtrate inside (40). However, depending on the membrane geometry, this latter may be less attractive. When dealing with anisotropic membranes it is advisable to apply the complex medium to the smooth side of the membrane.

A range of different applications are described in the literature. A stainless steel module with only one fiber inside has been reported (41). The fiber had an inner diameter of 5.5 mm and a length of about 200 mm. The dead volume of the module was 2.5 cm^3; and it was successfully used for sampling in conjunction with determination of ammonium, glucose, and phosphate. Reports on the use of several in-house built hollow-fiber modules can be found in the literature, covering vastly different applications in mammalian cell culture (42), lignocellulose hydrolysate fermentations (43), and biodegradation of naphthalene sulphonic acid (44). Systems are also available commercially from Bio-FIO (Glasgow, U.K.) and used for monitoring different types of fermentation components (45,46).

Despite the potential complications associated with operating an external loop filtration system, it remains a popular approach. The great advantage is that when membrane clogging occurs, it is possible to intervene without ruining the fermentation.

In dialysis, a membrane is used to separate a complex solution from a more well defined solution. Pores in the membrane allow exchange of small molecules between the two liquid volumes. The driving force is concentration difference. The different modes of dialysis originate from whether the donor and acceptor phases are stagnant or moving. In equilibrium dialysis both are stagnant and, at equilibrium, the concentration in both phases will be the same of those molecules able to pass the membrane. In continuous dialysis, compounds passing the membrane are continuously removed. This results in a larger concentration gradient, and a higher flux is maintained.

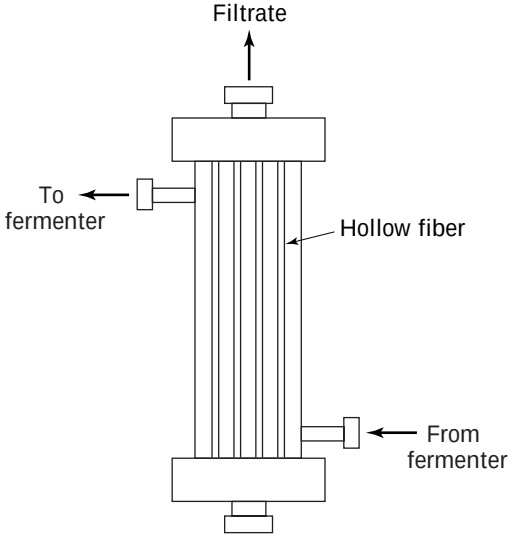

Figure 4. Schematic presentation of the hollow-fiber modules for sampling. A perfusion buffer is passed through the lumen of the fibers, and the fermentation broth is introduced on the shell side of the unit.

The membranes used for dialysis are classified according to their molecular weight cut-off. Most dialysis membranes are made from cellulose materials, but because many organisms are able to hydrolyze cellulosic materials, this limits their applicability. There are several sampling units that incorporate dialysis membranes. They are usually placed in the fermentor, and a receiving dialysis carrier buffer is circulated on the permeate side of the membrane. The carrier buffer is thus pumped into the bioreactor and, after having received the dialysate molecules, removed again. The major problem associated with this approach is the deposition of cells and fouling of the membrane on the fermentor side. The accumulated layer of cells may reduce the mass transfer from the fermentor to the accepting solution and also cause decreases in concentration of metabolites passing through the membrane because they run the risk of being metabolized by the cell layer before entering the dialysis membrane. To help reduce fouling it is possible to place the dialysis probe into the zone of the fermentor where the impeller creates the greatest turbulence (47).

Another means of obtaining similar results, but with fewer design restrictions, is to construct a dialysis probe that besides containing the membrane unit also has a stirring function, so that a high tangential liquid flow is generated over the membrane. This approach was used by Mandenius et al. (48) in constructing a system for use in dense particulate suspensions. The membrane is placed in the front of the probe, and membrane fouling is avoided by means of the rotating magnet driven by an electrical motor inside the probe (Fig. 5).

Zabriskie and Humprey (49) developed a dialysis probe situated within one baffle of a stirred fermentor. They were able to take samples for glucose analysis during cultivation of yeast cells on a synthetic medium. The disadvantage of this dialyzer is that it can be used only in this type of bioreactor. Another sampling device was presented by Glaxo Laboratories, Ltd. (50). This unit consist of an elongated support with a milled helical groove. A tubular membrane made of cellulosic materials or polytetrafluoroethylene was fixed to the support using ring seals.

An in situ dialysis membrane module was developed at the University of Hannover and is marketed by Advanced Biotechnology Corporation (ABC). The module consists of a unit supporting the membrane, and one or more extension units. The membrane module is usually inserted through a standard 19- or 25-mm port in the top of the bioreactor or, alternatively, through a 25-mm port below the liquid surface. When inserted from the top of the bioreactor, one or more extension tubes are needed to place the membrane below the liquid surface. Liquid passing the

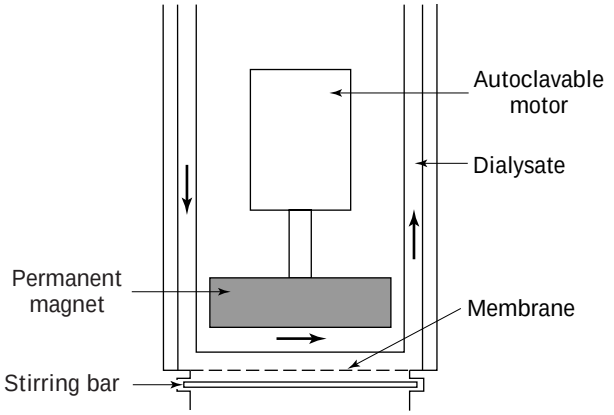

Figure 5. Cross section of the dialysis probe. The stirring bar is rotated by the rotating magnetic field when the motor is on. Receiving solution is pumped over the inner side of the membrane where dialysate is received and removed for analysis *Source*: From Ref. 48.

membrane is collected in 16 grooves, and these 16 permeate streams are joined in four openings placed evenly along the membrane holding unit. Through these four openings the permeate enters the central channel (10 mm i.d.), and a continuous sample stream to the analyzer leaves the unit from the top of the probe (51).

Gibson and Woodward (52) have also described an internal dialysis module, based on the same principle but without a stirrer. Ethanol and glucose could be sampled with this unit, and the results from the subsequent analyses agreed well with the on-line data.

Another modified technique is the microdialysis used for continuous in vivo sampling, which has been described in reviews (3,53,54). The microdialysis sampling unit is a probe, and it is a miniaturized form of a dialysis unit. It is manufactured in several different configurations, one is seen in Figure 6.

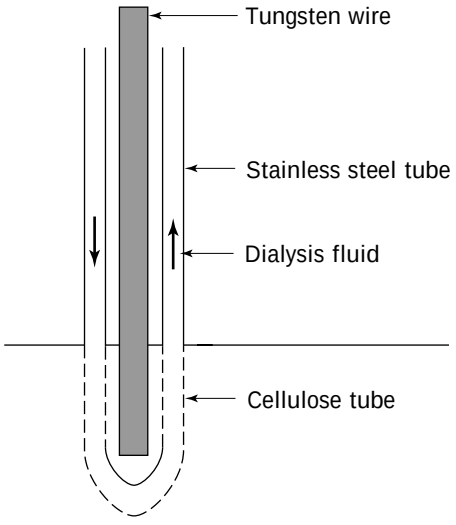

Figure 6. The microdialysis unit.

Typical flow rates of the perfusion liquid are 0.5–25 μL/min, and to avoid pulses in the flow, a peristaltic pump or preferably a syringe pump should be used. Due to its ease of operation and the general approach, the number of applications increases rapidly. It can easily be coupled on-line to a number of separation and detection techniques. This technique was used in fermentation processes for the production of ethanol, penicillin, and so on (55). However, the slow flux of liquid and thus the long response time from an analysis based on this sampling technique, compared with the conventional sensing devices, should be considered.

The major problem in dialysis units is the fouling and clogging by macromolecules on the membrane surface. This can be overcome by adding molecules that compete for the binding site of the protein, adding a displacer (56), changing the pH (57), or pumping the solution tangentially over the membrane surface. An excellent review on dialysis for flow injection analysis has been published (26).

MODES THAT AVOID OR AT LEAST REDUCE THE NEED FOR SAMPLE TREATMENT

As already noted a major concern in sample handling is clogging. Quite often packed-bed systems are used, and then particulate matter constitutes a major obstacle. In these cases, particulate matter has to be removed prior to analysis. However, with the introduction of expanded-bed chromatography, it is possible to handle large-scale chromatographic processes without separating out the cells (58). This made it tempting to investigate the possibility of using the same approach in an analytical system.

Enzyme-based analysis was studied using glucose oxidase immobilized to Streamline® particles. These particles are characterized by being of heterogeneous size and density distribution, such that when used in an expanded bed, a stable expanded bed can be obtained. Glucose was monitored using this technique (59). A more challenging issue is whether the same system would allow binding reactions to take place. If so, one should be able to run immunoassays in whole broth and maybe even in cell homogenates. Assays of human serum albumin in the presence of increasing amounts of heat-killed yeast cells was used as a model system. Antibodies against albumin were present on the Streamline® (60). The assays seemed successful, and therefore the model was also studied to see if the intracellular enzyme β-galactosidase could be quantified in a cell suspension or a cell homogenate. The results were so encouraging that it is safe to say that this technique allows binding assays without the preceding separation of particulate matter from the sample.

PRETREATMENT OF SAMPLES

Another vital part of the analysis is the pretreatment of the samples. This includes dilution, centrifugation, extraction, and filtration, depending on the nature of the samples. Certain samples can be analyzed without pretreatment; however, for complex samples extensive clean-up is required before introduction into the flow system. This topic has been discussed in several reviews (61,62). The

reproducibility and rapidity of flow injection analysis promotes its applicability for on-line pretreatment of samples with less manual intervention (63–65) (Fig. 8). Additionally pretreatment steps by FIA are rapid. The pretreatment and analysis, including chemical conversion, usually require less than a minute. Furthermore, when samples are toxic or pathogenic, FIA offers the advantage of removing, or at least minimizing, human exposure. An excellent review on sample pretreatment by FIA was published by Clark et al. (66) and includes a description of the theoretical background of sample pretreatment.

Disintegration of Cells

Monitoring levels of intracellular compounds has so far been possible only via off-line analyses. However, after the recent development of an on-line disintegration system that can be used together with expanded-bed adsorption in a flow system, a new possibility seems to have emerged. The important issues are that the whole broth is taken and treated and after that the whole homogenate can be processed in, for example, a binding assay.

The whole broth is introduced into an FIA system where it first passes an expanded bed containing Streamline® with immobilized lysozyme. On passage of *Micrococcus lysodeiticus* cells it has been proven that a high degree of disintegration is achieved, as judged from the amount of protein released (23). When adding a subsequent step involving sonication using a flow cell, the disintegration is even more efficient. The experimental set-up is shown in Figure 7. A culture of *E. coli* was studied and its level of β-galactosidase production was monitored. The detection step consisted of an expanded bed containing Streamline® with immobilized antibodies to β-galactosidase.

Upon introduction of the whole broth, homogenization takes place by treatment in the two units; and afterward liberated enzyme is trapped by the immunosorbent. The enzyme is quantified by reading the amount of *o*-nitrophenol liberated after passing a pulse of *o*-nitrophenyl-β-galactopyranoside over the sorbent. After the assay the immunocomplex is broken and the system is ready for another assay (24).

Centrifugation

Centrifugation is commonly used for separating cells and particulate materials from the fermentation broth. It is possible to include a small-scale centrifuge in an FIA system, with recycling of the sample to the reaction vessel (67).

Liquid–Liquid Extraction

Liquid–liquid extraction is based on the partitioning of the analytes between an aqueous and an organic phase and is widely used for gas chromatographic analysis. Integrating this technique into FIA is difficult because it is difficult to automate, laborious, and expensive. Solid-phase extraction (SPE) is based on sorption of analytes in solution to a sorbent packed in a cartridge or reactor, typically the size of a precolumn (10–20 $\times$ 2–4.6 mm in length and i.d., respectively) (68). While the analyte is trapped into the packing material, compounds with little or no affinity for the sorbent pass through the column. After washing the column to further remove the interfering substances, the analytes are then desorbed and eluted by a small volume of an appropriate solvent. Recently, Vreuls et al. (69) demonstrated the coupling of on-line SPE to gas chromatography. A precolumn packed with mixed anion/cation exchange materials was used on-line in a flow system for removal of ionic substances in aliquots of a filtrate from fermentation.

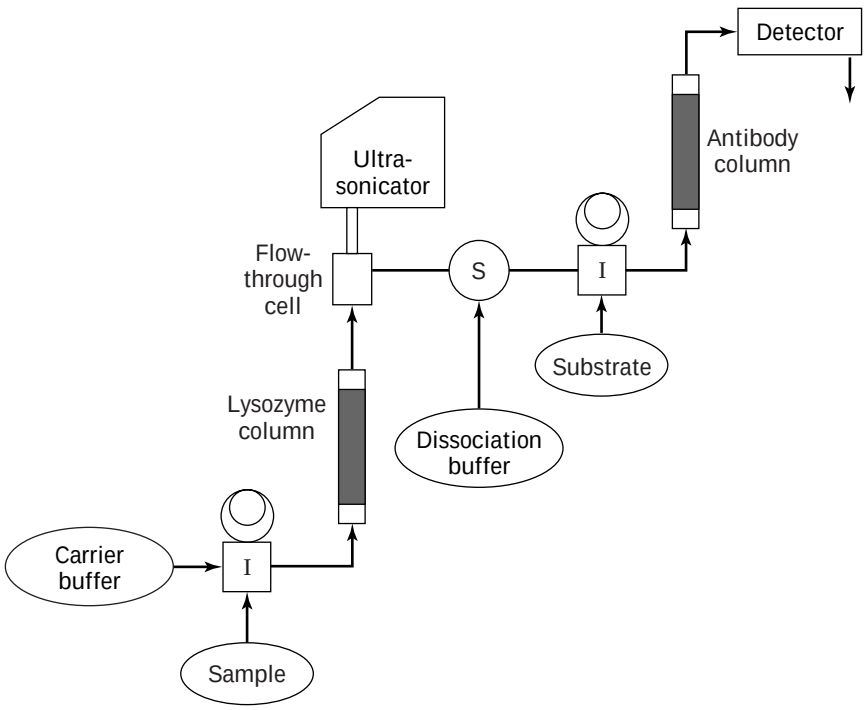

Figure 7. Schematic presentation of a complete flow system, including an expanded flow column with immobilized lysozyme and ultrasonicator flow cell. An expanded column with immobilized antibodies is also included for the subsequent ELISA.

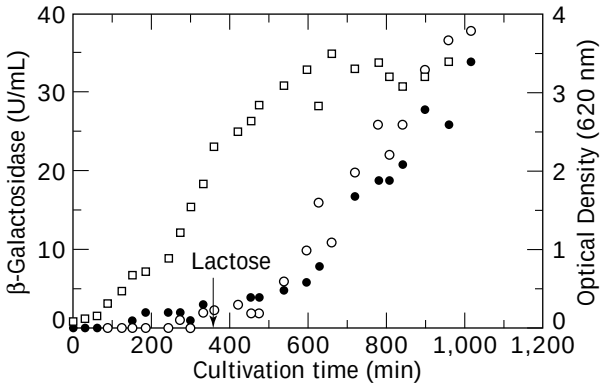

Figure 8. Monitoring of a shake-flask experiment. On-line (●) and off-line (○) *β*-galactosidase activity and o.d. (□) measurements. At the arrow the inducer lactose was added.

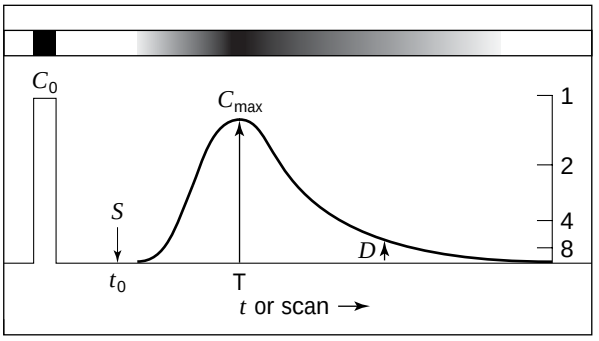

Figure 9. In addition to peak height a dispersed sample zone yields an infinite number of vertical readouts. The initial concentration, C_0, is injected at time t_0, and the pulse appears as a continuum of concentrations as exemplified by the peak. At time T, C_{max} is the highest value read, but a reading could be done anywhere along the peak (e.g., a diluted value at point D).

Preconcentration Techniques

If the analyte concentration is less than the concentration range of the detection method, the sample must be concentrated. Most of the manual pretreatment methods are time-consuming and expensive. Microcolumns with ion exchange materials can be used to significantly reduce the volume of the analyte by adsorbing the sample into a solid support in the column and by a further elution (70).

Dilution of Samples

If the analyte concentration is more than that of the detectable range of the analytical system, the sample must be diluted. The same goes for a sample in which inhibiting or otherwise disturbing substances are present in high concentrations. Manual dilution is used for off-line analysis. On-line dilution is now widely applied for fermentation processes (66) and includes the use of gradient dilution, zone sampling, and cascade dilution.

In the gradient dilution, an originally homogeneous sample zone disperses during its movement through the FIA conduit. The zone undergoes a change from an initial plug shape with a concentration C_0, to an exponentially modified gaussian shape with a maximum concentration in the zone of C_{max}. If the peak maximum does not lie in the calibration range of the measurement, the zone can be made at a time on the profile that yields a decreased response. By selection of measurement times longer than the time of peak maximum (T in Fig. 9), an element with a decreased concentration is measured, yielding a proportionally decreased absorbance. This measurement is reproducible from sample to sample and can be calibrated.

In zone sampling a small portion of the sample zone injected into a second flowing stream results in dilution (71,72). In cascade dilution the sample volume is reduced through stream splitting using differential pumping coupled with a true dilution by merging with a subsequent carrier stream.

Sample Injection

Sample handling and pretreatment can be achieved by using many techniques in FIA. The method of injection is equally important. The purpose of sample injection in FIA is to deliver a well-defined sample bolus reproducibly into a continuously flowing carrier stream. Ruzicka and Hansen (73) described that changing the injected sample volume is a powerful way to change the dispersion. An increase in peak height and sensitivity of measurement is best achieved by increasing the volume of the injected sample solution. Conversely, dilution of overly concentrated sample material is achieved by reducing the sample volume.

There are two methods of injection: time-based injection (a sample loaded for a precise time at a given flow rate) and volume-based injection (the sample fills a geometrically defined volumetric cavity). This well-defined sample bolus is then inserted into the carrier stream. Volume-based injections are performed using rotary valves, commutators, and hydrodynamic injections. A detailed methodology used for injection has been published (74).

Calibration of Sampling System

For any kind of analysis, whether it is on-line or off-line, the system needs to be calibrated to ensure that the compound of interest is being measured reliably. It is easy to calibrate an off-line system. However, the continuous systems described so far commonly have no possibility for calibration and recalibration on-line without disrupting the monitoring procedure. Thus, any changes occurring in the sample during the recalibration, are not registered (5). Another important limitation is the fact that the calibration solution and the sample solution are usually not treated in the same manner.

In-line calibrating systems are used in medical monitoring. Attempts were made for in-line calibration during fermentation with *E. coli* using a double-lumen catheter. The calibration was done by closing the sample inlet from the fermentor and substituting it with a sample of known analyte concentration (20) (Fig. 10). A further development of this technology was the use of the coaxial catheter for sampling. In on-line monitoring of glucose and lactate in blood, the calibration solution was introduced as a pulse

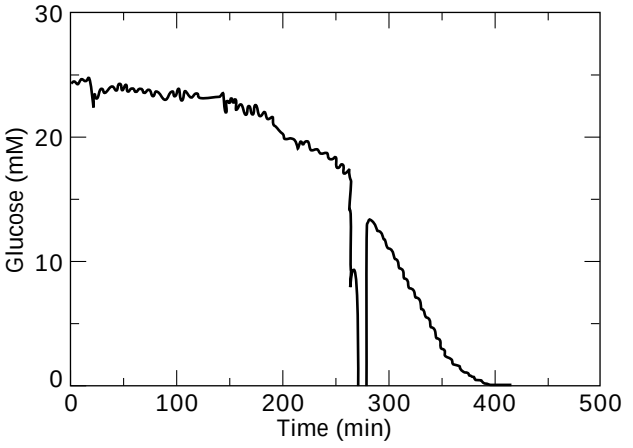

Figure 10. Monitoring of glucose in batch cultivation of *Escherichia coli*. After approx. 270 min a calibration solution is introduced, and the reading is back approx. 10 min later. *Source*: From Ref. 20.

in the heparin stream fed via the outer space in the coaxial catheter. This led to an on-line monitoring of the process without having to interrupt the reading (Fig. 11). Furthermore, by introducing the calibration solution at the tip of the sampling catheter, the whole system is calibrated. Thus a more true calibration value is obtained (75,76).

CONCLUSION

Sampling and sample treatment are extremely important when applying good analytical technique to the monitoring and control of biotechnological processes. Too often much effort is spent on developing a sensitive assay, but very little or no concern has been given to sampling and sample handling. The examples given in this article clearly demonstrate that many good techniques can be applied. Which method to use will be governed by the system studied, the equipment available, and also the earlier experience of the researcher.

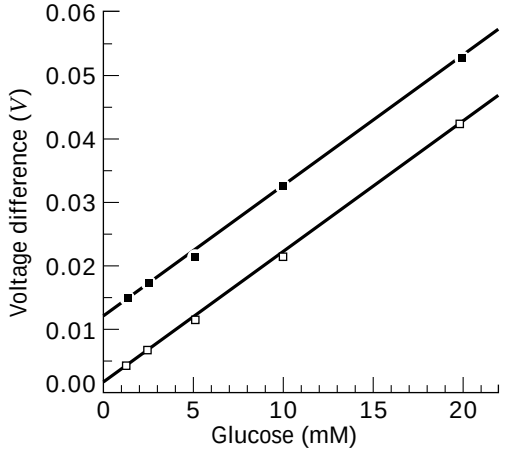

Figure 11. On-line outlet signal (V) as a function of glucose concentrations (mM); (■) glucose standard solution with added internal standard (5 mM), $y = 1.14 \times 10^{-2} + 2.05 \times 10^{-3}\,x$, $r^2 = 1.000$; (□) glucose standard solution, $y = 1.09 \times 10^{-3} + 2.04 \times 10^{-3}\,x$, $r^2 = 1.000$.

BIBLIOGRAPHY

1. D.J. Clarke, B.C. Blake-Coleman, M.R. Calder, R.J.G. Carr, and S.C. Moody, *J. Biotechnol.* **1**, 135–158 (1984).
2. R.T. Hatch, *Annu. Rep. Ferment. Proc.* **5**, 231–235 (1982).
3. N.C. van de Merbel, H. Lingeman, and U.A. Th. Brinkman, *J. Chromatogr. A* **725**, 13–27 (1996).
4. I. Karube, T. Matsunaga, S. Suzuki, T. Asano, and S. Hob, *J. Biotechnol.* **1**, 286–291 (1984).
5. B. Mattiasson and H. Håkanson, *Trends Biotechnol.* **11**, 136–142 (1993).
6. Hun.-C. Shu, Ph.D. Thesis Lund University, Lund, Sweden, 1994, ISRN LUTKDH/TKBT–94/1020-SE.
7. T. Buttler, Ph.D. Thesis Lund University, Lund, Sweden, 1996, ISRN LUNDKL/(NDKAK-1034).
8. K.D. Vorolop, J.W. Becke, and J. Klein, *Biotechnol. Lett.* **5**(8), 509–512 (1983).
9. J.H. Lee, J.C. Woodard, R.J. Pagan, and P.L. Rojers, *Biotechnol. Lett.* **3**, 351–356 (1981).
10. C.F. Mandenius and B. Mattiasson, *Eur. J. Appl. Microbiol. Biotechnol.* **18**, 197–200 (1983).
11. O.F. Fiho, J.F. de Andrade, A.A. Suleiman, and G.G. Guilbault, *Anal. Chem.* **61**, 746–748 (1989).
12. T. Buttler, C. Nilsson, L. Gorton, G. Marko-Varga, and T. Laurell, *J. Chromatogr. A* **725**, 41–56 (1996).
13. T. Lorenz, W. Schimidt, and K. Schugerl, *Chem. Eng. J.* **35**, B15–B22 (1987).
14. B. Mattiasson and B. Danielsson, (1996) in R.F. Taylor and J.S. Schultz eds., *Handbook of Chemical and Biological Sensors*, IOP Publishing, Philadelphia, pp. 533–552.
15. J. Nielson, *Process Qual. Control.* **2**, 371–384 (1982).
16. N. Vriezen and J.P. Van Dijken, *Biotechnol. Tech.* **11**(6), 427–430 (1997).
17. T. Kullick, U. Bock, J. Schubert, T. Scheper, and K. Schügerl, *Anal. Chim. Acta* **300**, 25–31 (1995).
18. K. Nikolajsen, J. Nielsen and J. Villadsen, *Anal. Chim. Acta* **214**, 137–145 (1988).
19. J. Nielsen, K. Nikolajsen, and J. Villadsen, *Biotechnol. Bioeng.* **33**, 1127–1134 (1989).
20. O. Holst, H. Håkanson, A. Miyabayashi, and B. Mattiasson, *Appl. Microbiol. Biotechnol.* **28**, 32–36 (1988).
21. H. Håkanson, M. Nilson, and B. Mattiasson, *Anal. Chim. Acta* **249**, 61–65 (1991).
22. S. Benthin, J. Nielsen, and J. Villadsen, *Anal. Chim. Acta* **247**, 45–50 (1991).
23. M.P. Nandakumar, A. Tokaj, and B. Mattiason, *Bioseparation*, in press.
24. A. Tokaj, M.P. Nandakumar, O. Holst, and B. Mattiasson, *Bioseparation*, in press.
25. K. Schügerl, in H.J. Rehm, G. Reed, A. Puhler, and P. Stadler eds., *Biotechnology*, 2nd ed., vol. 4, VCH, Weirheim, 1991, pp. 152–156.
26. J.F. van Staden, *Fresenius J. Anal. Chem.* **352**, 271–302 (1995).
27. K.H. Kroner and N. Papamichel, *Process Biochem.* **23**(10), 3–4 (1991).

28. A. Reckenwald, K.H. Kroner, and M.R. Kula, *Enzyme Microb. Technol.* **7**, 607–612 (1985).
29. M. Garn, M. Gasin, C. Thommen, and P. Cevey, *Biotechnol. Bioeng.* **34**, 423–428 (1989).
30. T. Lorenz, W. Schimidt, and K. Schügerl, *Chem. Eng. J.* **35**, B15–B22 (1987).
31. K.H. Kroner and M.R. Kula, *Anal. Chim. Acta* **163**, 3–15 (1984).
32. L.H. Christensen, J. Nielsen, and J. Villadsen, *Chem. Eng. Sci.* **46**(12), 3304–3307 (1991).
33. K.M. Pedersen, M. Kummel, and H. Soeberg, *Anal. Chim. Acta* **238**, 191–199 (1990).
34. N.C. van de Merbel, I.M. Kool, H. Lingeman, U.A.Th. Brinkman, A. Kolhorn, and L.C. de Rijke, *Chromatographia* **33**, 525–532 (1992).
35. T.A. Butler, A.J. Kristina Johanson, L. Gorton, and G.A. Markovarga, *Anal. Chem.* **65**(19), 2628–2636 (1993).
36. L.F. Forman, B.D. Thomas, and F.S. Jacobson, *Anal. Chim. Acta* **249**, 101–111 (1991).
37. F. Valero, J. Lafuente, M. Poch, C. Sola, A.N. Aranjo, and J.L.F.C. Lima, *Biotechnol. Bioeng.* **36**, 647–651 (1990).
38. M.J. Hayward, T. Kotiano, A.K. Lister, R.G. Cooks, G.D. Austin, R. Narayan, and G.T. Tsao, *Anal. Chem.* **62**, 1978–1804 (1990).
39. U. Brand, B. Reinhardt, F. Ruther, T. Scheper, and K. Schügerl, *Sensors Actuators* **4**, 315–318 (1991).
40. H. Hoffman, Ph.D. Thesis, University of Hannover, Hannover, Germany, 1985.
41. K. Schügerl, *Anal. Chim. Acta* **213**, 1–9 (1988).
42. S.S. Ozturk, J.C. Thrift, J.D. Blackie, and D. Nareh, *Biotechnol. Bioeng.* **48**, 201–208 (1995).
43. C.F. Mandenius, *Biotechnol. Bioeng.* **32**, 123–129 (1988).
44. J. Meschke, H. Bennemann, M. Herbst, S. Dormeier, and D.C. Hempel, *Bioprocess Eng.* **3**, 151–157 (1988).
45. N.C. van de Merbel, H. Lingman, U.A.Th. Brinkman, A. Kolhorn, and L.C. de Rijke, *Anal. Chim. Acta* **279**, 39–50 (1993).
46. N.C. van de Merbel, P. Zuur, Frijlink, J.J.M. Holthuis, H. Lingeman, and U.A.Th. Brinkman, *Anal. Chim. Acta* **303**, 175–186 (1995).
47. T. Lorenz, W. Schimidt, and K. Schügerl, *Chem. Eng. J.* **35**, B15–B22 (1987).
48. C.F. Mandenius, B. Danielsson, and B. Mattiasson, *Anal. Chim. Acta* **163**, 135–141 (1984).
49. D.W. Zabriskie and A.E. Humphery, *Biotechnol. Bioeng.* **20**, 1295–1301 (1978).
50. U.S. Pat. 3,830,106 (1974), Glaxo Laboratories, Ltd.
51. L.H. Christensen, J. Nielsen, and J. Villadsen, *Anal. Chim. Acta* **249**, 123–136 (1991).
52. T.D. Gibson and J.R. Woodward, *Anal. Chim. Acta* **213**, 61–68 (1988).
53. H. Benreniste and P.C. Huttemeier, *Prog. Neurobiol.* **35**, 365–372 (1991).
54. T.E. Robinson and J.B. Justice, Jr., Eds., *Microdialysis in the Neurosciences*, Elsvier Science, Amsterdam, 1991.
55. G. Marko-Varga, T. Buttler, L. Gorton, and C. Gronstervall, *Chromatographia* **35**, 285–289 (1993).
56. N.C. van de Marbel, J.M. Teule, H. Lingeman, and U.A.T. Britman, *J. Pharm. Biomed. Anal.* **10**, 225–231 (1992).
57. J.D.H. Cooper, D.C. Turnell, B. Green, and F. Verillon, *J. Chromatogr.* **456**, 53–69 (1988).
58. H. Chase, *Trends Biotechnol.* **12**, 296–303 (1994).
59. M.P. Nandakumar, A. Lali, and B. Mattiason, (1998) Submitted.
60. B. Mattiason and M.P. Nandakumar, (1998) Submitted.
61. M.C. Hennion, *Trends. Anal. Chem.* **10**, 317–322 (1991).
62. U.A.Th. Brinkman, *J. Chromatogr. A* **665**, 217–231 (1994).
63. S. Olsen, J. Ruzicka, and E.H. Hansson, *Anal. Chim. Acta* **136**, 101–112 (1982).
64. E. Martins, M. Bengtsson, and G. Johansson, *Anal. Chim. Acta* **169**, 31–42 (1985).
65. B. Karlsberg and S. Thelander, *Anal. Chim. Acta* **98**, 1–7 (1978).
66. G.D. Clark, D.A. Whitman, G.D. Christian, and J. Ruzicka, *Crit. Rev. Anal. Chem.* **21**(5), 357–375 (1990).
67. N.F. Thornhill and N.B. Fish, *Biotechnol. Tech.* **7**, 19–24 (1993).
68. G.R. van der Hoff, R.A. Banmann, U.A.Th. Brinkman, and P. van Zoonen, *J. Chromatogr.* **644**, 367–373 (1993).
69. J.J. Vreulls, G.J. De Jong, R.T. Ghijsen, and U.A.Th. Brinkman, *J. AOAC Int.* **77**, 306–327 (1994).
70. J. Ruzicka and E.H. Hansen *Anal. Chim. Acta* **214**, 1–27 (1983).
71. B.F. Reis, A.O. Jacintho, J. Moratti, F.J. Krug, E.A.G. Zagatto, F.H. Bergamin, and L.C.R. Pessenda, *Anal. Chim. Acta* **123**, 221–228 (1981).
72. J. Ruzicka and E.H. Hansen, *Anal. Chim. Acta* **145**, 1–15 (1983).
73. J. Ruzicka and E.H. Hansen, *Flow Injection Analysis*, 2nd ed., Wiley, New York, 1988.
74. F.J. Krag, F.F. Bergamin, and E.A.G. Zagatto, *Anal. Chim. Acta* **179**, 103–107 (1986).
75. M. Kyrölainen, H. Håkanson, and B. Mattiasson, *Biotechnol. Bioeng.* **45**, 122–128 (1995).
76. R. Kok and P. Hoasi, *Biosensors* **3**, 89–100 (1987/88).

SCALE-UP. See DIMENSIONAL ANALYSIS, SCALE-UP; MAMMALIAN CELL CULTURE REACTORS, SCALE-UP; SCALE-UP, STIRRED TANK REACTORS.

SCALE-UP, STIRRED-TANK REACTORS

D.C. HEMPEL
H. DZIALLAS
Technische Universität Braunschweig
Braunschweig, Germany

KEY WORDS

Dispersing capacity
Mass transport
Mixing time
Newtonian fluids
Non-Newtonian fluids
Power input
Pumping capacity
Scale-up

Shearing stress
Stirred-tank reactor

OUTLINE

INTRODUCTION

The scale-up of a biotechnological process developed in the laboratory often presents problems that, owing to the many parameters involved and their complexity, do not permit any generalized solution. As a result, criteria for scale-up have always been developed on the basis of specific processes. The main problem in all considerations of scale-up is that no strictly defined criteria exist for conducting biotechnological processes and, hence, their scaled translation. Of the biological and physical factors important in scale-up, generally valid relationships can be established only for the latter. Thus in the following, the experimentally proven physical fundamentals of scale-up for conventional stirred-tank reactors are brought together in a way that reflects their importance in practical operation. Such considerations have been published in the past but were based on the scientific knowledge available at that time (1–5). This article is an updated short version. For further information about scale-ups of fermentation processes and extended literature see Ref. 5.

SCALE-UP METHODS

Balance Equation

A scale-up using a solution of the complete equations for momentum, energy, and mass balances is exceedingly difficult to determine for a complex microbiological process. Thus for a scale-up on the basis of mathematical models, there are still no practicable equations available at present that take into account the kinetics and transport processes in the stirred-tank reactor. Nonetheless, the application of simplified balance equations is often helpful in order to understand the processes involved (6,7).

Dimensional Analysis

Dimensional analysis, introduced successfully into chemical technology and already a classical method of scale-up, is also helpful when dealing with biotechnological processes. Using it, a number of dimensionless quantities (π-quantities) are derived from the relevant process-influencing quantities, which using the mathematical interrelationships of the similarity principle, provide criteria for scale-up (see also Refs. 8 and 9). The invariance of all dimensionless π-quantities relevant to the problem provides the simplest rule for scale-up, but the rule is dependent upon complete similarity. Whereas physical processes often do behave similarly upon change in scale, similarity in the presence of a chemical or microbial process is often unattainable. Even for purely physical processes, a complete similarity can often not be attained. As shown in the section "Performance Characteristics of the Stirred-Tank Reactor," the translation rule Re = idem (idem means that the numerical value of Re is held constant in scale translation) is valid for the energy input in scaling-up stirred-tank reactors, without formation of vortices. But if, nonetheless, a vortex should form, as in unbaffled vessels, then both the Reynolds number and the Froude number must retain their numerical value. From the definition of Re and Fr, it immediately becomes obvious that the requirements Re = idem and Fr = idem cannot be fulfilled because $n \cdot d^2$ = idem cannot equal $n^2 \cdot d$ = idem.

Because it is rarely possible to maintain all dimensionless characteristic quantities at the same numerical value, it becomes necessary to restrict oneself to partial similarities in which only some of the π-quantities remain fixed. To achieve this, the rate-determining step of the reaction for the complex microbial system must be known. That means that from the many process parameters, such as nutrient requirements, physicochemical conditions of growth, or transport processes, the limiting (or inhibiting) quantities have to be determined by careful analysis. Problems then arise when there is a shift in the effect of the individual limiting factors when the scale is altered. Such an approach to scale-up, in which each rate-determining step, both of the microbial reaction and of the transport processes, is mathematically correlated, has been put forward from time to time (for example, see Ref. 10) and has also been introduced highly successfully (11–14).

Maintenance of Identical Operating Conditions

A further simplification of the scale-up criteria, which follows from accepting the notion of partial similarity, is the maintenance of identical operating conditions (usually assuming that there is geometrical similarity). The most common examples of scale-up rules that have been published in the specialized biotechnological literature are based on this concept; extrapolation is often performed ac-

Table 1. Effects of Different Criteria in Linear Scaling-Up by a Factor of 5

		Scale-up criterion			
	Laboratory scale	P/V (kW/m^3)	n (s^{-1})	$n \cdot d$ (m/s)	Re
Diameter D (m)	1	5	5	5	5
Specific power input P/V (kW/m^3)	1	1	25	0.2	1.6×10^{-3}
Power input P (kW)	1	125	3125	25	0.21
Rotational speed of stirrer n (s^{-1})	1	0.34	1	0.2	0.04
Tip speed of stirrer $n \cdot d$ (m/s)	1	1.71	5	1	0.2
Reynolds number	1	8.55	25	5	1

Source: From Ref. 20.

cording to empirical rules of thumb that are still used today in the fermentation industry. Typical examples of this are the following:

- Identical volumetric power input P/V
- Identical mixing time or adaption of the mixing time to different stirred-tank reactor sizes according to purely empirical translation rules
- Identical tip speed of the agitator
- Identical volumetric mass transfer coefficient k_La
- Identical Reynolds number, Re

In fact, according to Ref. 15, about one third of plants employed the translation rules P / V = idem and k_La = idem, and about 20% used the tip speed of the stirrer (i.e., assuming shear stress). Another 20% of industrial plants employ a scale-up on the basis of mixing time and Reynolds number. The remainder scaled-up on the basis of a limiting or inhibiting substrate or product component—most commonly on the basis of the concentration of dissolved oxygen.

A scale-up founded on a single operating condition has diverse effects on the other operating quantities, as shown in Table 1 (see also Refs. 16–19). Using a linear scaling factor of 5 (corresponding to a volume scaling factor of 125) each column shows the change in the operating quantity that results from the respective scale-up criterion. Table 1 shows that it is not possible to simultaneously fulfill several of the scale-up criteria mentioned (20).

PHYSICAL FUNDAMENTALS OF SCALE-UP CONDITIONS

Performance Characteristics of the Stirred-Tank Reactor

The stirring power, P, which produces the three-dimensional flow field can be calculated from the dimensionless power number or Newton number:

$$Ne \equiv \frac{P}{\rho \cdot n^3 \cdot d^5} \tag{1}$$

From considerations of the similarity principle, the formal correlation of the performance characteristic for a given geometry is described by

$$Ne = f(Re, Fr, Q) \tag{2}$$

where the Froude number is $Fr \equiv n^2 \cdot d/g$, the Reynolds number is $Re \equiv n \cdot d^2/\nu$, and the dimensionless gasflow number is $Q \equiv q_G/n \cdot d^3$.

Power Input in Nongassed Systems of Newtonian Fluids. In systems that have no gas input ($Q = 0$) and no vortex formation (as is effectively the case in a vessel with baffles), the effect of the Froude number is negligible. The performance characteristics of the nongassed system of Newtonian fluids, which is then solely a function of the Reynolds number (21–23) is depicted in Figure 1 for a selection of stirrers. The geometrical arrangement and the working range of the stirrers have been standardized in some countries (e.g., DIN 28131 in Germany). Except for the helical and anchor stirrers which extend right to the wall, stirred vessels are equipped with baffles to avoid vortex formation. The reduction in the number of baffles from 4 to 3 or 2 generally lowers the energy input by 10 or 20% (23). In a completely turbulent system (a condition fulfilled with most stirrers at $Re > 10^4$), the performance characteristic is independent of the Reynolds number, that is, Ne = constant. If the scale-up considerations are based on a constant volumetric power input, $P/V \sim P/d^3$ = idem, then the following is valid for the scaled translation:

$$n^3 \cdot d^2 = \text{idem} \tag{3}$$

Power Input in Nongassed Systems of Non-Newtonian Fluids. In many fermentation broths, for example, those containing polysaccharides or mycelium-forming microor-

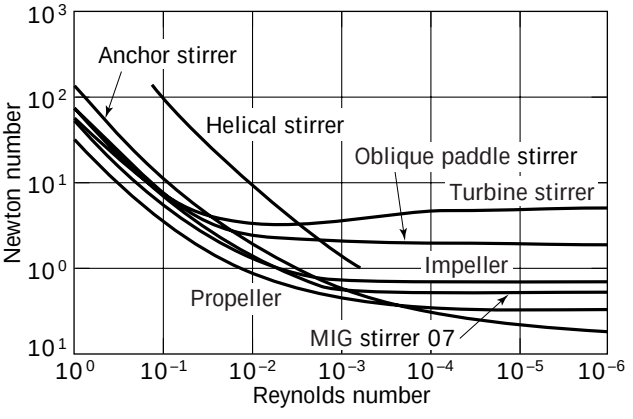

Figure 1. Performance characteristics of some types of stirrer with Newtonian fluids.

ganisms, non-Newtonian flow behavior is encountered: there is a complicated nonlinear relationship between the shearing stress, τ, and shear rate, $\dot{\gamma}$. For non-Newtonian fluids, the viscosity property can be defined only in the form of an apparent viscosity

$$\eta_a \equiv \frac{\tau}{\dot{\gamma}} \tag{4}$$

A number of models have been put forward to describe the non-Newtonian flow behavior. The most efficacious originate from the Ostwald-De Waele law for pseudoplastic fluids

$$\tau = K' \cdot \dot{\gamma}^{m'} \tag{5}$$

and from Herschel–Bulkley law for plastic fluids

$$\tau = \tau_0 + K'' \cdot \dot{\gamma}^{m''} \tag{6}$$

In order to determine the energy input in such fluids, the approach adopted by Metzner and Otto (24) and Metzner et al. (25) has proved itself. According to this concept, there is a direct proportionality between the rate of shear and the rotational speed of the stirrer

$$\dot{\gamma} = K \cdot n \tag{7}$$

whereby the apparent viscosity, η_a, is obtained from the rheological flow curve of the fluid involved. The coefficient K depends only slightly on the rheological behavior of the fluid but mainly on the stirring system, for example, $K \approx 11$ to 13 for turbine agitators and $K \approx 15$ to 25 for anchor agitators (15,26). In Figure 2 the performance characteristic of the turbine stirrer for pseudoplastic fluids is plotted versus the Reynolds number which has been modified by η_a (24,27).

A similar performance characteristic was measured by Sanchez et al. (28) and Velasco et al. (29) for a single and a dual Rushton turbine when mixing a mycelial broth under nonaerated conditions. As with Newtonian fluids, a constant Newton number is attained here at sufficiently high Reynolds numbers (i.e., the performance characteristic is independent of the viscosity). Whereas this independence of the viscosity is unequivocally valid in a nongassed system, considerable dependence on the viscosity occurs in a gassed system of non-Newtonian fluids, as is illustrated in a following section.

The apparently simple approach advocated by Metzner and Otto (24) is made more complicated by the fact that the rheological behavior of fermentation broths often changes drastically during the fermentation, as is shown in Figure 3 for a decrease of the apparent viscosity during the cultivation of *Cellulomonas uda* grown on printed newspaper (26).

Power Input in Gassed Systems at Low Viscosities. In gassed systems of aqueous-like fluids, a decrease in the stirring power input can be observed with increasing gas flow. This decrease is caused by gas cushions that form behind the stirrer blades and diminish the rotational resistance of the stirrer. The effect was first studied by Oyama and Endoh (30); the results are shown in Figure 4. Since then a series of measured values have been published; particularly extensive are the measurements made by Zlokarnik (31) and Judat (32). Judat (32) gives a relationship valid for a turbine stirrer in a turbulent region of flow ($Re > 10^4$) in water. This relationship is also applicable, in a somewhat modified form, to large vessels of up to $V = 900$ m^3:

$$Ne_G = Z \frac{Ne_0 + 187QFr^{-0.32}(d/D)^{1.53} - 4.6Q^{1.25}}{1 + 136Q(d/D)^{1.14}} \tag{8}$$

Here $Ne_0 \approx 4.9$ is the Newton number of the turbine stir-

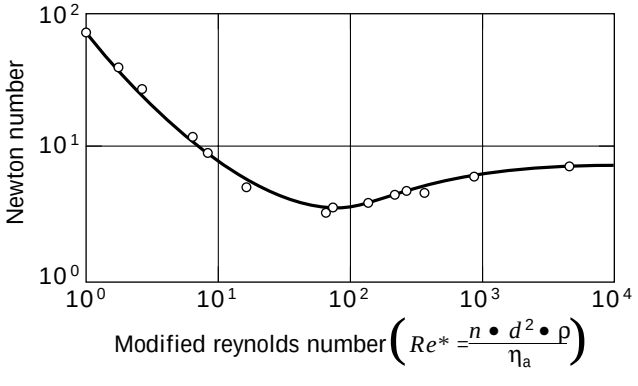

Figure 2. Performance characteristic of turbine stirrer with pseudoplastic fluid.

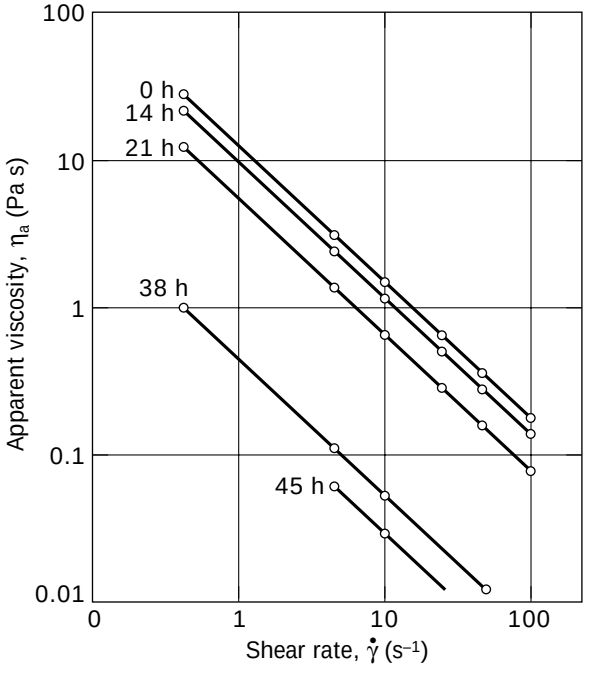

Figure 3. Time course of changes in apparent viscosity in the fermentation of cellulose.

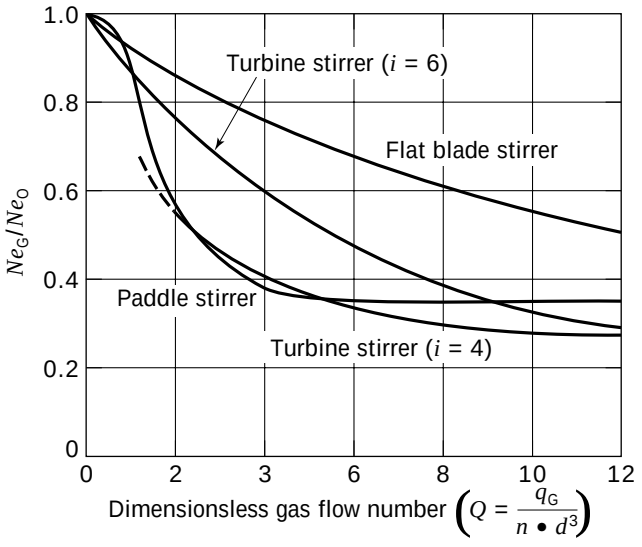

Figure 4. Power input of several types of stirrer in Newtonian fluids, dependent on the gas throughput.

ring in a turbulent region of flow without gassing, and Z is the number of stirrer blades. Equation 8 is valid for $Re > 10^4$, $Fr \leq 0.07(d/D)^3$, $0.2 \leq d/D \leq 0.42$, and $h/d > 0.75$.

Detailed investigations with other types of stirrers and multiple impellers were carried out by Schlueter and Deckwer (33). Their experimental results were well described by equation 8 with a maximum deviation of only 30%. Further investigations are necessary to describe properly the power input in stirred vessels if the impeller position is varied and multiple stirrer arrangements are used.

The influence of the Reynolds number on the power input in a gassed system has been studied by Zlokarnik (31) and is given, for the turbine stirrer, by

$$\frac{Ne_G}{Ne_0} = 1 + [(3.9Re^{0.12} + 6 \cdot 10^{-12}Re^{3.45}) \cdot (0.22Q^{0.1} + 6.25Q^3)]^{-1} \quad (9)$$

which is valid for $Q < 0.05$ and $800 \leq Re \leq 10^4$. Ne_G is the Newton number of the turbine stirrer gassed with Q at $Re > 10^4$.

Power Input in Gassed Systems of Newtonian and Non-Newtonian Fluids at Higher Viscosities. Whereas the influence of the gas on the energy input in aqueous-like fluids is about the same for the different types of stirrer, each stirrer type displays a very different effect when the viscosity increases. Detailed measurements on this have been published by Hoecker and Langer (34) and Hoecker (35). To illustrate the results, the form completely equivalent to equation 2 was chosen,

$$Ne = f(Q, Fr, Ga) \quad (10)$$

with the Galilei number

$$Ga \equiv \frac{Re^2}{Fr} = \frac{d^3 \cdot g}{\nu^2}$$

With turbine stirrers, a decrease in the power input is observed with increasing viscosity (Fig. 5). As in the correlation of the power input for nongassed systems of non-Newtonian fluids, the results with sparging can also be expressed by introducing an apparent viscosity, η_a, as results from the approach taken by Metzner and Otto (24) (i.e., equations 4 and 7). As Figure 5 shows, even the results for Newtonian glycerine–water solutions and for pseudoplastic carboxymethylcellulose–water solutions can be expressed by the same form of curve (34). With viscoelastic polyacrylamide–water solutions (Figure 5b), the decrease in the power input with viscosity is even more pronounced than with Newtonian and pseudoplastic fluids; this can probably be traced back to the development of orthogonal tension in viscoelastic fluids, which tends to damp the turbulence. The illustration of the performance characteristic for turbine stirrers in aqueous glycerine solutions in terms of the gas flow in Figure 6 clearly shows that at high viscosities a decrease in power input with the gas throughput hardly makes itself felt, but rather the Froude number exerts a more marked effect (34,35). The slight influence of the dimensionless gasflow number is due to the formation of gas cushions behind the stirrer blades, which is independent of the gas throughput.

The relationship given in equation 9 to calculate the influence of the Reynolds number on the power input with gassed turbine stirrers is roughly applicable to non-Newtonian fluids, too. In Figure 7 the results obtained by

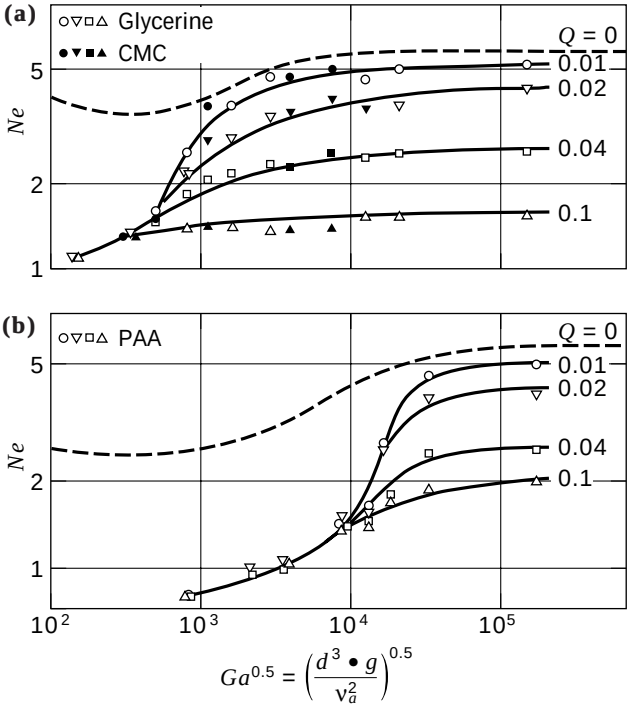

Figure 5. Power input with turbine stirrer ($d/D = 0.33$) in (**a**) Newtonian (glycerine) and pseudoplastic (CMC) and (**b**) viscoelastic (PAA) fluids.

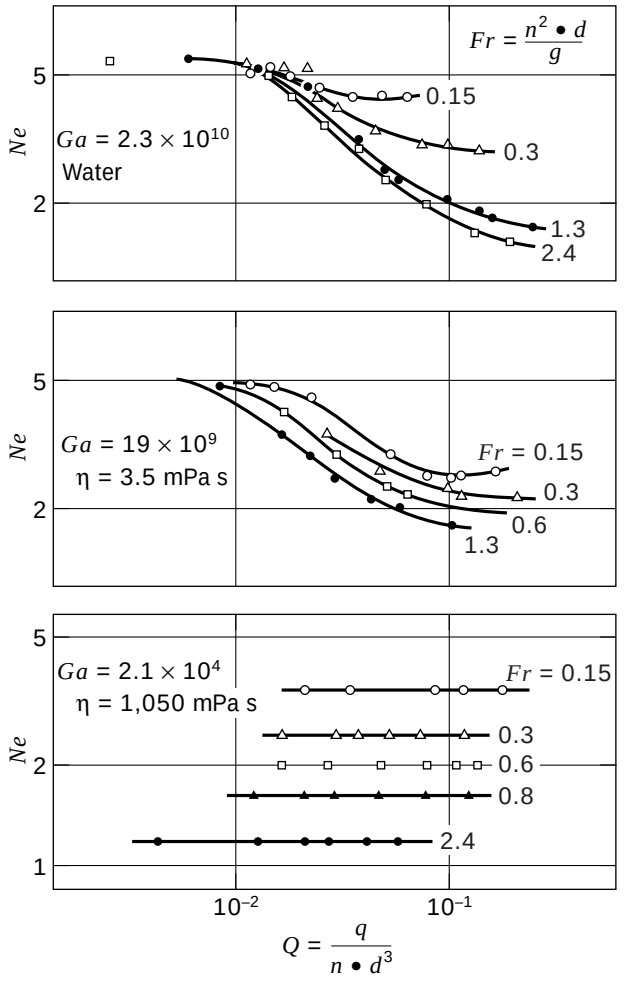

Figure 6. Power input with turbine stirrer ($d/D = 0.33$) in glycerine–water solutions.

Hoecker and Langer (34) are depicted for water, glycerine, carboxymethylcellulose (CMC), and polyacrylamide (PAA) solutions, plotted as $Ne \cdot f(Re, Q)$ corresponding to equation 9 as a function of $Q(1 + 38(d/D)^5)$. The dotted curve shows the results obtained by Zlokarnik (31). From the values taken from the line of the curve, the performance characteristics can be calculated exactly enough from Figure 7 with $Ne = Ne_G/f(Re, Q)$ with equation 9; this is the case for Newtonian and pseudoplastic fluids in the region $Ga > 10^6$ ($Re > 10^3$) and for viscoelastic fermentation broths with $Ga > 10^9$ (34,36).

Completely different behavior from that seen with a turbine stirrer is observed with a multistage impulse countercurrent (MIG) agitator: In Figure 8 the results obtained by Hoecker and Langer (34) and Hoecker (35) are plotted and are analogous to those in Figure 5. Here a decrease in the power input comparable in magnitude to that with the turbine stirrer cannot be established; this is due to the less marked formation of gas cushions with a MIG agitator. Because the interference multistage impulse countercurrent (INTERMIG) and the oblique arm paddle stirrer both exhibit hydrodynamic behaviour similar to that with a MIG stirrer, this result is to be expected in these cases, too.

Dispersing Capacity of the Stirrer

The dispersing capacity of a stirrer is limited by the so-called flooding point, which gives the maximum gas throughput that can be distributed by the stirrer, $q_{G,max}$. If this maximum gas throughput is exceeded, the stirrer is completely "flooded" by the gas, and the circulatory flow provided by the agitator breaks down. This flooding point exists in the transitional zone leading to turbulent flow and is particularly marked in the turbulent flow region. It manifests itself in a sudden decrease in the power input and mass transfer capacity. In the turbulent area of flow ($Re > 10^4$) the measured data can be correlated using the dimensionless form

$$Q = f(Fr, d/D) \tag{11}$$

Judat (32) reports that the flooding point for turbine stirrers for $Re > 10^4$ and $0.2 \leq d/D \leq 0.42$ is

$$Q_{max} = \frac{0.21Fr^{2.1d/D}}{[(d/D)^{-1} - 2.04]^{1.3}} + \frac{0.14Fr^{7.54d/D}}{[(d/D)^{-1} - 2.25]^{1.5}} \tag{12}$$

The flooding characteristic for different stirrers is depicted in Figure 9 (32). Because these results have all been acquired in laboratory experiments, comparison measurements must be carried out in order to achieve a dependable scale-up. A model to describe the flooding characteristic of stirrers by means of dimensional analysis was suggested by Zehner (37).

For fermentation processes that require low rotational speeds of the stirrer at high sparging rates or at very high gas throughput, Breucker et al. (38) made an interesting observation. For different types of turbine, propeller, or INTERMIG stirring systems they showed that sparge rings near the wall prevent the introduced gas flow from flooding the impeller. In the rotational speed range in which the stirrer is normally flooded, flooding did not occur. This extension of the operation range results in greater safety in vessel design. From the observations available for media of higher viscosity and for non-Newtonian fluids, conservative design considers the dispersing capacity of the agitator as lower than with Newtonian fluids.

Mixing Time Characteristics of Stirred-Tank Reactors

The mixing time is commonly defined as the time necessary to reduce concentration differences in the volume in question to a minimum. The mixing time should thus always be related to the method of measurement used and the degree of homogenity desired. From theoretical considerations of similarity, the mixing time characteristic in the case of Newtonian fluids (with negligible density and viscosity differences) is given by

$$n \cdot \theta = f(Re) \tag{13}$$

with the dimensionless characteristic mixing number $n \cdot \theta$.

In Figure 10 the mixing time characteristics of some types of agitator are illustrated. Those conditions of geometry (which deviate from the German norm DIN 28131) are given in the diagram. In the range of turbulent flow

Symbol				Ga	Fr
Water	Glycerine	CMC	PAA		
●	▲	△	○	$1.3 \times 10^9 - 2.3 \times 10^{10}$	
	▼			$1.37 \times 10^8 - 4.6 \times 10^8$	
	■	□		$10^7 - 6.8 \times 10^7$	> 0.6
	×	+		$1.3 \times 10^6 - 6.4 \times 10^6$	
	◄			$7.1 \times 10^5 - 9.06 \times 10^5$	
– – – – – – – – – – – – – – – – –				$2.2 \times 10^6 - 7.15 \times 10^7$	> 0.9

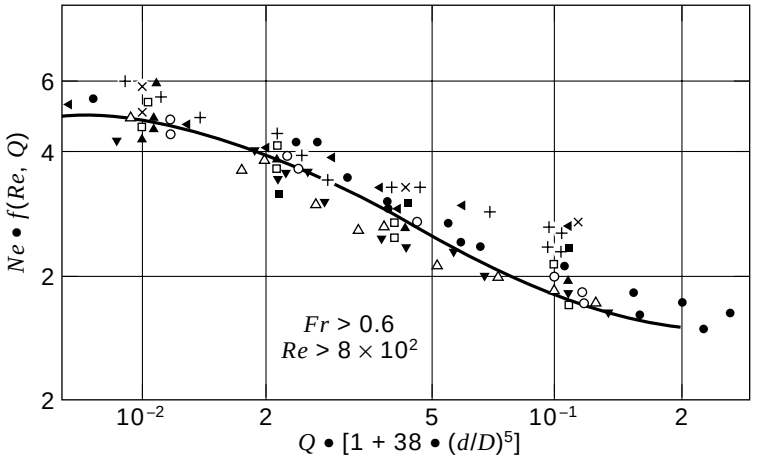

Figure 7. Power input with turbine stirrer (d/D = 0.33): Influence of Reynolds number and gas throughput [$f(Re, Q)$] according to equation 9.

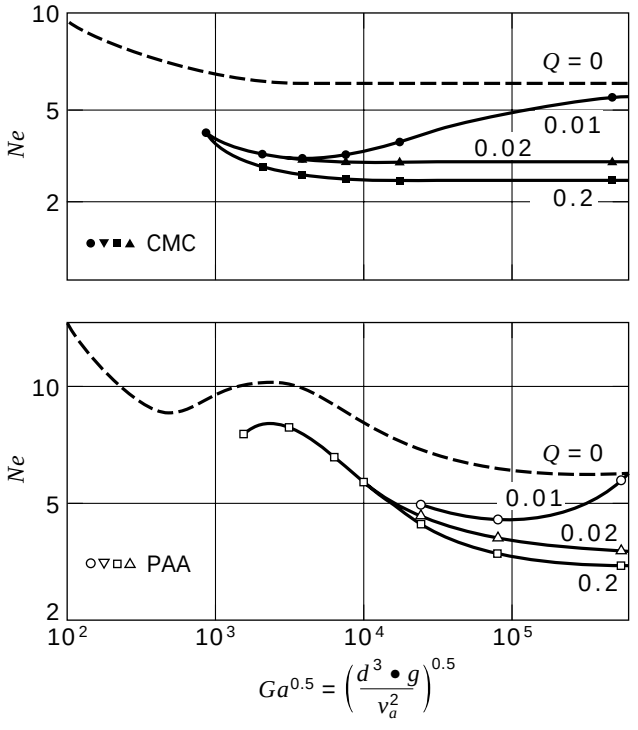

Figure 8. Power input with MIG stirrer (d/D = 0.6, 3 stirrers, H/D = 2), substance systems as in Figure 5.

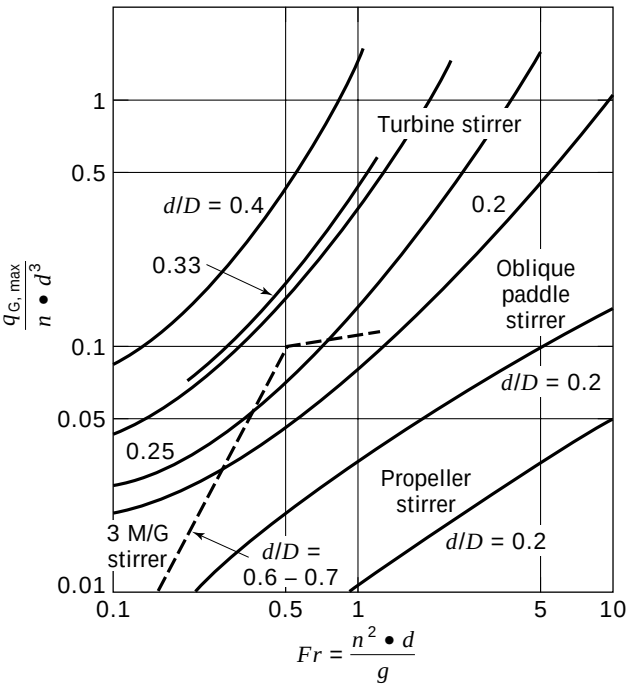

Figure 9. Dispersing capacity of several types of stirrer, $Re > 10^4$.

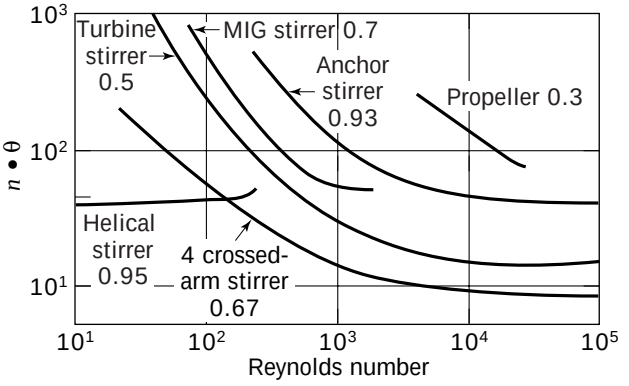

Figure 10. Mixing time characteristics of several types of stirrer in Newtonian fluids.

($Re > 10^4$) the characteristic mixing number is practically independent of the Reynolds number (39–41). Figure 11 shows a plot of the power input that is required to achieve those mixing times in the turbulent region given in Figure 10. The characteristic dimensionless numbers used in this diagram, which were formulated by Zlokarnik (42) on a theoretical consideration of similarity, permit the stirring power input to be determined for a given mixing time, or vice versa (43). For the most favorable conditions of geometry and operation, the stirring power input required in the region of turbulent flow (Ne = constant, $n \cdot \theta$ = constant) is obtained from the relationship

$$\frac{P \cdot \theta^3}{\rho \cdot D^5} = 300 \qquad (14)$$

For a scale-up with P/V = idem there is, from equation 14, a corresponding increase in the mixing time in the region of turbulent flow by

$$\frac{\theta}{D^{2/3}} = \text{idem} \qquad (15)$$

for example,

$$\frac{\theta}{V^{2/9}} = \text{idem} \qquad (16)$$

A scale-up on the basis of constant mixing times (θ = idem) requires, according to equation 14, an increase in the power input by

$$\frac{P/V}{D^2} = \text{idem} \qquad (17)$$

which leads to required energies that cannot be defended either on a technical or an economic basis. Bearing in mind the need for an economical stirring power input, it is indeed meaningful to allow an even longer mixing time when scaling-up than that given by equation 16.

The influence of non-Newtonian flow behavior on the mixing time characteristics can be derived from Figure 12

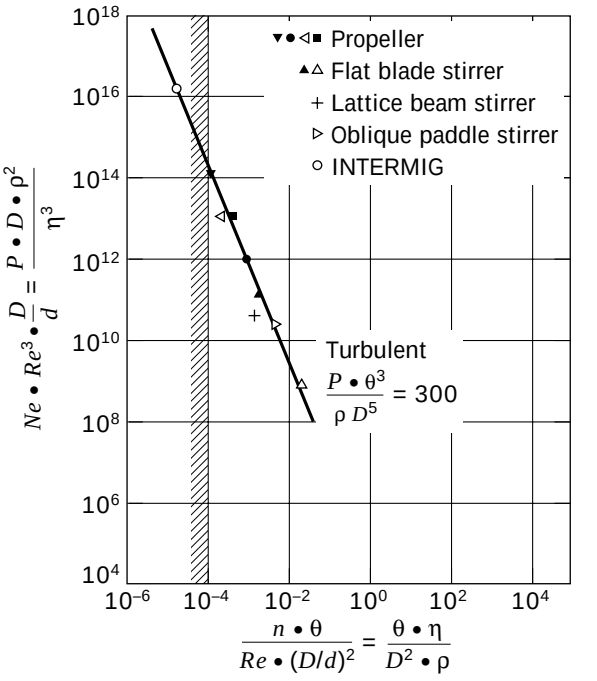

Figure 11. Power input to obtain given mixing times with favorable geometrical and operating conditions.

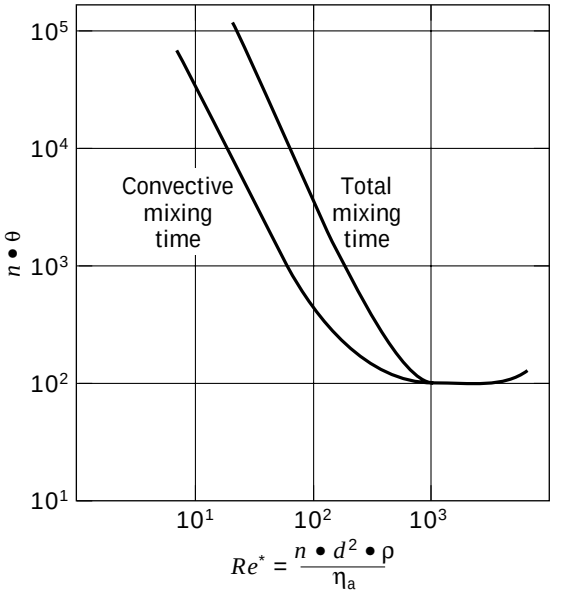

Figure 12. Mixing time characteristics in non-Newtonian fluids (crossed-arm stirrer in CMC solution).

(44). The Reynolds number here has again been modified by the apparent viscosity, as determined according to the method of approach used by Metzner and Otto (24) (equations 4 and 7).

For pseudoplastic fluids Opara (44) observed that in the laminar flow region, about 95% of the liquid is distributed very rapidly by convection, whereas the remainder is

mixed very slowly by diffusion. This convective mixing time corresponds roughly to the mixing time in Newtonian fluids (Fig. 10). The total mixing time in non-Newtonian fluids can be as much as a factor of 10 longer than the convective mixing time.

Mass Transport between Gas and Liquid Phase

Apart from the stirring power, mixing time, and dispersing capacity of the stirrer, mass transfer between gas and liquid is often the prime influence during an aerobic fermentation. The oxygen demand of the aerobic culture has to be the same as the oxygen transfer rate (OTR = $\dot{n}_{O_2}$) in the steady-state condition

$$\dot{n}_{O_2} = \frac{\dot{N}_{O_2}}{V} = k_L a (c^*_{O_2} - c_{O_2})_{av} \tag{18}$$

In this, it has been assumed that because oxygen is such a poorly soluble gas, the overall rate of mass transport is determined essentially by the mass transfer resistance in the liquid phase. In fact the transport coefficient in the gas phase is larger than that in the liquid phase by a factor of 100. The liquid-phase mass transfer coefficient, k_L, multiplied by the interfacial exchange area per unit volume, a, is termed the *volumetric mass transfer coefficient*.

The averaged concentration difference at the phase boundary $(c^*_{O_2} - c_{O_2})_{av}$ in the whole reaction vessel is, in the case of an ideally mixed liquid phase and complete segregation of the gas phase, equal to the logarithmic mean concentration

$$(c^*_{O_2} - c_{O_2})_{av} = \frac{c^*_{O_2,in} - c^*_{O_2,out}}{\ln\left(\dfrac{c^*_{O_2,in} - c_{O_2}}{c^*_{O_2,out} - c_{O_2}}\right)} \tag{19}$$

In stirred tank reactors the average concentration difference can be calculated from equation 19 with sufficient accuracy.

Mass Transfer in Aqueous Fluids. Many equations have been published for the calculation of the volumetric mass transfer coefficient, $k_L a$, in low-viscosity aqueous fluids (see Ref. 5). Regardless of the measuring system used, these equations give differences in the $k_L a$ value of up to a factor of 10. In particular, the influence of the coalescence behavior of the fluid system on $k_L a$ has not been elucidated. Consequently the $k_L a$ values found with the model system of sulfite oxidation in water must be viewed critically when applying such values to fermentation broths.

Theoretical considerations of the similarity of mass transfer between gas and liquid phase made by Zlokarnik (45) led to the formal relationship

$$k_L a = f\left(\frac{P}{V}, \frac{q_G}{V}, \ \ldots\right) \tag{20}$$

with a gas throughput per unit volume q_G/V. However, Judat (46) showed, by evaluating a series of published $k_L a$ values, that in order to fit the measured data better, the gas throughput related to the cross-sectional area of the reactor (i.e., the superficial gas velocity)

$$u_G = \frac{q_G}{A} \tag{21}$$

should be taken as the characteristic gassing quantity. This finding is in agreement with the empirical equation of the type

$$k_L a = K_1 \left(\frac{P}{V}\right)^{\alpha} u_G^{\beta} \tag{22}$$

which was compiled by Moo-Young and Blanch (3) for coalescent and noncoalescent aqueous solutions; their findings are listed in Table 2 (SI units, i.e., $k_L a$ in s^{-1}, P/V in W/m^3, and u_G in m/s). According to Van't Riet (47), differences of up to 35% arise in the $k_L a$ values in coalescent and noncoalescent systems. Van't Riet (47) gives the following correlations for low-viscosity fermentation broths from a series of published data (SI units as in equation 22):

$$\text{Coalescing medium:} \quad k_L a = 0.026\left(\frac{P}{V}\right)^{0.4} u_G^{0.5} \tag{23}$$

$$\text{Noncoalescing medium:} \quad k_L a = 0.002\left(\frac{P}{V}\right)^{0.7} u_G^{0.3} \tag{24}$$

In modifying the dimensionless quantities proposed by Zlokarnik there follows, for the calculation of the volumetric mass transfer coefficient, $k_L a$, the functional relationship

$$k_L a \left(\frac{\nu}{g^2}\right)^{1/3} = \left(\frac{P}{V \cdot \rho \cdot (g^4 \cdot \nu)^{1/3}}, \frac{u_G}{(g \cdot \nu)^{1/3}}, Sc, \sigma^*, S_i\right) \tag{25}$$

In this, $Sc \equiv \nu/\mathcal{D}$ is the Schmidt number, $\sigma^* \equiv \sigma/\rho(g \cdot \nu^4)^{1/3}$ is the dimensionless surface tension, and S_i represents characteristic quantities that are intended to describe the coalescence behavior of the fluid system but whose composition, as already mentioned, still remains largely unclear, though Breucker et al. (38) found that qualitatively the mass transfer coefficient for the noncoalescing system is up to a factor of 4 higher than for coalescing systems at comparable conditions. In the absorption of oxygen in fermentation broths, σ^* and Sc are practically determined only by the viscosity. The surface tension itself changes only very slightly and is not significant. The diffusion coefficient of aqueous solutions exhibiting Newtonian flow behavior can be correlated with the viscosity. On the other hand, the diffusion coefficient in non-Newtonian aqueous solutions is independent of ν and has the same value as water (48,49).

In the mass transfer of gases other than O_2, the Schmidt number and surface tension must also be considered in some cases. However the transport of CO_2, which is also of interest in fermentations, can be calculated without much error by using the same $k_L a$, owing to the very slight differences in diffusion coefficients between O_2 and CO_2. Indeed the overall transport rate is greater for CO_2 because it is 40 times more soluble in water than O_2.

Table 2. Sorption Characteristics of Aqueous Systems for Turbine Stirrers

Liquid	K_1	α	β	Range of validity P/V (kW/m^3)	Range of validity u_G (cm/s)
Water	0.024	0.4	0.5	0.26–5.3	0.3–1.8
Electrolyte solution	0.018	0.74	0.26	0.26–5.3	0.3–1.8
Water	–	0.4	0.35	0.03–18	0.1–0.5
KCl solution					
0.22 N	–	0.71	0.36	0.03–18	0.1–0.5
0.1N	–	0.63	0.62	0.03–18	0.1–0.5
Water	0.0275	0.42	0.43	0.44–10	0.37–1.11
Electrolyte solution (Na_2SO_4 + KOH)	0.017	0.52	0.43	0.44–10	0.37–1.11

Note: $Z = 6$, $d/D = 0.33$; according to Equation 22. For more information see Ref. 5.

By evaluating published data, Judat (46) proposed a correlation that for aqueous systems covers the entire region of technical interest:

$$k_L a\left(\frac{\nu}{g^2}\right)^{1/3} = \frac{9.8 \cdot 10^{-5}\left(\frac{P}{V \cdot \rho(g^4 \cdot \nu)^{1/3}}\right)^{\alpha}}{(B^{-\beta} + 0.81 \cdot 10^{-0.65/B})^{1.05}} \qquad (26)$$

The dimensionless gassing number is here given by

$$B \equiv \frac{q_G/D^2}{(\nu \cdot g)^{1/3}} \qquad (27)$$

The exponents are given as $\alpha = 0.42$ and $\beta = 0.6$. Although the exponents are dependent on the fluid system, the addition of the exponents, $\alpha + \beta \approx 1$, is approximately valid for all substances. Henzler (4) used this circumstance to evaluate the experimental results available with a relationship of the form

$$k_L a\left(\frac{\nu}{g^2}\right)^{1/3} = K_2\left(\frac{P}{V \cdot \rho(g^4 \cdot \nu)^{1/3}}\right)^{\alpha}\left(\frac{u_G}{(g \cdot \nu)^{1/3}}\right)^{\beta} \qquad (28)$$

Taking into account $\beta \approx 1 - \alpha$, the simplified form was derived:

$$\frac{k_L a}{u_G}\left(\frac{\nu^2}{g}\right)^{1/3} = K_2\left(\frac{P}{V \cdot u_G \cdot \rho \cdot g}\right)^{\alpha} \qquad (29)$$

which reflects the measured values with almost the same accuracy as equation 26.

In Figure 13 the sorption characteristics according to equation 29 are given for water and aqueous salt solutions. The results were obtained in reactor volumes of between 2.51 and 900 m^3. They lie close together, independent of the vessel volume. Equation 29 can thus be taken as a translation rule in scale-up on the basis of the oxygen transfer. In Table 3 the constant K_2 and exponent α are given for coalescent and noncoalescent fluid systems for turbine stirrers having $d/D = 0.14 - 0.5$.

Mass Transfer in Fluids of Higher Viscosity. For fluids of higher viscosity, in particular those with non-Newtonian flow behavior, there have been few systematic investigations published that deal with the determination of the volumetric mass transfer coefficient, $k_L a$. Figure 14 shows a plot of several sorption characteristics for millet pulp, aqueous glucose solutions, and aqueous CMC solutions using the same correlation (equation 29) as for low-viscosity fluids (4,35,49). Thereby the translation rule given by equation 29 is confirmed for all fluid systems, even though the viscosity and the diffusion coefficient change by a factor of 1,000 and 30, respectively. To illustrate the experimental results for non-Newtonian fluids it is necessary, however, as with the determination of the power input, to calculate the apparent viscosity with equations 4 and 7 according to the concept of Metzner and Otto (24).

In Table 3 all sorption characteristics compiled by Henzler (4) are shown. Because these sorption characteristics are valid only for the particular rheological behavior and coalescence properties of each system, such properties have to be measured in the fermentation medium before an exact calculation of the mass transport is possible. Perez and Sandall (50) proposed the following correlation to calculate the volumetric mass transfer coefficient for pseudoplastic non-Newtonian fluids according to an approach of Sideman et al. (51):

$$k_L a\left(\frac{d^2}{\mathcal{D}}\right) = 21.24 Re^{111} Sc^{0.5}\left(\frac{\eta_a \cdot u_G}{\sigma}\right)^{0.447}\left(\frac{\eta_G}{\eta_a}\right)^{0.694} \qquad (30)$$

The range of the flow behavior indices according to equation 5 is $m' = 0.916 - 1.00$ and $K' = (0.009 - 0.04)$ Pa $\cdot$ s$^{m'}$ with a vessel diameter of $D = 0.1524$ m. Kawase and Moo-Young (52) showed that the proposed model correlates reasonably well with the relatively wide variety of data measured by different authors for a range of vessel diameters of $D = 0.15 - 0.6$ m and for the flow behavior indices $m' = 0.59 - 0.95$ and $K' = (0.00355 - 10.8)$ Pa $\cdot$ s$^{m'}$.

A completely different correlation for the calculation of the volumetric mass transfer coefficient, $k_L a$, was suggested by Mooyman (53):

$$k_L a = C(270\varphi_G + 135\varphi_G \log(P_a/V)) \qquad (31)$$

Equation 31 expresses the overall transfer coefficient as an enhancement formula dependent on two variables: the gas holdup fraction, φ_G, that is given by

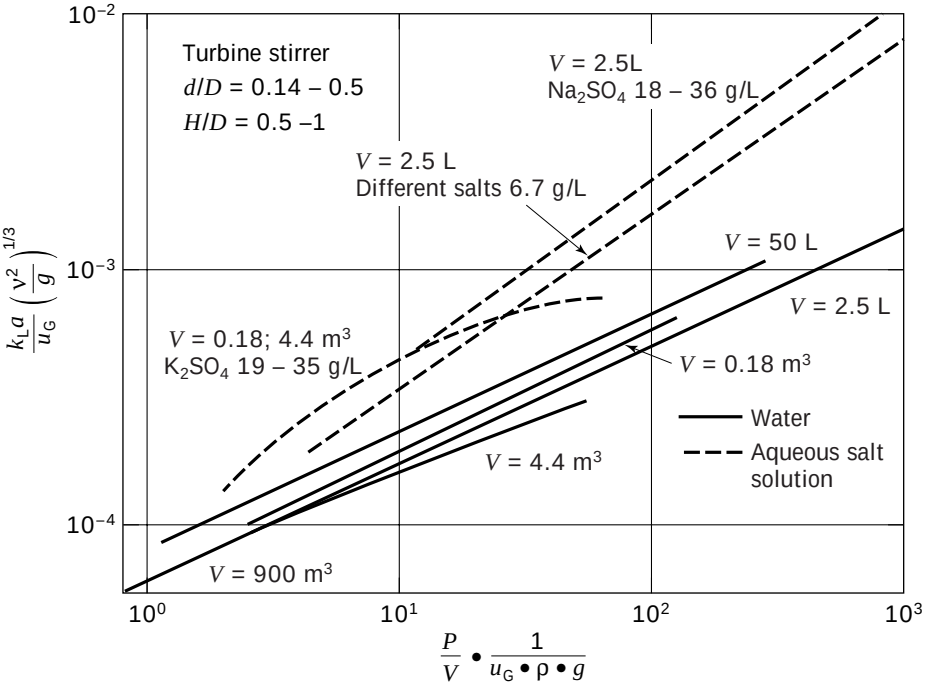

Figure 13. Sorption characteristics of aqueous systems for turbine stirrers.

Table 3. Sorption Characteristics of Different Fluid Systems for Turbine Stirrers

Liquid	Liquid	α	Range of validity		
			P/V (kW/m^3)	u_G (cm/s)	η (mPa s)
Water	7.5×10^{-2}	0.43	0.01–16.7	0.07–1.8	1
Aqueous salt solution					
6.7 g/L	7.2×10^{-5}	0.68	0.15–16	0.12–0.47	1
18–36 g/L	8.3×10^{-5}	0.71	0.23–18	0.12–1.8	1
Aqueous glucose solution	2.65×10^{-5}	0.7	–	–	12–267
Millet pulp	9.0×10^{-5}	0.7	0.23–2.2	0.19–0.78	1.3–70.2
Aqueous CMC solution, $m = 0.4$–0.82, equation 5	3.6×10^{-4}	0.55	0.06–6.2	0.22–1.9	16–1500

Note: $Z = 6$, $d/D = 0.14$–0.5; according to equation 29. For more information see Ref. 5.

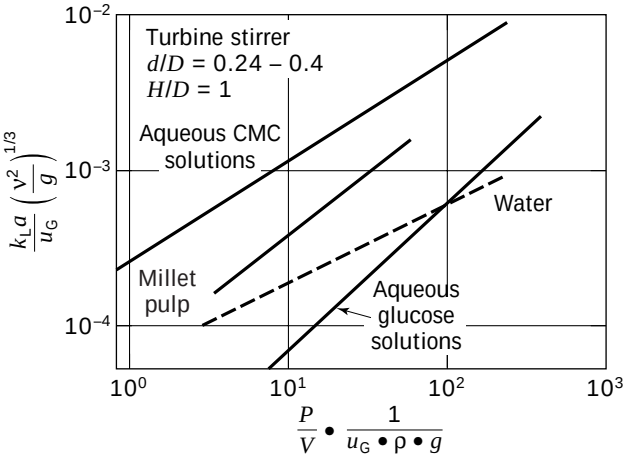

Figure 14. Sorption characteristics for millet pulp, glucose solutions, and CMC solutions.

$$\varphi_G = 0.1\left(\log\left(10.915 u_G \frac{p}{p_{av}}\right) - 0.9\right) \tag{32}$$

and the mechanical plus the adiabatic gas expansion power input per unit of volume, P_a/V; C is a multiplication factor required to correct published or calculated k_La data to actual values observed in industrial fermentations with operating volumes above 250 L (53).

The effects of the suspension of solids on the mass transfer in sparged tank reactors have been investigated by various authors (e.g., Mills et al. [54] and Oguz et al. [55]). Of particular note is the dimensionless correlation developed by Oguz et al. (55) for the k_La in air-sparged agitated tanks containing slurries of different materials:

$$k_L a \frac{V}{q_G} = 2.173 \cdot 10^{-3}\left[\frac{P/q_G}{\rho^{1/3}(\eta_a \cdot g)^{2/3}}\right]^{0.607} \tag{33}$$

The influence of the solid concentration becomes evident

in the calculation of the apparent viscosity of the slurries, which all showed non-Newtonian behavior. Consequently the viscosity was calculated with equations 4 and 7 according to the concept of Metzner and Otto (24). Oguz et al. (55) showed that an increase in the solid concentration leads to an increase of the slurry viscosity that corresponds to a decrease in k_La. The deviation of the measured data from the values calculated with equation 33 was in the range of 12.5%.

For a scale-up on the basis of constant volumetric mass transfer coefficients, there follows from the generally valid equation 29

$$\left(\frac{P}{V}\right)u_G^{(1-\alpha)/\alpha} = \text{idem} \tag{34}$$

for the power input required. The exponent α is approximately 0.67 for noncoalescing aqueous systems as well as for more highly viscous Newtonian fermentation fluids. From equation 34 it follows that

$$\left(\frac{P}{V}\right)u_G^{0.5} = \text{idem} \tag{35}$$

For example, with $u_G \sim q_G/D^2$

$$\left(\frac{P}{V}\right)\frac{q_G^{0.5}}{D} = \text{idem} \tag{36}$$

If surface-active substances, such as chemical antifoam agents, are added to the fermentation medium, the volumetric mass transfer coefficient at the interfacial surface usually drops, and the mass transfer behavior tends toward a coalescing fluid system. In a coalescing fluid system and for non-Newtonian fluids, the exponent α is approximately 0.5. Consequently it follows from equation 29 that

$$\left(\frac{P}{V}\right)u_G = \text{idem} \tag{37}$$

and

$$\left(\frac{P}{V}\right)\frac{q_G}{D^2} = \text{idem} \tag{38}$$

In applying this translation rule (equations 35–38), the dispersing capacity of the stirrer, as given by equation 12, also has to be taken into consideration.

Shearing Stress and Pumping Capacity of the Stirrer

The mixing of the fermentation broth, the distribution and dispersion of the gases, and the suspending of solid constituents of the culture medium and microorganism pellets are effected in the stirred tank by a complex three-dimensional flow field. In only a few isolated cases (those that have a defined flow field) can the shearing stress and the pump capacity of the stirrer be calculated. With turbulent mixing it is possible, however, only to estimate both the longitudinal mixing by the pumping around of the vessel contents, and the shear stress on the fluid caused by the fluctuations in turbulence.

In a theoretical consideration of turbulent flow, Reynolds split up the measured local liquid velocity, u_L, into the sum of a mean (deterministic) velocity, $\bar{u}$, and a superposed stochastic fluctuation velocity, u'. According to this hypothesis, the turbulent Reynolds shear stress produced by the stirrer is proportional to the square of the local fluctuation velocity of the turbulence and is approximately given by the tip speed of the stirrer

$$\tau_R \sim (n \cdot d)^2 \tag{39}$$

With the Reynolds shear stress, τ_R, the effects of the stochastic liquid fluctuation velocity, u', are mathematically seized. τ_R can be interpreted as a virtual shear stress, that is, a consequence of the impulse transport caused by the turbulent motions.

Hoffmann et al. (56) determined the shear stress in stirred-tank reactors by means of a model system consisting of flocculated clay. Their investigations showed that the proportionality between shear stress of the clay floc system and the tip speed of the stirrer is of little influence; this is caused by the distinctness of the length scale of the vortices resulting from the Reynolds shear stress and the size of the relatively small flocs. The clay floc system is suitable for describing the influence of shear stress on tissue cell cultures (57).

Therefore, the model of Cherry and Kwon (58) is proposed for the calculation of shear stress. It is based on Kolmogoroff's theory of local homogenous isotropic turbulence: the length scale of the microeddies in the dissipative area (with laminar flow of the eddies) yields

$$\lambda = \left(\frac{\nu^3}{\varepsilon}\right)^{0.25} \tag{40}$$

where ε is the energy dissipation rate (i.e., the energy input to the system that is completely dissipated by the formation of vortices)

$$\varepsilon = \frac{P}{\rho \cdot V} \tag{41}$$

To employ this model by Cherry and Kwon (58), the particles exposed to shear have to be smaller than 12 times the length scale, λ, a condition that is usually fulfilled in fermentation processes. Under these circumstances the microeddies induced by the energy input or the energy dissipation rate, respectively, cause the shear stress. The particles are put into rotation by the velocity gradients in the microeddies, which are significantly larger than the gradients caused by the liquid fluctuation velocities in Reynolds hypothesis. The pulsating shear stress that acts upon the flocs during the contact with the microeddies leads to

$$\tau = 5.33\rho(\varepsilon \cdot \nu)^{0.5} \tag{42}$$

that is,

$$\tau = 5.33\left(\frac{P}{V}\,\nu \cdot \rho\right)^{0.5} = K_3\left(\frac{P}{V}\right)^{0.5} \tag{43}$$

The influence of the liquid fluctuation velocities (i.e., the influence of the shear stress caused by the microeddies) has its maximum value if the dimension of the particles is close to the length scale of the microeddies. In Figure 15 the relationship between the experimentally determined shear stress of the clay floc system and the volumetric energy input for different types of stirrers is shown, using a relationship in analogy to equation 43

$$\tau = K_3\left(\frac{P}{V}\right)^{\alpha} \tag{44}$$

The experimentally determined maximum shear stress deviates from the data calculated with the model of Cherry and Kwon (58) by two to six times. This can be explained by the fact that, according to the type of impeller system, there exist areas with increased energy dissipation rates in the reactor in the area close to the stirrer. This effect was not taken into consideration in the model, which uses a mean energy dissipation rate over the entire reactor volume that can be up to 30 times smaller than the maximum value of the energy dissipation rate close to the stirrer (59). Because the main part of the energy input is dissipated near the impeller, the model has to be extended by a supplementary corrective term containing information about the type of stirrer and its geometry (i.e., about the area with increased dissipation rates). By analogy with the work of Liepe (60), who studied the ratio between the maximum and the mean dissipation rate, $\varepsilon_{max}/\varepsilon$, of different impeller systems for dispersion tasks, Hoffmann et al. (56) suggested a corrective function

$$f = f\left(\frac{V}{V_S \cdot Ne}\right)^{\beta} \tag{45}$$

with the effective energy dissipation volume, V_S, that is proportional to the volume of the stirrer ($V_S \sim d^2 \cdot h_B$). The values of V/V_S and Ne are given in Figure 15. By fitting the experimental data, Hoffmann et al. (56) finally determined the following correlation for the calculation of shear stress in stirred-tank reactors:

$$\tau = 0.367\left(\frac{P}{V}\left(\frac{V}{V_S \cdot Ne}\right)^{0.42}\right)^{0.55} \tag{46}$$

Figure 16 shows the calculated shear stress according to equation 46 compared with the experimentally determined data (56). The deviation of the model from the measured data is in a range of up to 30%, which means the model is suitable for a scale-up of the reactor performance on the basis of constant shear stress. In a sparged stirred-tank reactor the shear stress is also dependent on the gas input. Experimental investigations of Henzler and Biedermann (61) showed that there is a qualitative dependency of the shear stress on the pneumatic power input and the type of sparging system. They observed that with constant volumetric power input the shear stress increases with the increasing portion of pneumatic power input and with increasing superficial gas velocity. They described some of

Stirrer		d/D	V/V_S	Ne
●	Propeller	0.33	200.7	0.31
■	INTERMIG	0.65	40.7	0.65
▲	Turbine	0.33	310.1	5.0
△	Turbine	0.65	42.5	5.5
□	4-blade	0.33	135.7	9.6
——	Model according to Ref. 58			

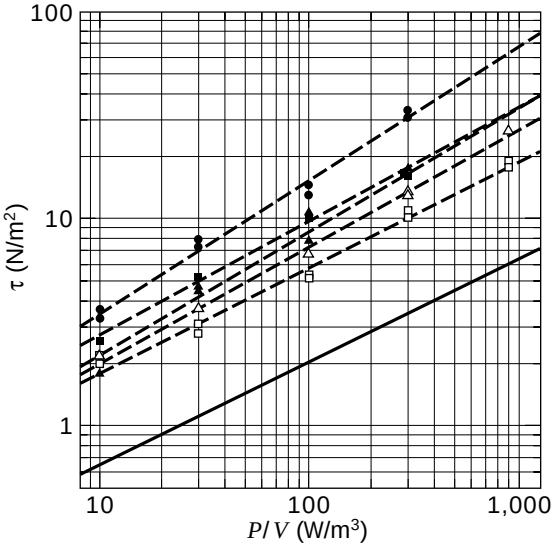

Figure 15. Experimentally determined maximum shear stress versus the volumetric power input, according to equation 44.

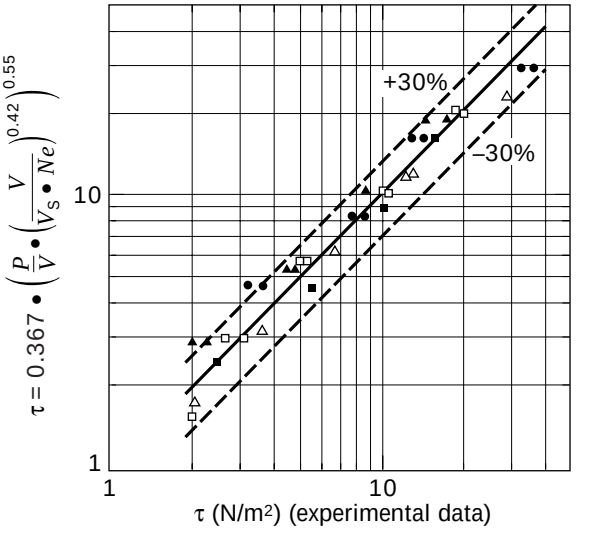

Figure 16. Experimentally determined shear stress compared with calculated data, according to equation 46; for symbols, see Figure 15.

the observed effects causing the increased shear stress, such as the turbulence in the lag zone of rising bubbles, coalescence or dispersion of bubbles close to the sparger, and the bursting of bubbles at the liquid surface (as is observed in bubble columns) (62). Because a model or correlations to describe these effects quantitatively are not yet known, further investigations are necessary to describe the effects of sparging and bubbles on the mechanical shear stress in stirred vessels.

A relationship for the circulating volumetric flow, which is produced by the pumping capacity of the stirrer, can be derived in a manner analogous to the principle that applies to rotary pumps. In this way Van de Vusse (39) calculated the circulating volumetric flow of propellers with the assumption that counterpressure is "zero" and obtained

$$\dot{V} = 0.5 \frac{\pi}{4} n \cdot d^2 \cdot h_S \tag{47}$$

where h_S is the pressure head produced by the propeller. With $h_S \sim d$, the generalized relationship

$$\dot{V} = K_4 \cdot n \cdot d^3 \tag{48}$$

follows from equation 47. K_4 is a constant that is essentially dependent on the type of stirrer (63) (see also Refs. 16, 19, and 64).

Varying details have been published regarding the suspension of solids in stirring apparatuses. Most authors say that in achieving the same suspension result in a larger vessel, the power input can be diminished (43). The circulating volumetric flow given by equation 48 is sufficiently large under the conditions of stirring that generally prevail in stirred-tank reactors so that a uniform distribution of cell pellets and solid constituents in the culture medium is guaranteed. This uniform distribution is supported by the very slight density differences between solid and liquid in the fermentation medium, and the relatively small solid particles and the small fraction of solid material ($d_P < 2$ mm, $\varphi_S < 20\%$) in the fermentation medium. Consequently the suspension process in general takes on no particular significance in scaling up stirred-tank reactors.

Mass Transport Processes in Mycelium Agglomerates

Mycelium-forming microorganisms can build up many morphological forms while submerged fermentation, depending on the conditions of fermentation. Forms include loose hyphae that are distributed homogenously throughout the medium or collect in agglomerates that appear as compact pellets. Whereas the filamentous forms result in highly viscous, non-Newtonian fermentation fluids, the mycelial pellets are usually present in Newtonian fluid systems at a considerably lower viscosity (65). An adequate shearing of the mycelium-forming microorganisms thereby leads to the preferred formation of pellets rather than a filamentous mycelial structure.

Regardless of whether the formation of pellets and compact cell agglomerates leads to fluids of lower viscosity (and thus to more turbulent conditions), problems regarding the oxygen supply to the cells can arise, in particular with large, compact pellets. When the inner and outer mass transport resistances are too large, the danger of autolysis exists, and only the external pellet layer is involved in the biotechnological process.

The effective diffusion coefficient of oxygen in mycelial pellets of *Aspergillus niger* was found to be about $\mathcal{D}_{Pe} = 10^{-4}$ cm^2/s (2). This value is larger by a factor of 10 than the molecular diffusion coefficient, $\mathcal{D}$, in the culture medium. Because the diffusion coefficient determined by Miura (2) also varied with the volumetric power input, this result must be interpreted as indicating that the mycelium forms a loose pellet structure that is penetrated by the turbulent microflow. Thus in such cultures an adequate but not excessive turbulence (i.e., shear stress) is required in order for pellets with a loose structure to form.

Whereas the mass transport inside mycelial aggregates has still not been widely researched, reliable equations exist for determining the mass transfer from fluid to pellet. The mass transfer coefficient k_{Pe} on the surface of the pellet of diameter d_{Pe} can be calculated from the formal relationship

$$Sh = f(Re_{Pe}, Sc) \tag{49}$$

where $Sh \equiv k_{Pe} \cdot d_{Pe}/\mathcal{D}$ is the Sherwood number, $Re_{Pe} \equiv u_{Pe} \cdot d_{Pe}/\nu$ is the Reynolds number formed with the relative velocity between pellet and fluid, and $Sc \equiv \nu/\mathcal{D}$ is the Schmidt number. The relative velocity at the pellet is determined solely by local turbulent fluctuation velocities, u', which are effected by the turbulent eddies of the scale of the pellets. According to the theory of isotropic turbulence put forward by Kolmogoroff, it follows for this velocity that

$$\sqrt{\overline{u'^2}} \sim (\varepsilon \cdot d_{Pe})^{1/3} \tag{50}$$

where ε is the mass-related energy of dissipation calculated with equation 41. Then the Reynolds number, formed with the relative velocity

$$u_{Pe} \sim \sqrt{\overline{u'^2}}$$

is

$$Re_{Pe} = \left(\frac{P}{V} \frac{d_{Pe}^4}{\rho \cdot \nu^3}\right)^{1/3} \tag{51}$$

In Figure 17 the experimental results according to equation 49, from different authors, are shown; the experimental data, following the theory, have been plotted as

$$\frac{Sh - 2}{Sc^{1/3}} = f(Re_{Pe}) \tag{52}$$

The only published equations that are mentioned here are those relationships reported by Liepe and Moeckel (66); with the relative velocity defined here they are given by

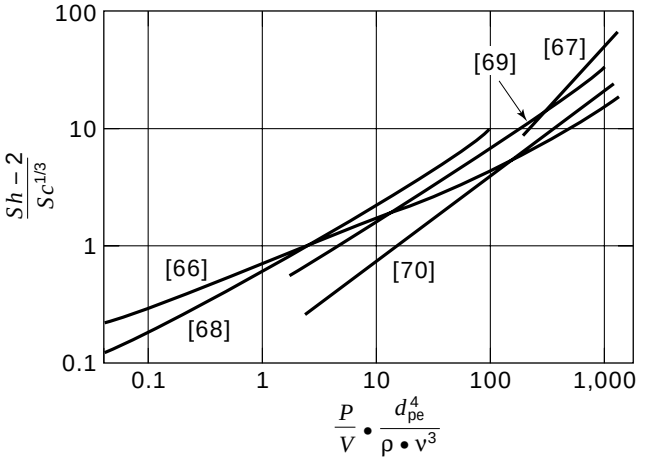

Figure 17. Mass transfer at the pellet surface as dependent on the particle Reynolds number. Numbers in brackets indicate reference.

$$\frac{Sh - 2}{Sc^{1/3}} = 0.35\left(\frac{\Delta\rho}{\rho}\right)^{1/3}\left(\frac{P}{V}\frac{d_{Pe}^4}{\rho \cdot \nu^3}\right) \qquad (53)$$

The curve given by equations 52 and 53 is illustrated in Figure 17, marked according to Liepe and Moeckel (66). Apart from the measurements made by Sicardi et al. (67), all measurements were performed in a nongassed system. Nevertheless the comparison of results shows that the presence of gas has virtually no influence on the mass transfer from fluid to pellet.

SCALE-UP EXAMPLES OF BIOTECHNOLOGICAL PROCESSES BY MAINTENANCE OF IDENTICAL OPERATING CONDITIONS

Scale-Up on the Basis of the Oxygen Transfer Rate

A scale-up of aerobic biotechnological processes is often performed successfully using the criterion of identical oxygen transfer rate (OTR = idem), or the same volumetric mass transfer coefficient (k_La = idem). The reason is that in the aerobic culture of yeasts and bacteria, which have high rates of respiration, the rate-limiting reaction step is often located in the oxygen transfer resistance at the gas–liquid interface. In the fermentation of mycelium-forming microorganisms there arises, under certain conditions, a further limiting mass transport resistance at the surface of or inside the mycelial pellet. That is the reason why a scale-up on the basis of both mass transport resistances is more successful.

Karow et al. (71) took the oxygen transfer rate as a scale-up criterion for the production of penicillin and streptomycin. In Figure 18 the relative penicillin concentrations are shown as a function of the oxygen transfer rate. The results for the production of streptomycin are very similar. The scale-up covers 4 orders of magnitude. At oxygen transfer rates of more than 0.5 mol/(L h) the product yield is maximal and nearly constant. The successful translation from the laboratory to a production scale, performed by

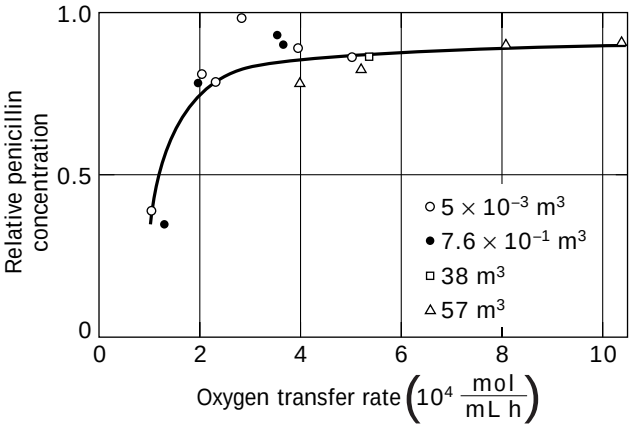

Figure 18. Production of penicillin as a function of the oxygen transfer rate.

Karow et al. (71), was also confirmed by Bylinkina et al. (72) for the fermentation of penicillin and streptomycin. They carried out a scale-up from the 15-L fermentor via a 100-L and 3-m^3 fermentor up to a 63-m^3 production fermentor on the basis of the mass transfer coefficient at the gas–liquid interface. Wegrich and Shurter (73) also described a successful scale-up of penicillin production. The same yields of penicillin were attained in an 8-m^3 fermentor as in a 100-m^3 fermentor. They did not only keep the superficial gas velocity constant but also the volumetric power input of the stirrer. According to equation 37, holding these parameters constant in non-Newtonian fluids corresponds to the scale-up rule k_La = idem.

A further, now "historical," example of scale-up on the basis of the oxygen transfer is shown in Figure 19, in which the production of baker's yeast is depicted (74). Although the oxygen transfer rate in the model system (sulfite oxidation), used as the scale-up criterion, was measured, no significant difference in the production of yeast could be

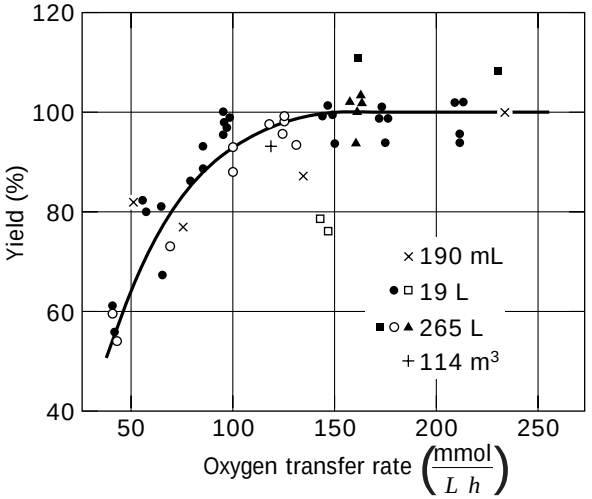

Figure 19. Scale-up of fermentation of baker's yeast based on oxygen transfer rate (sulfite oxidation).

established, which was dependent only on the size of the reactor. Those points plotted in Figure 19 were obtained using shaker flasks with a 190-mL liquid content and in 19-L, 265-L, and 114-m^3 fermentors. Jari (75) was able to show for the production of the primary metabolites alkaline and acid proteases and the secondary metabolites nystatin and fumagillin that a scale-up can be carried out using the same oxygen transfer rate (k_La = idem).

In the bacterial production of vitamin B_{12}, Bartholomew (76) established that the yield at high oxygen transfer rates is negatively influenced by a not very clearly described effect (Fig. 20). Since, moreover, this effect is dependent on the fermentor size, the oxygen transfer rate in this region cannot be used as a scale-up criterion. The dotted curve in Figure 20 applies to the yield only when small-scale equipment is used, and the continuous line represents the yield achieved in a production fermentor. In other words, the production fermentor is oversized. Takei et al. (77) studied protease production by *Streptomyces* sp. in a 0.03-m^3- and a 0.2-m^3-sized fermentor and found the same effect. The productivity of the cells in synthesizing protease is indeed determined by the oxygen transfer rate but is nonetheless diminished at higher oxygen transfer rates by a fermentor size–dependent effect.

In the production of glucoamylase by *Endomyces* sp., the enzyme yield is also not solely determined by the oxygen transport. A scale-up on the basis of identical k_La values also leads to oversizing of the production fermentor. The yields depicted in Figure 21, expressed in relative enzyme activities as a function of the volumetric mass transfer coefficients, were measured in fermentors of 0.06 m^3, 3 m^3, and 30 m^3 (78). In the latter three examples of fermentation described, no adequate scale-up among the fermentor sizes was achieved by using solely the oxygen transfer rate (i.e., the k_La value). The reasons for such deviations can be diverse. For example, in applying the same k_La values as a scale-up criterion, the influence of the surface aeration has to be taken into consideration. Fuchs et al. (79) showed that this effect makes itself felt at fermentor volumes smaller than 200 L.

The translation of the oxygen transfer rate from a laboratory fermentor to a production scale can still lead to

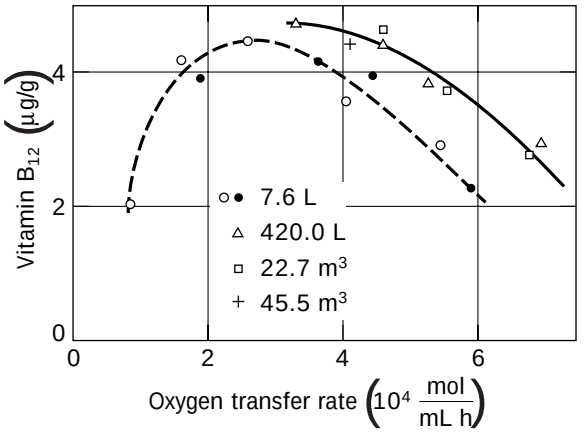

Figure 20. Production of vitamin B_{12} as function of the oxygen transfer rate.

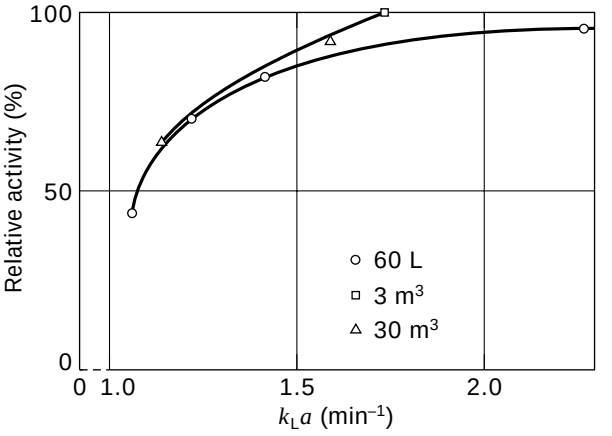

Figure 21. Relative glucoamylase activity as function of the k_La value.

considerable errors for other reasons. Thus, with the same k_La value, the oxygen transfer rate in the production fermentor can be larger than in the laboratory fermentor because, owing to the higher hydrostatic pressure, the driving force (concentration difference) will be larger. But with the same bubble size (identical rising velocity of the bubbles) the average residence time of the air bubble in the larger apparatus is longer; it is thus deficient in oxygen, and consequently, the positive effect of hydrostatic pressure, just cited, is diminished.

Scale-Up on the Basis of the Volumetric Power Input

One-third of the scale-up translations performed in the fermentation industry use the scale-up criterion "identical volumetric power input," as Margarites and Zajic (15) reported. Apart from the simplicity of the measurement in applying this scale-up rule, the reason for its industrial success probably lies in the fact that almost all hydrodynamic and mass transport phenomena can be correlated using the dissipated energy (and thus using P/V). Nevertheless, or maybe simply because of it, this criterion provides an extremely rough rule of thumb, which permits a scale-up only on an empirical basis.

Maxon (80) studied the influence of the volumetric power input on the production of novobiocin using *Streptomyces niveus*. In Figure 22 the novobiocin concentration produced is plotted against the volume-related power input for three different sizes of stirrer. Above P/V = 1 kW/m^3 the yields of the antibiotic are maximal and largely independent of P/V. Scale-up based on this criterion is not dependable because it has been established that there is a dependance on the diameter of the stirrer. According to Wang and Fewkes (81) a scale-up of this process is possible only owing to the partial similarity of the turbulent shearing stress and the pumping capacity of the stirrer.

In the fermentation of penicillin, the volumetric power input, P/V, was often used in the past as a criterion for scale-up. In Figure 23 the penicillin concentration is plotted as a function of the volume-related stirring power, as described by Gaden (82), who gave P/V values between 1.5

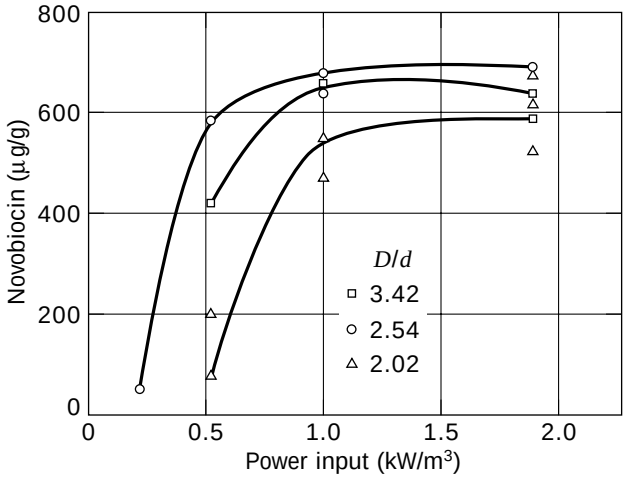

Figure 22. Novobiocin concentration after 115 h of fermentation duration, dependent upon the volumetric power input.

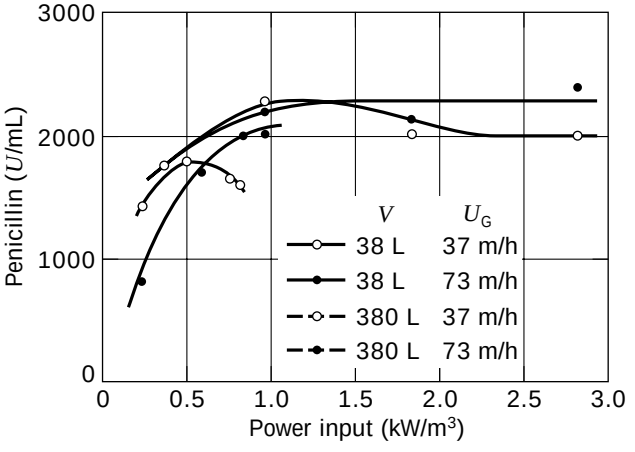

Figure 23. Influence of the volumetric power input on the synthesis of penicillin.

and 3 kW/m^3 as a scale-up rule. Similar results were achieved by Humphrey (83,84), who established a correlation between penicillin production and the volumetric power input and carried out a scale-up at a volume-related stirring power between 1 and 2.5 kW/m^3. Humphrey (84) reports a volumetric power input of 1.5 kW/m^3 for a scale-up of streptomycin production.

NOMENCLATURE

A	Reactor cross-sectional area (m^2)
a	Interfacial exchange area per unit volume (m^2/m^3)
$B \equiv (q_G/D^2)/(v \cdot g)^{1/3}$	Dimensionless gassing number
C	Factor
$c^*_{O_2}$	Saturation concentration of O_2 in fermentation medium (mg/L)
c_{O_2}	Concentration of O_2 in fermentation medium (mg/L)
$c^*_{O_2,in}$, $c^*_{O_2,out}$	Saturation concentration of O_2 at entrance and exit of reactor (mg/L)
D	Diameter of stirred-tank reactor (m)
$\mathscr{D}$	Diffusion coefficient of the liquid phase (m^2/s)
$\mathscr{D}_{Pe}$	Effective diffusion coefficient in mycelial pellets (m^2/s)
d	Diameter of the stirrer (m)
d_P	Diameter of solid particles (m)
d_{Pe}	Diameter of mycelial pellets (m)
$Fr \equiv n^2 \cdot d/g$	Froude number
$Ga \equiv d^3 \cdot g/v$	Galilei number
g	Acceleration due to gravity (m/s^2)
H	Liquid filling height in the reactor (m)
h	Distance between stirrers (m)
h_B	Height of stirrer blade (m)
h_S	Pressure head of the stirrer (m)
i	Number of stirrer blades
K	Proportionality constant
K'	Consistency index [(Pa s)m']
K''	Consistency index [(Pa s)m'']
K_1, K_2, K_3, K_4	Constants
k_L	Liquid-side mass transfer coefficient at gas–liquid interface (m/s)
k_{Pe}	Mass transfer coefficient at mycelium pellet surface (m/s)
k_La	Volumetric mass transfer coefficient at gas–liquid interface (s^{-1})
m', m''	Flow behavior parameters
$Ne \equiv P/\rho \cdot n^3 \cdot d^5$	Newton number
Ne_G	Newton number in gassed reactor at $Re > 10^4$
Ne_0	Newton number without gassing
$\dot{N}_{O_2}$	Oxygen mass flow (kg/s)
n	Rotational speed (s^{-1})
$\dot{n}_{O_2}$	Oxygen transfer rate (mass flow density) [kg/(s · m^3)]
P	Stirring power (kW)
P_a	Mechanical plus adiabatic gas expansion power input (kW)
p	Atmospheric pressure (N/m^2)
p_{av}	Average pressure at half the liquid height (N/m^2)
$Q \equiv q_G/n \cdot d^3$	Dimensionless gassing number
Q_{max}	Dimensionless gas flow number at flooding point of stirrer
q_G	Gas throughput (m^3/s)
$q_{G,max}$	Maximum gas throughput (m^3/s)

$Re \equiv n \cdot d^2/\nu$	Reynolds number
$Re^* \equiv n \cdot d^2 \cdot \rho/\eta_a$	Modified Reynolds number
$Re_{Pe} \equiv u_{Pe} \cdot d_{Pe}/\nu$	Pellet Reynolds number
S_i	Characteristic quantities for coalescence of fluids
$Sc \equiv \nu/\mathcal{D}$	Schmidt number
$Sh \equiv k_{Pe} \cdot d_{Pe}/\mathcal{D}$	Pellet Sherwood number
u'	Turbulent fluctuation velocity of the fluid (m/s)
$\bar{u}$	Mean velocity of the fluid (m/s)
u_G	Gas velocity based on empty cross section area of the reactor (m/s)
u_L	Local liquid velocity (m/s)
u_{Pe}	Relative velocity between pellet and fluid (m/s)
V	Reactor volume (m^3)
$\dot{V}$	Circulating volumetric flow by stirrer pumping (m^3/s)
V_S	Volume stirred up by the stirrer blades (m^3)
Z	Number of stirrer blades
α	Exponent
β	Exponent
$\dot{\gamma}$	Shear rate (s^{-1})
ε	Mass-related energy dissipation rate (kW/kg)
ε_{max}	Maximum energy dissipation rate (kW/kg)
η	Dynamic viscosity (Pa s)
η_a	Apparent dynamic viscosity (Pa s)
η_G	Dynamic viscosity of the gas phase (Pa s)
θ	Mixing time (s)
λ	Length scale of microeddies (m)
ν	Kinematic viscosity (m^2/s)
ρ	Density of fermentation fluid (kg/m^3)
σ	Surface tension (N/m)
$\sigma^* \equiv \sigma/[\rho(g \cdot \nu^4)^{1/3}]$	Dimensionless surface tension
τ	Shear stress (Pa)
τ_R	Reynolds shear stress (Pa)
τ_0	Yield stress (Pa)
φ_G	Gas holdup
φ_S	Solid holdup

BIBLIOGRAPHY

1. D.I.C. Wang and A.E. Humphrey, in D.J.D. Huckenhull ed., *Progress in Industrial Microbiology*, vol. 8, Temple Press Books, London, 1968, pp. 1–34.
2. Y. Miura, in T.K. Ghose, A. Fiechter, and N. Blakebrough eds., *Advances in Biochemical Engineering*, vol. 4, Springer-Verlag, Berlin, 1976, pp. 3–40.
3. M. Moo-Young and H.W. Blanch, in A. Fiechter ed., *Advances in Biochemical Engineering*, vol. 19, Springer-Verlag, Berlin, 1981, pp. 1–69.
4. H.-J. Henzler, *Chem.-Ing.-Tech.* **54**, 461–476 (1982).
5. D.C. Hempel, in R.K. Finn, P. Praeve, M. Schlingmann, W. Crueger, K. Esser, R. Thauer, and F. Wagner eds., *Biotechnology Focus 1*, Hanser Publishers, Munich, 1988, pp. 51–94.
6. J. Bryant, in T.K. Ghose, A. Fiechter, and N. Blakebrough eds., *Advances in Biochemical Engineering*, vol. 5, Springer-Verlag, Berlin, 1977, pp. 101–124.
7. R. Mann, P.P. Mavors, and J.C. Middleton, *Trans. Inst. Chem. Eng.* **59**, 271–278 (1981).
8. J. Pawlowski, *Die Ähnlichkeitstheorie in der physikalisch-technischen Forschung: Grundlagen und Anwendung*, Springer-Verlag, Berlin, 1971.
9. J. Stichlmaier, *Chem.-Ing.-Tech.* **63**, 38–51 (1991).
10. F. Kudrewizki, *Acta Biotechnol.* **4**, 89–104, 247–254 (1984).
11. M. Reuss, R.K. Bajpal, D. Debus, R. Lenz, H. Niebelschuetz, and A. Papalexiou, *6th Int. Ferment. Symp.*, London, Ontario, Canada, 1980.
12. R.K. Bajpal and M. Reuss, *Can. J. Chem. Eng.* **60**, 384–392 (1982).
13. N.M.G. Oosterhuis, N.M. Groesbeek, A.P.C. Olivier, and N.W.F. Kossen, *Biotechnol. Lett.* **5**, 141–146 (1983).
14. N.M.G. Oosterhuis, *Scale-Up of Bioreactors*, Proefschrift, Techn. Hogeschool, Delft, Netherlands, 1984.
15. A. Margarites and J.E. Zajic, *Biotechnol. Bioeng.* **20**, 939–1001 (1978).
16. J.Y. Oldshue, *Fluid Mixing Technology*, McGraw-Hill, New York, 1983.
17. J.Y. Oldshue, *Chem. Eng. Prog.* **5**, 33–42 (1989).
18. J.Y. Oldshue, *AlChE Symp. Ser.* **89**, 158–163 (1993).
19. J.Y. Oldshue, *Chem. Eng. Prog.* **93**, 70–73 (1997).
20. J.Y. Oldshue, *Biotechnol. Bioeng.* **8**, 3–24 (1966).
21. J.H. Rushton, E.W. Costich, and H.J. Everett, *Chem. Eng. Prog.* **46**, 395–404, 467–476 (1950).
22. M. Zlokarnik, in E. Bartholome, E. Biekert, H. Hellmann, H. Ley eds., *Ullmanns Enzyklopaedie der Technischen Chemie*, vol. 2, Verlag Chemie GmbH, Weinheim/Bergstrasse, 1972, pp. 259–281.
23. K. Kipke, *GVC-Vortragstagung: Verfahrenstechnische Fortschritte beim Mischen, Dispergieren und bei der Wärmeuebertragung in Fluessigkeiten*, VDI-Verlag, Duesseldorf, 1978, 21–36.
24. A.B. Metzner and R.E. Otto, *AlChE J.* **3**, 3–11 (1957).
25. A.B. Metzner, R.H. Feehs, H.L. Ramos, R.E. Otto, and J.D. Toothill, *AlCHE J.* **7**, 3–9 (1961).
26. R. Rapp, H. Reng, D.C. Hempel, and F. Wagner, *Biotechnol. Bioeng.* **26**, 1167–1175 (1984).
27. P.H. Calderbank and M.B. Moo-Young, *Trans. Inst. Chem. Eng.* **37**, 26–33 (1959).
28. A. Sanchez, A. Martinez, L.G. Torres, and E. Galindo, *Process Biochem.* **27**, 351–365 (1992).
29. D. Velasco, A. Martinez, L.G. Torres, and E. Galindo, in A.W. Nienow ed., *3rd International Conference on Bioreactor and Bioprocess Fluid Dynamics, BHR Group Conference Series Publication No. 5*, Mechanical Engineering Publications Limited, London, 1993, pp. 101–116.
30. Y. Oyama and K. Endoh, *J. Chem. Eng. Jpn.* **19**, 2–11 (1955).

31. M. Zlokarnik, *Chem.-Ing.-Tech.* **45**, 689–692 (1973).
32. H. Judat, Dissertation, Universitaet Dortmund, Germany, 1976.
33. V. Schlueter and W.D. Deckwer, *Chem.-Ing.-Tech.* **64**, 644–645 (1992).
34. H. Hoecker and G. Langer, *Rheol. Acta* **16**, 400–412 (1977).
35. H. Hoecker, Dissertation, Universitaet Dortmund, Germany, 1979.
36. H.-J. Henzler, *GVC-Vortragstagung: Verfahrenstechnische Fortschritte beim Mischen, Dispergieren und bei der Wärmeuebertragung in Fluessigkeiten*, VDI-Verlag, Duesseldorf, 1978, pp. 91–110.
37. P. Zehner, *Chem.-Ing.-Tech.* **60**, 531–539 (1988).
38. C. Breucker, A. Steiff, P.-M. Weinspach, *Proceedings of the European Conference on Mixing and Centrifugal Separation / Fluid Engineering*, vol. 6, British Hydromechanics Research Association, Cranfield, Bedford, 1988, pp. 399–406.
39. J.G. Van de Vusse, *Chem.-Ing.-Tech.* **31**, 583–587 (1959).
40. S. Nagata, *Mixing: Principles and Applications*, Kodansha, Tokyo, and Wiley, New York, 1975.
41. H.-J. Henzler, *Untersuchungen zum Homogenisieren von Fluessigkeiten oder Gasen, VDI-Forschungheft*, vol. 587, VDI-Verlag, Duesseldorf, 1978.
42. M. Zlokarnik, *Chem.-Ing.-Tech.* **39**, 539–548 (1967).
43. A. Mersmann, W.D. Einenkel, and M. Kaeppel, *Chem.-Ing.-Tech.* **47**, 953–996 (1975).
44. M. Opara, *Verfahrenstechnik* **9**, 446–449 (1975).
45. M. Zlokarnik, in T.K. Ghose, A. Fiechter, and N. Blakebrough eds., *Advances in Biochemical Engineering*, vol. 8, Springer-Verlag, Berlin, 1978, pp. 133–151.
46. H. Judat, *Chem.-Ing.-Tech.* **54**, 520–521 (1982).
47. K. Van't Riet, *Ind. Eng. Chem. Process Des. Dev.* **18**, 357–375 (1979).
48. K. Akita and F. Yoshida, *Ind. Eng. Chem. Process Des. Dev.* **13**, 84–91 (1974).
49. H. Yagi and F. Yoshida, *Ind. Eng. Chem. Process Des. Dev.* **14**, 488–493, (1975).
50. J.F. Perez and O.C. Sandall, *AlChE J.* **20**, 770–775 (1974).
51. S. Sideman, O. Hortacsu, and J.W. Fulton, *Ind. Eng. Chem. (Int. Ed.)* **58**, 32–47 (1966).
52. Y. Kawase and M. Moo-Young, *Chem. Eng. Res. Des.* **66**, 285–288 (1988).
53. J.G. Mooyman, *Biotechnol. Bioeng.* **29**, 180–186 (1987).
54. D.B. Mills, R. Bar, and D.J. Kirwan, *AlChE J.* **33**, 1542–1549 (1987).
55. H. Oguz, A. Brehm, and W.-D. Deckwer, *Chem. Eng. Sci.* **42**, 1815–1822 (1987).
56. J. Hoffmann, K. Buescher, and D.C. Hempel, *Chem.-Ing.-Tech.* **67**, 210–214 (1995).
57. J. Hoffmann, J. Tralles, and D.C. Hempel, *Chem.-Ing.-Tech.* **64**, 953–956 (1992).
58. R.S. Cherry and K.-Y. Kwon, *Biotechnol. Bioeng.* **36**, 563–571 (1990).
59. R.K. Geisler, Dissertation, Technische Universitaet Munich, Germany, 1991.
60. F. Liepe, *Verfahrenstechnische Berechnungsmethoden, vol. 4: Stoffvereinigen in fluiden Phasen*, VCH, Weinheim, 1988.
61. H.-J. Henzler and A. Biedermann, *Chem.-Ing.-Tech.* **68**, 1546–1561 (1996).
62. K. Buescher and D.C. Hempel, *Chem.-Ing.-Tech.* **68**, 1452–1455 (1996).
63. B.K. Revill, *4th Eur. Conf. on Mixing*, Paper B1, Noordwijkerhout, Netherlands, 1982.
64. J.Y. Oldshue, in C.S. Ho and J.Y. Oldshue eds., *Biotechnology Processes: Scale-Up and Mixing*, AlChE, New York, 1987, pp. 3–5.
65. B. Metz, N.W.F. Kossen, J.C. Van Suijdam, in T.K. Ghose, A. Fiechter, and N. Blakebrough eds., *Advances in Biochemical Engineering*, vol. 11, Springer-Verlag, Berlin, 1979, pp. 103–156.
66. F. Liepe, H.O. Moeckel, *Chem. Tech. (Leipzig)* **28**, 205–209 (1976).
67. S. Sicardi, R. Conti, G. Baldi, L. Franzino, *Chem.-Ing.-Tech.* **53**, MS 870/81 (1981).
68. P.L.T. Brian, H.B. Hales, T.K. Sherwood, *AlChE J.* **15**, 727–733 (1969).
69. P. Harriot, *AlChE J.* **8**, 93–102 (1962).
70. P.H. Calderbank, M.B. Moo-Young, *Chem. Eng. Sci.* **16**, 39–54 (1961).
71. E.O. Karow, W.H. Bartholomew, M.R. Sfat, *J. Agric. Food. Chem.* **1**, 302–312 (1953).
72. E.S. Bylinkina, V.V. Birukov, S.A. Voroshilova, in H. Dellweg ed., *Abstracts 5th International Fermentation Symposium*, Berlin, 1976.
73. O.G. Wegrich, R.A. Shurter, *Ind. Eng. Chem.* **45**, 1153–1160 (1953).
74. J. Strohm, R.F. Dale, H.J. Peppler, *Appl. Microbiol.* **7**, 235–238 (1959).
75. M. Jarai, in G. Terni ed., *4th International Fermentation Symposium Proceedings*, Fermentation Technology Today, Osaka, 1972, pp. 97–105.
76. W.H. Bartholomew, in Umbreit ed., *Advances in Applied Microbiology 2*, Academic Press, New York, 1960, pp. 289–300.
77. H. Takei, K. Mizusawa, and F. Yoshida, *J. Ferment. Technol.* **53**, 151–158 (1975).
78. H. Taguchi, T. Imomanaka, S. Teramoto, M. Takatsu, and M. Sato, *J. Ferment. Technol.* **46**, 823–828 (1968).
79. R. Fuchs, D.D.Y. Ryu, A.E. Humphrey, *Ind. Eng. Chem. Process Des. Dev.* **10**, 190–196 (1971).
80. W.D. Maxon, *J. Biochem. Microbiol. Tech. Eng.* **1**, 311–324 (1959).
81. D.I. Wang, R.C.J. Fewkes, in L.A. Underkofler ed., *Developments in Industrial Microbiology*, American Institute of Biological Science, Washington, D.C., 1977, pp. 39–56.
82. E.J. Gaden, Jr., *Sci. Rep. Inst. Superore di Sanita* **1**, 161–176 (1961).
83. A.E. Humphrey, *J. Ferment. Technol.* **42**, 265–278 (1964).
84. A.E. Humphrey, *J. Ferment. Technol.* **42**, 334–345 (1964).

See also BIOREACTORS, AIR-LIFT REACTORS; BIOREACTORS, FLUIDIZED-BED; BIOREACTORS, CONTINUOUS STIRRED-TANK REACTORS; DIMENSIONAL ANALYSIS, SCALE-UP; FERMENTATION MONITORING, DESIGN AND OPTIMIZATION; MAMMALIAN CELL CULTURE REACTORS, SCALE-UP; MASS TRANSFER.

SECONDARY METABOLITE PRODUCTION, ACTINOMYCETES, OTHER THAN STREPTOMYCES

ANN C. HORAN
Schering Plough Research Institute
Kenilworth, New Jersey

KEY WORDS

Actinomycetes
Cell wall composition
Chemotaxonomy
Fatty acids
Fermentation
Menaquinones
Phospholipids
Secondary metabolites

OUTLINE

INTRODUCTION

Actinomycetes are an industrially important group of microorganisms, producing, in fermentation, numerous therapeutically relevant natural products. In the pharmaceutical and biotechnology industries, they continue to be the focus of many natural product screening programs, especially in the search for novel antibiotics active against

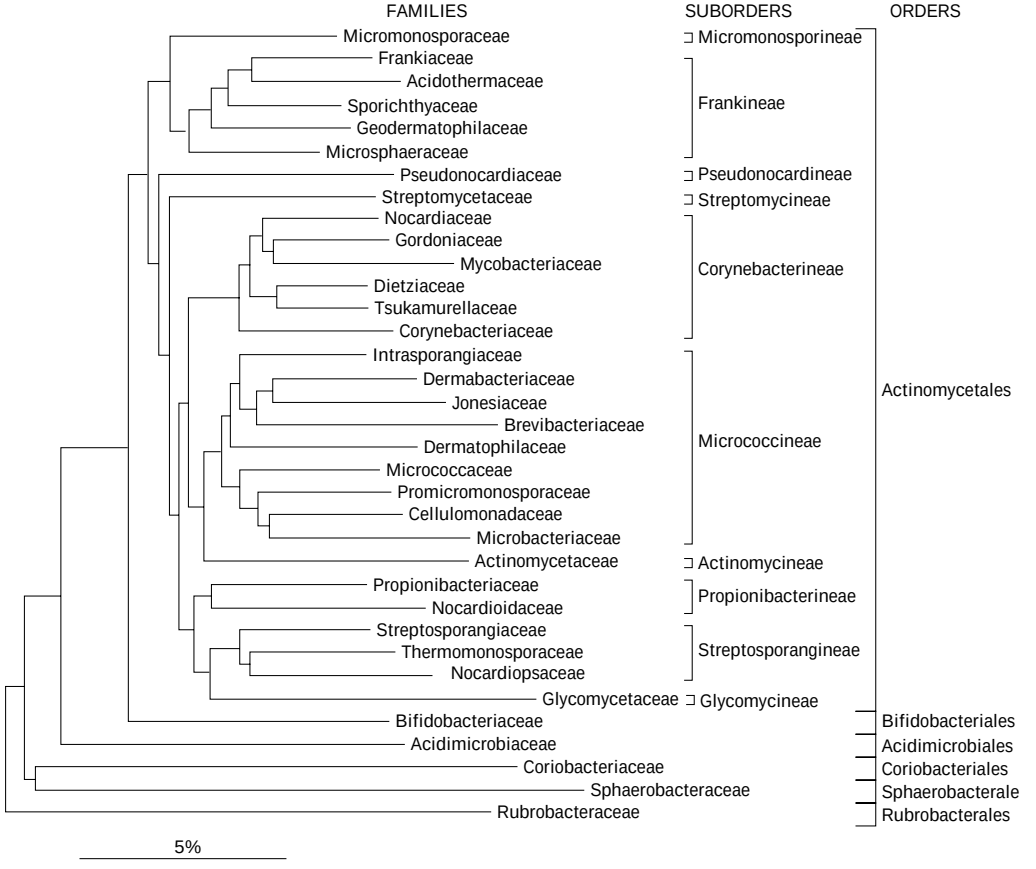

Figure 1. Relatedness of actinobacteria showing the presence of 6 orders and 10 suborders of the Actinomycetales based on 16S rDNA/rRNA sequence comparison. The scale bar represents 5 nucleotide substitutions per 100 nucleotides. *Source*: From Stackebrandt et al. (2).

Table 1. Morphological Characteristics of Members of the Families Streptosporangiaceae, Nocardiopsaceae, Thermomonosporaceae, Pseudonocardiaceae, Micromonosporaceae, and Glycomycetaceae

Family/genus	Substrate mycella	Aerial mycelia	Spore chains	Spores
		Streptosporangiaceae		
Streptosporangium	Branching, nonfragmenting; yellow, brown, orange, red	Present; white, pink to greenish-gray; spore vesicles borne on long or short sporangiophores, singly or clustered	Spore vesicles contain a coiled chain of arthrospores formed by septation of an unbranched, spiral hyphae within an expanded sporangiophore sheath.	Nonmotile; smooth, spherical, oval or rod-shaped
Herbidospora	Branching, nonfragmenting; colorless, tan to yellow-brown	Absent; spore chains, in mass, white	Straight, short chains, 10 to 30 spores, borne on tips of branching sporophores, in clusters, directly from the vegetative mycelium	Nonmotile; smooth, oval
Microbispora[a]	Branching, nonfragmenting; yellow, brown, orange, violet	Present; pink to white; bearing longitudinal pairs of spores often closely arranged along the hyphae, either sessile or on short sporophores	Spores in pairs	Nonmotile; smooth, spherical to oval
Microtetraspora	Branching, nonfragmenting; yellow, brown, orange, violet	Present; white, pink, blue-gray; short, sparsely branched	Spores in chains of 4	Nonmotile; smooth, warty, spherical to oval
Planobispora	Branching, nonfragmenting; colorless or rose	Present; white to light rose; bearing cylindrical to clavate sporangia, singly or in bundles, on short sporangiophores	Longitudinal pairs of spores in sporangia	Motile; peritrichous flagella; smooth, straight to slightly curved
Planomonospora	Branching, nonfragmenting; grayish-yellow, pink, reddish, orange	Present; white to rose; bearing cylindrical to clavate sporangia, sessile or on sporangiophores	Single spore in each sporangium	Motile; peritrichous flagella; straight to curved.
		Nocardiopsaceae		
Nocardiopsis	Branching, fragmenting into rods and coccal elements; yellow, yellowish-brown, olive	Present; white, yellowish-gray; long, moderately branched; straight to flexous, zigzag fragmentation	Fragmenting into long (greater than 50) chains of spores	Nonmotile; smooth, irregular
		Thermomonosporaceae		
Thermomonospora[b]	Branching, nonfragmenting; colorless to pale yellow	Present; white; differentiates into a single, heat sensitive spore	Single, sessile, or on the end of short branched or unbranched sporophores	Nonmotile; smooth to ridged
Actinomadura	Branching, nonfragmenting; colorless to yellow, orange, brown, red-brown, red, violet, gray-green	Present; white, yellow, pink, blue, green, gray; branching, carrying short to long chains of arthrospores	Straight, flexous, hooked, open loops, irregular spirals of 1 to 4 turns	Nonmotile; folded, irregular, smooth, spiny, or warty
Spirillospora[c]	Branching, nonfragmenting; white, pale yellow, pale pink, red to reddish brown	Present; white; bearing spherical sporangia on sporangiophores	Each spore vesicle contains coiled, branched aerial hyphae that differentiate into spores.	Motile, 1 to 7 subpolar flagella; smooth, rod-shaped, curved

Table 1. Morphological Characteristics of Members of the Families Streptosporangiaceae, Nocardiopsaceae, Thermomonosporaceae, Pseudonocardiaceae, Micromonosporaceae, and Glycomycetaceae (continued)

Family/genus	Substrate mycella	Aerial mycelia	Spore chains	Spores
		Micromonosporaceae		
Micromonospora	Branching, well developed; tan to orange, brown, blue-green, purple	Absent or a gray to white bloom	Borne singly, sessile or on short sporophores, in branched clusters	Nonmotile; smooth to warty, oval
Actinoplanes	Branching, nonfragmenting; tan to red, brown, violet	Absent or scanty, sporangia, spherical, subspherical, clavate, irregular, arising from the substrate mycelia, sessile or on short sporangiophores	Within the sporangia	Motile, polar flagella; spherical or short rods
Catellatospora	Branching, nonfragmenting; tan, yellow, mustard gold, orange, reddish brown.	Absent	Short, straight to flexous, branched chains of spores directly from the substrate mycelia	Nonmotile; cylindrical, ovoid, smooth to slightly rough
Couchioplanes	Branching, nonfragmenting; dark blue	Present; branching	Short spore chains in irregular spirals, directly from the substrate mycelia or on short aerial mycelia	Motile, polar flagellation; oval, short rods, smooth
Catenuloplanes	Branching, nonfragmenting; orange, red, brown	Present; sparse, branching	Short spore chains in spirals of 1 to 2 turns, from the substrate or aerial mycelia	Motile, peritrichous flagella; rod-shaped, straight to curved, smooth
Dactylosporangium	Branching, nonfragmenting; orange, rose, or wine.	Absent; sporangia present, borne on short sporangiospores, finger-shaped to claviform	Within the sporangia a single row of 3 to 4 spores	Motile, polar flagella; oblong, ovoid
Pilimelia	Branching, nonfragmenting; pale lemon-yellow, golden yellow, orange	Absent; sporangia present, spherical ovoid, pyriform, cylindrate, borne on sporangiospores	Within the sporangia, in parallel or swirl rows, and as conidia, in chains	Motile, sporangiospores, laterally inserted tuft of flagella; nonmotile, rod-shaped conidiospores
Spirilliplanes	Present, nonfragmenting, branching, yellow to orange	Absent	Short chains of spores arranged in spirals and clusters directly from the substrate mycelia	Motile, oval to short rods, smooth, flagella type not given
		Pseudonocardiaceae		
Pseudonocardia	Zigzag fragmentation and long chains of spore-like structures; mycelial wall with a characteristic electron dense outer layer	Present; white; fragmenting	Spore chains long, 50 or more per chain	Nonmotile; smooth, spiny, irregular
Actinopolyspora	Branching, occasionally fragments; buff	Present; white, with an outer sheath	Long chains of spores	Nonmotile; smooth
Actinosynnema	Fragmenting	Present; form synnemata (dome-like structures)	Chains of arthrospores at the tip of the synnemata	Motile arthrospores (flagellation not given)
Amycolatopsis	Fragments into long chains of squarish to ellipsoid structures	Rarely formed; when present, white; may fragment into chains of spores	Chains of squarish to oval fragments	Nonmotile; oval, smooth, warty
Kibdelosporangium	Zigzag fragmentation	Present; white; sporangia-like structures that do not contain spores but germinate when placed on agar	Long chains	Nonmotile; smooth, irregular

Table 1. Morphological Characteristics of Members of the Families Streptosporangiaceae, Nocardiopsaceae, Thermomonosporaceae, Pseudonocardiaceae, Micromonosporaceae, and Glycomycetaceae (*continued*)

Family/genus	Substrate mycella	Aerial mycelia	Spore chains	Spores
Kutzneria	Branching, nonfragmenting	Present; white, olive gray; branching with globose sporangia	Long chains formed by separation of coiled, unbranched hyphae	Nonmotile; spherical, rod-shaped or oval
Lentzea	Branching, nonfragmenting; yellow to yellow brown	Present; white to whitish-yellow; fragmenting into rod-shaped elements	Chains of rod-like structures	Nonmotile; smooth, rod-like
Saccharomonospora	Branching, rarely fragments; beige, lilac, green	Present; white becoming green; with an outer sheath	Single densely packed, on the aerial mycelia	Nonmotile; oval, smooth, warty
Saccharopolyspora	Fragmenting; spores often present	Present; white, pink to brownish gray, often sparse; with an outer sheath	Long and short chains	Nonmotile; spore sheath ornamentation hairy, spiny, smooth
Saccharothrix	Zigzag fragmentation; yellow to yellow brown	Present; white to yellowish-gray, zigzag fragmentation	Chains of ovoid to irregular elements	Nonmotile; smooth, ovoid
Streptoalloteichus	Branching, bearing spore-like vesicles containing one to several spores	Present; spore chains in clusters and sclerotia	Spore chains on the aerial mycelia, sporangiospores on the substrate mycelia	Motile sporangiospores by a single long polar flagellum
Thermocrispum	Branching, nonfragmenting; yellow to light brown	Present; white; aggregating into clusters that fragment into rod-like structures	Chains of rod-like structures	Nonmotile; smooth, rod-like
		Glycomycetaceae		
Glycomyces	Branching, nonfragmenting; pale yellow to tan	Present; white; forming spores	Short chains	Nonmotile; square-ended
		Genera of Uncertain Affiliation		
Actinobispora	Branching, nonfragmenting; bearing paired spores; light orange	Present; white; sparse; bearing paired spores	Longitudinal pairs	Nonmotile; smooth, spherical
Actinocorallia	Branching, nonfragmenting; ivory to pale yellow	Absent	Coralloid sporophores arising from the substrate mycelia bearing long chains (30+) of spores	Nonmotile; smooth, cylindrical
Actinokineospora	Branching, nonfragmenting; (on agar); colorless to yellow brown	Present; white; bearing chains of spores in a sheath	Irregularly curved; less than 50 per chain	Motile, peritrichous flagella; smooth, ovoid to squarish
Planotetraspora	Branching, nonfragmenting; ivory	Present; whitish gray; cylindrical sporangia on short sporangiophores	Single row of 4 spores per sporangium	Motile, a single polar flagellum
Thermobispora	Branching, nonfragmenting; yellow to yellow brown	Present; white; monopodially branched; bearing pairs of spores	In longitudinal pairs on the aerial hyphae	Nonmotile; smooth, spherical to oval

[a] *Microbispora bispora* has been removed from the genus to form a new, thermophilic single species genus, *Thermobispora* (7).
[b] The genus *Thermomonospora*, as defined by Kroppenstedt and Goodfellow (8), contains two species, *T. curvata* and *T. formosensis*.
[c] The genus *Spirillospora* was last placed in the family Streptosporangiaceae (9) based on 16S rDNA but has now been moved to the family Thermonomosporaceae (2).

Table 2. Cell Wall Types and Corresponding Whole-Cell Sugar Patterns of Aerobic Actinomycetes Containing *meso*-Diaminopimelic Acid

Cell Wall		Whole-cell sugar pattern		
Type	Distinguishing major constituents	Type	Diagnostic sugars	Representative genera
II	Glycine	D	Xylose, arabinose	*Micromonospora*
III	None	B	Madurose[a]	*Actinomadura*
		C	None	*Nocardiopsis*
IV	Arabinose, galactose	A	Arabinose, galactose	*Amycolatopsis*

Source: According to Lechevalier and Lechavalier (13).
[a]Madurose is 3-*O*-methyl-D-galactose.

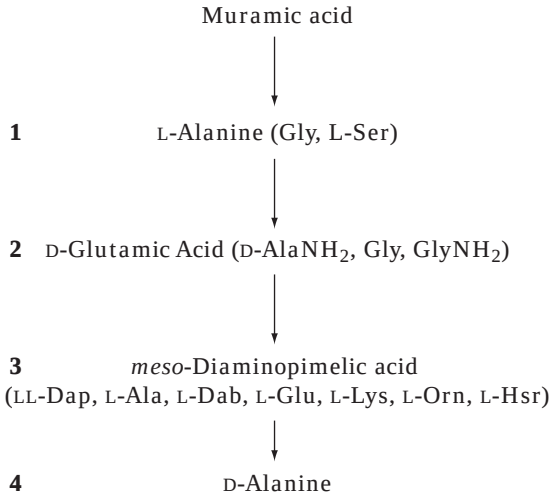

Figure 2. The peptide stem of the actinomycete (and other Gram-positive bacteria) peptidoglycan and the possible variations in amino acid content (in parentheses). Ala, alanine; Dab, diaminobutyric acid; Glu, glutamic acid; Gly, glycine; Hsr, homoserine; Lys, lysine; Orn, ornithine; Ser, serine. *Source*: From Suzuki et al. (15).

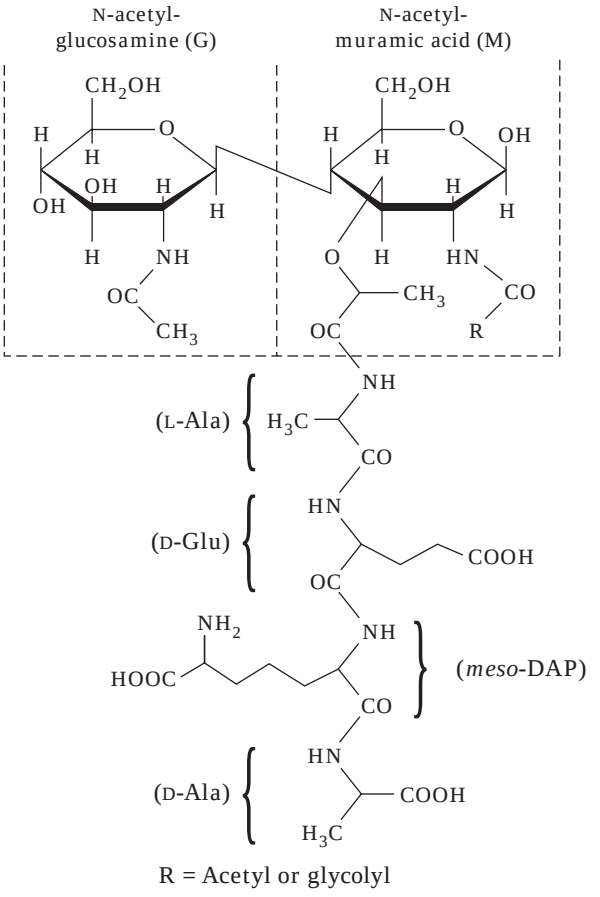

Figure 3. Complete structure of a single subunit of the peptidoglycan showing the linkage between the two amino sugars that make up the glycan strand and between muramic acid and the four amino acids in the peptide. Also indicated is the position of acetyl/glycolyl on muramic acid. *Source*: Modified from Suzuki et al. (15).

highly resistant, infectious Gram-positive pathogens. In an actinomycete-based natural product screening program, the organisms must be isolated from the environment, grown in pure state, preserved, and fermented, and the fermentation products must be tested for biological activity. Essential to this process is a knowledge of actinomycete ecology, taxonomy, and physiology, all of which contribute to the isolation of new strains with the potential of producing novel compounds.

Actinomycetes are Gram-positive, filamentous bacteria with a mol % G + C content of DNA greater than 50%. They can be divided into two broad groups: the fermentative organisms that are found in the natural cavities of man and animals and the larger group of oxidative organisms found in soil (1). The majority of oxidative soil actinomycetes can be further subdivided into two large groups based on the isomer of diaminopimelic acid in the peptidoglycan: the streptomycetes, containing LL-diaminopimelic acid (DAP) and the remainder containing *meso*-DAP. Further subdivisions to family, genus, and species relies on analysis of actinomycete morphology, determination of chemical constituents of cell walls and whole cells, biochemical characteristics, and resistance patterns. Sequence data generated from the analysis of small subunit RNA (16S) have been applied to the understanding of actinomycete phylogeny as well as molecular identification. A new hierarchical classification based on 16S rDNA/rRNA sequences (Fig. 1), proposed by Stackebrandt et al. (2), will be followed as phenotypic data are presented. Aerobic, saprophytic, filamentous actinomycetes containing *meso*-DAP in their cell

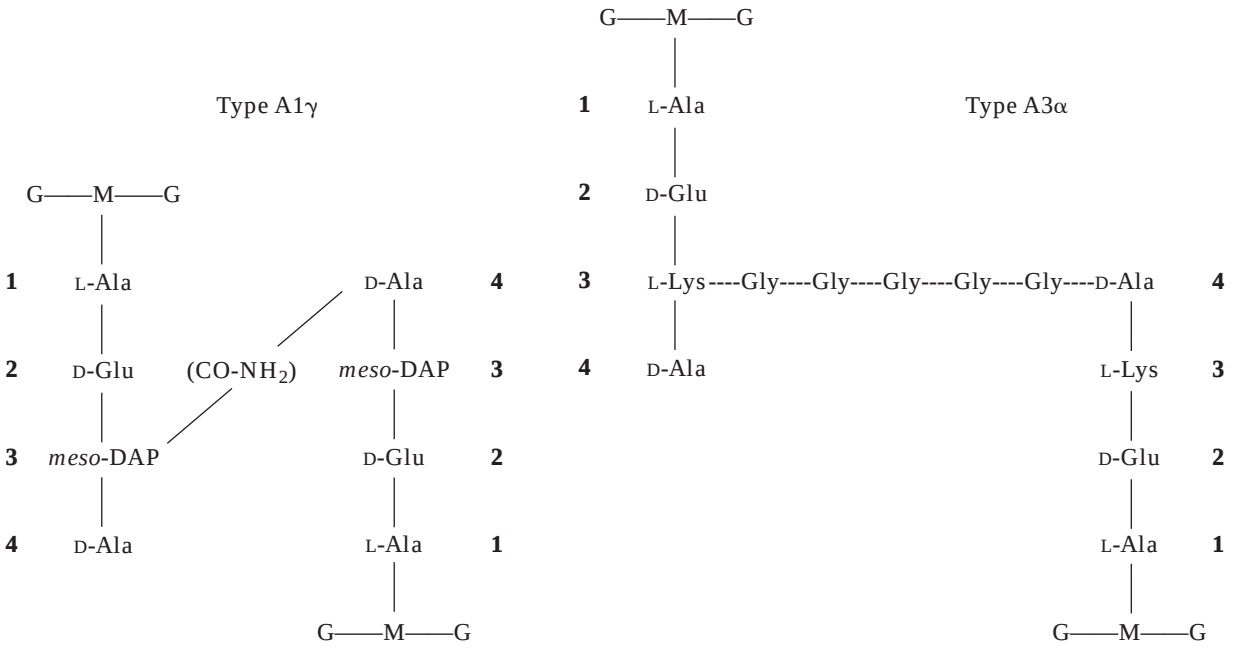

Figure 4. Example of a directly cross-linked *meso*-DAP–containing peptidoglycan of type A (cross-linkage between positions 3 and 4 of two peptide subunits), 1 (no peptide bridge), and γ (*meso*-DAP in position 3), and an example of cross-linking through a peptide bridge, A (as above), 3 (the bridge is an oligopeptide), and α (L-lysine in position 3. Ala, alanine; Dap, diaminopimelic acid; G, *N*-acetylglucosamine; Glu, glutamic acid; Gly, glycine; Lys, lysine; M, *N*-acetyl- or *N*-glycolylmuramic acid. *Source*: Modified from Suzuki et al. (15).

walls, which have not been placed in any of the actinomycete families defined by 16S rDNA sequence data, including Actinobispora (3), Actinocorallia (4), Actinokineospora (5), Planotetraspora (6), and Thermobispora (7) will also be described. The suborders Actinomycineae, Micrococcineae, Corynebacterineae, Propionibacterineae and Frankineae (2) will not be discussed in this article.

IDENTIFICATION OF NONSTREPTOMYCETE ACTINOMYCETES

Morphological Characterization

Meso-DAP–containing soil actinomycetes have a complex morphology. When grown on agar, a substrate mycelia forms that may penetrate the agar and that can bear spores, sporelike structures, or sporangia. Aerial mycelia may arise from the substrate mycelia and can be branching. The aerial mycelia may be in a sheath or in a sporangium and may fragment into motile or nonmotile spores. Morphological characteristics can be observed by growing the organisms on minimal media, for example, water agar (crude agar, 15 g; tap water, 1,000 mL), dilute Bennett's agar (agar, 15 g; glucose, 1 g; pancreatic digest of casein, 0.2 g; yeast extract, 0.1 g; beef extract, 0.1 g; distilled water, 1,000 mL), or dilute yeast–dextrose agar (agar, 15 g; yeast extract, 1 g; dextrose, 1 g; tap water, 1000 mL). After 7–28 days of incubation at 28 °C, plates can be examined directly under a light microscope using a long working distance, 40× objective. Detailed morphological analysis, such as spore and sporangiophore ornamentation, location and attachment of flagella on motile spores, and sporangial structures and spore formation within the sporangia will require either scanning or electron microscopic observations. In some cases, actinomycetes can be identified to genus based on their characteristic morphology (Table 1).

Chemical Characterization

Although the majority of actinomycetes readily form morphological structures, many do not, making preliminary identification based on this characteristic impossible. The laboratories of Huber and Mary Lechevalier at the Waksman Institute, Rutgers University, New Jersey, pioneered the extensive use of chemical markers to delineate genera of actinomycetes. The first large-scale, systematic application of chemical criteria to taxonomy focused on the analysis of cell-wall and whole-cell sugars and amino acids. Representatives of all the described actinomycete genera were analyzed, and distinct patterns were discerned (11,12) (Table 2). In conjunction with the data generated by Schleifer and Kandler (14) delineating the mode of cross-linking between subunits of the Gram-positive peptidoglycan (Figs. 2 to 4), a clearer understanding of the relationship of wall structure to wall chemotype was obtained (15) (Tables 3 and 4). The presence of either glycolyated or acetylated muramic acid in the cell wall (17,18) and lipids such as mycolic acids (19), phospholipids (20), menaquinones (21), and fatty acids (22,23) resulted in additional taxonomic discrimination. Phospholipid patterns are presented in Table 5, and the structure of typical ac-

Table 3. Peptidoglycan Classification

Position of cross-link	Peptide bridge	Amino acid at position 3
	Peptidoglycan A	
Cross-linkage between positions 3 and 4 of two peptide subunits	1. None	α-L-Lysine β-L-Ornithine γ-*meso*-DAP
	2. Polymerized subunits	α-L-Lysine
	3. Monocarboxylic L-amino acid or glycine or oligopeptides	α-L-Lysine β-L-Ornithine γ-LL-DAP
	4. Contains a dicarboxylic amino acid	α-L-Lysine β-L-Ornithine γ-*meso*-DAP δ-L-DAB
	Peptidoglycan B	
Cross-linkage between positions 2 and 4 of two peptide subunits	1. Contains an L-amino acid	α-L-Lysine β-L-Homoserine γ-L-Glutamic acid δ-L-Alanine
	2. Contains a D-amino acid	α-L-Ornithine β-L-Homoserine γ-L-DAB

Source: From Suzuki et al. (15) based on Schleifer and Kandler (14).
Note: DAB, diaminobutyric acid.

Table 4. Relationship Between Wall Chemotype and Peptidoglycan Type in Actinomycetes

Wall type[a]	Major wall amino acids[a]	Other distinguishing characteristics[b]	Peptidoglycan type[c]	Representative genera
I	Glycine, LL-DAP	None	A3γ	*Streptomyces*
II	Glycine, *meso*- or OH-DAP	None	A1γ	*Actinoplanes* *Micromonosporaa*
III	*meso*-DAP	Madurose in whole cells	A1γ	*Actinomadura* *Streptosporangium*
IV	*meso*-DAP	Arabinose and galactose in cell wall	A1γ	*Amycolatopsis* *Nocardia*
V	Lysine, ornithine	None	A5β	*Actinomyces*
VI	Lysine (aspartic acid, var.)	Galactose (var.)	A3α, A4α	*Couchioplanes, Oerskovia*
VII	Diaminobutyric acid, glycine (lysine, var.)	None	B2α	*Agromyces*
VIII	Ornithine	None	B2β	*Bifidobacterium*

Source: From Minnikin and Goodfellow (16).
Note: var. = variable
[a]Major constituents of actinomycete cell walls according to Lechevalier and Lechevalier (13).
[b]All cell wall preparations contain major amounts of alanine, glutamic acid, glucosamine, and muramic acid.
[c]From Schleifer and Kandler (14).

tinomycete fatty acids and the patterns obtained from their analysis are presented in Tables 6 and 7. Chemotaxonomic markers aid in the identification of actinomycetes to the genus level. Further discrimination to the species level can be achieved using physiological tests, including utilization of various carbon and nitrogen sources; hydrolysis of complex carbohydrates and macromolecules; and resistance to chemicals, including antibiotics (24,25). Sequence analysis, particularly of the 16S rDNA, may play a significant role in future definitions of actinomycete species. However, because of the highly conserved nature of small subunit RNA, very high similarity levels (greater than 97%) among related strains will be observed. In order to delineate species within these groups, DNA–DNA reassociation may be required (26).

The chemotaxonomic characteristics for each genus of the families described in the next section are presented in Table 8.

CHARACTERISTICS OF ACTINOMYCETE FAMILIES

Streptosporangiaceae

Streptosporangiaceae (9,27) are aerobic, Gram-positive, non-acid-fast, chemoorganotrophic actinomycetes that form stable substrate and aerial mycelia. Aerial mycelia

Table 5. Phospholipid Patterns of Aerobic Actinomycetes

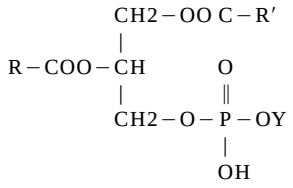

R, R′ = Long chain alkyl

Y = Polar head groups, PG, DPG,[a] PI,[a] PIM, PE, PC, PME

Phospholipid Pattern	Phosphatidyl-ethanolamine (PE)	Phosphatidylmethyl-ethanolamine (PME)	Phosphatidyl-choline (PC)	Phosphatidyl-glycerol (PG)	GluNU[a]
PI	Absent	Absent	Absent	Variably present	Absent
PII	Present	Absent	Absent	Absent	Absent
PIII	Variably present	Variably present	Present	Variably present	Absent
PIV	Variably present	Variably present	Absent	Absent	Present
PV	Absent	Absent	Absent	Present	Present

Source: According to Lechevalier et al. (20).
[a]DPG, diphosphatidy glycerol; PI, phosphatidylinositol; GluNU, phospholipids of unknown structure containing glucosamine.

Table 6. Structure of Representative Actinomycete Fatty Acids

Fatty acid type	Common example and structure
Straight-chain	*Hexadecanoic* CH_3-$(CH_2)_{14}$-COOH
Cis-unsaturated	*Oleic* CH_3-$(CH_2)_7$-CH = CH-$(CH_2)_7$-COOH *cis*
Tuberculostearic	*10-Methyloctadecanoic* CH_3 CH_3-$(CH_2)_7$-CH-$(CH_2)_8$-COOH
Cis-cyclopropane	*11,12-Methyleneoctadecanoic* CH_2 CH_3-$(CH_2)_5$-CH-CH-$(CH_2)_9$-COOH *cis*
Iso	*13-Methyltetradecanoic* CH_3 CH_3-CH-$(CH_2)_{11}$-COOH
Anteiso	*12-Methyltetradecanoic* CH_3 CH_3-CH_2-CH-$(CH_2)_{10}$-COOH

Source: From Minnikin and O'Donnell (16).

may carry chains of two or more spores or be differentiated into sporangia (spore vesicles) containing one, two, or more spores. Spores are either motile or nonmotile. Cell walls contain *meso*-DAP and N-acetylated muramic acid, but lack characteristic sugars; whole cells contain madurose. The peptidoglycan is of the A1γ type, having a cross-linkage between positions 3 and 4 of adjacent peptide subunits, with *meso*-DAP at position 3 of the peptide stem (14). Lipid profiles contain saturated, *iso*- and *anteiso*-fatty acids; major proportions of tetrahydrogenated menaquinones, with nine isoprene units saturated at sites III and VIII; and glucosamine-containing polar lipids. Mycolic acids are absent. The mol % G + C content of the DNA ranges from 66 to 74.

Nocardiopsaceae

Nocardiopsaceae (28,29) are aerobic, Gram-positive, non-acid-fast, chemoorganotropic actinomycetes that form well-developed, branching substrate mycelia that may fragment into coccoid to bacillary forms. Aerial mycelia are long and moderately branching, with zigzag fragmentation into irregular spores. The family is defined on the basis of chemotaxonomic markers because the morphological characteristics are the same for the genus *Saccharothrix* (family Pseudonocardiaceae). Cell walls contain *meso*-DAP, N-acetylated muramic acid, and no characteristic sugars. The peptidoglycan is A1γ. Lipid profiles contain phosphatidylcholine and phosphatidylmethylethanolamine; major portions of variably saturated menaquinones with 10 isoprene units; *iso*-branched, *anteiso*-branched, and 10-methyl-branched fatty acids; and high levels of octadecanoic acid. The combination of 15 to 20% *anteiso*-C17:0 (14-methylhexadecanoic acid) with 20 to 25% 10-methyl-C18:0 (tuberculostearic acid) or its precursor, oleic acid, is diagnostic and unique among bacteria. Mycolic acids are absent. The G + C content of the DNA is 64 to 69 mol %. The family contains only one genus, *Nocardiopsis*.

Thermomonosporacea

Thermomonosporacea (8) are aerobic, Gram-positive, non-acid-fast, chemoorganotrophic actinomycetes producing branched substrate mycelia bearing aerial mycelia that differentiate into single or short chains of arthrospores. Cell walls contain *meso*-DAP, N-acetylated muramic acid, and no characteristic sugars. The peptidoglycan type is

Table 7. Fatty Acid Types

Type	*Iso*-15:0	*Anteiso* 15:0	*Iso*-16:0	16:0	10-Methyl 16:0	*Iso*-17:0	*Anteiso*-17:0	17:0	17:1	10 Methyl 17:0	*Iso*-18:0	18:0	18.1	10-Methyl 18:0	OH_2	Cyclo-19
1a	−	−	−	+++	−	−	−	−	−	−	−	+	+++	−	−	−
1b	−	−	−	+++	++	−	−	−	−	+	−	+	++	+++	−	−
1c	−	−	−	+++	−	−	−	−	−	−	−	+	++	−	−	++
2a	+	−	+++	++	−	+	+	+	+	−	+	−	−	−	++	−
2b	++++	++	++	+	−	+++	+	−	−	−	−	−	−	−	−	−
2c	++	+++	+++	+	−	+	++	−	−	−	−	−	−	−	(V)	−
2d	+++	++	++++	++	−	++	++	+	+	−	+	+	++	−	−	−
3a	−	−	++	+++	+	−	−	+	+	+	+	+	++	++	−	−
3b	++++	+	++	−	−	++	++	+	++	+	−	−	+	−	−	−
3c	++	+	+++	+	+	+	+	++	+	++	+	+	−	−	++	−
3d	+	+	+++	+	−	+	+++	+	+	++	+	+	++	++	−	−
3e	++	−	++++	+	−	+	+	−	+	+	−	−	−	−	−	−
3f	++	+	++++	+	−	+	+	++	++	+	−	−	−	−	+	−
3g	++	+	++++	+	−	+	++	+	+	+	−	−	−	−	+	−

Source: From Kroppenstedt (23).
Note: + = 1.5%; ++ = 5–15%, +++ = 15–25%, ++++ = 25%; (V) = variable, usually less than 2% for one component.

A1γ. Whole cells contain madurose. Lipid profiles contain mixtures of straight- and branched-chain fatty acids; hydrogenated menaquinones with nine isoprene units; and major amounts of phosphatidylglycerol, phosphatidylinositol, and phosphatidylmannosides, some strains contain minor amounts of phosphatidylglycerol. The G + C content of the DNA is mol % 66 to 72.

Micromonosporaceae

Micromonosporaceae (10,30,31) are aerobic, Gram-positive, and non-acid-fast, forming nonfragmenting, branching substrate mycelia that, in the genus *Micromonospora*, form nonmotile spores, singly either sessile or on short sporophores. Aerial mycelia are rarely formed, but when present are scanty. Sporangia, which may be present and can contain two to five or numerous spores, are formed on sporangiophores arising directly from the substrate mycelia. Globose, subglobose, or rod-shaped spores are formed in the sporangia or in chains arising from the substrate mycelia. In water the spores become motile by means of polar or lateral tufts of flagella. Cell walls contain *meso*- or 3-hydroxy-DAP, or both. The peptidoglycan is of the A1γ type; glycine is the first amino acid (acetate in *Pilimelia*) in the stem peptide attached to a glycolated muramic acid. Whole-cell hydrolysates contain arabinose and xylose. Lipid profiles have saturated, *iso*-, and *anteiso*-fatty acids, and diphosphatidylglycerol, phosphatidylethanolamine, phosphatidylglycerol, and phosphatidylinositol as characteristic phopholipids; menaquinones are of varying lengths. Mycolic acids are absent. The mol % G + C content of the DNA ranges from 71 to 73.

Pseudonocardiaceae

Pseudonocardiaceae (32,33) are a heterogeneous grouping of organisms based on 16S rDNA/rRNA sequence data. Aerobic, Gram-positive, mesophilic or thermophilic, and chemoorganotrophic, one genus is halophytic. Heterogeneous morphologies include stable or fragmenting substrate and aerial mycelia; single or short chains of nonmotile spores on both the aerial and substrate mycelia; sporangial-like bodies not containing spores; and long chains of interwoven spores with motile spores at the tip. The peptidoglycan contains *meso*-DAP and is acetylated; many genera contain arabinose and galactose in their cell walls and whole cells, others do not. Rhamnose in combination with galactose in whole-cell hydrolysates appears to be diagnostic for some genera. Lipid profiles include mono-methyl-branched, straight-chain saturated and unsaturated, and hydroxy fatty acids and are genera specific; tetrahydrogenated menaquinones with 8, 9, or 10 isoprene units; phospholipid patterns II, III and IV are represented; mycolic acids are not present. The mol % G + C content of the DNA ranges from 64 to 79.

Glycomycetaceae

Glycomycetaceae (34) are aerobic, Gram-positive, non-acid-fast, and chemoorganotrophic, forming stable substrate mycelia and aerial mycelia that fragment into short chains of square-ended spores. The cell wall contains *meso*-DAP and glycine and N-glycolated muramic acid; the whole-cell sugar pattern is xylose and arabinose. The peptidoglycan is A1γ. Lipid profiles contain diphosphatidylglycerol and phosphatidylinositol; nitrogenous phospholipids are not found, nor are mycolic acids; tetra- and hexahydrogenated menaquinones with 10 isoprene units predominate. The mol % G + C content of the DNA is 71. The family contains only one genus, *Glycomyces*.

SCREENING ACTINOMYCETES FOR NATURAL PRODUCTS

Isolation from Natural Habitats

Studies have been performed (35–38) to discover appropriate conditions for isolating various groups of actinomycetes from natural habitats, thereby enhancing diversity and increasing the chances of discovering novel natural products. A testing paradigm was described by Horan (39) that evaluated the effect of soil type, media

Table 8. Chemotaxomic Characteristics of Members of the Families Streptosporangiaceae, Nocardiopsaceae, Thermomonosporaceae, Micromonosporaceae, Pseudonocardiaceae, and Glycomycetaceae

Family/genus	Diagnostic whole-cell sugars	Diagnostic cell-wall components[a]	Acyl type of muramic acid	Menaquinones	Phospholipid type	Fatty acid type[b]	mol % G+C
			Streptosporangiaceae				
Streptosporangium	Madurose	None	Acetyl	MK-9($H_{0,2,4}$)	IV	3c	69–71
Herbidospora	Madurose	None	Acetyl	MK-10($H_{2,4,6}$)	IV	3c	69–71
Microbispora	Madurose	None	Acetyl	MK-9($H_{0,2,4}$)	IV	3c	67–74
Microtetraspora	Madurose	None	Acetyl	MK-9($H_{0,2,4}$)	IV	3c	64–69
Planobispora	Madurose	None	Acetyl	MK-9($H_{0,2,4}$)	IV	3c	70–71
Planomonospora	Madurose	None	Acetyl	MK-9($H_{0,2,4}$)	IV	3c/a	72
			Nocardiopsaceae				
Nocardiopsis	None	None	Acetyl	MK-10($H_{4,6}$)	III	3d	64–69
			Thermomonosporaceae				
Thermomonospora	+/−Madurose	None	Acetyl	MK-9($H_{2,4,6,8}$)	I	3a/c	72
Actinomadura	Madurose	None	Acetyl	MK-9($H_{4,6,8}$)	I	3a	66–70
Spirillospora	Madurose	None	Acetyl	MK-9($H_{4,6}$)	I/II	3a	71–73
			Micromonosporaceae				
Micromonospora	Arabinose Xylose	OH-DAP Glycine	Glycolyl	MK-9(H_4) MK-10($H_{4,6}$) MK-12	II	3b	71–73
Actinoplanes	Arabinose Xylose +/−Galactose	OH-DAP Glycine	Glycolyl	MK-9(H_4) MK-10(H_4)	II	2d/2c	72–73
Catellatospora	Arabinose Xylose	OH-DAP Glycine 3-*O*-Methyl-rhamnose	Glycolyl	MK-10($H_{2,6}$) MK-9($H_{4,6}$)	III	2c	70.6 71.5
Couchioplanes	Arabinose Xylose Galactose	L-Lysine glycine Serine	Glycolyl	MK-9($H_{4,6}$)	II	2c	69.9 72.1
Catenuloplanes	Xylose +/−Galactose	L-Lysine Serine Glycine	Glycolyl	MK-9(H_8) MK-10(H_8)	III	2c	71–72
Dactylosporangium	Arabinose Xylose	Glycine	Glycolyl	MK-9($H_{2,6,8}$)	II	3b/2d	72–73
Pilimelia	Arabinose Xylose	Glycine	Glycolyl	MK-9($H_{2,4}$)	II	2d/2b	NR
Spirilliplanes	3-*O*-Methylmannose Xylose Galactose	Glycine	Glycolyl	MK-10(H_4)	II	2d	69
			Pseudonocardiaceae				
Pseudonocardia	Arabinose Galactose	Arabinose	Acetyl	MK-8(H_4)	III	3f/3e	68–79
Actinopolyspora	Arabinose Galactose Ribose	Arabinose Galactose	Acetyl	MK-9($H_{4,6}$)	III	2e/2c	64
Actinosynnema	None	None	Acetyl	MK-9($H_{4,6}$)	II	3d	71–73
Amycolatopsis	Arabinose Galactose	Arabinose Galactose	Acetyl	MK-9($H_{2,4}$)	II	3f	66–69
Kibdelosporangium	Arabinose Galactose tr-Madurose Rhamnose	Trace galactose	Acetyl	MK-9(H_4)	II	3f	66
Kutzneria	Galactose Rhamnose	None	Acetyl	MK-9(H_4)	II	3c/3e	70.3 70.7
Lentzea	None	None	Acetyl	MK-9($H_{0,2}$)	II	3d	68.6
Saccharomonospora	Arabinose Galactose	Arabinose Galactose	Acetyl	MK-9(H_4) MK-8(H_4)	II	2a	66–70

Table 8. Chemotaxomic Characteristics of Members of the Families Streptosporangiaceae, Nocardiopsaceae, Thermomonosporaceae, Micromonosporaceae, Pseudonocardiaceae, and Glycomycetaceae (*continued*)

Family/genus	Diagnostic whole-cell sugars	Diagnostic cell-wall components[a]	Acyl type of muramic acid	Menaquinones	Phospholipid type	Fatty acid type[b]	mol % G+C
Saccharopolyspora	Arabinose Galactose	Arabinose Galactose	Acetyl	MK-9($H_{2,4}$) MK-10(H_4)	III	3c	70–71.5
Saccharothrix	Galactose Rhamnose	None	Acetyl	MK-9(H_4)	II	3f	70–73
Streptoalloteichus	Galactose Rhamnose	Galactose	Acetyl	MK-9(H_6) MK-10(H_6)	II	NR	NR
Thermocrispum	Arabinose Trace galactose	None	Acetyl	MK-9(H_4)	II	3f	69–73
		Glycomycetaceae					
Glycomyces	Xylose Arabinose	Glycine	Glycolyl	MK-10($H_{2,4}$)	I	2c	71–73
		Genera of Uncertain Affiliation					
Actinobispora	Arabinose Galactose Xylose	None	Acetyl	MK-7(H_2) MK-9(H_2)	IV	NR	71
Actinocorallia	None	None	Acetyl	MK-9($H_{4,6}$)	II	1a	73
Actinokineosporia	Arabinose Galactose Rhamnose	Arabinose Galactose	Acetyl	MK-9(H_4)	II	3c	69–72
Planotetraspora	Arabinose Galactose Xylose Ribose	Glutamic acid	NR	NR	NR	NR	NR
Thermobispora	Madurose Galactose	None	Acetyl	MK-9($H_{0,2,4}$)	IV	3c	70

Note: NR, not reported.
[a]All organisms contain *meso*-DAP.
[b]Growth conditions may affect the profile (15).

constituents, and selective pressure on the isolation of actinomycetes. Resistance to antibiotics and physiological data, derived from taxonomic analysis of the various species of actinomycetes, formed the basis for the choice of selective pressures (antibiotics) and soil isolation media constituents. Soil samples were suspended in distilled water and serially diluted. The suspensions plated onto the surface of agar media containing various carbon and nitrogen sources and antibiotics, including the antifungal agent nystatin at 50 μg/mL. Resulting colonies were isolated to purity and identified microscopically to either genus or broad morphological group. Antibiotics in the agar medium had the most profound effect on the types of actinomycetes isolated, followed by soil type and media constituents. Novobiocin and spectinomycin at 20 μg/mL selectively enhanced the isolation of micromonosporae: up to 90% of isolates belonged to this group. Rifamycin (15 μg/mL), rosaramicin (10 μg/mL), everninomicin (10 μg/mL), and gentamicin (5 μg/mL) significantly reduced the streptomycete population, allowing diverse, *meso*-DAP containing actinomycetes to proliferate. Pretreatment of the soil sample, particularly air drying for 48 hours before plating, and rifamycin in the agar positively affected the isolation of nocardioform (fragmenting aerial and substrate mycelia) actinomycetes. Table 9 summarizes selective isolation techniques for non-streptomycete actinomycetes.

Growth and Fermentation of Isolates

Organisms are isolated from soil plates using sterile toothpicks, streaked onto the surface of a rich medium, usually American Type Culture Collection (ATCC) medium 72 (53); and grown at 28 °C for 5 to 7 days. Isolated colonies are transferred to broth (ATCC medium 172) in 25-mm tubes containing 10 mL of media. After 3 to 5 days' incubation at 28 °C on a rotary shaker at 200 to 250 rpm, the tubes are removed. Sterile glycerol is added to a final concentration of 10%, and 3 mL aliquots are distributed into sterile vials. The contents of a frozen vial are used as the inoculum that initiates the fermentation process. One milliliter of a thawed suspension is added to 10 mL of germination medium in a 25-mm tube stoppered with a Morton closure, and the tube is incubated for 3 to 5 days at 28 °C and shaken (200 to 250 rpm) on rotary shaker. After incubation, 1 mL of the germination tube growth (G1) is transferred into 10 mL of fermentation medium in 25-mm tubes and incubated as above. For primary screening, large numbers of diverse actinomycetes should be fermented in me-

Table 9. Methods for the Isolation of Actinomycetes from Natural Habitats

Genus	Habitat	Method
Streptosporangium *Kurtzneria*	Soil, possibly slightly acidic	Air dry soil, plate on AV agar containing penicillin G (0.8 μg/mL) and/or polymyxin (4 μg/mL) or gentamicin (2–5 μg/mL) (38,40)
Microbispora and *Microtetraspora*	Soil	Air dry soil, dry heat 120 °C/h, treat with 1.5% phenol, plate on AV, MGA-SE, and HV agars alone or on minimal media with rubromycin or streptomycin without phenol treatment (9,41)
Dactylosporangium, *Planobispora*, *Planomonospora*, *Spirillospora*	Soil	Baiting using organic substrates including grass, centrifugation for motile spored organisms, and plating on egg white agar containing nystatin (50 μg/mL) (42–44)
Herbidospora	Soil and plant material	Plant samples desiccated at 28 °C for 1 week, ground in blender with water, suspension incorporated into yeast extract agar containing nystatin and cyclohexamide; pour plates incubated 28 °C >2 weeks (45)
Thermonomonospora	Soil, mesophiles; overheated substances, bagasse, compost, fodders and manure, thermophiles	Sample heated to 100 °C, dilution plate onto media containing rifamycin (12 μg/mL) and/or kanamycin (25 μg/mL) (8,35)
Actinomadura	Soil	Air dry soil, dilution plate on media containing rifamycin (15 μg/mL), mefoxitin (10 μg/mL), or gentamicin (2–5 μg/mL) (38,39)
Micromonospora	Soil, lake muds, sediments	Air dry soil, dilution plate on soluble starch-yeast extract agar plus novobiocin (20 μg/mL), spectinomycin (20 μg/mL), or gentamicin (5–50 μg/mL) (39)
Actinoplanes *Couchioplanes* *Dactylosporangium*	Soil, sediments	Air dry soil, dilution plate on water agar, colloidal chitin agar or HV agar containing 0.1% potassium tellurite (30), or novobiocin (25 μg/mL) (27), or baiting and centrifugation (42)
Pilimelia	Soil, rarely encountered	Baiting using hair (30)
Catenuloplanes	Soil	Dilution plating on starch-casein agar plus nalidixic acid (25 μg/mL), kanamycin (12.5 μg/mL), cefsulodin (5 μg/mL), and kabicidin (6.25 μg/mL) (46)
Spirilliplanes	Soil	Dry heat 120 °C/h, dilution plating onto HV agar (10)
Amycolatopsis	Soil	Dilution plate on AV agar plus vancomycin (1–10 μg/mL) and polymyxin B (5 U/mL) (38); some species isolated from human specimens (47)
Saccharomonospora	Soil, thermophilic strains isolated from leaf litter, manure, compost	Isolate using Anderson Sampler, sedimentation chamber with penicillin G and polymyxin (5 μg/mL) added to half-strength nutrient agar (35)
Saccharopolyspora	Soil and decaying plant material	Dilution plate on yeast extract (1 g/L), glucose (1 g/L), agar (15 g/L) plus novobiocin (5 μg/mL) (A. Horan, unpublished data)
Kibdelosporangium	Soil	Ampicillin (4 μg/mL) and nalidixic acid (10 μg/mL) in complex medium incubated at 43 °C (48)
Saccharothrix	Soil	AV or starch-casein agars plus penicillin G (5–10 μg/mL) and nalidixic acid (15 μg/mL) or starch-casein-nitrate agar plus rifamycin (10 μg/mL) (38,39)
Streptoalloteichus	Soil, arid	Dilution plate on ISP-2 or Bennett's agars plus gentamicin or kanamycin (10 μg/mL), incubate 43 °C (49)
Thermocrispum	Municipal waste and mushroom composts	Dilution plate and Anderson Sampler, TSA plus rifamycin (10 μg/mL), erythromycin and oleandomycin (100 μ/mL), novobiocin (15 μg/mL), 50 °C (50)
Glycomyces	Soil	Dilution plate on Czapek-sucrose agar plus novobiocin (25 μg/mL) and streptomycin (15 μg/mL) (30)
Actinocorallia	Soil	Dilution plate on colloidal chitin-vitamin agar plus kabicidin (10 μg/mL) (4)
Actinokineospora	Soil, fallen leaves	Dilution plates plus kanamycin and/or nalidixic acid (50 μg/mL) or baiting and centrifugation (5,51)

Note: Detailed selective procedures are not reported for the following general: *Nocardiopsis*, *Actinoploy spora* (not isolated from a natural habitat, appeared as a contaminant), *Catellatospora*, *Pseudonocardia*, *Actinobispora*, and *Planotetraspora*. *Lentzea* has been isolated from human specimens (52).
[a]All media contain nystatin at 50–100 μg/mL.

dia that support the production of a wide variety of secondary metabolites. More than one medium is often used, three to four are optimal. The fermentation is harvested after 4 to 6 days and can either be extracted with solvent (butanol, methyl isobutyl ketone, or ethyl acetate) or filtered (paper or 10,000 mw cutoff filters). The extract or filtrate is tested for secondary metabolite production using biological activity or chromatography. Primary fermentations of wild-type strains, under the conditions outlined, can yield from 0.01 μg/mL to as much as 400 μg/mL of

Table 10. Methods for the Production of Actinomycete Secondary Metabolites

Parameter	Example 1 (54): saccharocarcins by *Saccharothrix aerocolonigenes*	Example 2 (55): megalomicin by *Micromonospora megalomicea*
Germination medium (per liter)	Glucose, 10 g; trehalose, 10 g; hydrolyzed casein, 5 g; soy flour, 5 g; yeast extract, 5 g; calcium carbonate, 2 g; tap water	Dextrose, 1 g; potato starch, 24 g; beef extract, 3 g; tryptone, 5 g; yeast extract, 5 g; calcium carbonate, 2 g; tap water
Germination conditions	G1 48 hr at 28 °C, 250 rpm; G2 48 h at 28 °C, 250 rpm	G1 72 h at 35 °C, 300 rpm
% inoculum	10	5
Fermentation medium (per liter)	Dextrin, 30 g; molasses, 10 g; soluble starch, 5 g; tap water	Dextrose, 10 g; starch, 20 g; yeast extract, 5 g; casein hydrolysate, 5 g; calcium carbonate, 4 g; tap water
Fermentation conditions	5 days at 30 °C, 250 rpm	60–70 hr at 31 °C, 300 rpm
Extraction procedure	Whole broth with ethyl acetate	Adjust whole broth to pH 9.5 and extract with ethyl acetate

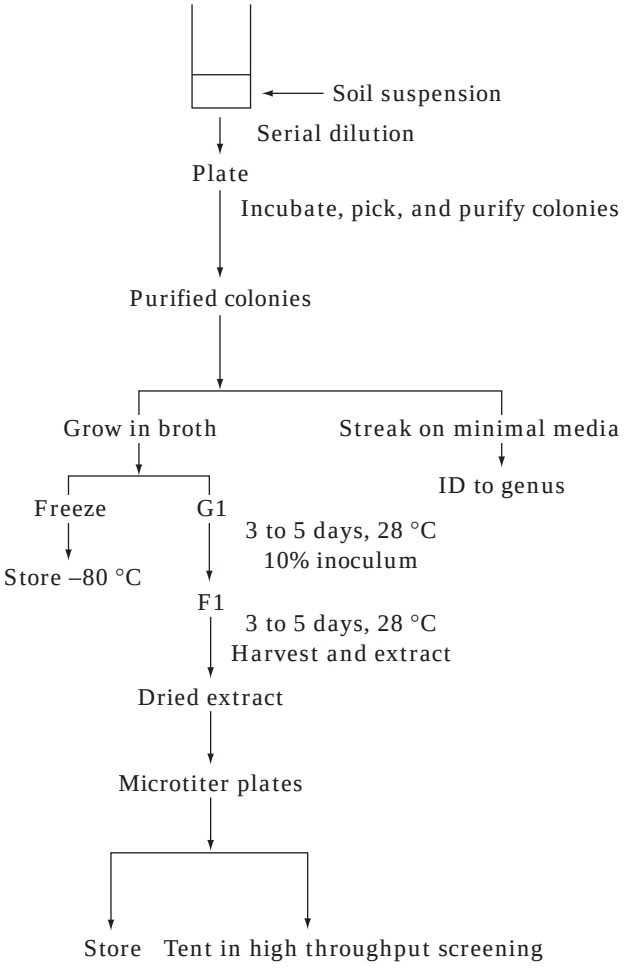

Figure 5. Outline of the primary screen process.

product. Examples of the production of secondary metabolites by two different genera of actinomycetes are presented in Table 10.

The advent of high throughput screening has resulted in a dramatic increase in the number of samples assayed, including natural products, with a concurrent decrease in the time required to test samples. In addition, an assay's lifetime has also decreased because all available samples can be tested in a relatively short time span (one month). For natural products to effectively compete with synthetic compounds and combinatorial libraries for available assay slots, a readily available source of samples is required. High throughput screening requires small amounts of test sample; a 10-mL fermentation results in enough extract for as many as 100 assays. Many natural product screening programs have addressed the issue of sample availability by developing libraries of extracts stored in 96-well microtiter plates. For each extract that is stored, the corresponding producing culture must also be preserved and its location catalogued. The nonstreptomycete actinomycetes described in this section can be stored at −80 °C in 10% glycerol for many years. However, data on the stability of natural product extracts stored over a period of years as well as the ability of preserved nonstreptomycete actinomycetes to maintain productivity have yet to appear in the literature. Figure 5 outlines the steps in a typical primary screen. Once activity has been detected in an extract or filtrate, the producing culture is fermented in a large enough volume to isolate enough material for characterization and structure elucidation. Many of the secondary metabolites produced by the *meso*-DAP containing actinomycetes are listed in Table 11.

SUMMARY

Nonstreptomycete actinomycetes continue to be a source of novel, therapeutically relevant natural products. Procedures described to effectively isolate a wide variety of genera rely on (*1*) collecting ecologically and geographically distinct soil samples, (*2*) using selective pressures (incorporating antibiotics and other chemicals into isolation media) that suppress streptomycetes while allowing diverse genera to survive, and (*3*) incorporating media constituents that favor the growth of rare actinomycetes. Evaluating the effectiveness of soil isolation procedures in obtaining diverse nonstreptomycete actinomycetes can quickly be achieved by identifying isolates macro- and microscopically. More definitive identification currently re-

Table 11. Secondary Metabolites Produced by *meso*-DAP-Containing Actinomycetes

Genus	Secondary metabolites[a]
Streptosporangium	Anthracyclines (figaroic acids, fragilomycins, carminomycin, carborubicin, sibiromycin; ansamycins (ansamitocin); bleomycins (platomycins, victomycin); glycopeptides (A-84575); macrolides (aculeximycin); peptides; phenazines; sugars (sporacuracins, 21906A); selenomycin; WS79089
Microbispora	Peptides (cochinmicins); phenazines; EV22 (SCH31828)
Microtetraspora	Amino acid containing (azaserine); talisomycin B; kistamicins; pyralomicins; macrolactam (fluvirucins); Bu-2313
Planobispora	Peptides; GE 2270
Planomonospora	Peptides (sporangiomycin); polyene
Thermomonospora	Naphthaquinone (SCH38519)
Actinomadura	Anthracyclines (akrobomycins, barminomycins, benanomicins, carminomycins, pradimicin, rubeomycins, rubstomycins); ansamycin (rifamycins); amino acid containing (madumycin); anthraquinones (oxanthromicin, maduramycin); indolocarabozole (AT2433); nucleosides (chloropentastatin, adenosine, coformycin, pentostatin); macrolactam (SCH38516, SCH38518, fluvirucin); macrocyclic lactone (kijanimicin); prodigiosins; polyethers (cationomycin, hidamicin, kijimycin); peptide related (formestin, luzopeptin, parvodicin), sugar containing (veractamycins, esperamicins); tetracyclin related (ES-119, SCH33256, SCH36969)
Spirillospora	Peptide macromolecular (Spirillomycin); polyene.
Micromonospora	Aminoglycosides (gentamicin, fortimicin, kanamycin, neomycin, sagamicin, sisomicin, verdamicin, G-52, G-418, Jl20); anthracyclines (daunorubicin, sibanomicin); anthraquinone (dynemicin); ansamycins (halomycins, rifamycins); benzodiazepine (sibanomicin); macrocyclic lactones (antlermicin, tetrocarcins); macrolides (clostomicin, erythromycin, juvenimicin, megalomicin, mycinamicin, izenamicin, rustmicin, primycin, rosaramicin); nucleosides (astromycin, dapiramicin); orthosomicins (everninomicins); peptides and amino acid containing (actinomycin, bottromycin, chalcidin, micromonosporin, 68-1147, glycine, negamicin); pigments (genistein, rubradirin, nocardiorubin); sugar containing (calicheamicin); xanthone (citreamicins); LL-E-19085
Actinoplanes	Glycopeptides (actaplanin, teicoplanin, ramoplanin); macrolides (lipiarmycin); peptides and amino acid containing (gardimycin, mycoplanecin, planothiocin, taitomycin, azetidine, azaserine, plauracins, virginiamycin, thristreptone); orthosomicin (SE737/74D); polyenes (octamycin, SE293); quinone (purpuromycin); chuangxinmycin; A/15104Y
Couchioplanes	Polyene (67-121)
Catenuloplanes	CP-54715
Dactylosporangium	Aminoglycosides (dactimicin, G-367); macrolides (clostomicin, tiacumin); orthosomicins (SF-2107); peptide containing (capreomycin, SF-2329); polyether (AC-7230, CP44161); quinone (DK-7814); tetracycline (SCH34164)
Pseudonocardia	Glycopeptides (azureomycins, boxazomycins, helvedardins); peptide (41043); polyene; quinones
Actinosynnema	Ansamycins (macbecins, C-33196); β-lactams (nocardicins)
Amycolatopsis	Ansamycins (rifamycins, kanglemycin); glycopeptides (avoparcin, vancomycin, orienticins, decaplanin, ristocetin, balhimycin); macrocyclic lactones (quartromycins); macrolides (A-59770); quinones (benzathrins, epoxyquinomicins, azicemicins); sugar (efrotomycin type); tetracycline (cetocycline); octacosamicins
Kibdelosporanglum	Glycopeptides (aridicins, kibdelins, decaplanin, A-80407); cycloviracins
Kutzneria	Chloramphenicol; glycoside macrolides (sporaviridins)
Saccharomonospora	Glycopeptide (AB-65)
Saccharopolyspora	Aminoglycosides (nebramycin, destomycin, saccharocin, sporaricin); alkaloids (hatomamicin); cinodines (coumamidines); lactones (belactins, nodusmicin); macrolides (erythromycin, sporeamicin); peptides (vanoxonin); CL307-24
Saccharothrix	Alkaloids (tetrazomine); glycopeptides (galacardins); indolocarbazoles (staurosporin, K-252a, rebeccamycins, SCH43228); macrolides (kayamycin, sekothrixide, N-814-103 factors); macrocyclic lactones (saccharocarcins); peptides (dopsisamine, madumycin, polynitroxin, nocamycin, sandramycin); polyether (portmicin); sugar (LL-C-19004); phosphonothrixin; karnamicins; tetrazomine
Streptoalloteichus	Aminoglycosides (kanamycins); bleomycins (talisomycins); siderochelin
Thermocrispum	Undescribed antifungal antibiotic (50)
Glycomyces	Amino acid containing (azaserine); LL-D05139
Actinocorallia	Peptide (azaserine related)

Note: Secondary metabolites not reported from *Herbidospora, Catellatospora, Pilimelia, Spirilliplanes, Actinopolyspora, Lentzea, Actinobispora*, and *Planotetraspora*.

[a]Data from Actinomycetes Antibiotic Data Base, Technomics Inc., C. P. O. Box 882, Tokyo, 00-91, Japan.

quires extensive chemical analysis of cell-wall and whole-cell components. Future identification of actinomycetes from natural habitats will rely on molecular approaches, particularly sequencing the gene encoding the small subunit of RNA (16S). This gene is a likely target because it is relatively small (1.5 kb), many actinomycete-type strains have been sequenced, and the data are readily available on-line for comparison to soil isolated, unknown strains. Numerous isolates can be fermented in small volumes. The fermentations are extracted or filtered, and the resulting samples are stored for testing against novel targets using high throughput screening methodologies. And so the quest for new metabolites with therapeutic potential from new organisms continues.

BIBLIOGRAPHY

1. M.P. Lechevalier and H.A. Lechevalier, in A.L. Demain and N.A. Solomon eds. *Biology of Industrial Microorganisms*, Benjamin/Cummins, Menlo Park, California, 1985, pp. 315–358.
2. E. Stackebrandt, F.A. Rainey, and N.L. Ward-Rainey, *Int. J. Syst. Bacteriol.* **47**, 479–491 (1997).
3. C. Jiang, L. Xu, Y. Yang, G. Guo, J. Ma, and Y. Liu, *Int. J. Syst. Bacteriol.* **41**, 526–528 (1991).
4. S. Iinuma, A. Yokota, T. Hasegawa, and T. Kanamaru, *Int. J. Syst. Bacteriol.* **44**, 230–234 (1994).
5. T. Hasegawa, *Actinomycetologica* **2**, 31–45 (1988).
6. H. Rumano, W. Guizhen, and L. Junying, *Int. J. Syst. Bacteriol.* **43**, 468–470 (1993).
7. Y. Wang, Z. Zhang, and J. Ruan, *Int. J. Syst. Bacteriol.* **46**, 933–938 (1996).
8. R.M. Kroppenstedt and M. Goodfellow, in A. Ballows, H.G. Trüper, M. Dworkin, W. Harder, K.H. Schleifer eds. *The Prokaryotes, Volume 2: A Handbook on the Biology of Bacteria: Ecophysiology, Isolation, Identification, Application*, 2nd ed., Springer-Verlag, New York, 1992, pp. 1085–1114.
9. M. Goodfellow, in A. Ballows, H.G. Trüper, M. Dworkin, W. Harder, K.H. Schleifer eds. *The Prokaryotes, Volume 2: A Handbook on the Biology of Bacteria: Ecophysiology, Isolation, Identification, Application*, 2nd ed., Springer-Verlag, New York, 1992, pp. 1115–1138.
10. T. Tamura, M. Hayakawa, and K. Hatano, *Int. J. Syst. Bacteriol.* **47**, 97–102 (1997).
11. M.P. Lechevalier, *J. Lab. Clin. Med.* **71**, 934–944 (1968).
12. M.P. Lechevalier and H.A. Lechevalier, *Int. J. Syst. Bacteriol.* **20**, 435–443 (1970).
13. H.A. Lechevalier and M.P. Lechevalier, in M.P. Starr, H. Stolp, H.G. Trüper, A. Balows, and H.G. Schlegel eds. *The Procaryotes: A Handbook on Habitats, Isolation and Identification of Bacteria*, Springer-Verlag, New York, 1981, pp. 1915–1922.
14. K.H. Schleifer and O. Kandler, *Bacteriol. Rev.* **36**, 407–477 (1972).
15. K. Suzuki, M. Goodfellow, and A.G. O'Donnell, in M. Goodfellow and A.G. O'Donnell eds. *Handbook of New Bacterial Systematics*, Academic Press, New York, 1993, pp. 195–238.
16. D.E. Minnikin and A.G. O'Donnell, in M. Goodfellow, M. Mordarski, and S.T. Williams eds. *The Biology of the Actinomycetes*, Academic Press, New York, 1984, pp. 337–388.
17. K. Uchida and K. Aida, *J. Gen. Appl. Microbiol.* **23**, 249–260 (1977).
18. K. Uchida and A. Seino, *Int. J. Syst. Bacteriol.* **47**, 182–190 (1997).
19. M.P. Lechevalier, A.C. Horan, and H.A. Lechevalier, *J. Bacteriol.* **105**, 313–318 (1971).
20. M.P. Lechevalier, C. DeBievre, and H.A. Lechevalier, *Biochem. Syst. Ecol.* **5**, 249–260 (1977).
21. M.D. Collins, in M. Goodfellow and D.F. Minnikin eds. *Chemical Methods in Bacterial Systematics*, Soc. for Applied Biotech., Tech. Series No. 20, Academic Press, London, 1985, pp. 267–287.
22. R.M. Kroppenstedt, in M. Goodfellow and D.F. Minnikin eds. *Chemical Methods in Bacterial Systematics*, Soc. for Applied Biotech., Tech. Series No. 20, Academic Press, London, 1985, pp. 173–199.
23. R.M. Kroppenstedt, in A. Ballows, H.G. Trüper, M. Dworkin, W. Harder, K.H. Schleifer eds. *The Prokaryotes, Volume 2: A Handbook on the Biology of Bacteria: Ecophysiology, Isolation, Identification, Application*, 2nd ed., Springer-Verlag, New York, 1992, pp. 1139–1156.
24. E.B. Shirling and D. Gottlieb, *Int. J. Syst. Bacteriol.* **16**, 313–340 (1966).
25. A.C. Horan and B.C. Brodsky, *Int. J. Syst. Bacteriol.* **32**, 195–200 (1982).
26. E. Stackebrandt and B.M. Goebel, *Int. J. Syst. Bacteriol.* **44**, 846–849 (1994).
27. M. Goodfellow, L.J. Stanton, K.E. Simpson, and D.E. Minnikin, *J. Gen. Microbiol.* **136**, 19–34 (1990).
28. J. Meyer, in S.T. Williams, M.E. Sharpe, and J.G. Holt eds. *Bergey's Manual of Systematic Bacteriology, Volume 4*, Williams & Wilkins, Baltimore, 1989, pp. 2562–2568.
29. F.A. Rainey, N. Ward-Rainey, R.M. Kroppenstedt, and E. Stackebrandt, *Int. J. Syst. Bacteriol.* **46**, 1088–1092 (1996).
30. G. Vobis, in A. Ballows, H.G. Trüper, M. Dworkin, W. Harder, K.H. Schleifer eds. *The Prokaryotes, Volume 2: A Handbook on the Biology of Bacteria: Ecophysiology, Isolation, Identification, Application*, Springer-Verlag, 2nd ed., New York, 1992, pp. 1029–1060.
31. C. Koch, R.M. Kroppenstedt, F.A. Rainey, and E. Stackebrandt, *Int. J. Syst. Bacteriol.* **46**, 765–768 (1996).
32. M.T. Embley, J. Smida, and E. Stackebrandt, *Syst. Appl. Microbiol.* **11**, 44–52 (1988).
33. M.T. Embley, in A. Ballows, H.G. Trüper, M. Dworkin, W. Harder, K.H. Schleifer eds. *The Prokaryotes, Volume 2: A Handbook on the Biology of Bacteria: Ecophysiology, Isolation, Identification, Application*, 2nd ed., Springer-Verlag, New York, 1992, pp. 996–1027.
34. D.P. Labeda, R.T. Testa, M.P. Lechevalier, and H.A. Lechevalier, *Int. J. Syst. Bacteriol.* **35**, 417–421 (1985).
35. T. Cross, in M.P. Starr, H. Stolp, H.G. Trüper, A. Balows, and H.G. Schlegel eds. *The Procaryotes: A Handbook on Habitats, Isolation and Identification of Bacteria*, Springer-Verlag, New York, 1981, pp. 2091–2102.
36. M. Goodfellow and S.T. Williams, *Ann. Rev. Microbiol.* **37**, 189–216 (1983).
37. S.T. Williams and E.M.H. Wellington, in J.D. Bu'lock, L.J. Nisbet, and D.J. Winstanley eds. *Bioactive Microbial Products: Search and Discovery*, Academic Press, London, 1982, pp. 9–26.
38. M.C. Shearer, *Dev. Ind. Microbiol.* **28**, 91–97 (1987).
39. A.C. Horan, in V.P. Gullo ed. *The Discovery of Natural Products with Therapeutic Potential*. Butterworth-Heinemann, Boston, 1994, pp. 3–30.
40. T.S. Whitham, M. Athalye, D.E. Minnikin, and M. Goodfellow, *Antonie Van Leeuwenhoek* **64**, 387–429 (1993).
41. M. Hayakawa and H. Nonomura, *J. Ferment. Technol.* **65**, 501–509 (1987).
42. C.E. Bland and J.N. Couch, in M.P. Starr, H. Stolp, H.G. Trüper, A. Balows, and H.G. Schlegel eds. *The Procaryotes: A Handbook on Habitats, Isolation and Identification of Bacteria*, Springer-Verlag, New York, 1981, pp. 2004–2010.
43. N.S. Makkar and T. Cross, *J. Appl. Bacteriol.* **52**, 209–218 (1982).
44. F.P. Mertz, *Int. J. Syst. Bacteriol.* **44**, 274–281 (1994).
45. T. Kudo, T. Ioth, S. Miyadoh, T. Shomura, and A. Seino, *Int. J. Syst. Bacteriol.* **43**, 319–328 (1993).
46. A. Yokota, T. Tamura, T. Hasegawa, and L.H. Huang, *Int. J. Syst. Bacteriol.* **43**, 805–812 (1993).
47. A.F. Yassin, B. Haggene, H. Budzikiewicz, and K.P. Schaal, *Int. J. Syst. Bacteriol.* **43**, 414–420 (1993).
48. K. Tomita, Y. Hoshino, and T. Miyaki, *Int. J. Syst. Bacteriol.* **43**, 297–301 (1993).
49. K. Tomita, in S.T. Williams, M.E. Sharpe, and J.G. Holt eds. *Bergey's Manual of Systematic Bacteriology, Volume 4*, Williams & Wilkins, Baltimore, 1989, pp. 2569–2572.

50. F. Korn-Wendisch, F. Rainey, R.M. Kroppenstedt, A. Kempf, A. Majazza, H.J. Kutzner, and E. Stackebrandt, *Int. J. Syst. Bacteriol.* **45**, 67–77 (1995).
51. T. Tamura, M. Hayakawa, H. Nonomura, A. Yokota, and K. Hatano, *Int. J. Syst. Bacteriol.* **45**, 371–378 (1995).
52. A.F. Yassin, F.A. Rainey, H. Brzezinka, K.D.-Jahnke, H. Weissbrodt, H. Budzikiewica, E. Stackebrandt, and K.P. Schaal, *Int. J. Syst. Bacteriol.* **45**, 357–363 (1995).
53. R. Gherna, P. Pienta, and R. Cote eds. *ATCC Catalogue of Bacteria and Bacteriophages*, 18th ed., American Type Culture Collection, Rockville, Md., 1992.
54. A.C. Horan, M.C. Shearer, V. Hegde, M.L. Beyazova, B.C. Brodsky, A. King, R. Berrie, K. Cardaci, and M. Nimeck, *J. Antibiot.* **50**, 119–125 (1997).
55. M.J. Weinstein, G.H. Wagman, J.A. Marguez, R.T. Testa, E.M. Oden, and J.A. Waitz, *J. Antiobiot.* **22**, 253–258 (1969).

See also CEPHALOSPORINS; FERMENTATION MONITORING, DESIGN AND OPTIMIZATION; MEDIUM FORMULATION AND DESIGN, *E. COLI* AND *BACILLUS* SPP.; METABOLITES, PRIMARY AND SECONDARY; MUTAGENESIS.

SECONDARY METABOLITES, ANTIBIOTICS

WILLIAM R. STROHL
Merck Research Laboratories
Rahway, New Jersey

KEY WORDS

Antibacterial drugs
Antibiotic drug discovery
Antibiotic markets
Antibiotic resistance
Anticancer drugs
Antifungal drugs
Beta-lactams
Macrolides
Natural products
Polyketides

OUTLINE

INTRODUCTION

Definition of Natural Product Antibiotics

The field of natural products owes its origins to the discovery of penicillin and its ability to kill bacteria. Since Fleming's original discovery in 1928 of the antibacterial effects of *Penicillium chrysogenum* and Flory and Chaim's efforts more than a decade later to bring that discovery to production, the field of natural products has undergone enormous changes.

Vuillemin first introduced the concept of antibiotic activity in 1889, using the term *influences antibiotiques* (antibiotic influences) to describe negative interactions between plants and animals (1). Waksman later coined the term *antibiotic* to describe "a chemical substance derived from microorganisms which has the capacity of inhibiting growth, and even destroying, other microorganisms in dilute solutions" (2). Natural product antibiotics are almost universally secondary metabolites, compounds generally produced at low growth rates or after growth has ceased, nonessential for growth of the producing organisms in pure culture, and typically possessing unusual structures not found in primary metabolites of central metabolism. Although natural product antibiotic biosynthesis is not essential to the producing organism in pure culture, these compounds are critical to the producing organisms in their natural environment, both for survival and competitive advantage (3).

In more recent years, the term *antibiotics* sometimes has been used more broadly to define anti-infective agents, essentially in line with Waksman's definition, as well as *bioactive natural products*. This latter group includes immunomodulatory agents, statins, antitumor drugs, antiparasitic compounds, insecticides, and other bioactive natural products, many of which also possess weak antibacterial or antifungal activities. Indeed, the immunosuppressive drug cyclosporin was originally discovered in an antifungal screening program. Additionally, the biosynthesis of bioactive antibiotics is often very similar to that of other bioactive natural products. As a result, cyclosporin, a weak antifungal antibiotic but an excellent immunosuppressive agent, is usually included in discussions of other peptide antibiotics. Similarly, when reviews are written about macrolide antibiotics, other bioactive natural products such as tacrolimus (formerly called FK-506) and rapamycin, both of which are immunosuppressive agents (4), are typically included in discussions with erythromycin, a bacteriostatic antibiotic; avermectin, a potent antiparasitic compound; and tylosin, an agricultural feed additive.

This certainly makes sense because all these bioactive natural products possess similar modes of biosynthesis.

An extensive table including all marketed antibiotics (both natural product-derived and chemosynthetic) as well as all other marketed bioactive natural products, as of December 1996, was recently compiled for the book entitled *Biotechnology of Antibiotics* (5). Additionally, a recent review by Shu (6) highlighted most of the recent important discoveries in the field of natural products, ranging from new antifungal activities to natural products active as neuromodulators. Thus, this review will focus on natural product anti-infective and antitumor agents.

Overview of the Natural Product Antibiotics Field

Cragg et al. (7) published in 1997 a well-cited review of the natural products field in which they analyzed the percentage of natural products in various fields. Of 520 new approved drugs between 1983 and 1994, 55.6% were chemically synthesized drugs, 24.4% were semisynthetic compounds, 5.8% were unmodified natural products, 8.8% were chemically synthesized drugs patterned after natural products, and 5.4% were "biologics" (e.g., recombinant proteins) (7). Thus, approximately 40% of all newly approved drugs over that period were derived from natural product leads. In breaking down the categories, however, natural products dominated the antibacterial markets (63% were derived from natural product leads) and the anticancer market, in which 61% of the new drugs were derived from natural product leads. Natural product leads also strongly contributed to the antihyperintensive market (48% were derived from natural product leads) and the anti-inflammatory market, in which one-third of the new drugs approved between 1983 and 1994 were derived from natural product leads. According to Cragg et al., however, natural products did not contribute in the period of 1983–1994 to newly approved drugs in the antifungal, analgesic, anxiolytic, antihistamine, antidepressant, cardiotonic, or hypnotic fields (7).

Strohl (5) conducted a similar analysis of bioactive natural products with antibiotic activities, identifying a list of 252 natural and synthetic compounds used clinically and agriculturally in the United States with selected compounds included from other countries. Thus, although this analysis was not all-inclusive, it represented the majority of commercially important antibiotics and antimetabolic drugs. Of those compounds identified, 75 (30%) were natural products, another 75 (30%) were semisynthetic compounds derived from natural products, and the remaining 40% were chemically synthesized compounds (5).

The discovery of new, novel natural products continues to rise dramatically (5). Based on an analysis of papers published in *Journal of Antibiotics*, Bérdy (8) indicated that about 11,900 antibiotics and bioactive natural products had been discovered through 1994, with increasing rates of discovery every year through 1990. He projected that the total of new, novel natural product structures discovered by the year 2000 would top 16,000 (8). The annual rate of new natural product descriptions published is now more than 500 per year, up from 200 to 300 per year 20 years ago (5,8). Nevertheless, there is the widespread perception in both the scientific literature and the popular press that the discovery of new natural products and natural product antibiotics is on the wane (5). This anomaly, however, can easily be explained. Because most new natural product drugs still are concentrated in the fields of anti-infectives and anticancer drugs, and natural product leads have been around long enough in both the anti-infectives and anticancer areas, the law of diminishing returns is most prevalent in these fields. For example, from 1962, when nalidixic acid was developed as the first quinolone antibiotic, to 1996, no new classes of clinical natural-product-derived antibacterials have been introduced to the market. In 1993, only one new natural product antibiotic was approved by the Food and Drug Administration for use in the United States, none in 1994, and only a few in 1995 and 1996. Overall, from 1980 to 1990, the worldwide discovery of more than 4,600 new bioactive natural products was published, yet only 20 new natural-product-derived drugs (3 natural products and 17 semisynthetic products) were commercialized in that period. Finally, in the period spanning from World War II to 1975, approximately 1.6% of all natural product antibiotics reported (either by publication or patent) were eventually commercialized. Since 1975, this number has dropped to about 0.11%. Thus, fewer antibiotics are being commercialized from an increasingly larger pool of isolated candidate compounds. These data suggest that the Golden Era of antibiotics, generally recognized as having begun shortly after World War II ended, lasted nearly 30 years before the law of diminishing returns caught up to it. Another major contributing factor for the dearth of commercialized natural product antibiotics from 1975 to the present is that the U.S. government, academic researchers, and pharmaceutical companies alike turned their efforts toward the defeat of cancer and heart disease, believing that infectious diseases were under control (5,9).

On the other hand, in pharmacological areas in which natural products are making new inroads, many discoveries of bioactive natural products have resulted in compounds that are still in preclinical or clinical trials. Since the late 1960s, Umezawa and colleagues in Japan showed interest in discovering non-anti-infective bioactive natural products, particularly in the area of protease inhibitors (10). Although researchers in U.S. pharmaceutical companies showed interest in developing natural products as bioactive molecules in areas other than the anti-infective and anticancer markets (i.e., whole cell assays), many viewed the Japanese mechanism-based assay approach more as a curiosity than a serious discovery effort. It was not until the publication of Merck's patent and paper in *Proceedings of the National Academy of Science* (11) in 1980 on lovastatin as a remarkable inhibitor of hydroxymethylglutaryl-CoA reductase, and ultimately an outstanding cholesterol-lowering drug, that the inclusion of natural products in mechanism-based screens was considered seriously.

Since that time much has changed, and although some pharmaceutical companies have minimized natural product screening efforts because of the perceived cost-to-benefit ratio, others have sought to expand the scope of natural products in their screening programs. As evi-

denced by publications in journals such as *Journal of Antibiotics*, patent applications, and clinical trial candidates (6), it has now become apparent that natural products can significantly augment synthetic chemical approaches for the discovery of new drug entities in a wide range of pharmacologically important areas. The two most significant recognized drawbacks of natural products in a broad-based screening program are the inclusion of crude extracts (which usually include salts, proteins, fatty acids and other potentially interfering materials) in in vitro assays (e.g., receptor-based, enzyme inhibition, or protein–protein interaction assays) and the time it takes to turn a crude-extract hit into a chemical structure. Despite these drawbacks, natural products now have been found to contribute to significant leads in most therapeutic areas (6).

The sources of natural products are also likely to change. Bérdy (8) showed that of the 11,900 antibiotics that had been discovered through 1994, approximately 6,600 (55%) were produced by *Streptomyces* spp. The remainder of producing organisms included the filamentous fungi, which produced 2,600 (22%); nonactinomycete bacteria, which produced 1,400 (12%); and non-*Streptomyces* strains of actinomycetes, which produced 1,300 (11%) (8). In the broader pharmacological field, it is widely recognized that a great percentage of pharmacologically derived products in use today are derived from or patterned after plant products (6). It can be expected that in the future a wider range of microorganisms, including well-known but underused groups such as the filamentous fungi, myxobacteria, bacilli, and pseudomonads, will contribute to the pool of natural products in larger ways (5).

Market for Natural Product Antibiotics

The total world sales for prescription pharmaceuticals was estimated in a September 1998 news release to be $308 billion. In a recent report of the 200 most-prescribed medicines in the United States (12), natural products accounted for 10 of the top 35 prescribed drugs (Table 1). All the top-prescribed natural products or semisynthetic drugs derived from natural products are anti-infective agents except for three statins: simvastatin, lovastatin and pravastatin. Although it is difficult to identify the entire contribution of natural products to the world pharmaceutical market economy, it should easily total more than $30 billion, including the natural-product-derived anti-infective agents (>$20 billion), the natural-product-derived anticancer agents (in which the anthracyclines and taxanes alone represent more than $3 billion in market size), the statins (with a market size estimated at more than $6 billion and rising at a rate of more than 20% annually), and the large pool of plant-derived natural products or compounds patterned after plant products.

The total world market for anti-infective agents in 1996 was reportedly $23 billion (13). The 1995 U.S. anti-infectives market alone was greater than $8 billion, with cephalosporins (45%), penicillins (15%), fluoroquinolones (11%), tetracyclines (6%), and macrolides (5%) comprising the majority of sales. Of these top-selling anti-infective agents, only the fluoroquinolones lack the distinction of being natural products, and even they are patterned after the original quinolone, nalidixic acid. Thus, in deference to their origins, antibacterial drugs are still natural products, semisynthetic compounds derived from fermentation products, or patterned after natural products.

The world antifungal market in 1995 was approximately $3 billion. Although this represents a much smaller market than the antibacterial market, the antifungal market is projected to grow at 20% annually. This rapid growth in antifungals unfortunately is driven by the dramatic increase in life-threatening fungal diseases, mostly as a result of opportunistic fungal pathogens infecting immunocompromised patients.

The antiviral market was $1.8 billion in 1995, and the projected 1998 market is $3 billion. Although the top product in 1995 was acyclovir (50% of the market [14]), more than 17 million people were infected with HIV, a number that is expected to reach 30 to 40 million by year 2000 (14). Because of the development of successful new anti-HIV drugs such as the HIV-proteinase inhibitors, it is expected that the antiviral market should increase substantially within the next few years.

Biogenesis of Natural Product Antibiotics

Since the discovery and elucidation of the structure of penicillin, there has been an enormous effort placed into finding new natural product antibiotics, particularly those of the antibacterial, antifungal, and anticancer therapeutic classes. Natural product antibiotics, for the most part, fall into several major classes of structures, as shown in Table 2, based on the precursors from which they are assembled and the mechanisms of assembly. Precursors common for the synthesis of natural products include short chain acyl-CoAs such as acetyl-CoA, malonyl-CoA, and propionyl-CoA, which are used to synthesize polyketides; activated amino acids, which are used to build peptides and β-lactams; various pyrimidines, which are the building blocks for nucleoside natural products; isoprene units, which form the basis of terpene, alkaloid, and substituted steroid natural products; and sugars and amino sugars, which are the building blocks for aminoglycosides as well as for the sugar moieties that decorate a wide variety of natural products. Many natural products result from the fusion of moieties arising from two or more different biogenic classes. For example, 6-deoxyerythronolide B (DEB), the macrolide backbone of erythromycin, is synthesized by a type I modular polyketide synthase, but the molecule is not biologically active until the sugars desosamine, attached at C-5, and cladinose, attached at C-3, are added. Several other macrolides, including spiromycin and tylosin, have this same characteristic. Similarly, anthracyclines are comprised of the aglycone portions, derived from the activity of a type II iterative polyketide synthase system, and daunosamine, a 2,3,6-trideoxy-3-aminohexose synthesized from TDP-glucose (15). Glycopeptides such as vancomycin also contain core units derived from the activity of a nonribosomal peptide synthetase that are decorated by sugar units to make bioactive molecules. An exaggerated example of this is the antifungal compound pradimicin, which is synthesized by a type II iterative polyketide synthase and then decorated both with sugar moi-

Table 1. Ranking of Natural Product Pharmaceuticals as Prescription Medicines in the United States (1997)

Natural product[a]	Brand name	Company	Rank[b]
Amoxicillin	Trimox	Apothecon	1
Azithromycin	Zithromax	Pfizer	9
Amoxicillin-clavulanate	Augmentin	SmithKline Beecham	14
Simvastatin	Zocor	Merck	15
Clarithromycin	Biaxin	Abbott	24
Amoxicillin	Amoxil	SmithKline Beecham	25
Cephalexin	Cephalexin	Teva	26
Penicillin V (K^+)	Veetids	Apothecon	32
Amoxicillin	Amoxicillin	Teva	33
Pravastatin	Pravachol	Bristol-Meyers Squibb	34
Cephalexin	Cephalexin	Apothecon	54
Lovastatin	Mevacor	Merck	57
Cefprozil	Cefzil	Bristol-Meyers Squibb	58
Cefuroxime	Ceftin	Glaxo Wellcome	72
Erythromycin	Ery-Tab	Abbott	82
Neomycin/polymyxin B/HC	Neomycin/polymyxin B/HC	Schein	122
Mupirocin	Bactroban	SmithKline Beecham	130
Cefaclor	Cefaclor	Mylan	139
Doxycycline	Doxycycline	Zenith	168
Amoxicillin	Amoxicillin	Warner-Chilcott	184
Clarithromycin	Biaxin suspension	Abbott	192
Cefixime	Suprax	Wyeth-Ayerst	196

[a]Includes both natural products and semisynthetic compounds derived from natural products.
[b]Ranking based on number of prescriptions sold.
Source: Data from Ref. 12.

eties and D-amino acid moieties (16). Other molecules, such as the rifamycins, contain a unique building block such as 3-amino-5-hydroxybenzoic acid (AHBA), which is used as the primer with which to initiate the synthesis of the macrocycle (17). Thus, many natural products are derived from mixed biogenic origins. For more detailed information on specific antibiotics, recent books edited by Vining and Stuttard (18) and by Strohl (19) cover the biogenesis and biosynthesis of virtually all the major classes of antibiotics and bioactive natural products.

ANTIBACTERIAL AGENTS

Introduction

The most widely prescribed, best known, best characterized, and perhaps also the most widely disparaged natural products are the antibacterials. After the discovery of penicillin by Fleming in 1928 and its subsequent development as a drug during World War II, the pharmaceutical industry and well-known academics such as Waksman of Rutgers University worked feverishly to discover new antibacterials that would eliminate bacterial infections of all kinds. The natural product antibiotics gramicidin (1939), streptomycin (1944), chlortetracycline (1948), chloramphenicol (1948), cephalosporin C (1948), neomycin (1949), oxytetracycline (1950), erythromycin (1952), tetracycline (1953), vancomycin (1955), rifamycins (1959), lincomycin (1962), pristinamycin (1962), and nalidixic acid (1962), the predecessor to fluoroquinolones, were all discovered by 1962 (22). No new, truly novel classes of natural product antibacterial drugs have been marketed since then. Even in the cases of modern synthetic antibacterials, all successful synthetic antibacterials have been biomimetically derived from natural product structures (the best example being the fluoroquinolones, which are based on nalidixic acid). There are new classes of candidate antibacterials, such as the oxazolidinones (23), which are not derived from natural products, but these have yet to break into the market, in part because of associated toxicities exhibited by this class of compounds. The targets for these drugs, including cell wall biosynthesis, protein biosynthesis, and nucleic acid biosynthesis, all have been targeted many times over by analogues of them, as well as by other compounds, both synthetic and naturally derived. As we enter the 21st century, there is a critical need for new, potent antibacterials to which resistance is not easily gained.

Needs and Markets

With the emergence of new infectious diseases as well as the emergence of bacterial strains resistant to existing antibiotics, there is an enormous challenge to pharmaceutical companies, researchers, and governments to develop new methods for treating existing infectious diseases and those emerging as new health threats. As recently reviewed by Strohl (5), there are several reasons for the need to develop new antibiotics, preferably with novel structures and activities.

First and foremost, pathogenic bacteria are acquiring or developing resistance to existing antibiotics and classes of antibiotics in direct correlation with the use of those antibiotics to treat them (24). As Julian Davies stated, "it is frightening to realize that one single base change in a gene encoding a bacterial β-lactamase can render useless $100 million worth of pharmaceutical research effort" (25). Although this is an oversimplification of the problem, it

Table 2. Biogenic Classes of Natural Product Antibiotics

Biogenic class and subclass[a]	Example compounds or groups	Example activities
	Nonribosomal peptide synthetases	
Diketopiperazines	Gliotoxin	Antibiotic
Cyclic peptides	Cyclosporin	Immunosuppressive
	Gramicidin	Antibacterial
Depsipeptide	Enniatin, valinomycin	Ionophores
Lipopeptides	Echinocandins	Antifungal
Glycopeptides	Vancomycin	Antibacterial
	Bleomycins	Antitumor
β-Lactams	Penicillins, cephalosporins	Antibacterial
Lantibiotic	Nisin	Antibacterial
Peptidolactones	Actinomycin D	Antitumor
Phosphinopeptide	Bialaphos	Phytotoxic
	Polyketides	
Type I modular		
Macrolides	Erythromycin, tylosin	Antibacterial
Pentacyclic lactones	Avermectin, milbemycin	Insecticidal acaricidal
Ascomycins	Tacrolimus	Immunosuppressive
Ansamycins	Rifamycin, ansatrienins	Tuberculostatic, antibacterial
Polyenes	Nystatin, amphotericin B	Antifungal
Polyethers	Monensin	Growth promotants
Type I iterative		
Statins	Lovastatin, pravastatin	Cholesterol-lowering
Type II iterative		
Tetracyclines	Oxytetracycline	Antibacterial
Anthracyclines	Doxorubicin, aclarubicin	Cytotoxic antitumor
	Aminoglycosides	
Aminoglycosides	Streptomycin, kanamycin	Antibacterial
Aminocyclitols	Spectinomycin	Antibacterial
Cyclitol	Kasugamycin	Antibacterial
	Isoprenoids	
Steroidal	Squalamine	Antitumor, antibacterial
Sesquiterpene	Artemisinin (Qinghao), epolone	Antimalarial
Diterpene	Paclitaxel (Taxol)	Antitumor
Triterpene	Fusidic acid	Antibacterial
Indole alkaloid	Vinblastine	Antitumor
	Others	
Lincosamides	Lincomycin, clindamycin	Antibacterial
Chorismic acid-derived	Chloramphenicol	Antibacterial
Amino acids	Cycloserine	Antibacterial
Quinolones	Nalidixic acid, fluoroquinolones	Antibacterial
Nucleosides	Nikkomycins, polyoxins	Antifungal
Mitosanes	Mitomycin C	Antitumor, cytotoxic
Oligosaccharides	Everninomycin, avilamycin	Antibacterials

Source: Data from Refs. 5, 18–21.

succinctly sums up the problem with the development of antibiotic resistance by pathogenic bacteria. The most critical reason for the development of new antibiotics is the race to remain a step ahead of antibiotic-resistance development, which has proceeded at an alarming rate (26). Even since the earliest use of antibacterial agents, the emergence of resistance to the drugs used has been observed. For example, within 4 years after the introduction of penicillin during World War II, several strains of penicillin-resistant bacteria were isolated from infected patients (27). After the war, outbreaks of dysentery in Japan, caused by sulfonamide-resistant *Shigella* spp., presented a serious health hazard to the recovering population. Within just a few years after introduction in 1950 of the newly developed antibiotics, streptomycin, tetracycline, and chloramphenicol to help quell the problem, resistance to each of these antibiotics was observed (28). By 1969, 69% of shigellae were resistant to sulfonamides, streptomycin, tetracycline, and chloramphenicol (28). Thus, in fewer than 20 years, nearly 70% of all *Shigella* spp. in Ja-

pan became resistant to four antibiotics to which there was minimal resistance before their use (28). Widespread antibiotic use has resulted in the rapid spread of multidrug resistant pathogens, and it has become both a local and global health hazard of epidemic proportions. The incidence of methicillin-resistant *Staphylococcus aureus* (MRSA), vancomycin-resistant enterococci (VRE; particularly by *Enterococcus faecium* and *Enterococcus faecalis*), and *β*-lactam-resistant *Streptococcus pneumoniae* are among the most serious problems, but are by no means the only ones (29). The incidence of nosocomial infections (i.e., hospital-acquired) is on the rise, and of those, an increasingly greater percentage of the infectious agents (typically MRSA and VRE) are drug-resistant (30). The U.S. Centers for Disease Control and Prevention (CDC) estimates that of the 40 million hospitalizations in the United States each year, 2 million patients (5%) contract nosocomial infections, and that as many as 58,000 of them (0.15%) die of them (31). Unfortunately, VRE are nearly untreatable with current antibiotics, with the possible exceptions of the experimental drugs Synercid or teichoplanin, which have been used successfully to treat some cases of VRE (32). The mortality rate of patients infected with multiple-drug resistant enterococci is 70%, making this a serious health care problem (32).

Second, new pathogens are evolving at an alarming rate. For example, today there are more than 30 new infectious diseases (e.g., AIDS, Ebola, Legionnaires disease, hantavirus, Lyme disease, and food-borne *E. coli* O157:H7 infections) that were unknown 20 years ago (5,33). Third, even with the development of remarkable anti-infective drugs with outstanding biological activities, there are still certain pathogens that naturally defy even the best efforts to defeat them. Perhaps the best example of this is our current inability to treat successfully *Pseudomonas aeruginosa* infections resulting from cystic fibrosis (5).

Finally, many potentially important antibiotics have associated toxicities that limit their use. The best example of this is gentamycin and other aminoglycosides, which are limited in effectiveness because of their associated nephrotoxicity and ototoxicity (5). Thus, critical challenges lay ahead for the entire anti-infectives field, many of which may be met by the discovery and development of new natural product leads.

There are three critical needs in the antibacterial market. First, new parenteral drugs that can successfully treat MRSAs and VREs are absolutely required. This need will grow dramatically in the coming years as the once-rare incidence of vancomycin-resistant *S. aureus* strains, the single greatest worry of infectious disease experts (34), expands. Second, even with a seemingly crowded pediatric market, there is still a critical need (and market place) for an orally absorbed, pediatric-safe (which eliminates fluoroquinolones, which are not considered safe for children) antibacterial agent that can successfully treat upper respiratory tract infections (primarily otitis media caused by *β*-lactam resistant streptococci, moraxellae, and *Haemophilus influenzae*) and that is not compromised by *β*-lactam, aminoglycoside, or MLS (macrolide-lincosamine-streptogramin) resistance or degraded by extended spectrum *β*-lactamases (35).

The pediatric antibacterial market, which has grown sharply since the early 1980s, has become one of the most important anti-infective markets today. Pediatric antibacterials typically are prescribed for middle-ear infections (otitis media) caused by *H. influenzae*, *Moraxella* spp., and *Streptococcus pneumoniae*. By the year 2000, it is expected that the U.S. pediatric market alone will be $2.2 billion, with annual increases of approximately 15%. The current leading pediatric antibacterials are amoxicillin, Augmentin (amoxicillin plus clavulanic acid), azithromycin, and clarithromycin. It is expected that the ketolides may make a significant impact on this market. The final critical need is for a new tuberculocidal drug. Antibiotic resistance in *Mycobacterium tuberculosis* is considered to be a major growing problem. Currently, a combination treatment with isoniazid and rifamycin (both tuberculostats) is the method of choice, but many strains of *M. tuberculosis* have recently been found that are resistant to one or both of these antibiotics, and approximately 14% of all tuberculosis cases reported today involve *M. tuberculosis* strains that are resistant to one or more antibiotics (36). The problem facing doctors today is that there is no proved, effective alternative yet on the market to treat isoniazid- and rifamycin-resistant *M. tuberculosis* (36).

Antibiotic-Resistant Bacteria

Antibiotic resistance is a major clinical problem that will only get worse with time. In the case of bacteria, resistance can be mediated by several different types of mechanisms, including modification of the target to make it unsusceptable to the antibiotic, enzymatic modification of the antibiotic to render it inactive, exclusion of the antibiotic by modification of membrane permeability, active export of the antibiotic, and bypass of the critical physiological mechanisms or structures inhibited by the antibiotic. Resistance to some these mechanisms, encoded by chromosomal mechanisms, is attained at a rate of 1×10^{-8}, and others are obtained at much higher frequencies through horizontal plasmid transfer.

Plasmid-encoded TEM- and SHV-type *β*-lactamases are the most common mechanisms responsible for *β*-lactam resistance in Gram-negative bacteria (37). These *β*-lactamases have generally broad substrate specificities for penicillins as well as some first- and second-generation cephalosporins and are responsible for much of the resistance to *β*-lactams observed in the clinics. It is well documented that as new *β*-lactams have been developed to resist plasmid-borne *β*-lactamases, the *β*-lactamases themselves have evolved (25,37). In an extraordinary example of natural directed evolution, TEM- and SHV-type *β*-lactamases recently have been found containing specific point mutations, all falling in close proximity to the active site cavity, which confer resistance to third-generation cephalosporins and monobactams (37).

Vancomycin has long been the last line of defense against antibiotic-resistant bacteria, particularly MRSAs and *β*-lactam- and aminoglycoside-resistant enterococci. Just a little over a decade ago, it was thought that microorganisms would never become vancomycin resistant because of its unusual mechanism of action (38). This illusion

was shattered, however, when VREs were reported in England and France in 1987 (39). VREs now are being discovered at an alarming rate, with no new last line of defense substitute firmly entrenched on the market (40).

Not all clinically significant antibiotic resistance is plasmid- or transposon-mediated. *S. pneumoniae*, the primary causative agent in pediatric otitis media and pneumonia as well as bacterial meningitis and bacteremia, remained sensitive to penicillin for many years. Recently, however, an alarming number of penicillin-resistant *S. pneumoniae* strains have recently been isolated from infected patients, correlating with the use of penicillins to treat them (41). These penicillin-resistant *S. pneumoniae* were not found to produce β-lactamases, the common plasmid-borne mechanism for resistance. Instead, they had incurred chromosomal mutations giving rise to altered penicillin-binding proteins (PBPs), the target for penicillin activity (41). This discovery has a touch of irony, because *S. pneumoniae* is the bacterium with which plasmid-mediated transformation was first observed. Similarly, the Oxford strain of *S. aureus*, isolated 50 years ago, is sensitive to nearly every antibiotic tested against it (42). The staphylococci, however, acquired resistance to aminoglycosides very quickly, and by 1992, 32% of *S. aureus* strains tested were found to be resistant to methicillin, the drug of choice to treat staphylococcal infections, up from 2% in 1975 (42). Like pneumococci, MRSAs have altered PBPs, giving them a resistance mechanism that cannot be countered easily. Thus, vancomycin has become the drug of last resort to treat MRSAs. Ever since *Enterococcus faecalis* was shown to transfer vancomycin resistance to *S. aureus* in the laboratory in 1992 (43), one of the greatest fears of health professionals universally has been the emergence of vancomycin-resistant, methicillin-resistant staphylococci (44). Recently, such doubly resistant, nearly untreatable strains have appeared in sporadic cases, confirming the greatest fears of infectious disease professionals (45).

A new mechanism of antibiotic resistance recently was discovered in meropenem-resistant *Pseudomonas aeruginosa* strains (46). *P. aeruginosa* is an opportunistic pathogen that contributes to nosocomial infections, eye infections, and opportunistic infections of burn patients and those with cystic fibrosis. The mechanism was found to be based on the alteration of outer membrane proteins, causing a reduction in permeability of several antibiotics, including meropenem, through the outer membrane (46). This is a significant finding, because carbapenems (e.g., imipenem) have been considered the antibiotics of choice for the treatment of opportunistic pseudomonads.

β-Lactams

As is well known, the discovery of penicillin was the genesis of modern pharmaceutical efforts to produce antibiotics, the magic bullets that at one time were thought to cure the world of disease. β-Lactams function by binding to PBPs, especially transpeptidases, that normally function in peptidoglycan biosynthesis. Because peptidoglycan is novel to bacteria, these drugs specifically act on a bacterial target. Since bacteria cannot grow in normal environments without their cell wall, inhibition of cell wall biosynthesis results in killing of the bacteria; thus, all β-lactams by definition are bacteriocidal drugs.

The total antibacterial market tops $20 billion annually, with nearly all the top-selling antibacterial drugs being natural products, semisynthetics derived from natural products, or compounds patterned after natural products. Even more than a half century after the first widespread use of penicillin during World War II to treat bacterial infections, β-lactams as a whole still make up 60%, or more than $12 billion worth, of the total antibacterial market. The commercial β-lactam antibiotics are comprised of many types of several different classes, ranging from penicillin G to the monobactam biomimetic drug, aztreonam (Table 3).

The natural product β-lactams can be separated into five separate biogenic subclasses (47): penams (e.g., penicillins), cephems (cephamycin C, cephalosporins), clavams (clavulanic acid, clavamycins), carbapenems (thienamycin), and monobactams (aztreonam) (Table 4). The ring structures of the various β-lactams differ from the classical penicillin core as follows: cephems have an expanded 6-membered ring containing a double-bond but retaining the sulfur atom; clavams have an oxygen atom replacing the sulfur of penicillins, and they tend to differ at C-2 and C-6; in carbapenems, the sulfur is replaced by a carbon and a double bond is present; and the monobactams are monocyclic (48).

β-Lactams of the penicillin, cephamycin, and cephalosporin subclasses share a common biogenic origin, i.e., the condensation of three activated amino acids, L-α-aminoadipate, L-cysteine, and L-valine by aminoadipyl-cysteinyl-valine (ACV) synthase (*pcbAB* gene products) to form the tripeptide δ-L-(α-aminoadipyl)-L-cysteinyl-D-valine (ACV), which is then cyclized by the enzyme isopencillin N (IPN) synthase (*pcbC* gene product) to form isopenicillin N (49). ACV synthases comprise a subset of a larger class of nonribosomal peptide synthases, which have been characterized in detail, both biochemically and molecularly (49,50). Both ACV synthases (49,50) and IPN synthases (49) of all β-lactam producers are highly conserved, indicating common ancestral origins. IPN is either directly converted to penicillin G via IPN acyltransferase (*penDE* gene product), or via IPN epimerase (*cefD* gene product) to penicillin N, which is converted via deacetoxycephalosporin C (DAOC) synthase (*cefE* gene product; also called expandase because it expands the 5-membered ring of penicillins to the 6-membered ring of cephalosporins) to deacetoxycephalosporin C (DAOC) (49).

The clavam β-lactamase inhibitor, clavulanic acid, is produced by *Streptomyces clavuligerus*, which also produces cephamycins (49). Interestingly, the biogenesis of the bicyclic nucleus of clavulanic acid occurs via a completely different mechanism than does the biosynthesis of other β-lactams (49,51). In *S. clavuligerus*, the clavulanic acid biosynthesis genes are just downstream of the cephamycin C biosynthesis genes (51).

Not all β-lactam-producing taxonomic groups of organisms synthesize all subclasses of β-lactams, as depicted in Table 4. Filamentous fungi, for example, produce β-lactams only of the penam and cephem classes, whereas various actinomycetes produce β-lactams of all subclasses

Table 3. Important Clinical and Experimental β-Lactams

Subclass	Drugs on market[a]
Penicillins	Ampicillin, *amoxicillin*, bacampicillin, cloxacillin, floxacillin, mezlocillin, nafcillin, oxacillin, penicillin G, penicillin V
Penicillinase-resistant penicillins	*Methicillin*, dicloxacillin
Antipseudomonal penicillins	Carbenicillin indanyl, piperacillin, *ticarcillin*
First-generation cephalosporins	Cefadroxil, cefazolin, *cephalexin*, cephalothin, cephapirin, cephradine
Second-generation cephalosporins	*Cefaclor*, cefmetazole, cefonicid, cefotetan, *cefuroxime*
Third-generation cephalosporins	Cefamandole, *cefixime*, cefoperazone, cefotaxime, cefpodoxime proxetil, *cefprozil*, ceftazidime, *ceftibuten*, ceftizoxime, ceftriaxone
Oxycephams (third generation)	Flomoxef, latamoxef
Fourth-generation cephalosporins	*Cefepime*
Cefam	*Cefoxitin*
Carbacefem	*Loracarbef*
Carbapenems	*Imipemen/cilistatin*, meropenem, MK-826, panipenem (Japan only)
Monobactams	Aztreonam
Clavams (β-lactamase inhibitors)	*Clavulanate*, sulbactam, tazobactam
Penicillins/β-lactamase inhibitors	*amoxicillin/clavulanate (Augmentin*), ampicillin/sulbactam (Unasyn), pipericillin/tazobactam (Zosyn), ticarcillin/clavulante (Timentin)

[a]Compounds in italics are most important commercial antibiotics.

Table 4. Biogenic Classes of β-Lactams

		β-Lactams produced by[a]		
Subclass	Example compounds	Fungi	G^+ bacteria	G^- bacteria
Penams	Penicillin G	*Penicillium, Aspergillus*	—	—
Cephems	Cephalosporin C	*Cephalosporium*	—	—
	DAOC[b]	—	—	Various strains
	Cephabacins	—	—	*Lysobacter*
	Cephamycin C	—	*Streptomyces, Nocardia*	—
Carbapenems	Thienamycin	—	*Streptomyces cattleya*	*Serratia, Erwinia*
Monobactams	Aztreonam[c]	—	*Nocardia*	*Pseudomonas*
Clavams	Clavulanic acid	—	*Streptomyces*	—
	Clavamycins	—	*Streptomyces*	—

Note: See Cohen and Aharonowitz (47) for more information. Dash means not produced by this group.
[a]Example taxonomic groups are given by genus names rather than an exhaustive listing of producing organisms.
[b]DAOC = deacetoxycephalosporin C.
[c]Example given is the biomimetic synthetic compound of the class.

except the penams and cephalosporins of the cephem subclass. The cephems in general are produced by the taxonomically widest range of microorganisms, including filamentous fungi, Gram-negative bacteria (e.g., lysobacters), and actinomycetes. The cephem products accumulated by each group differs, however, likely indicating evolutionary branches in terms of enzymes present. The Gram-negative bacteria, *Flavobacterium* sp. SC 12.154 and *Lysobacter lactamgenes* accumulate a 7-formylamino analogue of cephalosporin called cephabacin (49,52), an unusual natural β-lactam structure that is highly resistant to β-lactamases (49). The actinomycetes *Streptomyces clavuligerus* and *Nocardia lactamdurans* produce cephamycin C, which is formed from DAOC by the enzymes (gene names in parentheses) DAOC hydroxylase (*cefF*), deacetylcephalosporin C (DAC) *O*-carbamoyltransferase (*cmcH*), cephalosporin 7-α-hydroxylase (*cmcI*), and 7-α-hydroxy-*O*-carbamoyldeacetoxycephalosporin C methyltransferase (*cmcJ*) (49). The filamentous fungus, *Cephalosporium acremonium*, on the other hand, converts DAOC to cephalosporin C in two steps: DAOC hydroxylase (*cefF*), and DAC acetyltransferase (*cefG*) (49).

As is well known, penicillin was the first widely used clinical antibiotic. The first oral penicillin, used primarily to treat Gram-positive bacteria, was the fermentation product phenoxymethylpenicillin (penicillin V), still sold today under the name Veetids (5). Second-generation penicillins include the aminopenicillin group of ampicillin, amoxicillin, and bacampicillin, which exhibited much better gastrointestinal tract absorption and possess longer half lives. These aminopenicillins also exhibit greater activity against Gram-negative bacteria at the expense of activity against Gram-positives. Unfortunately, these penicillins are highly susceptible to β-lactamases. Development of β-lactamase inhibitors such as clavulanic acid, sulbactam, and tazobactam, however, have greatly extended the use of these broad-spectrum penicillins (47,49). In fact, Augmentin (oral amoxicillin/clavulanic acid), Unasyn (injectable ampicillin/sulbactam), Timentin (injectable ticarcillin/clavulanic acid), and Zosyn (injectable pipericillin/ta-

zobactam) are widely used antibiotics. Carbenicillin indanyl, the first oral antipseudomonal β-lactam, and ticarcillin, a potent parenterally administered drug, are third-generation penicillins (53). The development of antipseudomonal fluoroquinolones, however, has rendered carbenicillin indanyl obsolete. Pipericillin, azlocillin, and mezlocillin are parenteral fourth-generation penicillins that have not found wide usage clinically (53).

First-generation cephalosporins typically inhibited Gram-positive bacteria other than the enterococci. Second- and third-generation cephalosporins typically inhibit Gram-negative bacteria at the expense of activity against Gram-positives. A new fourth-generation parenteral cephalosporin, cefepime (Maxipime), possesses activity against both Gram-positives and Gram-negatives (54). Additionally, cefipime penetrates bacteria well, is not susceptible to β-lactamases, and has a lower propensity to induce β-lactamases (55). Unfortunately, this broad-spectrum cephalosporin does not effectively treat either VREs or MRSAs (54). Ceftriaxone was very recently approved as a one-time-only injectable for treatment of pediatric otitis media. The concept behind the development of this drug is that the greatest problem, and reason for failure, with treatment of otitis media is patient compliance; the option of a one-time-only injectable removes this as an obstacle.

Carbapenems are very broad spectrum, β-lactamase-resistant β-lactams that contain a carbon atom instead of a sulfur atom in the 5-membered ring (47). Imipenem/cilistatin (Primaxin) was the first clinical carbapenem antibiotic, developed in the mid-1970s and made available commercially since 1986, as a synthetic biomimetic analogue of the natural product thienemycin (56). Imipenem is administered with cilistatin, an inhibitor of human renal dehydropeptidase, to protect the antibiotic from enzymatic degradation. Imipenem has broad-spectrum activity against Gram-negatives and anaerobic bacteria and moderate activity against Gram-positive bacteria (53). Unfortunately, imipenem also is limited by potential renal toxicity (56). Meropenem (Merrem) (57) is a new carbapenem antibiotic approved in 1996 for use as a broad-spectrum injectable antibiotic for treatment of intra-abdominal infections and for pediatric bacterial meningitis. The advantage of meropenem over imipenem is that meropenem is stable in the presence of renal dehydropeptidase, thereby bypassing the need for cotherapy with cilistatin (53). A third carbapenem called panipenem is available in Japan but not in the United States (58). Merck currently has a new, very potent, broad-spectrum, long-acting carbapenem, MK-826, in phase-II clinical trials (59). This new carbapenem drug candidate has been demonstrated to be highly resistant to β-lactamases, including plasmid-encoded extended spectrum β-lactamases (ESBLs) (59). Nevertheless, certain rarely pathogenic bacteria (particularly *Acinetobacter baumannii*) contain specific carbapenem-degrading enzymes known as carbapenemases (60), which may, through horizontal gene transfer, enter the broader pathogen field in the future.

An interesting new parenteral β-lactam drug candidate has recently been described. The new Glaxo-Wellcome experimental compound, GV129606, called a trinem, is a highly potent antibacterial with efficacy against Gram-positives, Gram-negatives, aerobes and anaerobes alike, plus marked resistance to extended spectrum, clinically relevant β-lactamases (61). This compound may mark a new path to be followed in the β-lactam field.

Macrolides

The macrolide antibiotics are a group of compounds produced by actinomycetes via type I modular polyketide synthases (62). The core aglycone of the prototype macrolide, erythromycin, is synthesized by the huge multifunctional enzyme, 6-deoxyerythronolide B synthase (DEBS), which consists of three, multidomain subunits, each subunit with a molecular weight around 300,000 Da. The macrolide chain is synthesized by a set of enzymatic functional domains within the proteins in a linear, stepwise fashion. Interestingly, the enzymatic active sites are arranged in the polypeptides in the same order as their apparent function (62).

Although macrolides theoretically can have ring sizes ranging from as few as 6-membered to over 30-membered, most of the clinically relevant macrolides possess 14-membered or 16-membered rings (Table 5). Current clinical antibacterial macrolides are mostly derived from erythromycin, although a wide variety of biologically active macrolides are used for several purposes across several therapeutic areas (Tables 5 and 6).

The macrolide antibiotic, erythromycin, was first discovered in 1952, the year the double-helical structure of DNA was first announced. Macrolides, which are bacteriostatic agents, inhibit bacterial protein synthesis by structure-based mechanisms: 14-membered macrolides such as erythromycin block translocation of peptidyl-tRNA, whereas 16-membered macrolides inhibit peptidyl-transfer reactions (64). There are apparently additional interactions of macrolides of both groups with ribosomes, but even after 30 years of research, these are not fully understood (64). Resistance to macrolides is most often via the MLS resistance mechanism, which is based on mechanism of action. MLS resistance, conferred by several different genes, results in methylation of adenosine-2058 of 23S rRNA. MLS-I resistance, exemplified by the *tlrD* gene, is result of monomethylation, whereas MLS-II (*ermE* -type) is the result of dimethylation (65).

Erythromycin itself is a poorly soluble, acid-labile molecule that nevertheless has enjoyed a long history of successful use. Erythromycin has been an important orally active antibiotic for many years. The efforts for years in the macrolide field have been aimed at developing new drugs that are acid-stable, possess a longer half-life, have broader ranges of activity, and are not subject to MLS resistance mechanisms. Recently, several semisynthetic macrolides arising from modifications of erythromycin, including clarithromycin (Biaxin) the 15-membered azalide, azithromycin (Zithromax), and most recently, dirithromycin (Dynabac), have made significant contributions to the antibacterials market. Among them, these macrolides represent more than $2 billion in market share.

The most exciting research area in antibacterials today may be the discovery of ketolides, erythromycin-analogue macrolides in which the L-cladinose at the 3-position of

Table 5. Clinical and Experimental Macrolides of Interest as Sorted by Ring Size

Compounds	Ring size	Comments
Spinosad (spinosyns)	12	New insecticidal (esp. against lepidopterans) drugs from Dow AgroSciences
Methymycin	12	Antibacterial; produced by same PKS and gene cluster as picromycin (63)
Clarithromycin	14	Biaxin; 6-*O*-methylerythromycin; acid stable form available in 1-day dosing
Dirithromycin	14	Dynabac; approved in 1995 as orally available, single dose/day formulation
Erythromycin A	14	Original 14-membered macrolide antibacterial agent
Flurithramycin	14	8-Fluoro-erythromycin
Galbonolides	14	Group of 14-membered antifungal macrolides
Ketolides	14	HMR3004 and HMR3647 are new, experimental, 3-oxo-semisynthetic macrolides
Oleandomycin	14	Antibacterial compound used as agricultural feed additive
Picromycin	14	Synthesized from same PKS and gene cluster as methymycin (63)
Roxithramycin	14	9-[*O*]-(2-Methoxyethoxy)methyloxime] derivative of erythromycin
Rustmicin	14	Experimental 14-membered ring antifungal agent of the galbonolide group
Troleandomycin	14	Acid-stable acetylated ester of oleandomycin; antibacterial
Azithramycin	15	Zithromax; Orally active azalide; semisynthetic analogue of erythromycin
Avermectin	16	Veterinary use; also use to treat human onchocerciasis (river blindness)
Doramectin	16	Mutational biosynthetic analogue of avermectin; antiparasitic
Epothilone	16	Experimental myxobacterial antitumor drug; targets microtubule formation
Ivermectin	16	Semisynthetic analogue of natural product avermectin; antiparasitic
Josamycin	16	Used in both human and veterinary treatments
Midecamycin A_1	16	Antibacterial agent
Milbemycin	16	Used in Europe as antiparasitic agent
Miocamycin	16	Acetylated ester of midecamycin gives oral bioavailability
Rokitamycin	16	Propionyl ester of leucomycin A5; active against macrolide-resistant Gram-positives
Spiramycin	16	Used in France as antibacterial agent
Tylosin	16	Veterinary use as antibacterial feed additive
Soraphen	18	Myxobacterial macrolide patented as an agricultural antifungal agent
Ascomycin	23	Also called FK-520 and immunomycin; immunosuppressive compound
Tacrolimus (FK-506)	23	Immunosuppressive agent
Rapamycin	31	Immunosuppressive agent

erythromycin has been replaced by a keto moiety. The ketolides are particularly interesting because they do not induce MLS-resistance mechanisms in pathogenic organisms. This is critical because MLS resistance is typically not constitutive. The two leading ketolide drug candidates, RU64004 (also known as HMR 3004) and RU66647 (also known as HMR 3647), have been shown to be potent inhibitors of Gram-positive bacteria, particularly the pneumococci, including those that show marked resistance to other macrolides such as erythromycin and azithromycin (66). The ketolides, however, show poor activity against Gram-negative bacteria.

Recently, a series of new, 14-membered macrolide antifungal compounds known collectively as galbonolides was discovered (67), of which one, rustmicin, has been investigated in more detail (68). The data indicate that rustmicin and, by extension, possibly the other galbonolides appear to interact with the α-mannan of the cell wall by a potentially novel mode of action (68). Several years ago, interest was sparked when a macrolide known as FK506 (Tacrolimus) was found to possess significant immunosuppressive action (69). Additional compounds of interest in this area included rapamycin, which is expected to be approved soon, and immunomycin, which was dropped because of a narrow efficacy-to-toxicity window (69). Both the milbemycins and avermectins have been used for several years as antiparasitic drugs (70). Ivermectin has been used and approved to treat human diseases such as river blindness and intestinal threadworm. Additionally, macrolides such as tylosin have long been important as animal-feed additive growth promotants in the agricultural area (71).

During the past few years, interest in macrolides as bioactive natural products has grown significantly in areas other than the anti-infective area. As shown in Table 6, there currently is active experimental interest in macrolides in multiple therapeutic areas, including antibacterial, antifungal, antiparasitic, anticancer, immunosuppressive, neuroimmunophilin, gastrointestinal, respiratory, and agricultural areas.

There are five human therapeutic areas in which macrolides have not been used clinically, but in which there is currently considerable interest. An acid-catalyzed breakdown product of erythromycin, called motilide, has been shown to be a potent agonist of the motilin receptor, but it is unstable. Abbott has the lead drug candidate in this area, ABT-229, a 12-deoxyerythromycin homologue possessing modification in the sugars, which is stable and has reasonably high potency (74). It has recently been demonstrated that tacrolimus (formerly FK506) and rapamycin possess additional activities other than those related to immunosuppression. Both tacrolimus and rapamycin have been demonstrated to promote neuron cell growth under conditions in which they can still bind the FK-binding protein in the absence of the second ligand (calcineurin or RAFT, respectively) (73). The macrolide, roxithramycin, currently an investigational drug for treatment of asthma (75), potentially has multiple modes of action for this indication, including inhibition of glycoconjugate secretion to

Table 6. Therapeutic Areas in which Macrolides Are Being Studied as Potential Bioactive Molecules

Therapeutic area	Example macrolides	Comments
Antibacterial	Erythromycin analogues	Traditional area of strength based on erythromycin (64)
Antifungal	Rustmicin, galbonolides	New activities of interest; interaction with mannans (67,68)
Antiparasitic	Avermectin, doramectin	Avermectin recently approved for human use in U.S. (70)
Anticancer	Epothilone	Tubulin stabilizer activity similar to Taxol (72)
Immunosuppressive	Tacrolimus, rapamycin	Substitutes for cyclosporin (69)
Neuroimmunophilin	Rapamycin and analogues	Stimulation of neuronal growth (73)
Motilin receptor	Motilide, ABT-229	Treatment of gastroesophageal reflux disorder (74)
Respiratory	Roxithramycin	Antiasthmatic by multiple potential mechanisms (75)
Agricultural	Tylosin	Antibacterial and growth promoting feed additive (71)

increase mucous clearance; clearance of *Chlamydia pneumoniae*, a possible causative or implicated agent in asthma; suppression of T-cell cytokines interleukins 2, 3, and 4; and inhibition of cholinergic neuroeffector transmission in airway smooth muscle cells. Finally, a macrolide produced by the myxobacterium, *Sorangium cellulosum*, was found to possess tubulin-stabilizing activity similar to Taxol (72), a $1 billion per year anticancer drug. Several companies and research laboratories have shown strong interest in trying to develop epothilone analogues as potential antitumor drugs.

Streptogramins

For more than 25 years, pristinamycin, a combination of two antibiotics, pristinamycin I_A (a peptidic macrolactone belonging to the streptogramin B group) and pristinamycin II_A (a polyunsaturated macrolactone belonging to the streptogramin group A) (76), has been used in Europe as a drug to combat severe infections caused by both Gram-positive and Gram-negative bacteria, without development of resistance against it (76). Each component of pristinamycin is bacteriostatic with poor efficacy, but the combination is bacteriocidal with good potency against a broad range of bacteria (76). The usefulness of pristinamycin, however, has been limited because of its poor solubility (77). In February 1996, however, Rhône-Poulenc Rhorer introduced Synercid, a new variation on pristinamycin. A mixture of the two water-soluble, semisynthetic streptogramins, quinupristin (RP57669) and dalfopristin (RP54476) (78), Synercid (RP 59500) is currently in phase III clinical trials worldwide and is currently available in the United States and Europe in an emergency-use program. More than 700 patients have received Synercid in this program. In one study, 70% of 115 patients with VRE infections were successfully treated (i.e., infection cleared) with Synercid (5). Synercid has been found to be bactericidal for most Gram-positive bacteria, but bacteriostatic for *Listeria monocytogenes* (78). In one study, 96% of all staphylococci tested were sensitive to Synercid in vitro (76), suggesting that this drug may become the "vancomycin of the future," a drug of last resort for use against severe bacterial infections. One hopeful aspect concerning Synercid is that it is unaffected by classical rRNA-methylase-conferred MLS resistance mechanisms, the most common resistance mechanisms found in staphylococci (79). Other MLS resistance mechanisms such as acetylation or hydrolysis of streptogramins still affect these compounds, however, so they are not completely impervious to bacterial resistance mechanisms (79). A recent study showed that Synercid at 2 μg/mL inhibited nearly 99% of vancomycin-resistant *E. faecium* clinical isolates tested in the United States (80), giving rise to hopes that Synercid will help to contain the growing VRE problem.

Tetracyclines

The tetracyclines are among the earliest of antibacterial antibiotics to be discovered, with chlortetracycline being discovered in 1948. The natural tetracyclines are produced by various species of actinomycetes; *Streptomyces aureofaciens* produces both chlortetracycline and tetracycline, the production of each which can be optimized by specific fermentation conditions (81), *Streptomyces rimosus* produces oxytetracyclines, and dactylocyclines are produced by *Dactylosporangium* spp. and *Actinomadura brunnea* (81).

Tetracyclines function as antibiotics by inhibiting protein translation, specifically by disrupting codon-anticodon interactions of tRNA and mRNA at the acceptor site of the ribosome. Because they inhibit protein synthesis, tetracyclines, like macrolides, are bacteriostatic. Tetracyclines are widely used not only in human health, but also in animal health programs; perhaps the widest current use of chlortetracycline and oxytetracycline is as prophylactic drugs in the fish husbandry industry (81).

Bacteria typically develop resistance to tetracyclines by acquiring a plasmid- and transposon-borne resistance gene (*tetA*) encoding an efflux pump (81). Thus, tetracycline resistance is one of the primary resistances observed as being transmitted horizontally among different groups of bacteria. Additionally, a second mechanism, mediated by TetM, gives resistance by inhibition of the interaction of the tetracyclines with the ribosome. This, unfortunately, has led to the diminution of use of the classical tetracyclines for most human health indications. Some of the more modern tetracyclines, such as minocycline, are important for treating MRSAs (81).

The most exciting advance in the tetracycline area has been the development of the glycylglycine tetracyclines (81). Two new semisynthetic glycylglycines, *N*,*N*-dimethylglycylamido-9-aminominocycline (DMG-MINNO) and 9-amino-6-demethyl-6-deoxytetracycline (DMG-DMDOT), have been developed by Lederle for their very broad spec-

trum of activity against Gram-positive, Gram-negative, aerobic, and anaerobic bacteria (54). Their spectrum includes, perhaps surprisingly, bacteria as widely disparate as mycoplasmas, MRSAs, VREs, *Neisseria* spp., *Haemophilus* spp., and *Moraxella* spp. Most importantly, glycylglycine tetracyclines bind the ribosome more tightly than traditional tetracyclines so that TetM, which mediates ribosomal resistance mechanism, cannot interfere with their activity, and they are not substrates for the TetA-mediated efflux mechanisms (81). Thus, there currently is no effective resistance mechanism yet known for these modified tetracyclines. For more information, Hunter and Hill (81) have recently described the tetracyclines in detail.

Glycopeptides

Vancomycin was first isolated in the early 1950s, making it another of the group of long-standing, well-known antibacterial drugs. For a long time, vancomycin was not used to a significant degree, but as the incidence of infections with drug-resistant organisms increased, the use for vancomycin became significantly greater. Because vancomycin is absorbed poorly by the gastrointestinal tract, it is rarely used as an oral drug. Instead, its primary use today comes as a parenteral drug as the last line of defense against many potentially lethal pathogenic bacteria, including MRSAs and antibiotic-resistant *Enterococcus faecium*. In 1987, however, after 30 years of vancomycin being on the market, resistant strains of *E. faecium* (VREs) were finally observed (39). The increased incidence of vancomycin resistance, especially in *S. aureus*, is of enormous concern (44).

Little more than a decade ago, resistance to vancomycin was unheard of and totally unsuspected, because its mechanism of action was so different from that of any other antibiotic class. Nevertheless, resistance to vancomycin and other glycopeptides was discovered and is on the rise. Vancomycin and other glycopeptides exert their activity by inhibiting peptidoglycan biosynthesis, making them potent bacteriocidal drugs. Peptidoglycan consists of a sugar backbone to which pentapeptide chains are attached. The terminal residues of the pentapeptide chain are D-alanine residues, which are critical to processing the peptidoglycan matrix as it is built. Vancomycin and other glycopeptides bind, through multiple hydrogen bonding, to the terminal D-alanine residue of the pentapeptide chain and prevent both transglycosylation and transpeptidation (82). Resistance occurs when a bacterium contains special genes (*vanAHXY*) that allow for incorporation of a D-lactic acid residue in place of the terminal D-alanine residue of the peptidoglycan pentapeptide chains, rendering the peptidoglycan unrecognizable to vancomycin binding. Two genetically distinct forms of resistance have emerged, although both operate by the same mechanism. VanA-mediated resistance gives high-level resistance to both vancomycin and teichoplanan, whereas VanB-mediated resistance is restricted to vancomycin (82). A recent study of clinical VRE isolates in the United States showed that 72% possessed the VanA phenotype, whereas only 28% possessed the VanB phenotype (80).

There are several relatively new analogues of vancomycin on the market to combat vancomycin resistance. Teichoplanan has been around for several years, but its use is restricted to Europe so far. Ramoplanan, another glycopeptide that has been around for a few years, is currently in phase II clinical trials at BioSearch Italia. Eli Lilly has developed a new chlorobiphenyl analogue of vancomycin, LY333328, that is considerably more potent than vancomycin (83). Moreover, LY333328 appears not only to inhibit bacterial growth, but to kill existing bacteria, which may give it a distinct clinical advantage over other existing antibiotics. LY333328 is very potent against VRE in vitro (84), giving hope for treatment of vancomycin-resistant pathogens.

Aminoglycosides

Aminoglycosides are not widely used in clinical therapy in the United States because of their relative toxicity profile as compared to other available antibacterials and to the rapid development of plasmid-borne resistance mechanisms through pathogen populations. Streptomycin and neomycin were first described in 1944 and 1949, respectively, so this group of antibacterials has a rich history. An incredible amount of knowledge about the biosynthesis, the genes, and the molecular mechanisms for regulation of aminoglycoside production is now known, and Piepersberg, the architect of much of this effort, has coalesced this enormous wealth of information in a recent review (85). One new aminoglycoside worth mentioning is the development in Japan of arbekacin, a new aminoglycoside that has potent activity against methicillin-, gentamycin- and tobramycin-resistant *S. aureus* strains (86). The incidence of methicillin-resistance in Japan has risen to nearly 60%, and only vancomycin and the newly developed arbekacin are approved for treatment of these strains. The new aminoglycoside is apparently effective because the widely distributed resistance mechanism, a bifunctional aminoglycoside phosphotransferase (APH[2″])-6′-acetyltransferase (AAC[6′]) which confers resistance to other aminoglycosides such as gentamycin and tobramycin, is relatively ineffective at modifying the new drug (86). It is probable that within a few years, APH(2″)-AAC(6′) will evolve so that it will be able to modify arbekacin.

Other Antibacterial Compounds and New Activities of Interest

Several new antibacterial drugs recently have been introduced to the market or in clinical trials that hold hope for containing the problems of newly emergent pathogens and increased resistance to existing drugs. Several of these are listed in Table 7. A comparison of the minimal inhibitory concentrations (MICs) to kill 90% of *S. pneumoniae* treated in vivo (MIC_{90}s, in μg/mL) was made of several of the new antibacterials with the following results (in order of efficacy) (87): ketolides (new macrolides containing keto groups at C-3), 0.016 to 0.25; everninomicins (novel oligoglycoside from marine organism), 0.06 to 0.25; glycylglycines (modified tetracyclines), 0.12 to 0.5; new fluoroquinolones (e.g., sparfloxacin and trovafloxacin), 0.12 to 0.5; oxazolidinones (new class of chemosynthesized antibacterials), 0.5 to 1.0; and new streptogramins (e.g., Synercid), 0.25 to 2.0. These can be compared to MIC_{90}s for the ex-

Table 7. Newly Approved and Experimental Antibacterial Agents

Compound or drug	Class[a]	Comments
Azithromycin	Azalide	New 15-membered macrolide containing a nitrogen in the ring; approved for pediatric use against otitis media
Trovafloxacin	Quinolone	New very broad-spectrum, high potency quinolone (Pfizer)
Mupirocin	Pseudomonic acid	The pseudomonad product, which inhibits bacterial isoleucyl tRNA synthetase, was recently approved in the U.S. as a topical drug
Cefepime	Cephalosporin	Fourth generation very broad spectrum cephalosporin; has potency of cefotaxime against Gram-positive bacteria and of ceftazidime against Gram-negative bacteria
Oxazolidinones	Chemically made	Two new oxazolidinones are being tested as potential broad-spectrum antibiotics for use against VRE and staphylococci (Upjohn)
Synercid	Streptogramins	Now in phase III clinical trials; combination of quinupristin (RP57669) and dalfopristin (RP54476), both semisynthetic streptogramins
Ziracin (SCH27899)	Everninomycin	Although discovered in 1979, everninomycins were not pursued because of their narrow spectrum; now Ziracin is a leading clinical candidate for treatment of VRE and staphylococci
PA 1648	Ansamycin	Rifampin-derivative being developed that has excellent activity against *Mycobacterium tuberculosis* and *M. avium–M. intracellulare* complex, the most common opportunistic bacteria infection of AIDS patients (PathoGenesis)
Meropenem	Carbapenem	New, safer penem with better activity against Gram-negative bacteria
Rifapentine	Ansamycin	FDA approved in 1998 for treatment of pulmonary tuberculosis
MK-826	Carbapenem	Long-acting, stable, broad-spectrum carbapenem now in phase II clinical trials (Merck)
Trinem	Novel β-lactam	New, broad-spectrum β-lactam being tested that is resistant to β-lactamases (Glaxo-Wellcome)
LY333328	Glycopeptide	New chlorobiphenyl vancomycin analogue with improved potency over vancomycin; currently in phase II clinical trials (Eli Lilly)

[a]Natural product class, except where noted.

isting drugs on various (and variably resistant) strains of *S. pneumoniae*: amoxicillin-clavulanate (Augmentin), 0.06 to 1.0; cefuroxime (semisynthetic cephalosporin), 0.12 to 2.0; cefpodoxime (semisynthetic cephalosporin), 0.25 to 2.0; and cefixime (semisynthetic cephalosporin), 0.5 to 16 (87). As important as MICs are a low MIC does not alone make a good drug. The other critical factor is the development of antibacterials that can be taken orally in once-per-day doses to increase patient compliance. Thus, the time for a particular drug dose to maintain in vivo efficacy above MIC ($T > MIC$) value is also critical to dial into the structure of newly developed drugs (87).

Most of the new antibacterials on the market are modified analogues of existing, well-known classes of antibacterials: azithromycin and clarithromycin, as well as the new experimental ketolides, are based on modifications to the erythromycin core structure; trovafloxacin and sparfloxacin are new fluoroquinolones; cefepime is a new cephalosporin; meropenem and MK-826 are new carbapenems; trinem is a novel β-lactam; LY33328 is a new glycopeptide; and Synercid is comprised of two new streptogramins. Only the oxazolidinones, a chemical synthesis class, represents a new, novel class of antibacterials.

Pharmacia-Upjohn is testing two new oxazolidinones for their ability to treat multiple-drug-resistant strains of *Mycobacterium tuberculosis* (23). These new chemically synthesized antibiotics inhibit protein synthesis in a manner different from natural product protein synthesis-inhibitory antibiotics, have novel structures unrelated to structures of other antibiotics, and have a wide spectrum of activity (23). Experiments have shown that, at least in in vitro tests, pathogens do not form resistance against these antibiotics at significant frequencies.

Mupirocin (Bactroban) was approved in 1997 by the U.S. FDA for use as a topical agent, especially against nasal MRSA. Mupirocin has been used in the U.K. since 1985 and is currently approved in 90 countries. Produced as pseudomonic acid by *Pseudomonas fluorescens*, mupirocin is interesting because of its novel mode of action; it inhibits bacterial protein synthesis specifically through its binding to isoleucyl tRNA synthetase (88). Unfortunately, mupirocin-resistant MRSA have emerged, which is not surprising since the target is a single enzyme.

Ziracin is an interesting, if still-evolving story. The everninomycins have been known since the early 1960s as bacterial protein synthesis inhibitors, but they have attracted little attention for many years (89). Ziracin, an aromatic moiety-containing oligosaccharide, was first isolated in 1979 from a marine actinomycete, *Micromonospora cabonacea* (89). At that time, the everninomycin was not pursued because of its relatively narrow spectrum of being potent against only Gram-positive bacteria. With the increased resistance of Gram-positive bacteria to existing drugs, interest in the everninomycin, Sch27899, was revived. Now, Sch27899 is in clinical development as a novel antibacterial. The problem is that a similar everninomycin, avilamycin (MaxusG), has been used for several years in the European Union as a feed additive in the agricultural market. Recently, avilamycin-resistant isolates of *E. faecium* have been found in broiler chickens that are cross-resistant to Ziracin (90). This discovery is of great concern, potentially cutting short the effectiveness, and certainly the life span, of Ziracin if it is ever marketed (90).

ANTIFUNGAL AGENTS

The need for new antifungal drugs has never been greater for a variety of reasons. Fungal infections fall into two ma-

jor categories, those that are localized, dermal, and mostly annoyances, such as ringworm, athlete's foot, and nail infections (onychomycoses), and those that are disseminated and life threatening. Life-threatening, disseminated fungal diseases have risen dramatically during the past few decades, making this an important area for new drug development. Typically, life-threatening fungal infections occur in patients with impaired defenses, such as patients with AIDS; with other debilitating diseases; who are under treatment with immunosuppressive drugs (usually after organ transplants, to prevent tissue rejection); who are receiving chemotherapy; or with severe burns. Additionally, with the potentially broader use of immunosuppressive drugs for other indications such as arthritis, the potential for fungal infections may be expanded.

The most important pathogenic fungi are *Candida albicans* (disseminated candidiasis), *Candida* spp., *Aspergillus fumigatus* (systemic aspergillosis), *Cryptococcus neoformans* (disseminated cryptococcosis leading to meningoencephalitis), *Pneumocystis carinii* (*P. carinii* pneumonia [PCP]), *Histoplasma capsulatum* (histoplasmosis), and *Coccidioides immitis*, the final example being a fungal pathogen very rich in chitin (91). The most important fungal pathogens associated with immunocompromised patients, such as those with AIDS or receiving immunosuppressive therapy, are *P. carinii*, *C. neoformans*, and *Candida* spp.

The current antifungal drugs and leading clinical candidates are listed in Table 8. Current potent antifungal drugs have problems that make them less than optimal for clinical use. For example, amphotericin B, the antifungal drug of choice in life-threatening cases, causes acute toxicity, resulting in it not being well tolerated in a large percentage of patients, although it is efficacious against PCP (92). Azoles (e.g., clotrimazole, fluconazole, ketoconazole), which target membrane ergosterol synthesis, are static in vitro; they stop fungi from growing but do not kill them. Such agents, which depend on the immune system to clear the existing fungal infection, are used in immunocompromised patients but, because they do not clear the infections, require lifelong therapy to prevent recurrence. Additionally, *Aspergillus* spp. are naturally resistant to azoles, preventing their use in typically aggressive systemic aspergillosis infections that result in high mortality rates. Finally, the incidence of azole-resistant fungi is increasing, particularly among *Candida* spp. such as *C. glabrata* and *C. krusei*.

Because most of the current antifungal drugs suffer from either toxicity (amphotericin B) or the limitations of being static in vitro and increasing resisted by target populations (azoles), there is a critical need for new antifungal agents that act against new targets. Azoles target lanosterol demethylase, a P450 enzyme involved in the synthesis of ergosterol (93), a sterol found in fungal cell membranes but not mammalian cell membranes. Antifungal polyenes, including amphotericin B, nystatin, candicidin, and faerifungin, also target the cell membrane of fungi, but in this case by the formation of transmembrane pores and other membrane-associated effects (94). Although polyene antifungal agents are typically fungicidal, they also are not generally well tolerated by a large majority of patients, making them drugs used as last resorts.

Drug resistance in fungi, which more closely resembles drug resistance in tumor cells, is inherently different from drug resistance in bacteria. First, there is no evidence for plasmid-borne drug resistance mechanisms in fungi, so resistance is limited to chromosomal and nontransferable resistance genotypes. Most fungal drug resistance is effected

Table 8. Clinical and Lead Experimental Antifungal Drugs

Antifungal drug	Type	Comments
Amphotericin B	Polyene (NP)	Clinical; broad-spectrum antifungal agent
Atovaquone	Substituted naphthoquinone (CS)	Clinical; used for *P. carinii* infections
Clotrimazole	Oral fluconazole (CS)	Clinical; for vaginal candidiasis and dermal use
Fluconazole	Bis-triazole (CS)	Clinical; Orally active, relatively broad spectrum
Flucytosine	Flurocytosine	Clinical; for cryptococcal meningitis and candidiasis
Itraconazole	Triazole (CS)	Clinical; used for histoplasmosis and blastomycosis
Ketoconazole	Triazole (CS)	Clinical; broad spectrum
LY303366	Lipopeptide echinocandin (NP)	Phase II clinical trials (Eli Lilly)
Miconazole	Azole (CS)	Clinical; oral, parenteral, and topical; broad spectrum
MK-0991	Lipopeptide pneumocandin (NP)	Phase III clinical trials (Merck); broad spectrum
Natamycin	Polyene (NP)	Clinical; for aphthalmic treatment
Nikkomycin Z	Nucleoside dipeptide (NP)	Phase I clinical trials; chitin synthesis inhibitor
Nystatin	Polyene (NP)	Clinical; orally active and broad spectrum
Pentamidine isethionate	Aromatic diamidine (NP)	Clinical; for *P. carinii* infections
Pradamycins	Benzonaphthacene quinone (NP)	Phase I clinical trials
Rustmicin	Macrolide (NP)	Unusual target; plasma protein interactions
Sordarin analogue	Unusual natural product (NP)	Experimental compound
Sulconazole nitrate	Imidazole (CS)	Clinical; for topical treatment
Sulfanilamide	Sulfonamide (CS)	Clinical; for topical vulvovaginitis
Terbinafine	Allylamine (CS)	Clinical (Lamisil); orally active; for nail fungal infections
Thiabendazole	Benzimidazole (CS)	Clinical; for treatment of worms and fungi
Trimetrexate	Diaminoquinazoline (CS)	Clinical; for treatment of *P. carinii*

Notes: This list may not represent all clinical or experimental antifungal drugs. Generic names are used. NP = natural product; CS = chemically synthesized.

by changes in membrane permeases, leading to exclusion of the drugs, induction of membrane-bound efflux mechanisms, modifications of activases required for the activation of some antifungal drugs into their active forms, and site-specific mutations of target enzymes. Degradation of antifungal drugs by target organisms (e.g., similar to the action of β-lactamases) or modification of antifungal drugs to inert forms (e.g., aminoglycoside phosphotransferases) has not been observed thus far.

With the sequencing of the entire *Saccharomyces cerevisiae* genome, a study was conducted to search for novel targets, unique to fungi or different enough in fungi, which might be used to develop new antifungal agents with novel mechanisms of action (95). Of 6,000 genes analyzed, only a dozen or so potential targets were identified, including chitin synthetase, β-1,4-glucan synthetase, tubulin, elongation factor 2,*N*-myristoyl transferase, acetyl-CoA carboxylase, inositol phosphoryl ceramide synthase, membrane ATPase, mannosyl transferase, tRNA synthetases, lanosterol dehydrogenase, lanosterol synthase, and squalene epoxidase.

The most widely considered new targets for fungicidal activity are all involved with cell wall biosynthesis or structure. Yeast cell walls, which make up 15 to 25% of the cell dry weight, are typically comprised of β-1,3- and β-1,6 glucan polymers (about 50%), α-mannan (highly glycosylated mannoproteins; about 50%), and chitin (about 2%). Although different species of fungi contain different percentages of these components in their cell walls, the major constituents are typically present (93). Thus, the biosynthesis or structural integrity of β-1,3-glucans, β-1,6-glucans, and α-mannans represent potential excellent targets. The pneumocandins and echinocandins, novel lipopeptides produced by *Glarea lozoyensis* and similar fungi, inhibit the synthesis of β-1,3-glucans (96). Two new drug candidates, Merck's MK-0991 and Eli Lilly's LY303366, are semisynthetic lipopeptide echinocandin derivatives that specifically target the Rholp dissociable subunit of the heterodimeric transmembrane 1,3-β-(D)-glucan synthase (92,93,96). Because there is apparently only a single gene that is responsible for the synthesis of this subunit, this is considered an excellent target. The pneumocandin experimental drug, MK-0991, has been shown to possess efficacy against *Aspergillus fumigatus, C. albicans, H. capsulatum*, and *P. carinii* (but not against *Cryptococcus neoformans*), suggesting that this would make an outstanding potential broad-spectrum candidate for disseminated, life-threatening fungal diseases, particularly in immunocompromised patients (92).

Other targets of interest that have been pursued recently include chitin and sphingolipid biosynthesis. Fungi contain three chitin synthetases (CSI, CSII, CSIII) that catalyze the synthesis of the polymer from individual units of UDP-*N*-acetylglucosamine. The leading antifungal chitin biosynthesis-inhibitor drug candidate is nikkomycin Z, a nucleoside dipeptide substrate analog of UDP-*N*-acetylglucosamine which competitively inhibits chitin synthases (91). Although nikkomycin Z is effective in vitro against *C. albicans, C. immitis*, and other fungi with relatively high chitin contents, it does not kill *Saccharomyces cerevisiae* (92,94). The polyoxins, also peptidyl-nucleoside natural products, also inhibit chitin synthase, but none of these has been developed yet as a clinical candidate. Rustmicin (also called galbonolide A), a 14-membered macrolide produced by *Micromonospora chalcea*, inhibits inositol phosphoceramide synthase at pM levels, resulting in the loss of all complex sphingolipids and the accumulation of ceramide (68). Although rustmicin was reasonably efficacious in a murine cryptococcosis model, it suffers from severe in vivo instability, brought about by serum protein binding, and by being an excellent substrate for *S. cerevisiae* efflux pump Pdr5 (68). The pradamycins are D-amino-acid-substituted benzonaphthacene quinone glycosides that appear to act by binding to the saccharide moieties of the mannoproteins in fungal cell walls, leading to a loss of intracellular potassium that results in gross morphological changes (6). Another unusual antifungal compound is sordarin, which exerts antifungal activity via inhibition of the elongation step in protein synthesis (6,97). Glaxo-Wellcome has developed a semisynthetic sordarin, GM237354, that possesses a broad spectrum of activity and high in vivo potency (6).

ANTICANCER AGENTS

The search for natural product anticancer agents began in the late 1950s and became a reality with the discovery in 1964 of daunorubicin, a cytotoxic, antitumor drug of the anthracycline class with efficacy against a wide variety of solid tumors and leukemias (15). Five years later, doxorubicin, the 14-hydroxy analogue of daunorubicin, was discovered at Farmitalia (15). Doxorubicin, which showed a wider range of efficacy for treatment of various cancers, has been a mainstay in chemotherapy for more than 25 years. It was shown recently that doxorubicin as well as many other cytotoxic antitumor drugs (e.g., etoposide) act by trapping topoisomerase II with DNA in what has been referred to as the cleavable complex, resulting in multiple DNA strand breaks (15). Another class of anthracyclines, exemplified by aclarubicin (aclacinomycin A), were recently shown to inhibit by a different mechanism of action, by inhibition of topoisomerae II–DNA interaction (15).

Table 9 shows a list of the major antitumor drugs derived from natural products. Other natural product antitumor chemotherapy agents used for several years, but more restrictively than doxorubicin, include mithramycin, discovered in the early 1950s; the mitomycins, first described in 1956; bleomycin, described by Umezawa in 1965; and the vinca alkaloids, vinblastine and vincristine, which were first described in the period of 1958–1962. In all these cases, the mode of action is cytotoxicity through drug-DNA interactions. With the ultimate desire to get away from cytotoxic drugs that are detrimental to all cells and not just cancerous cells, these cytotoxic natural product antitumor drugs are considered to be drugs of the past and not of the future.

Interest in natural product antitumor drugs was renewed, however, with the discovery of taxanes from the pacific yew tree. Paclitaxel (Taxol), a complex diterpenoid alkaloid, was discovered as a potential antitumor agent in 1971 (98), and it has taken nearly three decades to bring

Table 9. Clinical and Lead Experimental Natural Product-Derived Anticancer Drugs

Anticancer drug	Type	Comments
Aclacinomycin A	Anthracycline	Produced by *Streptomyces galilaeus*; used in Japan and France
Bleomycin	Glycopeptide	Produced by *Streptomyces verticillus*
Carminomycin	Anthracycline	Produced by *Actinomadura carminata*; used in Russia
Dactinomycin	Acylpeptidolactone	Produced by *Streptomyces parvulus*
Daunorubicin	Anthracycline	Produced by *Streptomyces peucetius*
Docetaxel	Taxane	Taxotere; recently approved for treatment of ovarian cancer
Doxorubicin	Anthracycline	Adriamycin; Produced by *S. peucetius* subsp. *caesius*
Epothilone	Substituted macrolide	Produced by *Sorangium cellulosum*; experimental only
Idarubicin	Anthracycline	Synthetic (mimetic), orally available analogue of doxorubicin
Irinotecan	Camptothecin	Approved in 1996 for metastatic colon and rectal cancers
Mitomycin C	Cytotoxic drug	Produced by *Streptomyces caespitosus*
Mitoxantrone	Anthracenedione	Biomimetic compound
Paclitaxel	Taxane	Produced by *Taxus* spp. (yew trees); approved for use in 1994
Pentostatin	Nucleoside analogue	Produced by *Streptomyces antibioticus*
Plicamycin	Polyketide	Mithramycin; Produced by *Streptomyces argillaceus*
Tenipocide	Podophyllotoxin	Cytotoxic antitumor drug
Topotecan	Camptothecin	Semisynthetic; from *Camptotheca acuminata* (Chinese tree)
Vinblastine sulfate	Vinca alkaloid	Produced by *Catharanthus roseus* (periwinkle)
Vincristine sulfate	Vinca alkaloid	Produced by *Catharanthus roseus* (periwinkle)
Vinorelbine tartrate	Vinca alkaloid	Semi-synthetic vinblastine analogue

it to the market. One of the unique features that helped move the taxanes from experimental drugs to clinical candidates was the finding that they acted as tubulin stabilizers, a novel mode of action (99). Docetaxel (Taxotere) and paclitaxel (Taxol) have excellent activity against ovarian and breast cancers. Additionally, Taxol and semisynthetic taxanes may be efficacious against a wide range of tumors. Thus far, the greatest impediment to the development of these drugs on a large scale was that they are only found at levels of about 0.01% (w/w) in the bark of several related yew trees, *Taxus brevifolia* (Pacific yew, an endangered species), *Taxus baccata*, *Taxus cuspidata* (Japanese yew), and others (100). Moreover, the chemical synthesis of paclitaxel is very difficult, requiring more than 30 steps. Thus, paclitaxel is currently made semisynthetically from 10-deacetylbaccatin III, produced by the needles of the Himalayan yew (100). Other novel antitumor drugs developed in recent years include irinotecan (Camptosa) and topotecan (Hycamptin), both which are inhibitors of topoisomerase I.

FUTURE DIRECTIONS IN NATURAL PRODUCTS DRUG DISCOVERY

Several approaches are being taken to address the issues of MRSA, VRE, other antibiotic-resistant bacteria, newly emerging infectious diseases and related problems. One approach is the use of genomics to help to identify new targets amongst bacteria and fungi. As mentioned previously, sequencing of the yeast genome helped to identify about a dozen unique targets for new antifungal drugs. It appears that the incidence of fungal resistance to new drugs targeted against single, critical enzymes, such as glucan synthase, is very low. Similarly, it is hoped that genomic analysis of bacteria is as useful in identifying new targets for novel antibacterials. Unfortunately, there is a significant difference between bacteria and fungi and between bacterial infections and fungal infections that must be considered. First, any single-site bacterial target for which single mutations can render resistance cannot be seriously considered because of the high frequency of mutations (10^{-8}) that occur in bacteria (77). Second, many resistance mechanisms are passed horizontally among bacterial populations by plasmid- and transposon-mediated transfer, which renders many antibiotics useless. Even the fluoroquinolones, which for years were thought to target only DNA gyrase, are now known to target at least two separate enzymes (101). This is critical, too, because single mutations in bacterial gyrases have been shown recently to yield resistance to several fluoroquinolones (102). What is the best answer? Although there is probably no single best answer for all resistance problems, the clear-cut best approach is still to inhibit cell wall biosynthesis, preferably with a novel mechanism of action or at several sites. Alternatively, inhibition of systems or processes, such as protein or nucleic acid synthesis, again at multiple sites, appears to be back in vogue. The conundrum, however, is that protein synthesis inhibitors are bacteriostatic agents, which in recent years have been thought not to be desired. Nevertheless, the newer macrolides, dirithromycin, clarithromycin, and azithromycin, all protein synthesis-inhibiting bacteriostats, are effective drugs.

The Pharmaceutical Research and Manufacturers of America organization announced that as of September 1998, 136 new anti-infective drugs were currently in advanced stages of development by 78 different companies. Of these, 27 compounds are antibacterials, 31 are antivirals, 12 are antifungals, 42 are vaccines, and 24 are in the "other" category, but still relating to anti-infection indications. As described throughout this review, there are unmet needs in all fields of antibiotics. The wealth of new

drugs on the horizon bodes well for the future of antibiotics of all classes.

BIBLIOGRAPHY

1. S.B. Levy, *The Antibiotic Paradox: How Miracle Drugs Are Destroying the Miracle*, Plenum, New York, 1992.
2. E.J. Vandamme, in E.J. Vandamme ed., *Biotechnology of Industrial Antibiotics*, Dekker, New York, 1984, pp. 3–31.
3. A.L. Demain, in C.L. Hershberger, S.W. Queener, and G. Hegeman eds., *Genetics and Molecular Biology of Industrial Microorganisms*, American Society for Microbiology, Washington, D.C., 1989, pp. 1–11.
4. K.A. Reynolds and A.L. Demain, in W.R. Strohl ed., *Biotechnology of Antibiotics*, Dekker, New York, 1997, pp. 497–520.
5. W.R. Strohl, in W.R. Strohl ed., *Biotechnology of Antibiotics*, Dekker, New York, 1997, pp. 1–47.
6. Y.-Z. Shu, *J. Natl. Prod.* **61**, 1053–1071 (1998).
7. G.M. Cragg, D.J. Newman, and K.M. Snader, *J. Natl. Prod.* **60**, 52–60 (1997).
8. J. Bérdy, in V.G. Debabov, Y.V. Dudnik, V.N. Danilenko eds., *Proceedings of the Ninth International Symposium on the Biology of the Actinomycetes*, All-Russia Scientific Research Institute for Genetics and Selection of Industrial Microorganisms, Moscow, 1995, pp. 13–34.
9. E. Culotta, *Science* **264**, 362–363 (1994).
10. H. Umezawa, *Annu. Rev. Microbiol.* **36**, 75–99 (1982).
11. A.W. Alberts, J. Chen, G. Kuron, V. Hunt, J. Huff, C. Hoffman, J. Rothrock, M. Lopez, H. Joshua, E. Harris, A. Patchett, R. Monaghan, S. Currie, E. Stapley, G. Albers-Schonberg, O. Hensens, J. Hirschfield, K. Hoogsteen, J. Liesch, and J. Springer, *Proc. Natl. Acad. Sci. U.S.A.* **77**, 3957–3961 (1980).
12. American Druggist, *http://www.rxlist.com/top200a.htm*, Feb. 1998.
13. N. Pfeiffer, *Gen. Eng. News* **16**, 18–19 (1996).
14. SCRIP's 1995 Yearbook, PharmaBooks Ltd., New York.
15. W.R. Strohl, M.L. Dickens, V.B. Rajgarhia, A.J. Woo, and N.D. Priestley, in W.R. Strohl ed., *Biotechnology of Antibiotics*, Dekker, New York, 1997, pp. 577–657.
16. T.J. Walsh and N. Giri, *Eur. J. Clin. Microbiol. Infect. Dis.* **16**, 93–97 (1997).
17. P.R. August, L. Tang, Y.J. Yoon, S. Ning, R. Muller, T.W. Yu, M. Taylor, D. Hoffman, C.G. Kim, X. Zhang, C.R. Hutchinson, and H.G. Floss, *Chem. Biol.* **5**, 69–79 (1998).
18. L.C. Vining and C. Stuttard eds., *Genetics and Biochemistry of Antibiotic Production*, Butterworth-Heinemann, Boston, 1995.
19. W.R. Strohl ed., *Biotechnology of Antibiotics*, Dekker, New York, 1997.
20. L.C. Vining, in L.C. Vining and C. Stuttard eds., *Genetics and Biochemistry of Antibiotic Production*, Butterworth-Heinemann, Boston, 1995, pp. 499–504.
21. J. Mann, R.S. Davidson, J.B. Hobbs, D.V. Banthorpe, and J.B. Harborne, *Natural Products. Their Chemistry and Biological Significance*, Addison-Wesley Longman, Essex, U.K., 1996.
22. S. Budavari ed., *The Merck Index: An Encyclopedia of Chemicals, Drugs, and Biologicals*, 12th ed., Merck Research Laboratories, Merck and Co., Whitehouse Station, 1996.
23. C.W. Ford, J.C. Hamel, D. Stapert, J.K. Moerman, D.K. Hutchinson, M.R. Barbachyn, and G.E. Zurenko, *Trends Microbiol.* **5**, 196–200 (1997).
24. J.E. McGowan, *Rev. Infect. Dis.* **5**, 1033–1048 (1983).
25. J. Davies, *Science* **264**, 375–382 (1994).
26. M.L. Cohen, *Science* **257**, 1050–1055 (1992).
27. J. Travis, *Science* **264**, 360–362 (1994).
28. S. Falkow, *Infectious Multiple Drug Resistance*, Pion Ltd., London, 1975.
29. J. Lederberg, R.E. Shope, and S.C. Oaks eds., *Emerging Infections: Microbial Threats to Health in the United States*, Institute of Medicine, National Academy of Sciences Press, Washington, D.C., 1992.
30. R.A. Weinstein, *Emerg. Infect. Dis.* **4**, 416–420 (1998).
31. Centers for Disease Control and Prevention, *Morb. Mortal. Wkly. Rep.* **42**, 597–599 (1993).
32. E. Rubinstein and F. Bompart, *J. Antimicrob. Chemother.* **39**, 139–143 (1997).
33. *World Health Report 1996*, Office of World Health Reporting, World Health Organization, Geneva, 1996.
34. J. May, K. Shannon, A. King, and G. French, *J. Antimicrob. Chemother.* **42**, 189–197 (1998).
35. K. Sunakawa, H. Akita, S. Iwata, Y. Sato, and R. Fujii, *Infection* **23**, S74–S78 (1995).
36. B.R. Bloom and C.J.L. Murray, *Science* **257**, 1055–1064 (1992).
37. E. Collatz, R. Labia, and L. Gutman, *Mol. Microbiol.* **4**, 1615–1620 (1990).
38. P.M. Rowe, *Lancet* **347**, 252 (1996).
39. A.H.C. Uttley, C.H. Collins, J. Naidoo, and R.C. George, *Lancet* **1**, 57–58 (1988).
40. G.L. French, *Clin. Infect. Dis.* **27**, S75–S83 (1998).
41. P. Moreillon and A. Wenger, *Schweiz. Mediz. Wochensch.* **126**, 255–263 (1996).
42. W. Brumfitt and J.M.T. Hamilton-Miller, *Drugs Exptl. Clin. Res.* **20**, 215–224 (1994).
43. W.C. Noble, Z. Virani, and R.G.A. Cree, *FEMS Microbiol. Lett.* **93**, 195–198 (1992).
44. H.C. Neu, *Scand. J. Infect. Dis.* **91** 7–13 (1993).
45. K.J. Christensen and P.O. Gubbins, *Ann. Pharmacother.* **30**, 288–290 (1996).
46. Y. Sumita and M. Fukusawa, *Chemotherapy* **42**, 47–56 (1996).
47. G. Cohen and Y. Aharonowitz, in P.A. Hunter, G.K. Darby, and N.J. Russell eds., *Fifty Years of Antimicrobials: Past Perspectives and Future Trends*, Soc. Gen. Microbiol. Ltd., Cambridge, 1995, pp. 139–163.
48. H. Vanderhaeghe, *Verh. K. Acad. Geneeskd. Belg.* **53**, 39–58 (1991).
49. A.S. Paradkar, S.E. Jensen, and R.H. Mosher, in W.R. Strohl ed., *Biotechnology of Antibiotics*, Dekker, New York, 1997, pp. 241–277.
50. P. Zuber and M. Marahiel, in W.R. Strohl ed., *Biotechnology of Antibiotics*, Dekker, New York, 1997, pp. 187–216.
51. B.O. Bachmann, R. Li, and C.A. Townsend, *Proc. Natl. Acad. Sci. U.S.A.* **95**, 9082–9086 (1998).

52. H. Palissa, H. von Dohren, H. Kleinkauf, H.H. Ting, and J.E. Baldwin, *J. Bacteriol.* **171**, 5720–5728 (1989).
53. D.M. Allen and M.L. Ling, *Singapore Med. J.* **35**, 626–630 (1994).
54. P.M. Southern, *Compr. Ther.* **23**, 575–582 (1997).
55. M.A. Wynd and J.A. Paladino, *Ann. Pharmacother.* **30**, 1414–1424 (1996).
56. R.C. Moellering Jr., G.M. Eliopoulos, and D.E. Sentochnik, *J. Antimicrob. Chemother.* **24**, 1–7 (1989).
57. D.N. Fish and T.J. Singletary, *Pharmacotherapy* **17**, 644–669 (1997).
58. J. Shimada and Y. Kawahara, *Drugs Exptl. Clin. Res.* **20**, 241–245 (1994).
59. C.J. Gill, J.J. Jackson, L.S. Gerckens, B.A. Pelak, R.K. Thompson, J.G. Sundelof, H. Kropp, and H. Rosen, *Antimicrob. Agents Chemother.* **42**, 1996–2001 (1998).
60. D.M. Livermore, *J. Antimicrob. Chemother.* **39**, 673–676 (1997).
61. E. Di Modugno, R. Broggio, I. Erbetti, and L. Lowther, *Antimicrob. Agents Chemother.* **41**, 2742–2748 (1997).
62. L. Katz and S. Donadio, in L.C. Vining and C. Stuttard eds., *Genetics and Biochemistry of Antibiotic Production*, Butterworth-Heinemann, Boston, 1995, pp. 385–420.
63. Y. Xue, D. Wilson, L. Zhao, H.-W. Liu, and D.H. Sherman, *Abstr. 8th Intl. Symp. Genet. Industr. Microorg.*, Jerusalem, 1998, p. 39.
64. T. Mazzei, E. Mini, A. Novelli, and P. Periti, *J. Antimicrob. Chemother.* **31**, 1–9 (1993).
65. J.L. Pernodet, S. Fish, M.H. Rouault-Blondelet, and E. Cundliffe, *Antimicrob. Agents Chemother.* **40**, 581–585 (1996).
66. R.R. Reinert, A. Bryskier, and R. Luetticken, *Antimicrob. Agents Chemother.* **42**, 1509–1511 (1998).
67. H. Achenbach, A. Muhlenfeld, U. Fauth, and H. Zahner, *Ann. N.Y. Acad. Sci.* **544**, 128–140 (1988).
68. S.M. Mandala, R.A. Thornton, J. Milligan, M. Rosenbach, M. Garcia-Calvo, H.G. Bull, G. Harris, G.K. Abruzzo, A.M. Flattery, C.J. Gill, K. Bartizal, S. Dreikorn, and M.B. Kurtz, *J. Biol. Chem.* **273**, 14942–14949 (1998).
69. K.W. Mollison, T.A. Fey, R.A. Krause, V.A. Thomas, A.P. Mehta, and J.R. Luly, *Ann. N.Y. Acad. Sci.* **685**, 55–57 (1993).
70. D.J. MacNeil, in L.C. Vining and C. Stuttard eds., *Genetics and Biochemistry of Antibiotic Production*, Butterworth-Heinemann, Boston, 1995, pp. 421–442.
71. F.G. Day, *J. Am. Vet. Med. Assoc.* **208**, 655–656 (1996).
72. D.M. Bollag, P.A. McQueney, J. Zhu, O. Hensens, L. Koupal, J. Liesch, M. Goetz, E. Lazarides, and C.M. Woods, *Cancer Res.* **55**, 2325–2333 (1995).
73. J.P. Steiner, M.A. Connolly, H.L. Valentine, G.S. Hamilton, T.M. Dawson, L. Hester, and S.H. Snyder, *Nature Med.* **3**, 421–428 (1997).
74. P.A. Lartey, H.N. Nellans, R. Faghih, A. Petersen, C.M. Edwards, L. Freiberg, S. Quigley, K. Marsh, L.L. Klein, and J.J. Plattner, *J. Med. Chem.* **38**, 1793–1798 (1995).
75. S. Konno, K. Asano, M. Kurokawa, K. Ikeda, K. Okamoto, and M. Adachi, *Int. Arch. Allergy Immunol.* **105**, 308–316 (1994).
76. J.C. Barrière, D.H. Bouanchaud, J.M. Paris, O. Rolin, N.V. Harris, and C. Smith, *J. Antimicrob. Chemother.* **30** 1–8 (1992).
77. L.L. Silver and K.A. Bostian, *Antimicrob. Agents Chemother.* **37**, 377–383 (1993).
78. T. Nichterlein, M. Kretschmar, and H. Hof, *J. Chemother.* **8**, 107–112 (1996).
79. R. Leclercq, L. Nantas, S.-J. Soussy, and J. Duval, *J. Antimicrob. Chemother.* **30**, 67–75 (1992).
80. G.M. Eliopoulos, C.B. Wennersten, H.S. Gold, T. Schuelin, M. Souli, M.G. Farris, S. Cerwinka, H.L. Nadler, M. Dowzicky, G.H. Talbot, and R.C. Moellering Jr., *Antimicrob. Agents Chemother.* **42**, 1088–1092 (1998).
81. I.S. Hunter and R.A. Hill, in W.R. Strohl ed., *Biotechnology of Antibiotics*, Dekker, New York, 1997, pp. 659–682.
82. T.I. Nicas and R.D.G. Cooper, in W.R. Strohl ed., *Biotechnology of Antibiotics*, Dekker, New York, 1997, pp. 363–392.
83. T.I. Nicas, D.L. Mullem, J.E. Flokowitsch, D.A. Preston, N.J. Snyder, M.J. Zweifel, S.C. Wilkie, M.J. Rodriguez, R.C. Thompson, and R.D.G. Cooper, *Antimicrob. Agents Chemother.* **40**, 2194–2199 (1996).
84. R.S. Schwalbe, A.C. McIntosh, S. Qaiyum, J.A. Johnson, R.J. Johnson, K.M. Furness, W.J. Holloway, and L. Steele-Moore, *Antimicrob. Agents Chemother.* **40**, 2416–2419 (1996).
85. W. Piepersberg, in W.R. Strohl ed., *Biotechnology of Antibiotics*, Dekker, New York, 1997, pp. 81–163.
86. M. Inoue, M. Nonoyama, R. Okamoto, and T. Ida, *Drugs Exptl. Clin. Res.* **30**, 233–240 (1994).
87. W.A. Craig, *Diagn. Microbiol. Infect. Dis.* **27**, 49–53 (1997).
88. J.S. Bertino Jr., *Am. J. Health Syst. Pharm.* **54**, 2185–2191 (1997).
89. A.L. Demain, *Nature Biotechnol.* **16**, 3–4 (1998).
90. F.M. Aarestrup, *Microb. Drug Resist.* **4**, 137–141 (1998).
91. J.R. Graybill, L.K. Najvar, R. Bocanegra, R.F. Hector, and M.F. Luther, *Antimicrob. Agents Chemother.* **42**, 2371–2374 (1998).
92. M.A. Powles, P. Liberator, J. Anderson, Y. Karkhanis, J.F. Dropinski, F.A. Bouffard, J.M. Balkovec, H. Fujioka, M. Aikawa, D. McFadden, and D. Schmatz, *Antimicrob. Agents Chemother.* **42**, 1985–1989 (1998).
93. M.B. Kurtz, *ASM News* **64**, 31–39 (1998).
94. J.A. Gil and J.F. Martin, in W.R. Strohl ed., *Biotechnology of Antibiotics*, Dekker, New York, 1997, pp. 551–575.
95. Y. Koltin, *Abstr. 8th Intl. Symp. Genet. Industr. Microorg.*, Jerusalem, 1998, p. 5.
96. W.W. Turner and W.L. Current, in W.R. Strohl ed., *Biotechnology of Antibiotics*, Dekker, New York, 1997, pp. 315–334.
97. M.C. Justice, M.-J. Hsu, B. Tse, T. Ku, J. Balkovec, D. Schmatz, and J. Nielsen, *J. Biol. Chem.* **273**, 3148–3151 (1998).
98. M.C. Wani, H.L. Taylor, M.E. Wall, P. Coggen, and A.T. McPhail, *J. Am. Chem. Soc.* **93**, 2325–2327 (1971).
99. P.B. Schiff, J. Fant, and S.B. Horowitz, *Nature* **277**, 665–667 (1979).
100. Y. Yukimune, H. Tabata, Y. Higashi, and Y. Hara, *Nature Biotechnol.* **14**, 1129–1132 (1996).
101. X.-S. Pan and L. Fisher, *Antimicrob. Agents Chemother.* **41**, 471–474 (1997).
102. B. Waters and J. Davies, *Antimicrob. Agents Chemother.* **41**, 2766–2769 (1997).

SECRETION FROM ANIMAL CELLS

RANDAL J. KAUFMAN
University of Michigan Medical School
Ann Arbor, Michigan

KEY WORDS

Disulfide bond formation
Endoplasmic reticulum
Glycosylation
Golgi apparatus
Posttranslational modification
Protein chaperones
Protein folding
Protein trafficking
Proteolytic processing
Tyrosine sulfation

OUTLINE

INTRODUCTION

The specialized process of secretion in mammalian cells is directed through membrane-enclosed compartments composed of vesicles. Each compartment is unique to ensure specificity and directionality for the secretion process. The compartments are maintained by mechanisms of selective targeting of newly made proteins to their correct vesicle. As proteins destined for the cell surface transit the different compartments, they attain their final conformation through a maturation process that involves protein folding facilitated by molecular chaperones, covalent modification of the polypeptide backbone, and assembly into higher-order structures.

PROTEIN TRANSLOCATION INTO THE ENDOPLASMIC RETICULUM

Targeting to the Endoplasmic Reticulum

All proteins destined for the cell surface, the extracellular space, or intracellular organelles such as lysosomes or the Golgi apparatus are first translocated across the membrane of the endoplasmic reticulum (ER). In mammalian cells the process of protein transport across the ER membrane occurs in the majority of cases while the polypeptide is being translated, which is called cotranslational translocation. In contrast, in yeast, translocation can occur either cotranslationally or after translation of the polypeptide is complete, that is, posttranslational translocation. Proteins that are targeted for transport across the ER must contain a signal that directs the process. Most secretory proteins contain an amino-terminal set of amino acids that compose the signal that directs cotranslational translocation of the protein across the ER membrane. The signal peptide is exposed as the polypeptide emerges from the 60S ribosomal subunit and mediates association of the nascent polypeptide with the cytosolic face of the ER. Although the exact amino acid sequence of signal peptides is not conserved for a given protein across species, its general character is very conserved. The signal sequence may be approximately 30–60 amino acids in length and is composed of three regions: (*1*) an amino terminal segment of variable length that has a net positive charge, (*2*) a central hydrophobic core of 6–15 residues, and (*3*) a C-terminal region that often has a helix-breaking amino acid residue such as glycine proline or serine (1). In yeast, the more hydrophobic the character of the signal peptide, the more likely the transport process occurs by a cotranslational mechanism.

The signal recognition particle (SRP) is a complex of six polypeptides and one 7S RNA molecule that targets substrates for cotranslational translocation (for review see Ref. 2). The 300-nucleotide RNA component is very conserved across all species and is homologous with the highly repetitive Alu DNA family. The mechanism by which cotranslational translocation occurs was elucidated using in vitro studies of protein import into canine pancreatic microsomes, because they are efficient at directing SRP-dependent translocation. Analysis of the SRP has identified subcomplexes that perform different functions. SRP54 (the number refers to the molecular weight of the protein) binds the signal sequence and targets it to the ER membrane. SRP54 contains a stretch of methionine residues that provide a flexible surface, much like bristles of a brush, for interaction with the variable hydrophobic stretches of amino acids in different signal peptides. After interaction with SRP54, translation elongation pauses by a subcomplex of SRP9 and SRP14. This pause helps ensure proper targeting to the ER membrane before significant portions of the polypeptide are synthesized and begin to fold.

After SRP binds the signal sequence of the nascent chain–ribosome complex, it targets the complex to the ER translocation machinery (Fig. 1). The SRP receptor (SRPR) on the ER membrane is composed of two subunits SRα and SRβ and receives the nascent polypeptide after release from SRP. SRP then recycles back to the cytosol. Both SRP54 of the SRP and each of the SRP receptor subunits are GTPases. SRP and SRPR reciprocally stimulate each others' GTPase activity. SRP in the GTP-bound form promotes high-affinity association with SRPR (4). Subsequent transfer of the signal to the translocation apparatus depends on GTP binding by SRα (5). For recycling, SRP must be released from SRPR, a process that requires GTP hydrolysis by SRP54 (6). The nascent chain–associated complex (NAC), an ER-localized protein complex, ensures fidelity of cotranslational targeting to the translocon in the ER membrane by binding nascent polypeptides that lack signal sequences, preventing their targeting to the ER membrane, and preventing free ribosomes from interacting with the ER membrane (7–9). In addition, some polypeptides also require the translocating chain–associated membrane protein (TRAM) for translocation. TRAM can be cross-linked to the signal peptide of some secretory proteins (10). The signal-containing polypeptide inserts into the membrane, and the polypeptide threads through the protein channel, composed of Sec61α, into the lumen of the ER as an extending loop.

Translocation into the ER

The proteins that are required for translocation in vitro and in vivo have been identified through genetic studies in yeast. The most important protein is Sec61p (40 kDa), a protein predicted to span the ER membrane a number of times; it is the primary subunit of the protein translocation channel (11). Sec61p is part of a heterotrimeric complex with Sbh1p and Sss1p, which are the yeast homologues of mammalian Sec62β and Sec61γ (12). In addition to the Sec61p complex, another complex, Sec62p, Sec63p, Sec71p, and Sec72p, is required for posttranslocational translocation in yeast. Sec63p has a luminal region homologous to the J-domain that is highly conserved in the DnaJ protein family, a protein family that stimulates the ATPase activity of Hsp70 family members. The yeast homologue of BiP, Kar2p, is required for posttranslational translocation, probably through its ATPase activity, which is regulated by the J-domain of Sec63p. In mammalian cells, purified SRP, SRPR, and Sec61p are the only proteins required for cotranslocational translocation (12). TRAM is required for only a subset of precursors and stimulates translocation of others.

The role of resident proteins in the lumen of the ER was studied by selectively solubilizing and reconstituting microsomal translocation activity into proteoliposomes (13). Alkaline extraction at pH 9.5 releases a class of luminal proteins that is essential for completion of polypeptide translocation (14). Among the proteins released are the stress proteins BiP/GRP78, GRP94, protein disulfide isomerase, calreticulin, and peptidyl prolyl *cis-trans*-isomerase enzymes (cyclophilin and FKBP). These studies demonstrated that BiP/GRP78 was required for translocation in these yeast-derived proteoliposomes. However, experiments in mammalian systems have not provided compelling evidence that BiP/GRP78 is required for translocation. In addition, expression of an ATPase-defective BiP only prevented the secretion of selective proteins, supporting the view that the BiP ATPase activity is not absolutely required for the secretion of all proteins (15).

Proteins that become integral membrane proteins pose a unique problem for the translocation machinery. Type I transmembrane proteins contain a cleavable N-terminal signal peptide and an internal transmembrane domain. They are oriented such that their amino terminus is in the extracellular space. For these proteins, a span of hydro-

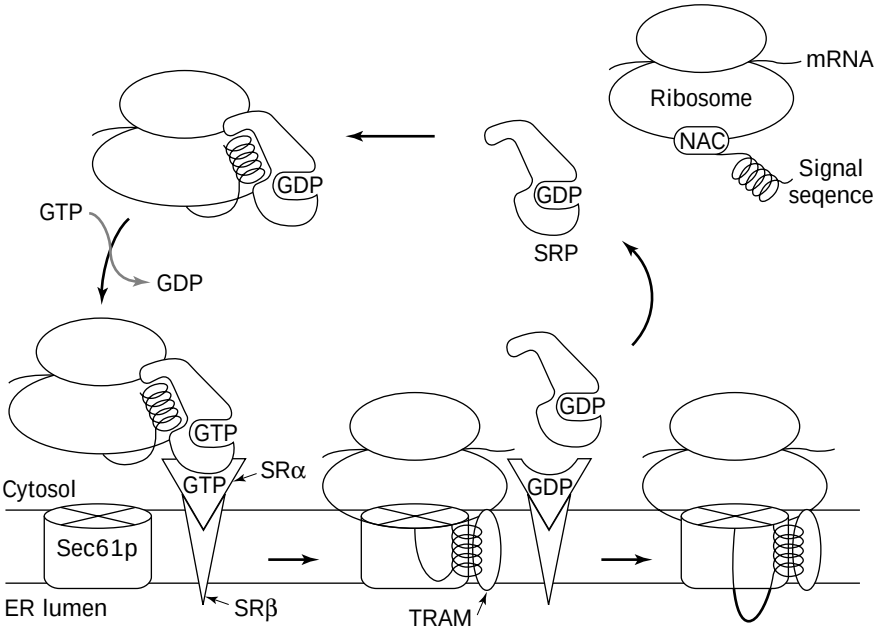

Figure 1. SRP-dependent cotranslocational translocation into the ER. SRP binds to the signal sequence of a nascent polypeptide emerging from the 60S ribosome to form a targeting complex in which elongation is arrested. SRP in the targeting complex then binds SRP receptor (composed of SRα and Srβ subunits) in the ER membrane. After GTP binding, SRP interacts with SRP receptor to result in formation of the ribosome-translocon junction, and translation elongation resumes. GTP hydrolysis stimulates the dissociation of SRP from SRP receptor so they can be recycled. As the nascent chain grows, the translocon pore allows passage of the nascent protein across the membrane. In most cases, the signal sequence is removed on the luminal side of the ER membrane by signal peptidase (not shown). *Source*: Reprinted from Ref. 3, with permission.

phobic amino acids (called the stop-transfer sequence) anchors the polypeptide in the lumen of the ER. In type II transmembrane proteins the carboxy terminus of the protein is in the extracellular space. The topology of type I and type II membrane proteins is determined by the charge distribution of polar amino acids flanking the signal-anchor domain (16). The side of the signal anchor that has more positively charged flanking residues remains intracellular, likely reflecting interactions with the negatively charged phospholipid bilayer. For multiple-spanning transmembrane proteins, each transmembrane domain displaces the prior one from the protein conducting channel where it moves laterally into the lipid bilayer. During the process of translocation, the channel is always gated, either by the ribosome on the cytoplasmic side or by BiP/GRP78 on the luminal side (17).

The cleavage site for signal peptidase is marked by small amino acids (alanine or glycine) in the 3- and 1-positions, relative to the cleavage site. Insertion into the ER membrane involves the formation of a loop structure with the amino terminus remaining in the cytoplasm and the growing carboxy terminus being continuously translocated across the membrane through Sec61p, a protein-conducting channel (18). Cleavage of the signal sequence by the signal peptidase (19,20) then releases the mature amino terminus into the lumen of the ER and is required for translocation of proteins into the secretory pathway.

The transport of a polypeptide across the ER membrane requires energy. GTP is used in the cycling of SRP and SRPR. The energy in cotranslational translocation is derived from the process of translational elongation. For posttranslational translocation, ATP is required for both function of Hsp70 in the cytosol and BiP function in the lumen of the ER. Depletion of intracellular ATP can block the secretion of some proteins, presumably by preventing dissociation of proteins from BiP (21). An ER ATP transporter has been characterized (22), and studies have directly detected ATP in the lumen of the ER by directing firefly luciferase expression to be localized in the ER (23). It is possible that increases in the intraluminal concentration of ATP will increase the secretion capacity in mammalian cells.

POSTTRANSLATIONAL MODIFICATIONS WITHIN THE SECRETORY PATHWAY

Protein translocation into and transport through the secretory pathway in eukaryotic cells is accompanied by a multitude of covalent modifications that occur on the polypeptide backbone. The sequence of posttranslational modifications that occur on a polypeptide is carefully regulated both temporally and spatially; specific modifications occur only within vesicles of the ER or Golgi compartment (Fig. 2). In many cases these modifications are required for proper polypeptide folding and secretion. In addition, posttranslational modifications can affect the half-life of the protein in the plasma and may be required for functional activity of the polypeptide. The mechanisms that direct posttranslational modifications recognize specific structural determinants within the polypeptide backbone. The efficiency of these modifications is determined by the specific host cell enzymatic machinery, the availability of substrates and cofactors, as well as structural properties of the polypeptide. To evaluate the role of posttranslational modification in protein function, investigators have studied proteins treated with chemicals or enzymes to remove modifications, proteins synthesized in the presence of inhibitors of specific modification reactions, proteins expressed in either different cell types or in cell mutants with defects in specific enzymatic machinery required to perform modifications, or proteins engineered through recombinant DNA technology that contain mutations that prevent modifications. The interpretation of results utilizing different strategies needs to be qualified to consider secondary effects due to the approach utilized. As a consequence, it is desirable to utilize several independent approaches to confirm the importance of any specific modification.

Protein Folding and Catalysts of Protein Folding in the ER

Analysis of protein folding in vitro has identified several key steps that occur during spontaneous refolding of a protein upon dilution from a denaturant. First, the polypeptide chain collapses into a compact shape to bury hydrophobic structures; this coincides with formation of secondary structures. Then native tertiary structures form as the protein passes through kinetically defined intermediates; this process may take several minutes. The partially folded intermediate is called the molten globule. Finally, the rate-limiting step lies close to the native folded state and involves formation of hydrogen bonds and disulfide bonds. Although proteins can fold into correct tertiary conformations in vitro (25), additional factors such as protein chaperones assist protein folding in vivo. Molecular chaperones compose a group of unrelated proteins that mediate the correct assembly of other proteins but are not themselves components of the final folded structure. Some molecular chaperones actually catalyze protein folding, whereas others maintain proteins in a folding-competent state and prevent protein aggregation.

A number of protein chaperones bind and stabilize partially folded polypeptides. One of the most well studied members of this family is the immunoglobulin binding protein (BiP) that is the same as the glucose-regulated protein of 78 kDa (GRP78) within the lumen of the ER (26). BiP is a member of the heat shock protein family, which exhibits a peptide-dependent ATPase activity (27), and for which expression is induced by the presence of abberently folded protein or unassembled protein subunits within the ER (28,29). Polypeptide release from BiP and transport out of the ER requires high levels of intracellular ATP (21); however, not all proteins require functional BiP for secretion (15). Intensive investigation into the role of BiP in protein folding has led to two different, but not mutually exclusive, functions for BiP. One hypothesis is that BiP assists protein folding by maintaining proteins in a conformation where they are folding competent, (30,31). This model is supported by the transient association with polypeptides destined for secretion (32–35) and an ATP dependence for proper folding and disulfide bond formation (36). In

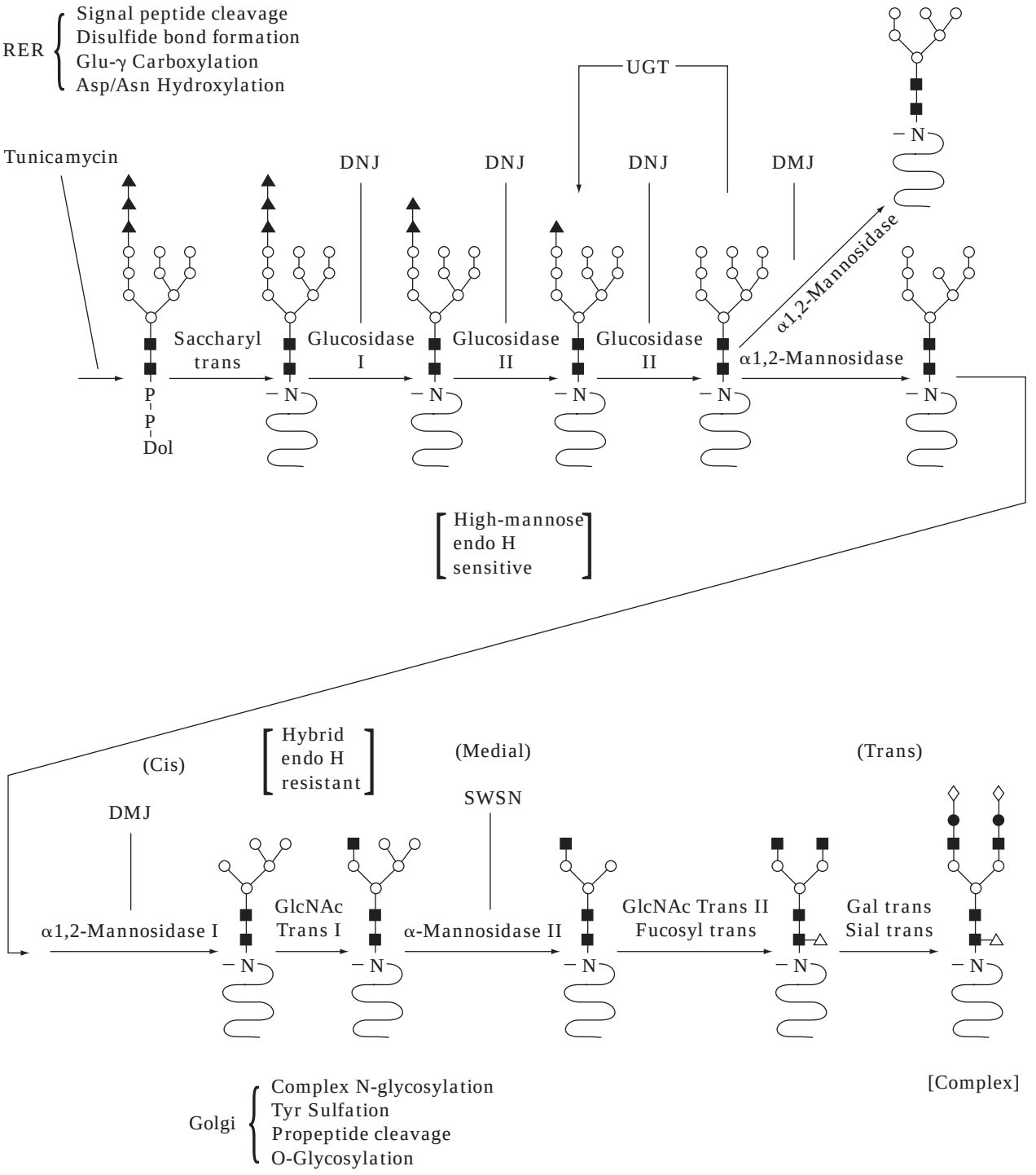

Figure 2. Posttranslational modifications within the secretory pathway. The posttranslational modifications that occur within the rough endoplasmic reticulum (RER, top) and the Golgi compartment (below) are shown. In addition, the sequence of oligosaccharide processing of N-linked oligosaccharides is shown, including the enzymes responsible and the known inhibitors (DNJ, deoxynojirimycin; DMJ, deoxymannojirimycin; SWSN, swainsonine). The point at which N-linked oligosaccharides become resistant to endoglycosidase H is shown. Sugars: ▲, glucose; ○, mannose; ■, *N*-acetylglucosamine (GlcNAc); △, fucose; ●, galactose (Gal); ◇, sialic acid (Sial) trans, transferase. UGT, UDP-glucose:glycoprotein glucosyltransferase. *Source*: Adapted from Ref. 24, with permission.

contrast, other studies (37–40) suggest that these proteins act as a retention mechanism for quality control to prevent aberrantly folded proteins from exiting the secretory pathway. However, despite many efforts to date, there is no direct demonstration that BiP binding to protein substrates actually catalyzes protein folding (41).

Disulfide bond formation occurs in the oxidizing environment of the ER. The tripeptide glutathione (γ-glutamyl, cyteinyl, glycine) is the major thiol-containing molecule in eukaryotic cells and prevents disulfide bond formation in the cytosol and catalyzes their formation in the ER. Glutathione is in equilibrium between a reduced form (GSH) and an oxidized form (GSSG). In the ER the ratio of GSH to GSSG is 5:1, an optimum for formation of disulfide bonds. In contrast, the ratio is 50:1 in the cytosol (42). Oxidized glutathione is reduced by glutathione reductase in a reaction that uses NADPH as a cofactor and occurs in the cytosol. One identified catalyst of protein folding is protein disulfide isomerase (PDI), which exchanges disulfide bonds on substrates and ensures proper disulfide bond formation, and exchange occurs prior to exit from the ER (43). PDI is also the β-subunit of prolyl hydroxylase, which catalyzes posttranslational hydroxylation of proline residue in pro-α-collagen. PDI is a soluble protein of the ER and is the most effective catalyst of protein folding known. PDI does not change the intermediates in the folding reaction but increases the kinetics of the overall process. Proper pairing of disulfide bonds is essential for transport through the ER, and pairing does not always occur in a sequential order.

Another rate-limiting step in protein folding is proline isomerization. Proteins that catalyze isomerization around peptidyl-prolyl bonds are peptidyl-prolyl isomerases (PPIases). There are two classes of these enzymes, based on their different substrate specificities and sensitivities to cyclophilin or FK506. Cyclophilin binds to cyclosporin A, a PPIase that has broad specificity. FK506 binds to FKBP, a PPIase that has narrower specificity with preference for hydrophobic residues in the P1 position. There are some very specific PPIases, one of the best studied is NinaA, a PPIase of the ER that specifically folds rhodopsins 1 and 2. *Drosophila* that have mutations in NinaA lack proper visual responses.

Asparagines and Serine/Threonine-Linked Glycosylation

High-mannose-containing oligosaccharide structures are added to asparagine residues of glycoproteins as an obligatory event for the folding and assembly of many newly synthesized polypeptides (44). This is an essential process in eukaryotic cells (45). The presence of oligosaccharides may be required for the efficient transport of individual glycoproteins through the secretory pathway (33,46), to increase the plasma half-life, or for the biological activity of glycoproteins. The luminal enzyme oligosaccharyltransferase catalyzes the transfer of a preassembled high-mannose-containing oligosaccharide core structure [glucose $(Glc)_3$mannose $(Man)_9$*N*-acetylglucosamine $(GlcNAc)_2$] from a dolichol pyrophosphate precursor onto asparagine acceptor sites within the consensus sequence Asn-X-Ser/Thr, where X can be any amino acid except proline. The mammalian oligosaccharyltransferase is a heterotrimeric transmembrane complex of ribophorin I, ribophorin II, and the oligosaccharyltransferase, which has been purified and molecularly cloned (47). The utilization of a particular consensus site for N-linked oligosaccharide attachment is determined by the structure of the growing polypeptide. As a consequence, proteins expressed in heterologous cells most frequently exhibit occupancy of N-linked sites very similar to that of the native polypeptide (48). To date there is no evidence that the N-linked oligosaccharide addition machinery can be saturated at high expression levels of glycoproteins.

After addition of the high-mannose-containing oligosaccharide core structure, trimming begins with the removal of the three terminal glucose residues, which is mediated by the action of glucosidases I and II (Fig. 2). Glucosidase I removes the terminal α1-3-glucose, and glucosidase II subsequently removes the two α1-2-glucose residues. Glucose trimming is required for binding to the protein chaperones calnexin and calreticulin within the lumen of the ER (49) (Fig. 3). Calnexin (IP90, p88, or CNX; an integral transmembrane protein) (50) and calreticulin (CRT; an ER luminal protein) (51) are homologous lectin-binding protein chaperones that transiently and selectively bind to overlapping sets of newly synthesized glycoprotein folding intermediates, thereby preventing their transit through the secretory pathway. Prolonged association with CNX and/or CRT is observed when proteins are unfolded, misfolded, or unable to oligomerize. CNX and CRT bind most avidly to monoglucosylated forms of the N-linked core structure and promote folding, delay oligomerization, and prevent degradation of some glycoproteins (52). In contrast, interaction with CNX correlates with intracellular degradation of some glycoproteins (53). Removal of the third glucose from the oligosaccharide core structure correlates with release from CNX and CRT and transport to the Golgi apparatus. It is proposed that the selective binding of unfolded glycoproteins to CRT and CNX is mediated by reglucosylation of the deglucosylated N-linked oligosaccharide. This reglucosylation activity is performed by a UDP-glucose:glycoprotein glucosyltransferase (UGT). The activity of the UGT is activated by unfolded protein (54). Thereby, only unfolded, mutant, or unassembled proteins are subject to reglucosylation. Reglucosylated proteins can rebind CNX and/or CRT and in this manner; unfolded proteins are retained in the ER through a cycle of CNX/CRT interaction, glucosidase II activity, and UGT activity. Inhibition of glucose trimming by inhibitors of glucosidase I and II, such as deoxynojirimycin or castanospermine, can inhibit this cycle and the secretion of some proteins. Because glucosidase inhibitors are fairly nontoxic and can inhibit the secretion of HIV envelope glycoprotein gp160, they have been used in the treatment of AIDS (55). Subsequent to glucose trimming in the ER, at least one α1-2-linked mannose is removed by an ER α1-2-mannosidase prior to transport out of the ER. Transit out of the ER is the rate-limiting step in secretion for the majority of proteins and may vary from 15 min to days, depending upon the rate at which a polypeptide attains a properly folded conformation.

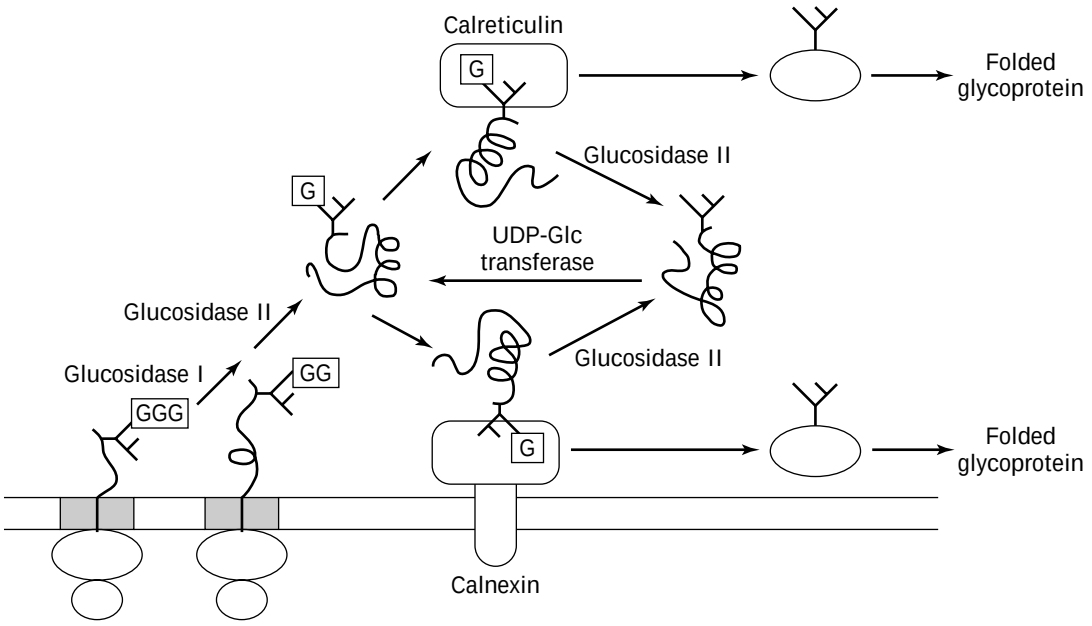

Figure 3. Role of calnexin/calreticulin and UDP-glucose:glycoprotein glucosyltransferase in the recognition and retention of unfolded glycoproteins in the ER. As a protein is cotranslationally translocated into the lumen of the ER, high-mannose core oligosaccharides are attached to asparargine residues. Subsequently, the glucose residues on the core-N-linked oligosaccharides are trimmed by the action of glucosidases I and II to expose a monoglucosylated core oligosaccharide that is a ligand for calnexin (a transmembrane protein) and/or calreticulin (a luminal ER protein) binding. After further action by glucosidase II, the glycoprotein is released from calnexin and calreticulin interaction. Unfolded glycoproteins are recognized as a substrate for the UDP-glucose:glycoprotein glucosyltransferase to form a monoglucosylated ligand to promote another round of calnexin and/or calreticulin binding. Folded glycoproteins bypass reglucosylation and are subsequently transported to the Golgi compartment. *Source*: Adapted from Ref. 44, with permission.

A sequential series of additional carbohydrate modifications occur that are separated spatially and temporarily as the protein transits through the *cis*, *medial*, and *trans* Golgi compartments. Mannose residues are removed by Golgi mannosidases I and II, and then *N*-acetylglucosamine, fucose, galactose, and sialic acid residues are added. These reactions are catalyzed by specific glycosyltransferases that modify the high-mannose carbohydrate to complex forms. Also within the Golgi apparatus, O-linked oligosaccharides are attached to the hydroxyl of serine or threonine residues through an O-glycosidic bond to *N*-acetylgalactosamine. Serine and threonine residues subject to glycosylation are frequently clustered together and contain an increased frequency of proline residues in the region, especially at positions -1 and $+3$, relative to the glycosylated residue (56). Galactose, fucose, and sialic acid are frequently attached to the serine/threonine-linked *N*-acetylgalactosamine. O-glycosylation occurs in the Golgi complex concomitant with complex processing of N-linked oligosaccharides.

The role of N- and O-linked oligosaccharide addition in glycoprotein function can be studied by using specific enzymatic inhibitors, glycosidases, and mutant cell lines (24). N-linked glycosylation is most easily evaluated by using specific glycosidases. The acquisition of resistance to endo-β-*N*-acetylglucosaminidase (Endo-H), which cleaves high-mannose and some hybrid-type oligosaccharides at the GlcNAcβ1-4GlcNAc linkage to leave a single GlcNAc residue attached to the asparagine (57), is frequently used to monitor movement of the protein from the ER to the medial Golgi apparatus. Resistance to Endo-H occurs in the medial Golgi following action of GlcNAc transferase I and mannosidase II. Peptide-*N*4-(*N*-acetyl-β-glucosaminyl)-asparagine amidase (N-gly) removes all N-linked oligosaccharides, regardless of the complexity of their structure, to leave a free aspartic acid residue (58). Also of use are a number of inhibitors that are specific for selective steps in the N-linked oligosaccharide processing pathway (see Fig. 2). In addition, a number of cell lines have been isolated that are defective in specific steps in oligosaccharide processing (59).

There are no specific inhibitors that can be used to study the requirement for O-linked glycosylation. It is possible to inhibit O-glycosylation, as well as complex modification of N-linked oligosaccharides, by depletion of the divalent metal ion manganese from the secretory pathway, and this may be used as an indication of whether O-linked sugars are present on the polypeptide (60). Of greater utility is a mutant cell line, ldlD, that is deficient in the UDP-galactose and UDP-*N*-acetylgalactosamine-4-epimerase and cannot synthesize Gal or GalNAc under normal growth conditions in the presence of glucose (61,62).

Finally, it is possible to enzymatically remove O-linked glycans with endo-α-*N*-acetyl-D-galactosaminidase (*O*-glycanase) that cleaves the Galβ1-3GalNAc disaccharide unit linked to serine or threonine residues (63). Sialic acid residues on the Gal or GalNAc will inhibit *O*-glycanase cleavage and therefore need to be removed by prior digestion with neuraminidase.

Glycosylphosphatidylinositol Anchor Addition

The addition of glycosylphosphatidylinositol (GPI) to many cell-surface-associated proteins occurs in order to anchor the protein in the lipid bilayer. The addition of GPI anchors occurs in the ER. A signal in the carboxy terminus of the polypeptide substrate contains a hydrophobic sequence of 17–30 amino acids followed by a spacer of 5–10 amino acids and a cleavage/attachment site. The attachment site must be an amino acid with a small side chain. The reaction is catalyzed by GPI:protein transamidase. This activity is defective in individuals with paraxysmal nocturnal hemoglobinuria. This disease results from a defect in the cell surface expression of inhibitors of complement-mediated cell lysis (such as decay accelerating factor). As a consequence, hemolytic anemia occurs because blood cells are unprotected from complement-mediated lysis.

Gamma-Carboxylation of Glutamic Acid Residues

The precursor of the vitamin K–dependent coagulation factors and a number of bone proteins and growth factors contain a propeptide that directs γ-carboxylation of up to 12 glutamic acid residues at the amino terminus of the mature protein (64). The propeptides of these proteins exhibit amino acid conservation within the γ-carboxylase recognition site and the site for cleavage of the propeptide. NMR structural analysis identified that the propeptide is an amphipathic α-helix with the carboxylase recognition site N-terminal to the helix (65).

The vitamin K–dependent γ-glutamyl carboxylase enzyme converts glutamate residues to γ-carboxyglutamate Gla residues. In the presence of CO_2, O_2, and vitamin K hydroquinone (KH_2) the enzyme is able to carboxylate a peptide containing glutamic acid residues, yielding a Gla-containing peptide, vitamin K epoxide, and H_2O (66). The vitamin K epoxide formed is subsequently reduced to regenerate KH_2 by either a thiol or the enzyme vitamin K epoxide reductase. The bovine (67) and human (68) cDNAs encoding the vitamin K–dependent γ-glutamyl carboxylase were isolated and demonstrate that the protein is a single-chain polypeptide of 94,000 kDa that spans the membrane 3 to 5 times. The overexpressed protein product directed increased carboxylation activity in vitro using isolated microsomes from transfected mammalian or insect cells and a synthetic peptide substrate (67,69). The ability to express γ-carboxylase activity from the cloned cDNA has permitted identification of the propeptide binding site between residues 50 and 225 (70) and the γ-carboxylase active site for glutamate binding within 218 residues of the amino terminal (71), whereas the vitamin K–reactive site is in the carboxy terminus of the protein (72). Vitamin K epoxidase activity is also catalyzed by the enzyme, and the carboxy terminus of the enzyme is required for this activity.

High-level expression of the vitamin K–dependent plasma proteins in transfected mammalian cells is limited by the ability of the mammalian host cell to efficiently perform γ-carboxylation of amino-terminal glutamic acid residues and also to efficiently cleave the propeptide (73,74). Analysis of factor IX expressed in CHO cells revealed that the protein had a much lower specific activity compared with the natural human plasma–derived protein. The reduced specific activity was attributed to both the limited ability of CHO cells to cleave the propeptide of factor IX and its ability to efficiently perform γ-carboxylation (67,73). Overexpression of the γ-carboxylase cDNA yielded increased activity in microsomal fractions when measured in vitro using small substrates (67). However, overexpression of the γ-carboxylase did not improve γ-carboxylation of factor IX when coexpressed in transfected mammalian cells (67). These results suggest that the amount of carboxylase protein is not a limiting factor to direct vitamin K–dependent γ-carboxylation in vivo. Several possibilities exist for the inability of the overexpressed γ-carboxylase to improve γ-carboxylation in vivo. First, the overexpressed γ-carboxylase may be mislocalized within the secretory pathway. It is possible that another protein, such as a protein chaperone, may be required to utilize a more complex protein substrate as opposed to a small peptide substrate. It is possible that another cofactor, possibly reduced vitamin K, is limiting for factor IX carboxylation in vivo. Further information on the mechanism of γ-carboxylation reaction in vivo is required in order to elucidate the rate-limiting step for γ-carboxylation in vivo.

β-Hydroxylation of Amino Acids: Aspartic acid, Asparagine, Lysine, and Proline

Proline and lysine residues are hydroxylated in procollagen by prolyl-3-hydroxylase and prolyl-4-hydroxylase. Prolyl-4-hydroxylase acts on prolines if the amino acid sequence is G-X-P, where X is any amino acid. This reaction requires O_2, Fe^{2+}, ascorbic acid, and α-ketoglutarate. This modification is important for stability of the collagen triple helix. Vitamin C deficiency results in scurvey because of reduced proline hydroxylation to form a stable collagen triplex.

A number of proteins that contain epidermal growth factor (EGF) domains, such as blood coagulation factor IX, have an aspartic acid or asparagine that is β-hydroxylated (75). This modification occurs by posttranslational hydroxylation of aspartic acid and/or asparagine within the ER. The β-hydroxylase has been molecularly cloned and characterized to some extent in recent years (76,77). β-Hydroxylation does not require the propeptide, vitamin K, or concomitant γ-carboxylation. A consensus β-hydroxylation site within EGF domains (Cys-X-Asp/Asn-X-X-X-X-Phe/Tyr-X-Cys-X-Cys) was proposed (75). Hydroxylation of both aspartic acid and asparagine is catalyzed by aspartyl β-hydroxylase, requires 2-ketoglutarate and Fe^{2+} (78,79), and is inhibited by agents that inhibit 2-ketoglutarate-dependent dioxygenases (80). It is interesting that only 0.3 mol/mol of plasma factor IX is modified by β-hydroxylation at Asp64, and this same amount of β-hydroxylation occurs

in recombinant factor IX expressed at high levels in CHO cells (80). Thus, the low efficiency of β-hydroxylation appears to be a consequence of the factor IX polypeptide backbone and independent of the cell type used for expression.

Sulfation of Tyrosine Residues

Sulfate addition to tyrosine as an *O*4-sulfate ester is a common postranslational modification of secretory proteins that occurs in the trans Golgi apparatus (81) and is mediated by tyrosylprotein sulfotransferase that utilizes the activated sulfate donor 3′-phosphoadenosine 5′-phosphosulfate (PAPS) (82,83). Although the enzyme has been biochemically characterized (83), to date the enzyme has not been molecularly cloned. This modification occurs on many secretory proteins including a number of proteins that interact with thrombin, such as hirudin (84), fibrinogen (85), heparin cofactor II (86), α2-antiplasmin (87), vitronectin (88), bovine factor X (89), factor V, and factor VIII (90–92). Comparison of all known tyrosine sulfation sites yielded a consensus sequence that is primarily characterized by a large number of acidic amino acid residues. The consensus tyrosine sulfation site has three aspartic acid and/or glutamic acid residues near the sulfated tyrosine (± 5 amino acids), a turn-inducing residue within $+7/-7$, and the absence of cysteine or N-linked glycosylation sites within 7 residues of the sulfated tyrosine (81). Although tyrosine sulfation modification is found on many proteins that transit the secretory apparatus, there are few examples where this modification is required for secretion or functional activity of the molecule; for example, tyrosine sulfation in the hormone cholecystokinin is required for its biological activity (93). However, tyrosine sulfation can modulate the biological activity, binding affinities, and secretion of specific proteins (81). For example, tyrosine sulfation at the carboxy terminus of hirudin increases its binding affinity to the anion binding exosite of thrombin (94,95).

The most direct method to measure sulfation of a particular protein is to measure incorporation of [^{35}S]-sulfuric acid into protein as it is synthesized in cultured cells as described in Ref. 24. [^{35}S]-Sulfuric acid will not be incorporated in cysteine. Sodium chlorate is an inhibitor of ATP sulfurylase, the first of two enzymes involved in the synthesis of 3′-phosphoadenosine 5′-phosphosulfate (PAPS). PAPS is the donor for sulfation of both tyrosine and carbohydrate residues in intact cells (96). Analysis of proteins synthesized in the presence of sodium chlorate can provide a useful means to study the role of tyrosine sulfation.

Proteolytic Processing of Precursor Polypeptides

Early studies demonstrated that the budding yeast *Saccharomyces cerevisiae* gene product Kex2 could cleave mammalian precursor polypeptides after paired basic residues (97), suggesting that a human homologue of Kex2 may be the protease required for propeptide processing. Kex2 is a membrane-bound Ca^{2+}-dependent subtilisin-like serine protease that cleaves substrates, such as alpha mating factor, within the *trans*-Golgi compartment (98,99). A computer search identified a human homologue of Kex2 upstream of the c-*fes*/*fps* protooncogene and was subsequently named furin (fes/feps upstream coding region) or PACE, an acronym for "paired basic amino acid cleaving enzyme." The cDNA was subsequently cloned and shown to encode a protein that could cleave pro-vWF (100,101), pro–nerve growth factor (102), proalbumin (103), complement pro-C3 (104), and pro–factor IX (73) after pairs of basic amino acids. PCR-based cloning strategies subsequently identified over a half dozen members of this subtilisin-like serine protease family (105). Expression of some of these enzymes (PC1/PC3, PC2, and PC4) is restricted to neuroendocrine tissues, and the activities are likely responsible for processing of neuropeptides and endocrine hormones (106,107). In contrast, furin/PACE and PACE4 are ubiquitously expressed, but to a greater extent in the hepatocyte (108,109), and are likely candidates for processing of many other proteins including coagulation factors.

Propeptide cleavage occurs in the trans Golgi compartment just prior to secretion from the cell. The activity of the propeptide processing enzymes is uniquely regulated where a calcium-dependent induced autocatalytic activation occurs within the trans Golgi compartment to activate these proteases to their active form (110–113). In the process of activation, a propeptide is cleaved away from the zymogen. The specific localization of propeptide processing to the trans Golgi compartment ensures that the propeptide is associated with the mature polypeptide as proteins transit the secretory compartment.

Characterization of the amino acid requirements around the propeptide cleavage site has identified that both the P1 and P4 arginine are important for efficient processing mediated by furin/PACE and PACE4 (114,115). Cotransfection experiments were performed to test whether these enzymes could process pro–factor IX and or pro-vWF. Whereas both furin/PACE and PACE4 were effective at enhancing pro-vWF processing, only furin/PACE was capable of improving pro–factor IX processing. Thus, it appears that different members of this class of enzymes recognize and process overlapping sets of substrates. Overexpression of furin/PACE in transfected cells (103) as well as in transgenic animals (116) improves the ability to yield fully processed proteins. Recombinant factor IX is produced by coexpression with furin/PACE to ensure complete processing of the propeptide.

VESICULAR PROTEIN TRANSPORT

Transport vesicles are the intermediates for the trafficking of proteins between compartments of the secretory pathway (117). The principal mechanism of transport vesicle formation is through cytosolic coat proteins that bind to specific sites on the membrane (118). Interactions between these coat proteins and the cytosolic tails of membrane proteins play a fundamental role in sorting cargo into vesicles (119,120). Binding of coat proteins to the membrane induces the configuration of the membrane into a coated bud. Membrane fission at the neck of this bud releases the vesicle. The most well-characterized coat protein is the clathrin coat that is responsible for endocytic vesicle formation

at the plasma membrane. Two additional types of coat components mediate vesicle formation and fusion within the secretory pathway. COP II (*co*at *p*rotein) components are required for the formation of vesicles that export cargo from the ER. COP I components were identified as coat proteins that form Golgi-derived transport vesicles (121,122) (Fig. 4).

Protein transport through the secretory pathway begins at the ER. Secretory proteins leave the ER in vesicles that bud from a specialized region of the ER. Protein transport between the ER and the intermediate compartment occurs in both directions. Retrograde transport from the intermediate compartment to the ER was first demonstrated for ER-resident proteins. If such proteins are erroneously incorporated into transport vesicles and leave the ER, they are efficiently recycled by retrograde transport. COP I–coated vesicles mediate the recycling of ER-resident proteins from intermediate compartments back to the ER, and COP II–coated vesicles mediate the export from the ER. The interaction of COP I and COP II components with the cytosolic tail domains of secretory transmembrane and ER-resident transmembrane proteins is likely to play an important role in sorting cargo into transport vesicles (119,120). Recently studies have used green fluorescent protein fused to vesicular stomatitis virus glycoprotein to visualize protein trafficking between the ER and Golgi compartments in living cells. The results demonstrate that the COP II–coated vesicles that are derived from the ER membrane have their coat proteins replaced by COP I and then move in a manner that depends on microtubules to the Golgi complex (Fig. 4). In addition, the vesicles are more elongated (appearing more like tubules) and are juxtaposed to microtubules that probably guide their movement (122,123).

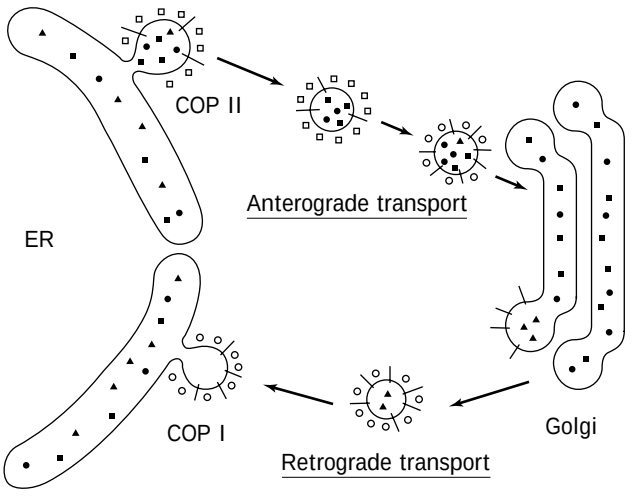

Figure 4. Proposed roles of COP I and COP II in vesicle traffic between the ER and cis Golgi. COP II vesicles transport normal cargo, some escaped ER resident proteins, and some anterograde targeting membrane proteins from the ER to the intermediate compartment where the COP II coat is exchanged for a COP I coat. The COP I–coated vesicle then fuses with the cis Golgi compartment. COP I vesicles are also shown mediating retrograde transport to the ER for escaped ER proteins.

Secretory proteins pass through the Golgi in the cis to trans direction. As proteins pass through the Golgi compartments they are modified by sequence of glycosylation and deglycosylation steps (124). Best understood is the modification of N-linked glycans in the Golgi. Initial trimming of mannose residues is followed by attachment of *N*-acetylglucosamine (GlcNAc), which is followed by more trimming of mannose residues and attachment of more GlcNAc. Mannose trimming and GlcNAc addition occur in cis and medial Golgi compartments. Although each Golgi subcompartment differs from its neighboring compartments in the specific set of enzymes contained within it, this separation is not complete. The same enzymes may even have different localization in different cell types. Golgi enzymes are not restricted to just one cistern. When the distributions of two different Golgi enzymes were determined relative to each other in the same samples, both were found spread out over several cisternae. The maximum concentration of each enzyme was in different in different compartments, but their distribution showed considerable overlap. Furthermore, Golgi enzymes seem to be in flux. Experiments with yeast demonstrated that a Golgi enzyme that is predominantly localized in the early Golgi was modified by late-acting Golgi enzymes (125). In a similar study using mammalian cells it was shown that an enzyme that was localized in the medial Golgi could be modified by an enzyme in the cis Golgi, even after the medial Golgi enzyme had reached its localization (126). These results indicate that Golgi enzymes must be efficiently recycled from late to early Golgi compartments and move again forward with the secretory flow. Golgi enzymes are not immobile in Golgi cisternae, but rather are freely diffusable.

Two models are proposed to explain protein transport through the Golgi: the vesicular transport model and the cisternal maturation model (127–129). The vesicular transport model assumes several distinct subcompartments that exchange cargo by vesicular transport in the anterograde and retrograde direction. The cisternal maturation model proposes that cisternae form de novo by fusion of ER-derived transport vesicles. These ER-derived transport intermediates would acquire Golgi enzymes by fusion with Golgi-derived retrograde transport vesicles from the cis-most compartment of the Golgi stack. At the same time, resident Golgi enzymes would move by retrograde transport in the trans to cis direction, from cisternae that formed earlier to more recently formed cisternae. Ultimately, cisternae would emerge on the trans face of the Golgi stack and disperse into vesicles of the constitutive and regulated secretory pathways and into transport vesicles to endosomes and lysosomes. Both models were first formulated shortly after the Golgi apparatus was characterized by electron microscopy, and which one best describes the Golgi has been controversial ever since.

Fusion of the vesicle membrane with its target membrane requires the cytosolic protein NSF (NEM-sensitive factor for fusion). NSF interacts with another cytosolic protein, SNAP (soluble NSF attachment protein), and SNARE (SNAP receptor) membrane proteins (130). It is the interaction of vesicle SNARE (v-SNARE) with target SNARE (t-SNARE) that is thought to play an important role in

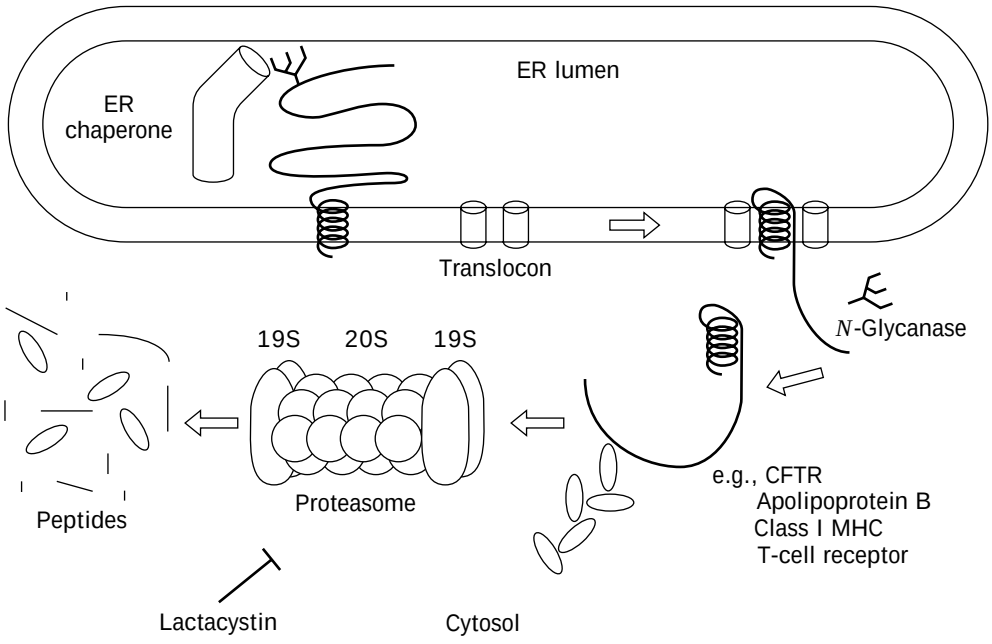

Figure 5. Degradation of ER-associated proteins. A putative ER chaperone facilitates association of a protein, with the Sec61 translocon. Reverse translocation from the lumen to the cytosol occurs with subsequent deglycosylation by *N*-glycanase. The protein may be subject to modification by ubiquitination and eventual targeting to the proteasome. Soluble proteins of the ER may also be degraded by reverse translocation through the Sec61 translocon, or alternatively they may associate with transmembrane proteins, such as CNX, that mediate their degradation. *Source*: Adapted from Ref. 141, with permission.

controlling the specificity of the vesicle fusion reaction. The precise role of NSF in this reaction is unclear. NSF action disrupts a v-SNARE/t-SNARE complex (131). This disruption could be what mediates the rearrangement of SNAREs that is required during fusion (132). These results therefore support the hypothesis that NSF directly mediates vesicle fusion. However, in yeast NSF mutants, vesicles accumulate in the cytosol, and this observation lends support to a model in which NSF is required for vesicle docking (133). Consistent with this hypothesis is that although yeast vacuole fusion is NSF dependent, the NSF action in this process precedes the docking of the membranes (134). These results indicate that NSF acts by activating the SNAREs for vesicle docking, rather than being involved in fusion itself. Small GTP-binding proteins of the rab family, as well as other proteins such as p115/Uso1p, are likely to be involved in further control of vesicle docking and fusion (135–138).

Mammalian cells constitutively transport proteins within vesicles from the ER to the plasma membrane, where they fuse through exocytosis. There are also specialized secretory cells, for example neuroendocrine cells, that store granules and release them upon appropriate stimulation through a regulated secretory pathway. Different proteins are sorted to the regulated secretory granules in different cell types through a common mechanism. The sorting process involves selective protein aggregation into clathrin-coated vesicles at the trans Golgi network. The aggregation occurs at pH 6.5 with 1 mM Ca^{2+}.

PROTEIN RETENTION AND DEGRADATION IN THE ER

A protein within the ER has several possible destinations that include transport to the Golgi compartment, degradation, and retention in the ER. What determines the fate of any particular polypeptide? For resident proteins of the ER, there are two primary mechanisms that ensure that proteins do not exit the ER compartment (139). Soluble luminal proteins of the ER, such as BiP and PDI, contain a carboxy-terminal tetrapeptide, with the consensus sequence KDEL, that is necessary and sufficient for preventing secretion of the polypeptide. A KDEL receptor, that is, a transmembrane-spanning protein, binds KDEL-containing proteins that leave the ER and retrieves them to the ER from the intermediate compartment. For transmembrane-resident proteins of the ER, there is a signal within the cytosolic domain that mediates retrieval from the intermediate compartment by COP proteins. Type I transmembrane-resident ER proteins contain a dilysine motif in the carboxy terminus (i.e., cytosolic tail). For type II transmembrane proteins, a diarginine motif in the amino terminus mediates the interaction with COP proteins. COP I vesicles then retrieve these proteins to the ER from the intermediate compartment.

As mentioned earlier, for many years investigators searched for signals that direct protein transport out of the ER. Although it is now known that specific short sequences exist that facilitate export from the ER, it appears now that the majority of polypeptides have retention signals

that prevent their export. As a polypeptide folds, these retention signals become buried within the polypeptide, and thus, the polypeptide can transit to the Golgi compartment. A variety of polypeptides that recognize and bind unfolded proteins have been identified, including BiP/GRP78, CNX, and CRT, which were discussed earlier. These protein chaperones play a fundamental role in preventing unfolded proteins from exiting the ER compartment.

Proteins that are unable to attain their native conformation are targeted for degradation. A nonlysosomal pathway has been identified in the degradation of these proteins (140,141). The discovery that lactacystin, a fungal metabolite that specifically binds and inhibits the cytosolic 26S proteasome, inhibits the degradation of many ER-associated proteins pointed to the involvement of the cytosolic proteasome in the degradation of ER-localized proteins. There are now a number of examples of ER-associated proteins, such as the cystic fibrosis transmembrane conductance regulator, the T-cell receptor, factor VIII, class I MHC molecules, and so forth, that are degraded by this pathway (53,142–146). Insight into the mechanism of degradation was obtained by studying how human cytomegalovirus (HCMV) evades the immune system (Fig. 5). HCMV encodes two gene products, US2 and US11, that are able to dislocate ER MHC class I proteins to the cytosol (146,147). This dislocation occurs through the Sec61 protein conducting channel (148). Once in the cytosol, the class I molecules are deglycosylated by an *N*-glycanase and are then polyubiquitinated. The ubiquitinated protein is then degraded by the cytosolic 26S proteasome. How are unfolded proteins identified to be degraded? The answer to this question is unknown, but present data suggest that CNX may be involved in this quality control decision. Proteins that are destined to be degraded are bound to CNX but not to CRT (53,143,149,150). CNX is a transmembrane protein that is in close proximity to the Sec61p translocon. It is speculated that CNX may mediate the transfer of unfolded proteins in the lumen of the ER to the proteasome.

ACKNOWLEDGMENTS

I thank Joe Nowak and Renee Strauss for assistance in preparation of this article.

BIBLIOGRAPHY

1. H. Nielsen, J. Engelbrecht, S. Brunak, and G. von Heijne, *Protein Eng.* **10**, 1–6 (1997).
2. P. Walter and A.E. Johnson, *Annu. Rev. Cell Biol.* **10**, 87–119 (1994).
3. A.K. Corsi and R. Schekman, *J. Biol. Chem.* **271**, 30299–39302 (1996).
4. P.J. Rapiejko and R. Gilmore, *J. Cell Biol.* **117**, 493–503 (1992).
5. P.J. Rapiejko and R. Gilmore, *Mol. Biol. Cell* **5**, 887–897 (1994).
6. J.D. Miller, H. Wilhelm, L. Gierasch, R. Gilmore, and P. Walter, *Nature* **366**, 351–354 (1993).
7. B. Wiedmann, H. Sakai, T.A. Davis, and M. Wiedmann, *Nature* **370**, 434–440 (1994).
8. B. Lauring, G. Kreibich, and M. Weidmann, *Proc. Natl. Acad. Sci. U.S.A.* **92**, 9435–9439 (1995).
9. B. Lauring, H. Sakai, G. Kreibich, and M. Wiedmann, *Proc. Natl. Acad. Sci. U.S.A.* **92**, 5411–5415 (1995).
10. S. Voigt, B. Jungnickel, E. Hartmann, and T.A. Rapoport, *J. Cell Biol.* **134**, 25–35 (1996).
11. C.J. Stirling, J. Rothblatt, M. Hosobuchi, R. Deshaies, and R. Schekman, *Mol. Biol. Cell* **3**, 129–142 (1992).
12. D. Gorlich and T.A. Rapoport, *Cell* **75**, 615–630 (1993).
13. T.A. Rapoport, *Science* **258**, 931–936 (1992).
14. C.V. Nicchitta and G. Blobel, *Cell* **73**, 989–998 (1993).
15. J.A. Morris, A.J. Dorner, C.A. Edwards, L.M. Hendershot, and R.J. Kaufman, *J. Biol. Chem.* **272**, 4327–4334 (1997).
16. S. High and B. Dobberstein, *Curr. Opin. Cell Biol.* **4**, 581–586 (1992).
17. B.D. Hamman, L.M. Hendershot, and A.E. Johnson, *Cell* **92**, 747–758 (1998).
18. B. Martoglio, M.W. Hofmann, J. Brunner, and B. Dobberstein, *Cell* **81**, 207–214 (1995).
19. R.E. Dalbey, M.O. Lively, S. Bron, and J.M. van Dijl, *Protein Sci.* **6**, 1129–1138 (1997).
20. K.U. Kalies, T.A. Rapoport, and E. Hartmann, *J. Cell Biol.* **141**, 887–894 (1998).
21. A.J. Dorner, L.C. Wasley, and R.J. Kaufman, *Proc. Natl. Acad. Sci. U.S.A.* **87**, 7429–7432 (1990).
22. P. Mayinger, V.A. Bankaitis, and D.I. Meyer, *J. Cell Biol.* **131**, 1377–1386 (1995).
23. A.J. Dorner and R.J. Kaufman, *Biologicals* **22**, 103–112 (1994).
24. A.J. Dorner and R.J. Kaufman, *Methods Enzymol.* **185**, 577–596 (1990).
25. C.B. Anfinsen, E. Haber, M. Sela, and F.H. White, *Proc. Natl. Acad. Sci. U.S.A.* **47**, 1309–1314 (1961).
26. S. Munro and H.R.B. Pelham, *Cell* **46**, 291–300 (1986).
27. G.C. Flynn, T.G. Chappell, and J.E. Rothman, *Science* **245**, 385–390 (1989).
28. Y. Kozutsumi, M. Segal, K. Normington, M.J. Gething, and J. Sambrook, *Nature* **332**, 462–464 (1988).
29. A.S. Lee, *Trends Biochem. Sci.* **12**, 20–24 (1987).
30. M.-J. Gething and J. Sambrook, *Nature* **355**, 33–45 (1992).
31. J.E. Rothman, *Cell* **59**, 591–601 (1989).
32. D.T.W. Ng, R.E. Randall, and R.A. Lamb, *J. Cell Biol.* **109**, 3273–3289 (1989).
33. A.J. Dorner, D.G. Bole, and R.J. Kaufman, *J. Cell Biol.* **105**, 2665–2674 (1987).
34. T. Hai, F. Liu, E.A. Allegretto, M. Karin, and M.R. Green, *Genes Dev.* **2**, 1216–1226 (1988).
35. P. Blount and J.P. Merlie, *J. Cell Biol.* **113**, 1125–1132 (1991).
36. I. Braakman, J. Helenius, and A. Helenius, *Nature* **356**, 260–262 (1992).
37. L. Hendershot, D. Bole, G. Kohler, and J.F. Kearney, *J. Cell Biol.* **104**, 761–767 (1987).
38. A.J. Dorner, M.G. Krane, and R.J. Kaufman, *Mol. Cell. Biol.* **8**, 4063–4070 (1988).
39. A.J. Dorner, L.C. Wasley, and R.J. Kaufman, *EMBO J.* **11**, 1563–1571 (1992).

40. B.A. Pollok, R. Anker, P. Eldridge, L. Hendershot, and D. Levitt, *Proc. Natl. Acad. Sci. U.S.A.* **84**, 9199–9203 (1987).
41. A. Zapun, T.E. Creighton, P.J.E. Rowling, and R.B. Freedman, *Proteins* **14**, 10–15 (1992).
42. C. Hwang, A.J. Sinskey, and H.F. Lodish, *Science* **257**, 1496–1502 (1992).
43. R. Noiva and W.J. Lennarz, *J. Biol. Chem.* **267**, 3553–3556 (1992).
44. A. Helenius, *Mol. Biol. Cell* **5**, 253–265 (1994).
45. S. Silberstein, P.G. Collins, D.J. Kelleher, P.J. Rapiejko, and R. Gilmore, *J. Cell Biol.* **128**, 525–536 (1995).
46. J.L. Guan, C.E. Machamer, and J.K. Rose, *Cell* **42**, 489–496 (1985).
47. D.J. Kelleher, G. Kreibich, and R. Gilmore, *Cell* **69**, 55–65 (1992).
48. Y. Gavel and G. von Heijne, *Protein Eng.* **3**, 433–442 (1990).
49. D.N. Hebert, B. Foelimer, and A. Helenius, *Cell* **81**, 425–433 (1995).
50. J.J. Bergeron, M.B. Brenner, D.Y. Thomas, and D.B. Williams, *Trends Biochem. Sci.* **19**, 124–128 (1994).
51. K.H. Krause and M. Michalak, *Cell* **88**, 439–443 (1997).
52. D.N. Hebert, B. Foellmer, and A. Helenius, *EMBO J.* **15**(12), 2961–2968 (1996).
53. S.W. Pipe, J.A. Morris, J. Shah, and R.J. Kaufman, *J. Biol. Chem.* **273**, 8537–8544 (1998).
54. S.E. Trombetta and A.J. Parodi, *J. Biol. Chem.* **267**, 9236–9240 (1992).
55. A.D. Elbein, *Semin. Cell Biol.* **2**, 309–317 (1991).
56. I.B. Wilson, Y. Gavel, and G. von Heijne, *Biochem. J.* **275**, 529–534 (1991).
57. A.L. Tarentino and F. Maley, *J. Biol. Chem.* **249**, 811–817 (1974).
58. A.L. Tarentino, C.M. Gomez, and T.H. Plummer, Jr., *Biochemistry* **24**, 4665–4671 (1985).
59. P. Stanley, in M.M. Gottesman ed., *Molecular Cell Genetics*, Wiley, New York, 1985, pp. 745–772.
60. R.J. Kaufman, M. Swaroop, and P. Murtha-Riel, *Biochemistry* **33**, 9813–9819 (1994).
61. C.L. Wasley, P. Horgan, G. Timony, J. Stoudemier, M. Krieger, and R.J. Kaufman, *Blood* **77**, 2624–2632 (1991).
62. D.M. Kingsley, K.F. Kozarsky, L. Hobbie, and M. Krieger, *Cell* **44**, 749–759 (1986).
63. J. Umemoto, V.P. Bhavanandan, and E.A. Davidson, *J. Biol. Chem.* **252**, 8609–8614 (1977).
64. M.J. Jorgensen, A.B. Cantor, B.C. Furie, C.L. Brown, C.B. Shoemaker, and B. Furie, *Cell* **48**, 185–191 (1987).
65. D.G. Sanford, C. Kanagy, J.L. Sudmeier, B.C. Furie, B. Furie, and W.W. Bachovchin, *Biochemistry* **30**, 9835–9841 (1991).
66. J.W. Suttie, *FASEB J.* **7**, 445–452 (1993).
67. A. Rehemtulla, D.A. Roth, L.C. Wasley, A. Kuliopulos, C.T. Walsh, B. Furie, B.C. Furie, and R.J. Kaufman, *Proc. Natl. Acad. Sci. U.S.A.* **90**, 4611–4615 (1993).
68. S.M. Wu, W.F. Cheung, D. Frazier, and D.W. Stafford, *Science* **254**, 1634–1636 (1991).
69. D.A. Roth, A. Rehemtulla, R.J. Kaufman, C.T. Walsh, B. Furie, and B.C. Furie, *Proc. Natl. Acad. Sci. U.S.A.* **90**, 8372–8376 (1993).
70. M. Yamada, A. Kuliopulos, N.P. Nelson, D.A. Roth, B. Furie, B.C. Furie, and C.T. Walsh, *Biochemistry* **34**, 481–489 (1995).
71. A. Kuliopulos, N.P. Nelson, M. Yamada, C.T. Walsh, B. Furie, B.C. Furie, and D.A. Roth, *J. Biol. Chem.* **269**, 21364–21370 (1994).
72. D.A. Roth, M.L. Whirl, L.J. Velazquez-Estades, C.T. Walsh, B. Furie, and B.C. Furie, *J. Biol. Chem.* **270**, 5305–5311 (1995).
73. L.C. Wasley, A. Rehemtulla, J.A. Bristol, and R.J. Kaufman, *J. Biol. Chem.* **268**, 8458–8465 (1993).
74. R.J. Kaufman, L.C. Wasley, B.C. Furie, B. Furie, and C.B. Shoemaker, *J. Biol. Chem.* **261**, 9622–9628 (1986).
75. J. Stenflo, A. Lundwall, and B. Dahlback, *Proc. Natl. Acad. Sci. U.S.A.* **84**, 368–372 (1987).
76. K. McGinnis, G.M. Ku, W.J. VanDusen, J. Fu, V. Garsky, A.M. Stern, and P.A. Friedman, *Biochemistry* **35**, 3957–3962 (1996).
77. S. Jia, W.J. VanDusen, R.E. Diehl, N.E. Kohl, R.A. Dixon, K.O. Elliston, A.M. Stern, and P.A. Friedman, *J. Biol. Chem.* **267**, 14322–14327 (1992).
78. R.S. Gronke, W.J. VanDusen, V.M. Garsky, J.W. Jacobs, M.K. Sardana, A.M. Stern, and P.A. Friedman, *Proc. Natl. Acad. Sci.* **86**, 3609–3613 (1989).
79. J. Stenflo, E. Holme, S. Lindstedt, N. Chandramouli, L.H. Huang, J.P. Tam, and R.B. Merrifield, *Proc. Natl. Acad. Sci.* **86**, 4440–4447 (1989).
80. C.K. Derian, W. VanDusen, C.T. Przysiecki, P.N. Walsh, K.L. Berkner, R.J. Kaufman, and P.A. Friedman, *J. Biol. Chem.* **264**, 6615–6618 (1989).
81. W.B. Huttner, *Annu. Rev. Physiol.* **50**, 363–376 (1988).
82. P.A. Baeuerle and W.B. Huttner, *J. Cell Biol.* **105**, 2655–2664 (1987).
83. C. Niehrs and W.B. Huttner, *EMBO J.* **9**, 35–42 (1990).
84. P.J. Braun, S. Dennis, J. Hofsteenge, and S.R. Stone, *Biochemistry* **27**, 6517–6522 (1988).
85. D.H. Farrell, E.R. Mulvihill, S.M. Huang, D.W. Chung, and E.W. Davie, *Biochemistry* **30**, 9414–9420 (1991).
86. G. Hortin, D.M. Tollefsen, and A.W. Strauss, *J. Biol. Chem.* **261**, 15827–15830 (1986).
87. G. Hortin, K.F. Fok, P.C. Toren, and A.W. Strauss, *J. Biol. Chem.* **262**, 3082–3085 (1987).
88. D. Jenne, A. Hille, K.K. Stanley, and W.B. Huttner, *Eur. J. Biochem.* **185**, 391–395 (1989).
89. T. Morita and C.M. Jackson, *J. Biol. Chem.* **261**, 4008–4014 (1986).
90. D.D. Pittman, J.H. Wang, and R.J. Kaufman, *Biochemistry* **31**, 3315–3323 (1992).
91. D.D. Pittman, K.N. Tomkinson, D. Michnick, U. Selighsohn, and R.J. Kaufman, *Biochemistry* **33**, 6952–6959 (1994).
92. D.A. Michnick, D.D. Pittman, R.J. Wise, and R.J. Kaufman, *J. Biol. Chem.* **269**, 20095–20102 (1994).
93. V. Mutt, in G.B.J. Glass ed., *Gastrointestinal Hormones* Raven Press, New York, 1980, pp. 169–221.
94. C. Niehrs, W.B. Huttner, D. Carvallo, and E. Degryse, *J. Biol. Chem.* **265**, 9314–9318 (1990).
95. T.J. Rydel, K.G. Ravichandran, A. Tulinsky, W. Bode, R. Huber, C. Roitsch, and J.W. Fenton, *Science* **249**, 277–280 (1990).
96. E. Friederich, H.J. Gritz, and W.B. Huttner, *J. Cell Biol.* **107**, 1655–1667 (1988).

97. D.C. Foster, R.D. Holly, C.A. Sprecher, K.M. Walker, and A.A. Kumar, *Biochemistry* **30**, 367–372 (1991).

98. I.C. Bathurst, S.O. Brennan, R.W. Carrell, L.S. Cousens, A.J. Brake, and P.J. Barr, *Science* **235**, 348–350 (1987).

99. D. Julius, A. Brake, L. Blair, R. Kunisawa, and J. Thorner, *Cell* **37**, 1075–1089 (1984).

100. R.J. Wise, P.J. Barr, P.A. Wong, M.C. Kiefer, A.J. Brake, and R.J. Kaufman, *Proc. Natl. Acad. Sci. U.S.A.* **87**, 9378–9382 (1990).

101. W.J. van de Ven, J. Voorberg, R. Fontijn, H. Pannekoek, A.M. van den Ouweland, H.L. van Duijnhoven, A.J. Roebroek, and R.J. Siezen, *Mol. Biol. Rep.* **14**, 265–275 (1990).

102. P.A. Bresnahan, R. Leduc, L. Thomas, J. Thorner, H.L. Gibson, A.J. Brake, P.J. Barr, and G. Thomas, *J. Cell Biol.* **111**, 2851–2859 (1990).

103. S.O. Brennan and R.J. Peach, *J. Biol. Chem.* **266**, 21504–21508 (1991).

104. Y. Misumi, K. Ohkubo, M. Sohda, N. Takami, K. Oda, and Y. Ikehara, *Biochem. Biophys. Res. Commun.* **171**, 236–242 (1990).

105. P.A. Halban and J.C. Irminger, *Biochem. J.* **299**, 1–18 (1994).

106. S. Benjannet, N. Rondeau, R. Day, M. Chretien, and N.G. Seidah, *Proc. Natl. Acad. Sci. U.S.A.* **88**, 3564–3568 (1991).

107. L. Thomas, R. Leduc, B.A. Thorne, S.P. Smeekens, D.F. Steiner, and G. Thomas, *Proc. Natl. Acad. Sci. U.S.A.* **88**, 5297–5301 (1991).

108. A.J. Roebroek, J.A. Schalken, J.A. Leunissen, C. Onnekink, H.P. Bloemers, and W.J. van de Ven, *EMBO J.* **5**, 2197–2202 (1986).

109. M.C. Kiefer, J.E. Tucker, R. Joh, K.E. Landsberg, D. Saltman, and P.J. Barr, *DNA Cell Biol.* **10**, 757–769 (1991).

110. A. Rehemtulla, A.J. Dorner, and R.J. Kaufman, *Proc. Natl. Acad. Sci. U.S.A.* **89**, 8235–8239 (1992).

111. R. Leduc, S.S. Molloy, B.A. Thorne, and G. Thomas, *J. Biol. Chem.* **267**, 14304–14308 (1992).

112. E.D. Anderson, J.K. VanSlyke, C.D. Thulin, F. Jean, and G. Thomas, *EMBO J.* **16**, 1508–1518 (1997).

113. S.S. Molloy, L. Thomas, J.K. VanSlyke, P.E. Stenberg, and G. Thomas, *EMBO J.* **13**, 18–33 (1994).

114. A. Rehemtulla and R.J. Kaufman, *Blood* **9**, 2349–2355 (1992).

115. A. Rehemtulla, P.J. Barr, C.J. Rhodes, and R.J. Kaufman, *Biochemistry* **32**, 11586–11590 (1993).

116. R. Drews, R.K. Paleyanda, T.K. Lee, R.R. Chang, W.N. Drohan, A. Rehemtulla, and R.J. Kaufman, *Proc. Natl. Acad. Sci. U.S.A.* **92**, 10462–10466 (1995).

117. J.E. Rothman, *Protein Sci.* **5**, 185–194 (1996).

118. R. Schekman and L. Orci, *Science* **271**, 1526–1533 (1996).

119. M.J. Kuehn, J.M. Herrmann, and R. Schekman, *Nature* **391**, 187–190 (1998).

120. P. Cosson and F. Letoumeur, *Science* **263**, 1629–1631 (1994).

121. R. Schekman and I. Mellman, *Cell* **90**, 197–200 (1997).

122. S.J. Scales, R. Pepperkok, and T.E. Kreis, *Cell* **90**, 1137–1148 (1997).

123. J.F. Presley, N.B. Cole, T.A. Schroer, K.J. Hirschberg, K.J. Zaal, and J. Lippencott-Schwartz, *Nature* **389**, 81–85 (1997).

124. R. Kornfeld and S. Kornfeld, *Annu. Rev. Biochem.* **54**, 631–664 (1985).

125. J. Ting, S.K. Wooden, K.S. Kelleher, R. Kritz, R.J. Kaufman, and A.S. Lee, *Gene* **55**, 147–152 (1987).

126. R.J. Jenny, D.D. Pittman, J.J. Toole, R.W. Kriz, R.A. Aldape, R.M. Hewick, R.J. Kaufman, and K.G. Mann, *Proc. Natl. Acad. Sci. U.S.A.* **84**, 4846–4850 (1987).

127. S.I. Bannykh and W.E. Balch, *J. Cell. Biol.* **138**, 1–4 (1997).

128. B.S. Glick, T. Elston, and G. Oster, *FEBS* **414**, 177–181 (1998).

129. H.D. Love, C.C. Lin, C.S. Short, and J. Ostermann, *J. Cell Biol.* **140**, 541–551 (1998).

130. T. Sollner, S.W. Whiteheart, M. Brunner, H. Erdjument-Bromage, S. Geromanos, P. Tempst, and J.E. Rothman, *Nature* **362**, 318–324 (1993).

131. J.E. Rothman, and G. Warren, *Curr. Biol.* **4**, 220–233 (1994).

132. T. Sollner, M.K. Bennett, S.W. Whiteheart, R.H. Scheller, and J.E. Rothman, *Cell* **75**, 409–418 (1993).

133. C.A. Kaiser, and R. Schekman, *Cell* **61**, 723–733 (1990).

134. A. Mayer, W. Wickner, and A. Haas, *Cell* **85**, 83–94 (1996).

135. V. Rybin, O. Ullrich, M. Rubino, K. Alexandrov, I. Simon, C. Seabra, R. Goody, and M. Zerial, *Nature* **383**, 266–269 (1996).

136. V.V. Lupashin, and M.G. Waters, *Science* **276**, 1255–1258 (1997).

137. S.K. Sapperstein, V.V. Lupashin, H.D. Schmitt, and M.G. Waters, *J. Cell Biol.* **132**, 755–767 (1996).

138. N. Nakamura, M. Lowe, T.P. Levine, C. Rabouille, and G. Warren, *Cell* **89**, 445–455 (1997).

139. H.R. Pelham, *Curr. Opin. Cell Biol.* **7**, 530–535 (1995).

140. R.D. Klausner and R. Sitia, *Cell* **62**, 611–614 (1990).

141. R.R. Kopito, *Cell* **88**, 427–430 (1997).

142. C.L. Ward, S. Omura, and R.R. Kopito, *Cell* **83**, 121–127 (1995).

143. R. Halaban, E. Cheng, Y. Zhang, G. Moellmann, D. Hanlon, M. Michalak, V. Setaluri, and D.N. Hebert, *Proc. Natl. Acad. Sci. U.S.A.* **94**, 6210–6215 (1997).

144. D. Qu, J.H. Teckman, S. Omura, and D.H. Perlmutter, *J. Biol. Chem.* **271**, 22791–22795 (1996).

145. M.M. Hiller, A. Finger, M. Schweiger, and D.H. Wolf, *Science* **273**, 1725–1728 (1996).

146. E.J. Wiertz, T.R. Jones, L. Sun, M. Bogyo, H.J. Geuze, and H.L. Ploegh, *Cell* **84**, 769–779 (1996).

147. E.J. Wiertz, D. Tortorella, M. Bogyo, J. Yu, W. Mothes, T.R. Jones, T.A. Rapoport, and H.L. Ploegh, *Nature* **384**, 432–438 (1996).

148. M. Pilon, R. Schekman, and K. Romisch, *EMBO J.* **16**, 4540–4548 (1997).

149. K.S. Cannon, D.N. Hebert, and A. Helenius, *J. Biol. Chem.* **271**, 14280–14284 (1996).

150. W. Chen, J. Helenius, I. Braakman, and A. Helenius, *Proc. Natl. Acad. Sci. U.S.A.* **92**, 6229–6233 (1995).

See also PROTEIN SECRETION, *SACCHAROMYCES CEREVISIAE*.

SHEAR SENSITIVITY

YUSUF CHISTI
University of Almería
Almería, Spain

KEY WORDS

Air-lift bioreactors
Animal cell culture
Bioreactor hydrodynamics
Bubble columns
Cell damage
Shear damage
Shear protection
Shear rate
Shear stress

OUTLINE

INTRODUCTION

Susceptibility to hydrodynamic and mechanical shear forces affects performance of cultured cells of animals, plants, microalgae, and cyanobacteria. In addition, hydromechanical forces affect or otherwise damage some commercially relevant mycelial fungi, filamentous bacteria, microbial flocs, and biofilms. In specific cases, intense shear fields may also damage the larger bioactive molecules such as enzymes. This article details the shear sensitivity of the major types of biocatalysts and the approaches available for mitigating the damaging effects. Methods for estimating shear rate and shear stress are discussed for various configurations of bioreactors operated in process-relevant conditions.

Depending on its intensity, a shear field may be stimulatory, inhibitory, or outright destructive. Intense shear fields will disintegrate even the most robust of microorganisms (1). Lesser levels of turbulence impact upon cellular morphology (2,3), biochemistry and physiology (4), floc size (5), and attachment and detachment from surfaces (6,7). These influences of shear stresses are reflected in the industrially important aspects of production rate, productivity, product spectrum, and characteristics. Among the most susceptible to shear effects are the animal cells, plant cells, and cells of some microalgae and cyanobacteria. Shear-associated problems have the greatest economic impact in the animal cell culture industry because it is among the largest ones based on shear-sensitive cells and because of the high-value nature of most cell-culture-derived products (8). Damaging consequences of intense shear fields are also well documented for other microorganisms. For example, shear effects may alter characteristics of extracellular microbial polysaccharides by affecting the secretery process in some bacteria (9,10). Considerations of shear stress levels are also important in design and operation of biomedical devices such as dialysis machines, heart-lung machines, and transfusion filters. Shear stresses associated with implanted devices such as artificial heart valves can have medically significant implications. Increasingly, shear-sensitive human cells are being used to regenerate damaged tissue in vitro for later implanting or grafting. In other instances, susceptibility to shear may be beneficial, for example, during recovery of intracellular material by mechanical disruption (1,11,12). Some of the factors that determine shear sensitivity are summarized in Table 1.

SHEAR FORCES IN BIOREACTORS

Substantial information exists on the effects of hydrodynamic forces on cells in defined flow geometries such as viscometers and capillaries (5,13–18), but little is known about shear fields in bioreactors (19–21). Whereas selection of more shear-tolerant cell lines can be helpful, successful culture of shear-sensitive biocatalysts requires attention to bioreactor design and operation.

Table 1. Factors Determining Shear Sensitivity

1.	Type of cell and species
2.	Composition and thickness of cell wall when present
3.	Size and morphology of cell
4.	The intensity and nature of shear stress, whether turbulent or laminar, or associated with interfaces (e.g., during bubble rise and rupture)
5.	Growth history, both short-term (e.g., starvation) and long-term adaptation
6.	Growth environment (pH, temperature, agitation intensity, light in photosynthetic cultures)
7.	Growth medium (trace elements, vitamins, carbon and nitrogen sources)
8.	Growth rate
9.	Growth stage
10.	Type and concentration of shear-protective agents if present

The magnitude of the fluid mechanical forces is often expressed as shear stress, τ, or shear rate, γ. These quantities are related; thus, in laminar newtonian flow,

$$\tau = \gamma \mu_L \tag{1}$$

where μ_L is the viscosity of the fluid. Shear rate is a measure of spatial variation in local velocities in a fluid. Cell damage in a moving fluid is sometimes associated with the magnitude of the prevailing shear rate or the associated shear stress, but these quantities are neither easily defined nor easily measured in the relatively turbulent environment of most bioreactors. Moreover, shear rate varies with location within a vessel. Attempts have been made to characterize an average shear rate or a maximum shear rate in various types of bioreactors and process flow devices, as discussed later for the more common cases.

Bubble Columns and Airlift Bioreactors

Expressions for mean shear rate in bubble columns have been summarized by Chisti (21), Chisti and Moo-Young (19), and Shi et al. (22). These expression generally correlate the average shear rate with the superficial gas velocity; thus

$$\gamma = k U_G^a \tag{2}$$

where the parameter a equals 1.0 in most cases, but the k value has been reported variously as 1,000, 2,800, 5,000 m^{-1}, and so forth (20). The enormous disagreement among various authorities is obvious in Figure 1, where the shear rate calculated according to several available equations is shown as a function of the superficial aeration velocity in air–water system in a bubble column.

Equation 2 has also been applied to airlift bioreactors, using the superficial gas velocity in the riser zone as a correlating parameter; however, that usage is incorrect (19). A more suitable form of equation 2 for airlift reactors is

$$\gamma = \frac{k U_{Gr}}{1 + \dfrac{A_d}{A_r}} \tag{3}$$

where U_{Gr} is the superficial gas velocity in the riser, A_r is the cross-sectional area of the riser, and A_d is the cross-sectional area of the downcomer. In addition to the already-noted discrepancies (Figure 1), equations 2 and 3 have other significant flaws. The shear rate should depend also on the momentum transfer capability of a fluid, that is, on the density and the viscosity of the fluid, but equations 2 and 3 show no such dependence. Indeed, it is well known that the bubble size in a turbulent field depends on the viscosity and the density of the fluid as well as on the specific energy input rate. It is therefore reasonable to assume that correlations that express the shear rate as a function of U_G (or U_{Gr}) alone are incomplete (19). Furthermore, correlations such as equation 2 have generally been based on observations of phenomena at solid–liquid interfaces (e.g., heat transfer from coils or jackets), and their extension to phenomena at the gas–liquid interface or the bulk fluid is absurd at best. Shear stress and, hence, shear rate at walls of riser and downcomer zones of an airlift device are readily calculated using methods developed for pipes and channels, as discussed in a later section.

Another equation for estimation of an "effective" shear rate in airlift reactors is

$$\gamma = 3.26 - 3.51 \times 10^2 U_{Gr} + 1.48 \times 10^4 U_{Gr}^2 \tag{4}$$

which was developed for $0.004 < U_{Gr}\ (m\ s^{-1}) < 0.06$ (22); the shear rate range covered was 2–35 s^{-1}. Equation 4 was developed in an external-loop airlift reactor. First, the effect of viscosity on the induced liquid circulation velocity in the downcomer was established using Newtonian glycerol solutions at various gas flow rates. The maximum Reynolds number in the downcomer was about 3,200, or barely in the turbulent regime. In a second step, pseudoplastic media were used in the reactor, and the effective viscosity (μ_{ap}) of these fluids in the circulation loop was determined as being equal to the viscosity of the Newtonian glycerol solutions, when the two systems were at identical aeration rates and liquid circulation rates. The effective viscosity and the known values of K and n were used in the power law equation to calculate the prevailing shear rate:

$$\gamma = \left(\frac{\mu_{ap}}{K}\right)^{1/n-1} \tag{5}$$

The calculated shear rates were correlated with the superficial gas velocity in the riser, as noted in equation 4 (22). Although written in terms of the superficial gas velocity in the riser, equation 4 may usefully be expressed in terms of the specific power input in the reactor, as recommended elsewhere (19).

Because the procedure employed by Shi et al. (22) equated the viscosity-associated reduction in the liquid cir-

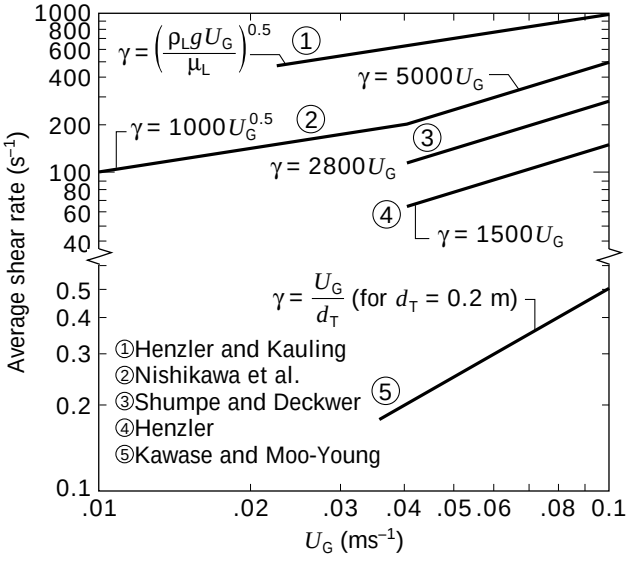

Figure 1. Average shear rate in air–water system in a bubble column according to various sources. *Source*: Based on Ref. 21.

culation velocity in different fluids, it gave in some sense a shear rate in the vicinity of the interface between the fluid and the walls of the reactor; shear rate in the bulk flow, which is the quantity of interest in most cases, was not quantified. Furthermore, the method of analysis used (22) applies strictly to a laminar flow regime, quite unlike the flow situations encountered in most practical operations.

Compared with bubble columns, equation 4 yields quite low values for shear rates in airlift reactors, as noted by Shi et al. (22). In such comparisons, care needs to be taken to ensure that the devices are being compared at identical values of specific power inputs (19,21). Although Shi et al. (22) did not adhere to this criterion, the specific geometry of the reactor they used was such that the error was small. Unlike what Shi et al. (22) concluded, equation 4 is not suitable for correlating mass transfer from gas bubbles or suspended solids because it does not give shear rates at gas–liquid or particle–liquid interfaces. Similarly, the usefulness of the shear rate calculated using equation 4, for correlating survival of fragile biocatalysts, remains questionable. An alternative, mechanistic approach to quantifying the bulk shear rate in various zones of airlift bioreactors has been advanced by Molina Grima et al. (14). Because the hydrodynamic environment in various zones of airlift reactors tends to be quite different, characterization of shear rate by a single global value is not sensible. The overall shear rates can be deceptively low even though damaging levels may be experienced in the high-shear zones (14); hence, the approach of Molina Grima et al. (14) is preferred.

Yet other attempts at characterizing the hydrodynamic forces relied on measurement of noises associated with events such as bubble formation at the sparger, bubble disengagement at the surface, and liquid flow over the baffle into the downcomer (23). Spectra of acoustic signals were measured in water, a salt solution, and aqueous glycerol media in a bubble column and split-cylinder airlift reactor (23). Because several events occur simultaneously in bubbling reactors, there were substantial ambiguities in assignment of the noise signals to specific events. The practical significance of the results was unclear even though the intended aim was to somehow relate the data to damage of fragile cells that has been reported by others in such reactors. Yet other work (24) examined the structure of turbulence in water and power law solutions ($K = 0.0194$ Pa $s^{0.973}$ and 0.0596 Pa $s^{0.958}$) in an external-loop airlift reactor. The reactor achieved complete gas–liquid separation and there was no gas in the downcomer. Measurements of local root mean square velocity fluctuations as an indicator of turbulence intensity showed a slight decrease from the center of the riser to the wall. These measurements were at a constant gas velocity of 2.05×10^{-2} m s^{-1}. The magnitudes of the velocity fluctuations were similar for all media; however, the velocity fluctuations were much lower in the gas-free downcomer than in the riser despite similar values of Reynolds numbers in the two zones. Based on measurements of one-dimensional energy spectra in the center of the riser (24), turbulence could not be considered isotropic, particularly in power law fluids. Other substantial evidence for the absence of isotropic turbulence in airlift and bubble column reactors has been documented (25,26).

Stirred-Tank Fermenters

The local velocity at a fixed position in any vessel fluctuates around a mean value; hence, the shear rate fluctuates. The extent of fluctuations is position dependent. In stirred tanks with radial-flow impellers such as Rushton turbines, the velocity fluctuations are greatest near the impeller tip and decline rapidly as one moves radially outward from the tip. Elsewhere in the vessel, the velocity fluctuations are reduced yet further. The time-averaged mean shear rate generated by a six-bladed Rushton turbine agitating a Newtonian fluid in a baffled vessels of diameter d_T is given as (27)

$$\gamma_{av} = 4.2N\left(\frac{d_i}{d_T}\right)^{0.3}\frac{d_i}{W} \tag{6}$$

where W is the width of the impeller blade, d_i is the impeller diameter, and N is it's rotational speed. The time averaged maximum shear rate value is 2.3-times γ_{av} (27). Another expression for the maximum shear rate at Rushton turbine blades is (28)

$$\gamma_{max} = 3.3N^{1.5}d_i\left(\frac{\rho_L}{\mu_L}\right)^{1/2} \tag{7}$$

which applies to Newtonian and non-Newtonian liquids when $100 \leq (Nd_i^2\,\rho_L/\mu_L) \leq 29{,}000$. The uncertainty in the coefficient (equation 7) is said to be $\pm 20\%$. For non-Newtonian fluids, μ_L in equation 7 is the zero shear viscosity. A different equation has been proposed by Wichterle et al. (28):

$$\gamma_{max} = N(1 + 5.3n)^{1/n}\left(\frac{N^{2-n}d_i^2\rho_L}{K}\right)^{1/1+n} \tag{8}$$

Equation 8 provides the maximum shear rate on a Rushton turbine blade. An average shear rate expression applicable to a broader range of impellers and media is (29):

$$\gamma_{av} = k_i\left(\frac{4n}{3n+1}\right)^{n/n-1}N \tag{9}$$

where n, the flow index of a fluid, equals 1.0 for a Newtonian liquid. In equation 9, k_i is an impeller-dependent constant. Some typical k_i values are noted in Table 2. The various shear rate correlations discussed here are compared in Figure 2 for water in a standard stirred tank (30) agitated

Table 2. The k_i Values for Use in Equation 9

Impeller	k_i
Six-bladed disc turbines	11–13
Paddle impellers	10–13
Propellers	~10
Helical ribbon impellers	~30

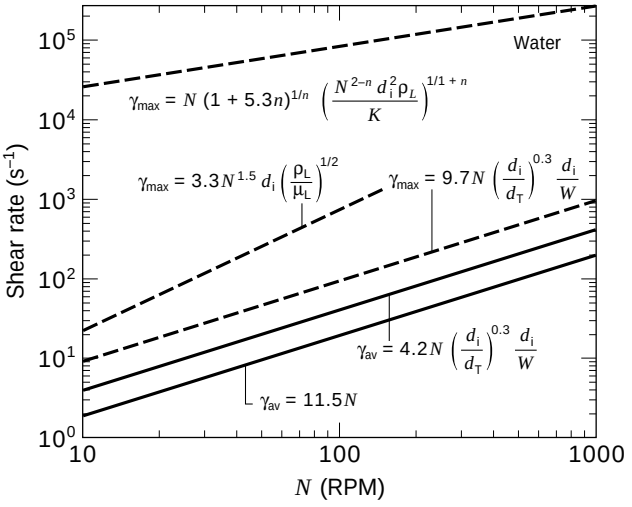

Figure 2. Comparison of the various shear rate correlations for water in a standard stirred-tank agitated with a 0.1-m-diameter six-bladed Rushton turbine. The dashed lines are for the maximum shear rate; the solid ones are for the average shear rate. See text for additional details.

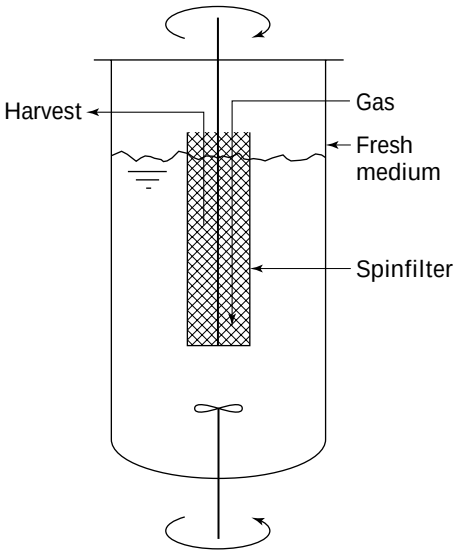

Figure 3. Perfusion culture with spinfilter for hydrodynamics-based cell retention in bioreactors.

with a 0.1-m diameter six-bladed Rushton turbine. For some contexts, the shear rate around a rising bubble may be approximated as the ratio of the terminal rise velocity to the bubble diameter (or radius); hence,

$$\gamma_{av} = \frac{2U_B}{d_B} \tag{10}$$

In air–water, under conditions typical of bubble columns and airlift reactors, the bubble rise velocity is about 0.2 m s^{-1}, and the bubble diameter is about 0.006 m. Thus, the interfacial shear rate approximates to 67 s^{-1} if the interface is nonmobile. Lower shear rates are expected at circulating interfaces.

Spinfilter

Spinfilters—rotating cylinders made of wire screen with openings that are significantly bigger (e.g., 25 μm) than the cells—are used to retain suspended animal cells in perfusion culture continuous bioreactors. Most of the cells are kept on the upstream side of the wire mesh by a hydrodynamic mechanism that depends on rapid rotation (e.g., 500 rpm) of the cylindrical screen (Fig. 3). The spent, largely cell-free medium is withdrawn from the zone within the rotating screen. Shear stresses associated with rotation of spinfilters do not generally damage animal cells (31). Sometimes the cell-free zone within the confines of the screen is also used for submerged aeration.

Other Flow Devices

Bioreactors and process vessels are where much of the shear-sensitive material is processed; however, at least part of the processing usually requires transfer of material between vessels. Transfer is accomplished through pipework, and centrifugal pumps are sometimes used. Methods of estimating shear stress levels in these devices are briefly summarized next.

Pipes, Tubings, and Flow Channels. ***Newtonian Fluids.*** In developed laminar flow of a Newtonian fluid through a straight tube of diameter d, the wall shear rate is given as

$$\gamma_w = \frac{8U_L}{d} \tag{11}$$

where U_L is the mean flow velocity. For rectangular channels of height h, the maximum or wall shear rate in developed laminar flow is

$$\gamma_w = \frac{6U_L}{h} \tag{12}$$

where U_L is again the mean flow velocity.

The wall shear stress (i.e., the maximum value) in a flow channel such as the riser of an airlift reactor is related to the pressure drop (ΔP), the length L of channel, and the hydraulic diameter (20); thus,

$$\tau_w = \frac{d}{4L}\,\Delta P \tag{13}$$

Consequently, in turbulent flow, the wall shear stress is

$$\tau_w = \frac{1}{2}\,C_f\rho_L U_L^2 \tag{14}$$

where ρ_L is the liquid density and C_f is the Fanning friction factor. The latter is related with the Reynolds number as follows:

$$C_f = 0.0792\left(\frac{\rho_L U_L d}{\mu_L}\right)^{-0.25} \quad (15)$$

where d is the hydraulic diameter of the flow channel or pipe. From equations 14 and 15, the wall shear stress can be shown to depend on Newtonian viscosity of the fluid: $\tau_w \propto \mu_L^{-0.75}$ (14). Use of equations 11 and 12 and others given later that are similar presupposes that the liquid velocity is known. This is normally the case in pipes and channels; however, with airlift vessels the induced liquid circulation rate will often need to be estimated using available methods (20,21,32).

Non-Newtonian Power Law Fluids. Methods for calculation of wall shear stress in laminar and turbulent flow of power law fluids with and without dispersed gas, have been discussed by Chisti (21) and Chisti and Moo-Young (33). For a non-Newtonian pseudoplastic medium flowing through a tube such as the riser or the downcomer of an airlift bioreactor, the flow is laminar when (34)

$$Re \leq 2300\,\frac{3n+1}{4n} \quad (16)$$

where the Reynolds number is calculated using the equation

$$Re = \frac{8U_L^{2-n}d^n\rho_L}{K\left(\frac{6n+2}{n}\right)^n} \quad (17)$$

In the laminar regime, the wall shear stress for flow of a gas-free liquid has been expressed as (35)

$$\tau_w = \frac{8\rho_L U_L^2}{Re} \quad (18)$$

When the flow is turbulent (i.e., the Reynolds number exceeds the value calculated with equation 16), the wall shear stress in a gas-free liquid is (34,35)

$$\tau_w = \frac{0.316n^{0.121}\rho_L U_L^2}{8Re^{2/n(x-1)+2}} \quad (19)$$

In presence of a gas, the shear stress is a complex function of τ_w, the gas holdup, the properties of the liquid (ρ_L, K, n), and the superficial velocities of the gas and the liquid phases, as discussed elsewhere (21,33). In equations 16–19, d is the channel diameter, U_L is the superficial liquid velocity, K is the consistency index, and n is the flow behavior index. The parameter x in equation 19 is given as

$$x = 0.70n^{-0.591} \quad (20)$$

as reported by Chisti and Moo-Young (33) based on data of Sokolov and Metkin (34).

Submerged Jets. Submerged jets are encountered wherever a pipe or nozzle discharges a fluid beneath the surface of the same fluid in a larger reservoir. For example, culture broth recirculating from a tank to an ultrafiltration module and back to the tank could form a submerged jet. If the cross-sectional area of the discharge nozzle is less than about 25% of that of the reservoir, the wall effects can be neglected and the jet is said to be "free." In a stable submerged turbulent jet, the maximum shear stress occurs in the direction of discharge, six to seven nozzle diameters downstream from the orifice. This shear stress is given as

$$\tau_{max} = 0.018\rho_L u_o^2 \quad (21)$$

where u_o is the velocity at the orifice.

Centrifugal Pumps. Centrifugal pumps are commonly employed in bioprocessing; hence, a knowledge of the shear rate in these devices is essential to assessing their suitability for a given use. The shear rate in a Newtonian fluid adjacent to the rotating impeller of a centrifugal pump depends on the radial position. The local shear rate at any position has been expressed as

$$\gamma = 6.30NRe_L^{0.5} \quad (22)$$

where the local Reynolds number at the local diameter d_L is

$$Re_L = \frac{Nd_L^2\rho_L}{\mu_L} \quad (23)$$

Equation 22 is based on theoretical considerations, but it has closely correlated measured shear rate data over the range $10^2 \leq Re_L \leq 2 \times 10^6$ in a centrifugal pump with the impeller rotating in a standard volute casing (36). Over the approximate impeller rotational speed range of 0.01–100 s^{-1}, the shear rate values ranged over 1–10^5 s^{-1} in aqueous electrolyte solutions (36).

As a general guideline, centrifugal pumps may be used to transfer most low-viscosity microbial broths and enzyme solutions so long as gas–liquid interfaces are rigorously excluded. Centrifugal pumps should not be used for animal cells, biofilm supporting particles, soft immobilized enzyme supports, suspensions of nematodes and protozoa, protein precipitates, and plant cells. These pumps will be satisfactory for some microalgae but not for others.

Shear Rate in Isotropic Turbulence

Irrespective of the bioreactor configuration, a turbulence field is deemed isotropic when the size of the primary eddies generated by the turbulence-producing mechanism is a thousandfold or more compared with the size of the energy-dissipating microeddies. The length scale of the primary eddies is often approximated as the width of the impeller blade or the diameter of the impeller in a stirred tank. In bubble columns and airlift bioreactors, the length scale of primary eddies is approximated as the diameter of the column (or the riser tube), or the diameter of the bubble issuing from the gas sparger.

Shear stress, shear rate, the dimensions of microeddies, and other characteristics of flow are linked ultimately to the energy input and dissipation rates in the fluid. The local shear rate in the vicinity of an eddy in an isotropically

turbulent field may be estimated as the ratio of the velocity and the length of the eddy; hence,

$$\gamma_i = \frac{u}{l} = \frac{\mu_L}{\rho_L l^2} \tag{24}$$

where ρ_L and μ_L are, respectively, the density and the viscosity of the fluid. The mean length, l, and the velocity, u, of the microeddies are related with the energy dissipation in the turbulence field; thus,

$$l = \left(\frac{\mu_L}{\rho_L}\right)^{3/4} E^{-1/4} \tag{25}$$

and

$$u = \left(\frac{\mu_L E}{\rho_L}\right)^{1/4} \tag{26}$$

where E is the rate of energy dissipation per unit mass of fluid. In most cases, all the energy input to the fluid is dissipated in fluid eddies, and E equals the rate of energy input. Equations 24–26 apply when local isotropic turbulence prevails.

Energy dissipation rate in bubble columns and airlift vessels is a function of the superficial aeration velocity (20,21); thus

$$E = gU_G \text{ (bubble columns)} \tag{27}$$

and

$$E = g\frac{U_{Gr}}{1 + \frac{A_d}{A_r}} \text{ (airlift bioreactors)} \tag{28}$$

Methods for calculating the specific energy dissipation rate in stirred vessels have been discussed elsewhere (30,37). The energy dissipation varies greatly from the mean value in a stirred tank. The maximum energy dissipation occurs in the vicinity of the impellers. This maximum value can be calculated using the equation

$$E = \frac{\mathrm{Po}N^3 d_i^2}{\rho_L} \tag{29}$$

where Po is the power number, d_i is the diameter of the impeller, and N is the rotation speed (s^{-1}). In developed turbulent flow in stirred vessels, the power number is generally constant for a given type of impeller and tank geometry. For single-phase pipe flow, the specific energy dissipation rate is

$$E = \frac{U_L \Delta P}{\rho_L} \tag{30}$$

where ΔP is the pressure drop per unit length, and U_L is the mean flow velocity.

Generally, if the dimensions of the biocatalyst particle are much smaller than the calculated length, l, of the microeddies, the particle is simply carried around by the fluid eddy; the particle does not experience any disruptive force. On the other hand, a particle that is larger than the length scale of the eddy will experience pressure differentials on its surface, and if the particle is not strong enough it could be broken by the resulting forces.

In addition to turbulence within the fluid, other damage-causing phenomena in a bioreactor include interparticle collisions; collisions with walls, other stationary surfaces, and the impeller; shear forces associated with bubble rupture at the surface of the fluid; phenomena linked with bubble coalescence and breakup; and bubble formation at the gas sparger. Some of these aspects are discussed elsewhere in this article. Summarizing, several possible shear rate values may be calculated for a given situation in a bioprocess device. Not every calculated value is appropriate or relevant to the problem at hand. For pneumatically agitated bioreactors, when the turbulence characteristics in the bulk fluid are the relevant ones, the preferred approach is to use equation 24 for shear rate in the vicinity of eddies. The same applies to mechanically stirred tanks. In some cases, the relevant shear rate may be that at the interface of a rising bubble unless turbulence is so intense that bubbles do not rise freely. Other situations would be controlled by the bubble rupture events, as discussed later. In yet other cases, the fluid eddy shear rate and the maximum shear rate at the impeller will need to be taken into account. Factors such as the frequency of passage of a sensitive biocatalyst through high-shear regions may need consideration.

RESPONSE TO SHEAR

Response to shear has been characterized using various indices, including growth rate (38–40); cell viability (41); regrowth potential (42); release of intracellular material (38,43,44); changes in oxygen uptake rate, ATP, productivity of metabolites, and biochemical composition of the cells; and alterations in morphology of cells and cell aggregates (2,42,44).

Most studies of shear response of cells have utilized batch culture with or without aeration. Such cultures contain cells at different stages of growth; hence, the size and metabolic state of cells are nonuniform. In contract, continuous culture is time-consuming (38), differs substantially from the culture methodologies that are typically employed commercially, and, through natural selection, the cells in continuous culture adapt to shear fields, hence, masking the effect of shear. For example, Wu et al. (45) noted for insect cells that the beneficial effect of shear-protective agents (serum, methyl cellulose, Pluronic F68) were not as important as the effect of passage number. Similar results have been alluded to for plant cells (38). To overcome problems associated with cell growth and adaptation to shear, Zhang et al. (43) recommended the use of erythrocytes for comparative evaluation of the hydrodynamic environment in bioreactors. A nongrowing, well-defined, and shear-susceptible cell population such as that provided by erythrocytes can help identify suitable regimes of operation of a given reactor. In addition, shear-

damaging potential of different bioreactor configurations can be assessed on a common basis using cells such as erythrocytes. Specific information on shear susceptibility of animal, plant, and various microbial cells is discussed in the following sections.

Bacteria, Yeasts, and Mycelial Microfungi

Yeasts, bacteria, and mycelial microfungi are generally quite robust and not easily damaged under typical processing conditions; however, even the most robust cells are broken when subjected to suitable combinations of high stress and exposure time (1). Often, genetically modified strains of an otherwise robust microorganism are less shear tolerant (1,10,46–48). With microorganisms, the composition of the growth medium and the specific growth rate used for the culture are known to influence the robustness of the cell (1). Cells grown in fully defined media that may lack one or more components essential to synthesis of a normal cell wall are often less robust (1). Growth at a higher specific rate will often produce weaker cells (1). When the shear field is insufficiently intense to damage cells, it may still affect product formation and characteristics (9,10). In one case, properties of a shear-sensitive polymer were affected, but not the producing bacterial cells (10). Cells experiencing physiological stress (e.g., starvation) are more susceptible to shear-stress-related damage (44).

Reports cited by Märkl et al. (44) document increasing release of intracellular material from mycelium of *Rhizopus javanicus* and *Mucor javanicus* as the stirrer speed increased. Increasing release of nucleotides was noted with increasing speed of agitation, or with increasing agitation time at a constant agitation speed. Effect of Rushton turbine tip speed on performance of a process for converting cellulose to protein-enriched microbial biomass were clearly demonstrated by Moo-Young et al. (39). The process utilized the filamentous microfungus *Neurospora sitophila* for the conversion. Increasing impeller tip speed from 2.35 m s^{-1} to 3.29 m s^{-1} reduced the specific protein production rate and the final yield (Fig. 4). In addition, a distinct lag phase was observed at the higher agitation rate (Fig. 4) when the inoculum grown in a more quiescent environment was transferred to the fermenter. At the highest tip speed shown in Figure 4, the specific protein production rate was only 55% of that at the lowest tip speed. Similarly, the yield of crude microbial protein was reduced to ~67% of the value obtained at the lowest agitation speed used (39). Further work revealed that agitation-associated damage could be reduced substantially by replacing the Rushton turbines with axial flow hydrofoil impellers (40); thus confirming that different types of impellers generate very different shear fields at identical tip speeds. For equal or lower power draw, hydrofoil impellers are typically better bulk mixers than Rushton turbines (30,37).

In *Penicillium chrysogenum* fermentations performed in turbine-impeller-agitated vessels with working volumes of 0.005–1 m^3, operated at impeller tip speeds of 2.5–6.3 m s^{-1}, the specific penicillin production rate and the mean length of the main hyphae were lower at high agitation intensities (2). High agitation speeds affected the fungal

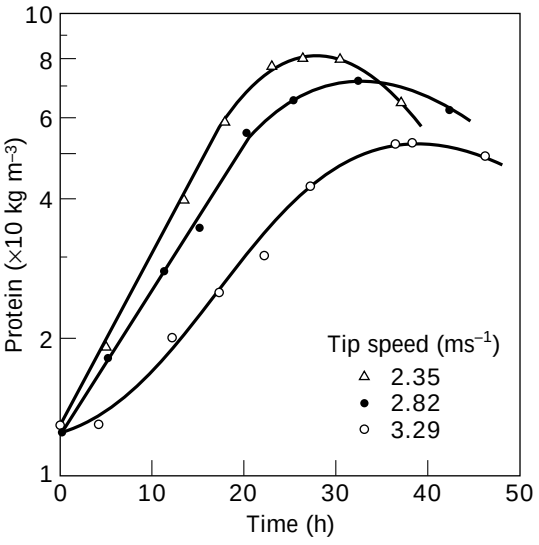

Figure 4. Effect of Rushton turbine tip speed on protein production by the mold *N. sitophila*. *Source*: From Refs. 39 and 40.

morphology, promoting mycelial fragmentation and a greater frequency of branching (2). The behavior of the fermentation at various scales correlated poorly with the impeller tip speed, but correlation was superior in terms of a parameter that took into account the frequency of passage of the culture through the intensely agitated zones around the impellers (2). This behavior suggests that the degree of hyphal damage in stirred bioreactors depends on a combination of the shear intensity in the impeller zone and the cumulative time of exposure of the microbial solids to the shear field.

Sometimes, especially with certain mycelial microfungi, the biomass yield may not be affected by agitation rate, but the cell morphology and production of metabolites may be influenced greatly. Using different strains of citric acid–producing *Aspergillus niger*, Ujcova et al. (3) showed that the yield of citric acid first increased with increasing agitation rate, presumably because of improved oxygen supply, but the yield declined because of cell damage if the agitation speed was increased further. The yield maxima occurred at different agitation rates for different strains, and the sensitivity to agitation differed among strains. Other morphological effects of nondamaging shear levels include changes in growth form, whether pelletlike or pulplike; changes in the degree of branching; the extent of entanglement; and whether growth occurs in filamentous or spherical cell form in certain dimorphic species.

Evidence suggests that even a supposedly robust cell such as *Saccharomyces cerevisiae* (1,11) is susceptible to mechanical shear damage in fermenters (49,50). In one study, *S. cerevisiae* suspended in isotonic saline lost viability at increasing rate over a 25-h period as the agitation speed of the paddle impeller was increased (50). At 1.43 m s^{-1} impeller tip speed, >90% of the cells were dead over the course of 25 h. In contrast, at 0.66 m s^{-1} tip speed, only about 15% of the cells died over the same period (50). Excessive shear has been alleged to also influence the pro-

ductivity of ethanol in fermentations employing *S. cerevisiae* (49).

Among methane bacteria, *Methanobacterium thermoautotrophicum* with rodlike cells that exceeded 2 μm in length was highly resistant to shear stress (44). In contrast, and surprisingly, the relatively smaller (<2 μm) spheroidal cells of *Methanococcus vanielii* were quite sensitive to shear stresses (44). Supplementing the medium with carboxymethyl cellulose viscosity enhancer increased the extent of the cell damage (44). Failure to provide an essential nutrient, selenium is this case, also enhanced shear susceptibility of the culture (44). Although many authors have successfully correlated cell damage with the tip speed of the impeller, Märkl et al. (44) believe that power input per unit culture volume is a superior correlating parameter that is also suitable for comparing the cell damage effects of mechanically stirred and other nonmechanically agitated bioreactors. A constant power input per unit culture volume has also been suggested as a bioreactor scale-up criterion for fragile biocatalysts (44). This recommendation notwithstanding, average power input alone cannot be a universally satisfactory determinant of cell damage; as noted in an earlier section, the maximum shear rate and the frequency of passage (or cumulative exposure) through the high-shear zone need to be taken into account, especially when the shear rate in a given device is strongly position dependent. Several studies confirm that frequency of passes through a high-shear environment have a clear impact on biocatalyst survival (1,2,11,12,16,20,51). Effects of variously intense shear fields on microbial cells are further discussed by Thomas (5,52), Prokop and Bajpai (53), and Chisti and Moo-Young (1). Shear effects on microbial flocs and pellets are treated in a separate section of this article.

Microalgae and Cyanobacteria

Cell fragility has been referred to as the key problem of culture of microalgae in photobioreactors (54); however, the real situation is not quite that bad. Among microalgae, the sensitivity to shear varies greatly with the species. Algae such as *Dunaliella* are indeed extremely fragile, but many other species will tolerate high levels of turbulence and sparging with gas. Thus, gas-sparged airlift devices are commonly used to circulate algal cultures through the solar receivers of photobioreactors (20,55–57). Similarly, relatively low-shear positive displacement rotary pumps have been successfully employed. High-shear centrifugal pumps have also been used; however, at least in some cases, the centrifugal pumps are known to be more damaging than the other fluid-moving systems. In one case, for otherwise equivalent conditions, replacement of the centrifugal pump with a positive displacement device doubled the productivity of *Porphyridium cruentum* (54), a producer of phycoerythrin and polyunsaturated fatty acids. Irrespective of the method used to circulate the culture, the culture flow velocities through tubular solar receivers typically range over 0.3 to 0.5 m s^{-1} in tubes up to 0.06 m in diameter. These conditions have been used with a variety of algae.

In cultures of *Haematococcus pluvialis*, a producer of astaxanthin, early onset of the stationary phase has been associated with turbulence-induced deflagelation of the cells (54). Fragility of species such as *H. pluvialis* depends also on the phase of growth; thus, tailoring the bioreactor operational regime to the growth phase can improve overall productivity (54). The stationary phase red cysts of *H. pluvialis* are significantly more robust than the green vegetative cells (54). The cyanobacterium *Spirulina*—a healthfood and source of the food colorant phycocyanin—is another species that is susceptible to damage by excessive shear forces. The marine alga *Dunaliella* is particularly fragile: the cell lacks a ridged wall; only a thin cytoplasmic membrane encloses it. *Dunaliella* is a good source of natural β-carotene; hence, it is commercially useful. The cell also produces glycerol. Silva et al. (58) showed that *Dunaliella* was susceptible to damage by gas bubbles as well as by turbulence in the liquid. Supplementing the culture with carboxymethyl cellulose or agar improved cell survival.

In one study with *Dunaliella tertiolecta*, culture in a bubble column was quite successful, but when the bubble column was converted to an airlift device by inserting a vertical baffle, the productivity declined (59). Under conditions that were earlier identified as optimal, no growth was observed in the airlift reactor, whereas good growth occurred in the bubble column. Microscopic examination showed significant disruption of the cells in the airlift device (59). This was associated with the hydrodynamic stresses generated as the culture flowed over the upper edge of the baffle into the downcomer (59). This effect could have been avoided, or at least minimized, by hydrodynamic smoothing of the upper and lower parts of the baffle to prevent flow separation (20). In the bubble column, the growth was sensitive to aeration rate: growth rate increased with increasing superficial gas velocity until a velocity of about 0.6 m min^{-1}. Further increase in aeration rate reduced growth, apparently because of hydrodynamic stresses in the fluid (59). Under nongrowth conditions (no light), the specific death rate in the bubble column was shown to increase with superficial gas velocity for velocities exceeding 0.6 m min^{-1} (59). At a fixed aeration velocity ($U_G = 1$ m min^{-1}), the specific death rate decreased with increasing height of the culture fluid in the column (59), probably because the specific power input and, hence, the turbulence intensity declined (20). Similar behavior has been reported with animal cells in bubble columns (60–64).

For otherwise fixed conditions, increasing the number of aeration nozzles (i.e., decreasing the gas jet velocity) caused a marginal reduction in the specific death rate of *D. tertiolecta* (59). This led to the conclusion that the events at the gas sparger did contribute to cell death (59), although the effect was minimal. Unlike Suzuki et al. (59), others (56,57) have quite successfully cultured various microalgae in pilot-scale airlift devices. Continuous culture of the green alga *Chlorella pyrenoidosa* in a rectangular airlift device with multiple light-emitting diodes was reported by Matthijs et al. (65). With a relatively robust photosynthetic organism such as *Chlorella*, increasing turbulence within limits improves productivity in photobioreactors because of enhanced fluid interchange between the dimly lit interior and the better-illuminated exterior parts of a photobioreactor.

In addition to an organism's morphology, the biochemical composition of the cell wall has been associated at least qualitatively with the cell's susceptibility to hydrodynamic stresses. The microalga *Chlorella vulgaris*, which is shear tolerant, has a thick (100–200 nm) cell wall composed of cellulose, pectin, and sporopollenin (44). The somewhat more sensitive alga *Chlorella reinhardii* has only glycoproteins in its relatively thin (40 nm) cell wall (44), whereas a highly sensitive cell wall defective mutant of *C. reinhardii* is devoid of cell wall (44). Similarly, the cyanobacterium *Synechococcus*, with a murein-containing cell wall, and the methane bacterium *M. thermoautotrophicum*, with a pseudomurine-containing wall, are noticeably more resistant than methane bacteria such as *Methanococcus vanielli*, which has a protein-based wall.

Although earlier work with the mold *M. javanicus* showed a reduced extent of damage to mycelia as the viscosity was increased at constant agitation rate, and similar reports exist with animal cells (66,67) and the halotolerant alga *Dunaliella* (58), Märkl et al. (44) observed an opposite effect: with a highly shear-sensitive strain of *C. reinhardii*, even slight increase in viscosity enhanced cell damage (44). The viscosity was increased by adding carboxymethyl cellulose to the culture broth. With a relatively less shear sensitive strain of *C. reinhardii*, increasing the viscosity reduced the impeller agitation speed at which the damaging effects were first discerned (44). Apparently, at least with the less sensitive strain, supplementing the medium with the viscosity enhancer caused the cells to grow in clumps, and aggregation supposedly was an effective shield against cell damage (44). Increasing shear damage with increasing culture viscosity has been seen before with a protozoan (68). These apparently contradictory results are easily explained: whether changes in viscosity increase or reduce shear damage depends on the peculiarities of the mechanism causing the damage. For a given impeller tip speed, increasing viscosity will not affect the tip speed–associated shear rate, but the turbulence will be reduced; hence, the shear rate in the fluid should be lower. However, the shear stress around a particle may increase if the fluid eddy length scale remains comparable to the dimensions of the particle. In other cases, increased viscosity may reduce both shear rate and shear stress: only eddies that are larger than the particle may survive and there may be little or no relative motion between the fluid and the particle. In yet other cases, the frequency of passage through high-shear zones may decline with increasing viscosity.

Plant Cells

Cultured plant cells are a potential source of numerous high-value compounds, although few production processes have been commercialized (13,69). Low culture productivities continue to be the primary limitation. Investigational culture in large bioreactors has been carried out since at least 1959. A variety of reactors have been used, including bubble columns, airlift devices, stirred vessels, rotary-drum reactors, and immobilized cell systems (13). Airlift bioreactors have proven especially effective for large-scale culture of heterotrophic, photomixotrophic, and photosynthetic plant cell suspensions (20,70). Relatively low values of pneumatic power inputs have given satisfactory results during cultivation of plant cells. For example, Fischer and Alfermann (70) obtained good results with about 13 W m^{-3} specific power input during culture of *Chenopodium rubrum* cells in a concentric draft-tube airlift device. Similarly, Ballica and Ryu (71) obtained maximum biomass and product yield at an approximate power input value of 35 W m^{-3}, also in a draft-tube airlift reactor, while culturing *Datura stramonium* cells. In the latter case, power inputs above ~60 W m^{-3} caused large declines in biomass and product yields. The size of the cell aggregates declined with increasing specific power input (71). Reinhard et al. (72) described culture of *Digitalis lanata* in a 300-L airlift bioreactor for producing β-methyldigoxin.

Plant cells in suspension tend to be large: 20–50 μm in diameter and 100–500 μm in length. The cells have a cellulose-based wall. Most of the cell's volume is taken up by a vacuole that may occupy >95% of the available space. The fluid in the vacuole is much less viscous than the cytoplasm; hence, a cell with a large vacuole is likely to be less resistant to certain types of deformations than one with a smaller vacuole. Cells frequently occur as aggregates of up to a hundred cells. The aggregates settle easily. Plant cells grow slowly, with doubling times of the order of 20–100 h. Cells may secrete extracellular polysaccharides, producing non-Newtonian broths. Also, the biomass concentration may be high, up to 70 kg m^{-3}. Heterotrophically growing plant cells require oxygen, but demands are low, of the order of 10^{-6} kg O_2 kg^{-1} cell s^{-1}. Critical dissolved oxygen concentration generally tends to be ≤20% of air saturation. The polysaccharide-containing cultures tend to foam a lot when aerated. Also, excessive aeration may reduce productivity by stripping carbon dioxide and other essential volatiles produced by the cells themselves (5,69).

As has been demonstrated with some microorganisms (1), the composition of the culture medium, the culture conditions, and the specific growth rate of a cell may affect the wall strength of plant cells also. For otherwise identical conditions, agitation intensity is reported to influence the composition of plant cell walls. Thus, the relative amounts of pectin, cellulose, and hemicellulose in walls of *Catharanthus roseus* were affected by the intensity of agitation in one case (73). In another case cited by Doran (13), the mass ratio of cell wall relative to the whole cell increased with increasing intensity of shear, suggesting adaptation of the cell to the prevailing environment even over short periods. Even though the turbulence level may be insufficient to affect individual cells, aggregates may be affected; hence, a shear-related metabolic response may occur due to altered cell–cell interactions (69).

Based on laminar flow viscometric measurements, a critical shear stress level of 80–200 N m^{-2} has been suggested for *Morinda citrifolia* cells. Whereas for *Daucus carota*, a shear stress level of 50 N m^{-2} has been associated with cell damage. In another study, carrot cells in a laminar flow Couette viscometer lost the ability to grow and divide in the shear stress range of 0.5–100 N m^{-2} (53). The intracellular enzyme activity was impaired at shear stress levels above 3,000 N m^{-2}, but significant lysis did not occur until a shear stress level of 10,000 N m^{-2} was applied over a prolonged period (≥1 h) (53). In contrast to behavior in

laminar flow, the cells were quite sensitive to turbulent impeller agitation. Impeller tip speeds of ~1.1 m s^{-1} lysed a significant proportion of the cells within 40 min (53).

In studies with *Perilla frutescens* cell suspensions, Zhong et al. (74) noted that the cell viability declined with increasing shear rate (constant exposure time) or increasing shear time at constant rate of shear in a concentric cylinder shearing device. A constant shear rate of about 140 s^{-1} produced a noticeable loss of viability within 20 min. At higher shear rate of ~860 s^{-1}, less than 75% of the cells were viable after 20 min (74). In marine propeller–agitated fermenters, the impeller tip speed affected the specific growth rate and the yield of the cells (74). Tip speeds >0.6 m s^{-1} reduced the specific growth rate and the cell biomass yield (74). In other cases, impeller tip speeds as low as 0.35 m s^{-1} have extensively lysed certain plant cells.

With *M. citrifolia* cells subjected to 25–350 N m^{-2} turbulent shear stress in a capillary, the viability decline followed first-order kinetics in which the rate constant increased with the applied shear stress (75). The culture was circulated through the capillary by a peristaltic pump, which also contributed to cell damage (75). The specific death rate constant was linearly related with the cumulative energy dissipated (75). Cell aggregates subjected to shear were reduced in size. For the same species, damage was reported when cells grown in a quiescent environment were subjected to turbulent jet flow through 1- and 2-mm nozzles (51). Cells lost viability with increasing number of passes through the nozzles. The viability loss was first order in the number of passes (51). For a fixed number of nozzle passes, increased nozzle flow velocity enhanced the death rate constant. Similarly, the maximum and the mean aggregate size were reduced when the suspension was subjected to jet flows (51). The average aggregate size was lower for higher jet velocities. The average energy dissipation rates in the jet ranged over 10^3–10^5 W kg^{-1} (51).

Meijer et al. (38) assessed the hydrodynamic stress sensitivity of *C. roseus, Nicotiana tabacum, Tabernaemontana divaricata,* and *Cinchona robusta* in a 3-L Rushton turbine-stirred vessel. Effects of stress were quantified in terms of culture growth rate, respiration rate, and release of organic compounds from the cells. Cultures of *C. roseus* carried out at 0.59 m s^{-1} and 2.36 m s^{-1} impeller tip speeds showed identical behavior in terms of biomass growth rate and glucose consumption rate; hence, hydrodynamics-associated stress was concluded to not affect the cells over the ranges examined (38). Similarly, *N. tabacum* was little affected by differences in agitation rate, although the growth rate and the final yield were noticeably greater at the lower agitation speed. Cells of *C. robusta* responded differently: at 0.59 m s^{-1} impeller tip speed the cells grew and there was little release of intracellular protein; however, at 2.36 m s^{-1}, there was no growth and the specific protein concentration increased with culture time, indicating leakage from damaged cells (38). The *T. divaricata* cells also were damaged at 2.36 m s^{-1}, but less than the cells of *C. robusta*. The damage to *T. divaricata* was reduced at a lower impeller tip speed of 0.59 m s^{-1}. In separate experiments, cells of *N. tabacum* that had earlier withstood higher shear stress levels were shown to be more susceptible to damage after a prolonged period (10 days) of starvation (38). This effect is similar to that noted with other cells (44).

Table 3 is a summary of the damage thresholds levels—either impeller tip speed or the specific power input due to aeration—noted for various plant cell suspensions in stirred fermenters and airlift bioreactors. The studies just referenced clearly affirm that the susceptibility to shearing forces varies a great deal with cell line. Moreover, for the same cell line, cultivation history (e.g., prolonged starvation) and age of cell affect the cell's response to shear fields (38,44,69), which is consistent with similar findings for microorganisms (1). That plant cells adapt to shear fields is also well known: cells cultured in high-shear environments better withstand hydrodynamic forces after many generations.

Protozoa

Midler and Finn (68) provided a clear demonstration of shear-related damage to cells of the large (~80-μm cell diameter) ciliated protozoan *Tetrahymena pyriformis*. Lysis correlated with impeller tip speed. Agitation at impeller tip speeds approximately ≥0.5 m s^{-1} destroyed most of the cells. In a Couette viscometer, the critical shear stress level when lysis first occurred was ~24 N m^{-2} (68). Eighty percent of the cells lysed within the first minute when exposed to shear stress levels of 10^3 N m^{-2}. The extent of damage increased with shear stress level and exposure time. At a given shear rate, increasing the broth viscosity made the protozoan more susceptible to shear damage, implying that the damage was associated with shear stress rather than shear rate (68). The cells were more sensitive to turbulent shear stress: an average turbulent shear stress of ~10 N m^{-2} lysed over half the population within 10 min. In contrast, in laminar flow, similar levels of damage occurred at shear stress levels of almost 300 N m^{-2}. Note that *T. pyriformis* cells are larger than most animal cells, but smaller than most cultured plant cells.

Animal Cells

Animal cells are the most shear-susceptible of biocatalysts. Animal cells are relatively large—typically 10–20 μm in diameter—and they lack a protective cell wall. Osmotic

Table 3. Damaging Threshold Values of Impeller Tip Speed or Specific Power Input for Some Plant Cells

Stirred fermenters	Impeller tip speed (m s^{-1})
Catharanthus roseus	≥2.36
Nicotiana tabacum	~2.36
Cinchona robusta	<2.36
Daucus carota	<1.10
Tabernaemontana divaricata	~0.59
Perilla frutescens	0.60
Others	≤0.35
Airlift bioreactors	**Power input (W m^{-3})**
Chenopodium rubrum	≥13
Datura stramonium	~60

shock is often sufficient to lyse animal cells. Other than blood cells, most normal animal cells are anchorage dependent. Cancerous cells, hybridomas, and established lines will normally grow in suspension. Because of these distinct growth characteristics, two types of culture methods are employed in industrial practice: free suspension culture, in which cells are freely suspended in a nutrient broth; and microcarrier culture, in which anchorage-dependent cells grow on surfaces of solid carriers that are suspended in a culture fluid. Irrespective of the culture method, the suspending fluid is invariably directly sparged with air or other gas mixture to supply the cells with oxygen. Although other aeration alternatives are available (see MASS TRANSFER article), direct sparging with a gas is likely to remain the dominant method of providing oxygen to animal cells (76). Both stirred tanks and airlift devices have been successfully employed for commercial processing of animal cells (77–79). Anchorage-dependent cells may also be cultured on surfaces of large static particles held in packed beds (80,81), but this method is uncommon. Devices used in generation of implantable tissue typically grow normal cells supported on stationary surfaces or within a static matrix of gel or woven fabric (82). The supporting surface may be flat or variously shaped.

Cells in bioreactors are subject to two main kinds of fluid mechanical forces: (*1*) those due to turbulence within the liquid, and (*2*) forces associated with the gas–liquid interface. The latter category includes effects of bubble formation, rise, and rupture. In addition in microcarrier culture, collisions among carriers and carrier–impeller (or carrier–wall) interactions may play a role. Furthermore, in tall bioreactors cells may be subjected to substantial changes in hydrostatic pressure as they circulate with the fluid. Cells in tissue regeneration bioreactors experience the same kind of forces as occur in flow past a flat plate, wall, or other submerged object. The specific considerations relevant to the various culture methodologies are treated in the following sections.

Resistance to shear stress is determined at least partly by the cytoskeletal structure of the cell. The cytoskeleton determines a cell's mechanical properties, shape, and movements such as occur during phagocytosis. The cytoskeleton is made of protein filaments, mainly of actin. The filaments interact closely with the cell membrane by anchoring to specific membrane proteins. A cell exposed to mechanical forces undergoes cytoskeletal reorganization. Cytoskeleton-mediated stress signal transmission to intracellular organelles (Fig. 5) has been associated with various biochemical, physiological, and gene-level responses in vascular cells (4). Some cells are known to have surface stress receptors (e.g., Ca^{2+} ion channels) that have been implicated in biochemical responses (4,83,84) independent of cytoskeletal mediation (Fig. 5). Cytoskeletal properties are known to affect the shear tolerance of hybridomas. Effects of turbulence on the cytoskeleton and other biological responses have been treated by several authors (4,53,85). Work cited by Al-Rubeai et al. (86) suggests that inhibitors of actin polymerization decrease a cell's resistance to shear forces, whereas inducers of polymerization make the cells more robust. Thus, supplementing the culture medium with actin polymerization inducers may be one way of improving performance of bioreactor-cultured animal cells, so long as the requisite production biochemistry is not adversely affected.

Plasma membrane fluidity (PMF), which is a measure of the degree of packing of the membrane and its constituent's freedom to move about laterally through the bilayer membrane, to rotate about their major axes, and to oscillate in the plane of the membrane, is another factor that appears to influence shear susceptibility of cells (41). Increasing membrane fluidity correlates with increasing shear sensitivity (41). PMF increases with increasing temperature and can be manipulated in both directions using various additives. In studies with a freely suspended mouse–mouse hybridoma in a laminar shear stress Couette flow device, conditions that yielded higher membrane fluidity produced more fragile cells (41). For example, cells sheared at elevated temperatures showed greater loss of viability than unsheard controls at the same temperature (41).

Shear Effects in Bubble-Free Environments ***Suspended Cells.*** Freely suspended cells in bubble-free bioreactors are not damaged by mechanical agitation even at intensities much greater than the ones used in typical processing. Exceptions occur in extensional or elongational flow in certain high-shear devices even when the flow is laminar. Extensional or elongational flow occurs whenever the cross-sectional area of the flow channel reduces (e.g., at an orifice on the wall of a tank or at the entrance of a capillary connected to a larger reservoir). The fluid elements undergoing extensional flow stretch and thin. Suspended particles also experience elongational forces in the direction of flow, and compression perpendicular to the flow streamlines. Drops subjected to extension flow can rupture. Similarly, extensional flow through orifices of high-pressure homogenizers contributes to rupture of even the very robust microbial cells (1). Rupture of erythrocytes at entrances to capillaries is well known (87). Shear effects on suspended erythrocytes are discussed in detail in a later section.

For a hybridoma line, Born et al. (88) reported that exposure to laminar shear stress (208 N m^{-2}) in unaerated flow in a cone-and-plate viscometer led to substantial loss in cell count and viability within 20 min. At a constant 180-s exposure, increasing shear stress over 100–350 N m^{-2} linearly enhanced cell disruption, with >90% of the cells being destroyed at 350 N m^{-2} stress level (88). Shear stress levels associated with bubble rupture at the surface of a bioreactor may range over 100–300 N m^{-2} (13). These values are remarkably consistent with shear rates that damaged hybridomas in *unaerated* laminar flow experiments (88).

For a suspended mouse myeloma line in turbulent capillary flow, McQueen et al. (18) noted a threshold average wall shear stress value of 180 N m^{-2} when lysis first commenced. Although the flow caused lysis, it had no effect on viability (18), suggesting that cells at various growth stages were equally affected. The sudden flow contraction at the entrance to the capillary may have contributed to cell lysis, but the residence time in the capillary also had an effect at otherwise constant average wall shear stress level. The rate of lysis was first order in cell number. Above

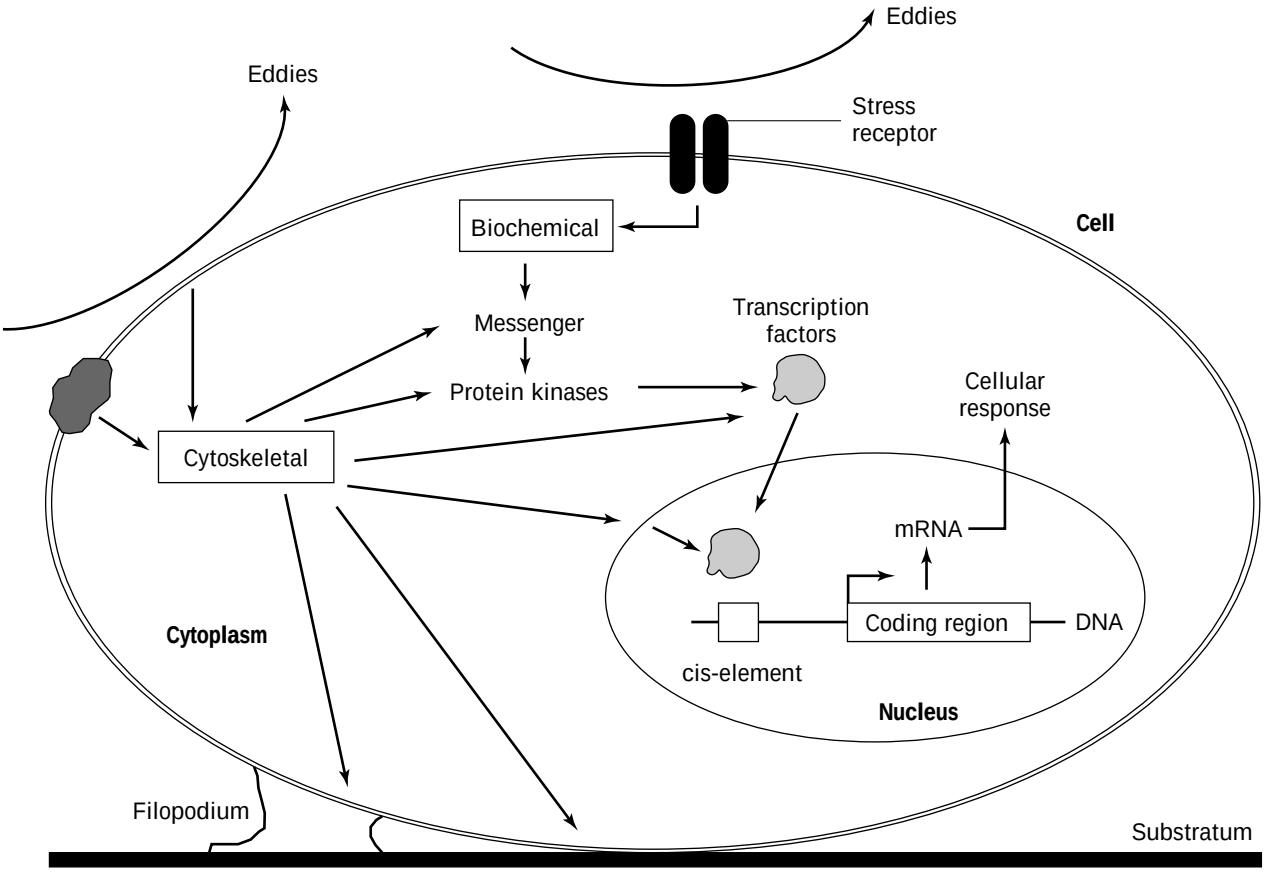

Figure 5. Stress signal transmission and transduction via cytoskeletal and biochemical routs in an anchored cell. *Source*: Adapted from Ref. 4.

the threshold shear stress value, the specific lysis rate increased with increasing level of shear stress (18). The growth rate and the DNA synthesis rate of the cells exposed to the shearing environment were unaffected when the surviving cells were returned to a normal quiescent growth environment (18). In other studies cited by McQueen et al. (18), the shear stress threshold for damage has been reported as 0.87 N m^{-2} for a mouse hybridoma and 1.5 N m^{-2} for insect cells. Higher shear sensitivity of another mouse cell line relative to a human carcinoma has been reported (16).

For human cervical carcinoma HeLa S3 and mouse abdominal fibroblast L929, Augenstein et al. (16) observed lysis of suspended cells in turbulent flow through stainless steel capillaries. Cell death could be correlated with the average wall shear stress level or the power dissipation within the capillaries. The L929 line was more sensitive than the human cell. Control experiments showed that the positive displacement pumps used to circulate the cells through capillaries contributed little to cell lysis (16). Average wall shear stress levels of 0.1–2.0 $\times$ 10^3 N m^{-2} were sufficient to induce cell inactivation for the two lines. According to Shiragami (17), the mean shear stress acting on cells suspended in capillary flow is 4/3 the shear stress at the capillary walls, so long as the ratio of the cell's diameter to that of the capillary is <0.08.

For a hybridoma examined by Shiragami (89), the specific rate of monoclonal antibody production in a surface-aerated spinner flask depended on the agitation speed. In a 250-mL spinner vessel an agitation rate of $\sim$180 rpm gave the highest specific antibody production rate. The specific productivities were reduced at higher or lower values of agitation speed. The increased antibody production with increasing agitation was associated supposedly with enhanced secretion in a more turbulent environment (89). Oxygen transfer effects may have better explained the observations (see MASS TRANSFER), but no data were reported on this aspect.

Damage to murine hybridomas was observed by Jan et al. (31) in stirred tanks equipped with marine impellers agitated at sufficiently high speeds that vortexing occurred and gas entrained into the medium. Even at these high speeds, damage could be prevented by baffling the tank, which suppressed vortex formation. Usually though, vortexing is not a problem in large-scale cell culture. Unbaffled, marine impeller–stirred tanks were successfully used by Chisti (78) in industrial culture of several hybridoma lines. Effects of agitation on hybridoma culture in the absence of sparging or surface entrainment were further examined by Smith and Greenfield (90). Culture growth was unaffected by agitation intensity (100 or 600 rpm) in the RPMI medium supplemented with fetal bovine serum

(10% vol/vol). However, in PFHM II medium supplemented with either Pluronic F68, fetal bovine serum, or bovine serum albumin, and agitated at 600 rpm (impeller tip speed = 1.6 m s^{-1}, power input = 1 kW m^{-3}) the results were different: the agitation intensity did not affect the exponential growth rate, but once growth had ceased, the decline phase was substantially faster than in control experiments (90).

A certain level of hydrodynamic shear is generally beneficial to culture processes, especially in intraparticle immobilized culture where mass transfer limitations can be severe. In producing engineered tissue of smooth muscle cells/polymer matrices (biodegradable 2-mm-diameter fibers of polyglycolic acid assembled into a nonwoven matrix), Kim et al. (82) noted that seeding of the matrix under agitation led to significantly higher intramatrix cell densities than when cells were seeded under static conditions. Moreover, the higher cell densities were attained more rapidly than the lower densities of static culture. In addition, the relative rates of synthesis of elastin and collagen were significantly greater in seeded matrices cultured with agitation than in ones grown statically (82). A lower possible supply of oxygen or other nutrient may have reduced the performance of static seeding methodology. In view of the above referenced studies and similar others, sufficiently intense fluid mechanical forces other than those associated with aeration do affect cells.

Adherent Cells. Quite low shear stress levels, for example, between 0.25 and 0.6 N m^{-2} in laminar flow (91), can interfere with the process of cell attachment to surfaces; however, once the cells are attached and spread out, they may tolerate higher stresses. Laminar shear stress of the order of 0.5–10 N m^{-2} may remove adherent cells from surfaces (92), but even lower values (e.g., 0.1–1.0 N m^{-2}) are known to affect cellular morphology, permeability, and gene expression (92). Sublethal shear stress levels cause no obvious physical damage but are known to produce various biochemical and physiological responses (4,83,84). In studies with rat aortic endothelial cells anchored on the internal walls of glass capillaries, laminar shear stress was shown to affect the cytosolic pH because of preferential leakage of certain ions out of the cells into the buffer saline (84). This reversible permeability enhancement occurred even at stress levels as low as 0.05 N m^{-2} applied over short durations (~2 min). Similar effects were noted with human aortic endothelial cells but not with human skin fibroblasts or rat intestinal epithelial cells exposed to shear stress levels of up to 1.34 N m^{-2} (84). With rat aortic cells, the flow-induced cytosolic acidification could be maintained for at least 30 min at 1.34 N m^{-2} shear stress level, but the cytosolic pH returned to unstressed levels within about 15 min when the sustained shear stress was $\leq$0.027 N m^{-2} (84).

In studies with anchorage-dependent cells attached to the flat glass walls of a rectangular flow channel, Shiragami and Unno (93) observed increased activity of lactate dehydrogenase (LDH) in cells that had been exposed to a steady-state shear stress of 0.5 N m^{-2} for 12 h: the activity was fourfold greater relative to controls. The LDH activity correlated with the transmission of energy from the fluid to the attached cells (93).

In vivo hemodynamic forces have been implicated in various physiological and pathophysiological processes (4). Atherosclerotic lesions in humans tend to develop in zones of flow separation (4) such as regions of arterial branching and sharp curvature. Arteries adapt to chronic changes in blood flow, increasing in circumference under high flow and declining under reduced flow (4). Shear stress signals transmitted throughout the vascular cell via cytoskeletal and biochemical elements result in changes to structure, metabolism, and gene expression (4).

Shear effects need to be considered also in perfusion devices that retain cells over long periods in continuous culture (94). Shear effects on adhering erythrocytes and leukocytes are treated separately.

Erythrocytes and Leukocytes. Mammalian erythrocytes, or red blood cells, are among the best studied of animal cells. Properties of erythrocytes and other blood cells are relevant to various pathologies and biomedical processes. Erythrocytes and leukocytes, being suspended cells in vivo, likely experience the kind of stresses encountered in bioreactors and various other industrial processing devices; hence, these cells may provide a broad general insight into mechanical behavior of other cells of mammalian origin. The normal lifetime of a human erythrocyte in circulation is 121 days. The normal daily destruction rate is about 2 $\times$ 10^{11} cells (87). Some cells lyse during circulation; most are destroyed in the spleen. Aging cells resist deformation more than the younger ones. All cells unable to deform in the 3-μm openings of the splenic circulation are delayed and ultimately phagocytized (87).

Erythrocytes are highly deformable cells that orient in laminar flow so that least possible surface area of the disc-shaped cell is perpendicular to the flow. The cytoplasm of erythrocytes is a viscous Newtonian fluid (95). The cell membrane behaves as an elastic solid: the cell deforms but almost instantly recovers its shape when the deforming force is removed. The membrane has little resistance to bending but substantially resists increase in area (95). Erythrocytes suspended in turbulent isotonic saline (viscosity ~1 $\times$ 10^{-3} Pa s) have been observed to undergo elongation and deformation; however, the cell appears to be less vulnerable to turbulent shear stress than a cell at the same stress level in a viscous suspending medium (87). Based on measurements in turbulent jets, a critical lytic shear stress level of 4,000 N m^{-2} has been reported for very brief exposures (~10^{-5} s) (87). Measurements on erythrocytes of different mammals reveal that the critical shear stress increases dramatically as the cell volume declines.

According to Blackshear and Blackshear (87), "Areal change occurs when the cell membrane is subjected to stress; hemolysis occurs when the area increases by approximately 6.4 percent." Hemolysis is associated at least in part with physical factors and flow, which produce the hemolysis threshold strain in membranes of erythrocytes (87). Once the threshold strain is exceeded, membrane pores open and the membrane eventually tears (87). A briefly (e.g., 10 ms) imposed uniaxial tension of 0.058 N m^{-1} is a sufficient criterion for lysis (87). When the cell is subjected to biaxial stress, a tension of about 0.029 N m^{-1}

may produce lysis. In viscometric stress for prescribed periods, time to lysis declines as the imposed stress is increased. However, it has been conclusively shown that shear stress alone is not a sufficient predictor of hemolysis rate or thresholds (87); cell shape and tumbling also play a role. Membrane shear appears to be far lower when the cells are suspended in higher-viscosity media in viscometric studies.

Erythrocytes allowed to adhere to a glass surface and then subjected to a fluid shear commence movement when the fluid shear force exceeds about 10^{-11} N (95). During this process the cell gradually moves downstream, but the membrane may remain attached to the surface (95). The membrane can be deformed permanently when the deforming force persists for more than a few minutes (95). Shear elasticities of nonnucleated mammalian red cells are generally similar, but elasticities are about an order of magnitude greater for cells of nucleated species. Small amounts of thiol reagents are known to decrease the elongation of human red cells suspended in a shear field (95), presumably by producing some sort of cross-linking. Potentially, this methodology may improve survival of any fragile cell with a significant amount of cross-linkable protein in the membrane. Other additives may render the cell more susceptible to shear damage. Certain chemical lysins and some antigen–antibody reactions cause perforation of the cell membrane and leakage of intracellular material (87). Cholesterol enrichment or depletion of the human erythrocyte membrane does not affect its viscosity.

Hemolysis of red cells is known to occur intravascularly in vivo as well as in various in vitro flow systems (87). A number of studies have correlated hemolysis to flow in pumps, valves, heart–lung machines, blood dialyzers, and transfusion filters. In flow through tubes, wall roughness of the scale of erythrocyte correlates with hemolysis (87). Bubbles trapped in surface imperfections appear to aid lysis. In flow through tubes, hemolysis correlates with the shear rate and the surface-to-volume ratio (87). This type of lysis occurs at shear stress thresholds lower than the ones required to produce lysis in a fluid shear field. Wall contact–associated lysis has been observed to depend on the chemical nature of the wall material. Lysis may decline with time as surfaces become passivated by prolonged contact with plasma proteins (87).

In capillaries of ~1 mm in diameter, an upper limit on the mean tube velocity of 6 m s^{-1} has been suggested for capillaries with sharp-edged entrances, and blood with a viscosity of 4×10^{-3} Pa s (87). This corresponds to a Reynolds number of 1,500 inside the capillary and an average wall shear rate of about 4,800 s^{-1}. Velocities as high as 17 m s^{-1} may be employed inside capillaries with carefully flared entrances (87). As with other animal cells, erythrocytes subjected to bubbling are susceptible to bubble rupture–associated damage, as shown in Figure 6 for porcine erythrocytes. The normalized cell number (Fig. 6) declined more rapidly in a sparged airlift bioreactor in comparison with cells in a surface-aerated shake flask (43). In surface-aerated shake flasks, increasing shaker platform speed over 100–400 rpm increased the specific cell lysis rate (Fig. 7). The slight decline in lysis rate at 100 rpm (Fig. 7) was associated with improved surface aeration

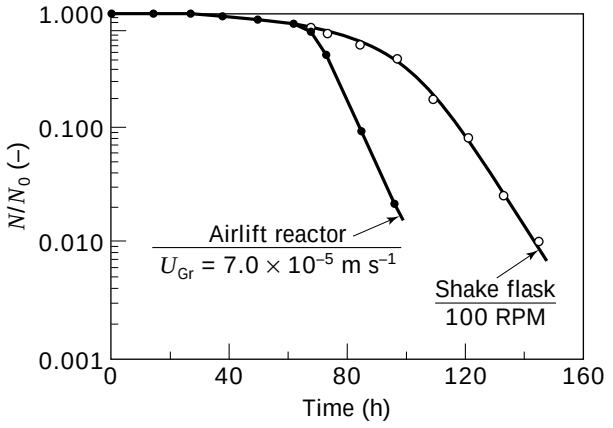

Figure 6. Survival of suspended porcine erythrocytes in a sparged airlift bioreactor and a surface aerated shake flask. Normalized cell count (N/N_0) is plotted as a function of time. *Source*: From Ref. 43.

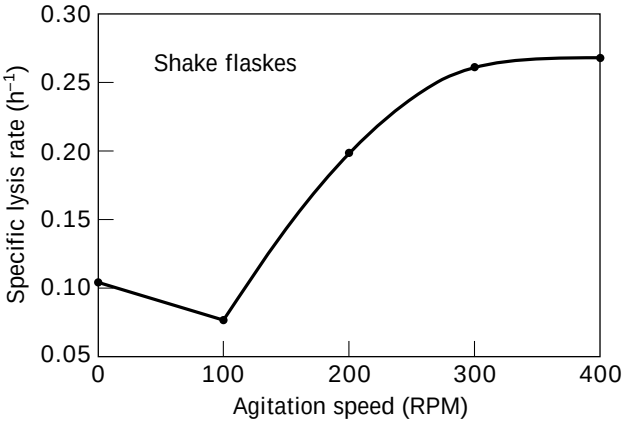

Figure 7. Effect of shaker platform agitation speed on specific lysis rate of suspended porcine erythrocytes in surface aerated shake flasks. *Source*: From Ref. 43.

relative to static flask. Because erythrocytes do not multiply in vitro, the effects of cell-damaging forces are not masked by growth-associated adaptation, changes in cell size, and stages of growth; hence, suitably chosen erythrocytes provide a well-defined cell population for comparative assessment of the damaging potential of various hydrodynamic environments (43).

In comparison with erythrocytes, the cytoplasm of leukocytes has markedly different rheological properties (96), but the properties of the leukocyte membrane are similar to those of the red cell membrane. Leukocytes adhering to vascular endothelium detach when the shear stress is between 26.5 and 106.0 N m^{-2} (96). According to work cited by Prokop and Bajpai (53), a shear stress level of 60 N m^{-2} applied over 10 min should lyse about one-fourth of a leukocyte population. In another study, sublethal shear stresses of 10 and 20 N m^{-2} applied over 10 min in a Couette viscometer affected the biochemical response of human T cells relative to unsheared controls (83). It seems,

therefore, that cells in vivo in circulation are apparently more shear resistant than ones studied in vitro.

Microcarrier Culture. Both stirred-tank and airlift bioreactors (97) may be used for suspended microcarrier culture. Microcarrier-supported cells likely experience hydrodynamic forces of greater magnitude than do freely suspended cells. This is because in highly agitated or aerated systems, the length scale of fluid eddies can be of the same order as the dimensions of microcarriers, resulting in high local relative velocities between the solid and the liquid phases (15,78,98). Furthermore, the carriers have greater inertia than free cells; hence, collisions among microcarriers and between the impeller and microcarriers likely damage attached cells. Similarly, fluid eddy impact and shear stress forces on a high-inertia particle are greater than on free cells.

Resistance of a cell to rupture by impact (i.e., burst resistance) is a possible measure of the cell's survivability in the culture environment. Measurements of burst force are potentially useful also for comparative assessment of cell strength and in establishing culture conditions that give rise to more robust cells. It may eventually be possible to correlate the sensitivity to shear of a cell to its resistance to mechanical rupture (99). Burst strength may be directly relevant in microcarrier culture where impact-associated damage is likely; however, in view of the cytoskeleton-mediated pressure signal transmission to internal parts of a cell, a more likely scenario is that the force required to cause impact-associated damage is far lower than the rupture threshold. This issue notwithstanding, resistance to rupture of a mouse hybridoma grown in serum-containing continuous culture has been measured by squeezing single cells between flat surfaces of micromanipulator arms (100). The bursting strength increased with cell size (101). The bursting force correlated with the initial cell diameter as follows:

$$S = 0.2d_c - 0.1 \times 10^{-6} \tag{31}$$

where the intercept was not significantly different from zero (100). The cell diameter ranged over $\sim(10\text{–}17) \times 10^{-6}$ m. Other similar data (101) have been correlated (99) as follows:

$$S = 0.27d_c - 0.86 \times 10^{-6} \tag{32}$$

where the burst strength S is in newtons, and the hybridoma cell diameter, d_c, is in micrometers. The calculated bursting tension had a mean value of $(1.8 \pm 0.5) \times 10^{-3}$ N m^{-1}, which was essentially independent of cell size (100). Because the bursting tension was size independent, the bursting pressure fell with increasing cell diameter. At $(0.8 \pm 0.3) \times 10^{-3}$ N m^{-1}, the calculated mean compressibility modulus of the cells was roughly independent of cell diameter (100).

Sinskey et al. (102) advanced the concept of an integrated shear factor (ISF)—a measure of the strength of the shear field between the impeller and the spinner vessel walls—to correlate shear damage to mammalian cells. The ISF was defined as

$$\text{ISF} = \frac{2\pi N d_i}{d_T - d_i} \tag{33}$$

or, effectively, the laminar shear rate between the impeller tip and the walls. For a range of stirred vessels (0.25–2.0 L, $0.032 \leq d_i$ (m) ≤ 0.085), cell damage occurred once the ISF value exceeded about 18 s^{-1} during culture of microcarrier-supported human fibroblasts (103). Damage could be correlated also with the impeller tip speed, but unlike the ISF, the damaging value of the tip speed depended on the size of the culture vessel (103).

Relying on the earlier work of Nagata, Croughan et al. (103) arrived at the following expression for a time-averaged shear rate:

$$\gamma_{av\cdot T} = \frac{112.8 r_i^{1.8}(r_T^{0.2} - r_i^{0.2})(r_c/r_i)^{1.8}}{r_T^2 - r_i^2} \tag{34}$$

where r_i and r_T are the impeller and the tank radii, respectively. The radius r_c of the formed vortex zone would need to be estimated using Nagata's expression:

$$\frac{r_c}{r_i} = \frac{Re_i}{1{,}000 + 1.6Re_i} \tag{35}$$

The impeller Reynolds number in equation 35 is calculated as follows:

$$Re_i = \frac{N d_i^2 \rho_L}{\mu_L} \tag{36}$$

Equation 34 was developed for unbaffled stirred tanks operated in the turbulent regime (103). For human fibroblasts on microcarriers in various stirred vessels, cell damage occurred when the time-averaged shear rate exceeded about 2.5 s^{-1} (103). For chicken embryo fibroblasts, also on microcarriers, the damage threshold was 6 s^{-1} time-averaged shear rate (103). Cell damage correlated also with the Kolmogoroff eddy length scale (l): for human fibroblasts the cell damage occurred when the length scale declined to approximately below 125 μm, whereas for the chicken embryo cells damage was observed when the l-value declined to below 100 μm (103).

Analyzing data from several sources, Croughan et al. (103) further showed that the specific death rate correlated with the average energy dissipation rate per unit mass; thus,

$$k_d \propto E^m \tag{37}$$

where m was 0.72, 0.76, and 0.82, respectively, for microcarrier-supported Vero cells, similarly supported human fibroblasts, and a freely suspended protozoan. For attaining a more homogeneous shear field in stirred culture vessels (i.e., for the minimum value of the maximum-to-average shear rate ratio) Croughan et al. (103) noted an optimal vessel geometry corresponding to $r_i/r_T = 0.74$.

In microcarrier culture, collisions between microcarriers and interactions between carriers and internals of a reactor are other possible causes of cell damage, particu-

larly in stirred bioreactors (15,104,105). Cherry and Papoutsakis (98,104,105) advanced the concept of "severity of collision" to account for at least some of the damage to cells in suspended microcarrier culture in stirred vessels. Severity of collision combined collision frequency and energy of the impact. Two collision severities were defined: a turbulent collision severity (TCS) for turbulence-associated particle-to-particle impacts, and an impeller collision severity (ICS) for particle-to-impeller collisions; thus,

$$\mathrm{TCS} = \left(\frac{E\rho_L}{\mu_L}\right)^{3/2}\left(\frac{\pi^2\rho_S d_p^5 \varepsilon_S}{72}\right) \tag{38}$$

and

$$\mathrm{ICS} = \frac{9\pi^4\rho_S n_B N^3 d_t^4 d_p^4}{512 V_L} \tag{39}$$

where E is the energy dissipation rate per unit liquid mass, ρ_S and d_p are the density and diameter of the microcarriers, ε_S is the volume fraction of the carriers, n_B is the number of impeller blades, N and d_i are the impeller rotational speed and diameter, and V_L is the volume of the liquid in the vessel. Improved cell growth was observed with smaller microcarriers, as predicted by equations 38 and 39. The specific cell death rate increased with increasing values of TCS and ICS (104,105); however, the influence of hydrodynamic forces on culture performance correlated also in terms of the ratio of Kolmogoroff eddy scale to bead diameter: the specific death rate declined as l/d_p increased. As culture viscosity was raised, damage to cells declined in conformance with equation 38 and in agreement with interpretations based on the l/d_p ratio (105).

Unlike in stirred tanks, animal cell microcarriers suspended in airlift bioreactors under typical operating conditions do not significantly interact with each other or with the walls of the vessel (106); instead, the microcarrier particles follow the laminar streamlines of the fluid (106). Consequently, in airlift reactors at least, the effects of particle–particle or particle–wall collisions on monolayers of cells may be disregarded. Observations of Ganzeveld et al. (106) spanned microcarrier loadings of up to 30 kg m^{-3}, with carriers of 150–300 μm diameter, and 1,030–1,050 kg m^{-3} density. The observations covered a power input value of up to 33 W m^{-3}, which is about the upper limit for cell culture in pneumatically agitated bioreactors. These results applied to a split-cylinder airlift bioreactor with an aspect ratio of 7.6, which would not normally be exceeded in large-scale cell culture systems. As an additional design constraint, the Reynolds number in the riser and the downcomer should not exceed about 3,000, or the flow will be more chaotic (106).

Numerical analysis of forces exerted by laminar flow on anchorage-dependent cells attached to flat surfaces suggests that shear stress between 0.25 and 0.6 N m^{-2} is sufficient to detach round cells, but much higher values are needed to dislodge spread out cells (91). These observations are relevant to microcarrier culture where, during inoculation, the round cells must first attach to microcarriers before spreading on the solid surface. During proliferation, bead-to-bead transfer of cells may also require a level of turbulence that is not so high as to hinder the reattachment process, yet not so low that bead-to-cell encounters are few.

Typically, the shear rate values in airlift bioreactors range over 250–4,000 s^{-1} for operational conditions that are relevant to animal cell culture (14). These shear rates are substantially lower than the $\sim 10^5$ s^{-1} that would be needed to damage cells if a 100-N m^{-2} shear stress value (13,88) is taken as the threshold of mechanical damage. However, based on the shear stress data of Olivier and Truskey (91), during the process of attachment of cells to microcarriers, shear rate levels of 250–600 s^{-1} may well be detrimental. Thus, during initial attachment of cells, the reactor would need to be operated at reduced aeration rates—a practice that is well established through empirical experience, but previously explained only intuitively (14).

Under conditions typical of microcarrier culture in airlift bioreactors, the specific energy dissipation rates are different in different zones of the vessel. The specific energy dissipation rates increase in the following order: downcomer $<$ riser $<$ bottom, for any fixed value of the aeration rate (14). The dissipation rates in all zones decline with increasing loading of microcarriers; however, the prevailing shear rates are not particularly sensitive to the density or the diameter of microcarriers within the ranges that are relevant to anchorage-dependent cell culture. In one case, typical shear rates ranged over 250–4,000 s^{-1} in microcarrier-containing systems, but much higher values, up to 12,000 s^{-1} could occur in solids-free media (14). These values compare favorably with shear rates of $\sim 10^5$ s^{-1} that have been reported as the threshold of damage to cells. Cells in airlift bioreactors would experience a substantial increase in the riser shear rate only when the fluid eddy length–to–microcarrier diameter ratio declines to ~ 1 (14).

Hydrostatic Pressure As the scale of operation increases, suspended animal cells will inevitably experience substantial hydrostatic pressure changes as they move with fluid elements in a large bioreactor. At least for hybridomas, artificially imposed pressure cycling of up to 1.2 atm (18 psig) has shown no harmful effect (79). This level of pressure fluctuation will be encountered in bioreactors that are about 12 m tall; hence, for a 2:1 aspect ratio, an animal cell culture vessel could be scaled up to about 340 m^3. If, as recommended for airlift and bubble column bioreactors (20,21), an aspect ratio of 5:1 is employed, a maximum vessel volume of about 50 m^3 should be feasible. Suspension cell culture vessels in current commercial use do not generally exceed 10 m^3, or about 20% of the feasible volume based on hydrostatic pressure considerations.

Bubble-Associated Damage That sparging damaged cells has been known since the 1960s; however, the specific events responsible for the damage—whether bubble formation at the sparger, bubble detachment, rise through the fluid, or events at the disengagement surface—and the mechanism(s) of damage remained unclear until recently.

The growth rate, viability, and antibody productivity of a mouse hybridoma in a surface-aerated stirred vessel were not affected by the agitation rate, but damage occurred when gas was sparged through the culture (107). In surface-aerated operation, the average and the maximum shear stress values varied over the respective ranges of 0.001–0.4 N m^{-2} and 0.06–6.4 N m^{-2}. Subsequent work showed that bubbles larger than 5 mm were significantly less damaging to cells than smaller bubbles (108). Furthermore, placing the sparger below the impeller enhanced cell damage, presumably because the impeller-associated bubble breakup gave rise to the more damaging smaller bubbles (108).

Cell lines differ tremendously in sensitivity to aeration as was demonstrated by Handa et al. (109). At constant aeration rates in geometrically identical bubble columns, smaller diameter bubbles (0.2 mm in diameter) were shown to be significantly more damaging to a hybridoma than larger bubbles (1.62 mm in diameter). In industrial-scale culture of several hybridomas, Chisti (78) preferred yet larger bubbles (10–20 mm diameter) for aeration. Similarly, Tramper et al. (63) observed that smaller bubbles were more damaging to insect cells than larger ones. However, the effect of bubble size may not be prevalent across cell types. Thus, in another study, baby hamster kidney (BHK-21) cells were not sensitive to the size of gas bubbles (110). Over a superficial gas velocity range of (0.42–8.5) $\times$ 10^{-4} m s^{-1}, higher velocities led to faster decline in cell viability of a hybridoma (109), which is consistent with other similar observations (61).

In commercial stirred-tank culture of several hybridoma lines at up to 0.3 m^3, Chisti (78) employed submerged aeration with bubbles of 0.01–0.02 m in diameter. Because of high rise velocities and mobile interfaces, such bubbles did not carry many attached cells to the surface. In contrast, during aeration with sintered metal spargers that produced slower rising bubbles of ~0.002–0.003 m in diameter, the cells were rapidly carried into a persistent foam layer at the top by a froth flotation mechanism (78). The foam produced by larger bubbles collapsed soon after the bubble rose to the surface. The reactors employed were agitated by magnetically coupled agitators with support bearings submerged in the culture. Reactors with submerged mechanical seals were also used. No loss in culture performance occurred relative to roller bottles. The impeller tip speeds >1 m s^{-1} produced no ill effects. Under typical operating conditions, the length scale of the microeddies was about 130 μm, or about 10-fold greater than the dimensions of the cells (78).

Based on energetics of bubble-associated damage to freely suspended cells, Wang et al. (111) concluded that the principal determinants of cell damage were the cell–bubble encounter rate, the rate of bubble breakup within the fluid, and the bursting rate at the surface. Cell death correlated linearly with specific gas–liquid interfacial area, with the proportionality constant being 0.0125 m h^{-1} for a murine hybridoma (111).

Using an elegant mechanistic analysis, Tramper et al. (62,63) related the first-order rate constant for cell death due to all causes to aeration rate in a bubble column; thus,

$$k_d = \frac{24QV_k}{\pi^2 d_B^3 d_T^2 h_L} \tag{40}$$

where k_d is the first-order death rate constant, Q is the volumetric aeration rate, h_L is the height of fluid, d_T is the column diameter, and V_k is a hypothetical killing volume associated with the bubbles. The latter is actually the total volume of fluid associated mainly with the bubble wakes; the cells entrapped in the circulating wake are carried with the bubble to the surface where most of the damaging events take place. According to equation 40, the specific cell death rate is proportional to the frequency of bubble generation, or $6Q/\pi d_B^3$. Alternatively, because at hydrodynamic steady state the bubble generation frequency equals the frequency of rupture at the surface, the death rate may be interpreted as being dependent on the frequency of bubble rupture and the killing volume associated with the bubbles.

Based on equation 40, the death rate constant should decline with increasing height of fluid, as experimentally confirmed: for otherwise fixed conditions, increasing liquid height in bubble columns improved survival of insect cells (62,63), myelomas, and hybridomas (60,64,110), supporting the view that cell death occurred predominantly in the bubble disengagement zone at the surface (109,110). For a myeloma grown in serum-supplemented medium, the minimum culture height that provided a performance equivalent to that of surface aerated flasks, was ~0.7 m, corresponding to a bubble column aspect ratio of ~14 (64). The 0.05-m diameter column was aerated through a sintered disc sparger (150- to 250-μm pore size). The aeration rate was 5 mL min^{-1} (64), corresponding to a specific power input of about 0.42 W m^{-3}.

If bubble rise were to predominantly contribute to cell death, then the specific cell death rate should be independent of the height of fluid (112). Because this is contrary to experimental observations, the rise events may be disregarded as principal contributors to cell damage (112). Whereas, if gas entry at the sparger contributed predominantly to cell damage, then at a given gas flow rate in the reactor, decreasing the number of sparger holes should enhance the specific cell death rate constant (112). In bubble columns, Jöbses et al. (112) noted that increasing the sparger hole gas velocity over 0.6–2.5 m s^{-1} at a constant volumetric gas flow in the reactors had no effect on the first-order rate constant for cell death; hence, events at the sparger could be disregarded as contributing to cell damage. This process of elimination identified bubble breakup at the culture surface as the principal cause of damage to suspended cells in sparged bioreactors such as bubble columns (112). Equation 40 applies also to airlift devices (61), especially ones in which gas is not carried into the downcomer. Because most agitated tanks used in animal cell culture operate at quite low mechanical power inputs and the impeller does not usually serve as a bubble breaking device, equation 40 should provide a lower limit on k_d also in such tanks.

Using a hybridoma culture van der Pol et al. (60) showed that the first-order death rate constant increased with increasing $1/d_T^2$ in bubble columns, as expected from equation 40. Equation 40 suggests that cell damage in-

creases in direct proportion to the superficial gas velocity in the column, or in direct proportion to the specific power input. Note that increasing liquid level at constant aeration rate in a column of fixed diameter decreases the specific power input (14,20,21). Equation 40 further suggests that for a given V_k, larger bubbles should be less damaging than smaller ones. This agrees with substantial empirical evidence (62,63,78,108,110,113).

That the death rate increases linearly with increasing aeration rate has been proven (62,63,113). Also, the killing volume, V_k, has been shown to be independent of the aeration rate and the height of fluid, so long as the bubble diameter is not affected (62,63). The killing volume apparently depends on bubble diameter, increasing with diameter but in such a way that the ratio V_k/d_B^3 declines as the bubble diameter increases. This has been confirmed by Wu and Goosen (113) using *Spodoptera frugiperda* insect cells in bubble columns that were sparged with bubbles of different mean diameters while maintaining a constant volumetric gas flow rate. Increasing bubble diameters reduced the specific death rate, as shown in Figure 8. In view of the numerous contrary observations, analyses suggesting lesser cell damage with smaller bubbles are clearly flawed.

The dimensionless specific killing volume, or $6V_k/\pi d_B^3$, in equation 40 depends on the concentration of serum in the culture medium. Van der Pol et al. (60) showed that the dimensionless killing volume declined as the serum concentration was raised over the range 0–2.5% (vol/vol); the dimensionless killing volume in the absence of serum was ~2.7-fold that at 2.5% serum in a hybridoma culture (60). This and other similar observations (61) at least partly explain the well-known protective effect of serum. Cell-protective effects of other proteins may be similarly explained. Serum-free media with 1 g protein L^{-1} (equivalent to supplementing the medium with 2% vol/vol serum) are commercially used in sparged airlift culture vessels (79).

Why rupture of larger bubbles is less damaging to cells than breakup of smaller ones has become clear through analyses of mechanics of rupture (114,115). Numerical simulations and experimental observations of bubble rupture at an air–water interface confirm that smaller bubbles rupture much more violently than larger ones (114,115). A bubble reaching the surface rises to different heights above the flat liquid surface before rupturing. For a bubble that is stationary at the surface, a part is always submerged below the flat surface of the liquid. The degree of submergence is generally greater for smaller bubbles. During rupture, the liquid drains from the film between the raised liquid surface and the bubble (116,117). As the film thins, a hole develops in the center of the dome, and the film rapidly retreats into the bulk liquid. The rupture of the film and consequent elongational and accelerational flow have been postulated to damage cells in the film and those adhering to the bubble cavity (116). A cell on the surface of a rupturing film would apparently not experience any motion until struck by the torroidal ring of fluid at the receding edge of the film (116). The force experienced by the cell will depend on the film thickness at the instance of rupture (116). Rupture of thinner films is likely to be less damaging than the breakage of a thicker film. Once the bubble ruptures, fluid rapidly accelerates and moves down the interior walls of the bubble cavity. The flow from around the walls impacts at a stagnation point located immediately below where the bubble had been. The high pressure produced by the impacting streams forces a jet of fluid upward into the gas phase above the liquid surface. A second opposing jet is forced into the fluid below the stagnation point. Intense accelerational flows around the bubble cavity and formation of liquid jets occur mostly during rupture of small bubbles. Bubbles larger than about 6 mm rupture much less violently.

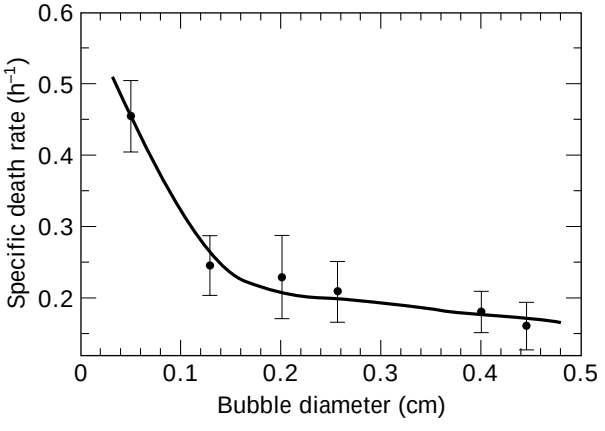

Figure 8. Effect of bubble diameter on the specific death rate of *S. frugiperda* insect cells in bubble columns aerated at a constant volumetric gas flow rate of 10 mL min^{-1}. *Source*: Adapted from Ref. 113.

According to Boulton-Stone and Blake (114), "one of the most important factors determining the motion following film rupture, in terms of the energy released, is the height of the top of the bubble above the equilibrium free-surface" of the liquid. Bubbles rupturing from a lower position beneath the equilibrium surface of the liquid release more energy because of their higher internal pressure. The energy is released as high-speed liquid jets. Bubbles larger than about 6 mm bursting at the surface do not form significant jets (114) which is consistent with numerous observations dating from 1950s and earlier. When a jet is produced, the speed of the jet declines as the size of the rupturing bubble increases: for example, for air bubbles rupturing on water, a maximum jet speed of 6.4 m s^{-1} has been calculated for rupture of a 1-mm bubble; for rupture of a 6-mm bubble the maximum jet speed declines to 0.94 m s^{-1} (114). In addition to a liquid jet rising into the atmosphere above the liquid, a second liquid jet moves down into the fluid from the region that had been below the base of the bubble. The maximum pressure produced during bursting of bubbles of various sizes declines with increasing bubble diameter, as illustrated in Figure 9. The maximum energy dissipation rate occurs just beneath the bubble immediately before the jet forms (114). The calculated maximum energy dissipation rates for the smallest bubbles are equivalent to a stress of about 10.4 N m^{-2} (114). The maximum energy dissipation rates decline with increasing bubble diameter, as depicted in Figure 10.

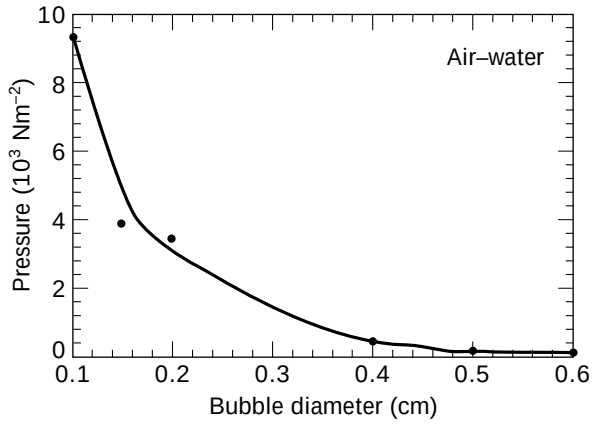

Figure 9. The maximum pressure produced during bursting of air bubbles of various sizes on the surface of water. *Source*: Adapted from Ref. 114.

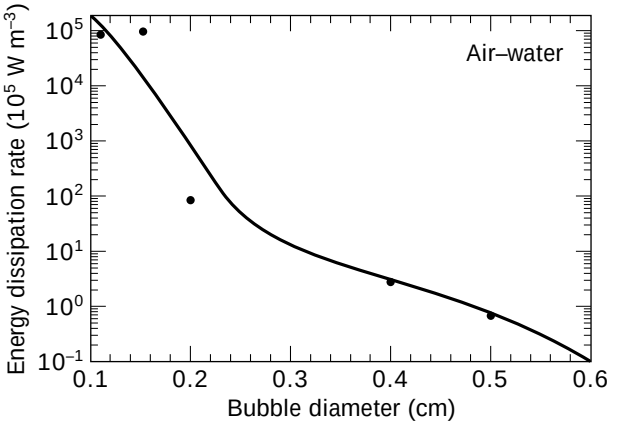

Figure 10. The maximum energy dissipation rates produced during bursting of air bubbles of various sizes on the surface of water. *Source*: Adapted from Ref. 114.

Even a violent bubble rupture event would be inconsequential if there were no cells in the vicinity. Unfortunately, cells attach to rising bubbles, and the fluid behind bubbles is especially rich in cells. That some animal cells will attach to rising bubbles has been shown with *Trichoplusia ni* and *S. frugiperda* insect cells (116,118). The cells adhered to rising microbubbles (diameter ≤3 mm) of the type used commonly in froth flotation. Hydrophobic interactions are apparently responsible for cell attachment—a mechanism observed also with ore particles attaching to bubbles during foam flotation. Although, very small bubbles are generally not suited to aeration of cell cultures (78), larger bubbles also transport cells to the surface, but not predominantly as adhering cells. Instead, the cells are trapped in the circulating wake carried behind large bubbles. The fluid associated with the wakes is known to be richer in particles than the bulk fluid.

More than 95% of the cells in the liquid ejected as jet during rupture of bubbles have been shown to be nonviable even when the cells in the bulk culture contained fewer than 10% dead cells (115). Clearly, the cells carried in the bubble wake are destroyed by the rupture event. Based on simulations of rupture of bubbles with diameters of 0.77 mm, 1.70 mm, and 6.32 mm, Garcia-Briones et al. (115) calculated maximum energy dissipation rate values (W m^{-3}) of 9.52×10^7, 1.66×10^7, and 9.40×10^4, respectively. Comparing these values with energy dissipation rates that have damaged cells in various unaerated flow devices (capillaries and viscometers), Garcia-Briones et al. (115) noted that values of the order of 5.81×10^2 W m^{-3} did not damage the cells significantly, whereas appreciable damage occurred when the energy dissipation rate exceeded about 2.25×10^4 W m^{-3}. Clearly, therefore, a 6.32-mm bubble still has a significant potential to damage cells, and a smaller bubble would produce instantaneous damage. For example, in gas-free capillary flow in experiments reported by Augenstein et al. (16), more than 80% of the cells died within 0.3 s of exposure to energy dissipation rates of about 4.80×10^7 W m^{-3} (115). Interpreting data from several sources, Garcia-Briones et al. (115) further note that average energy dissipation rates of the order of 2,990–29,000 W m^{-3} have generally produced a significant decline in growth rate in impeller-agitated bioreactors. These dissipation rates are average values; the cells probably experienced much higher local energy dissipation rates in the vicinity of the impellers.

If stable foam is not allowed to form, and relatively large bubbles (diameter ≈ 10–20 mm) are used for aeration so that the energy dissipated during rupture remains below the cell damaging threshold, then the cells carried in the wake will not be damaged or removed into a foam layer. For bubbles of a given size, the volume of the circulating wake can be reduced by increasing the viscosity of the culture broth. Small increases will reduce the rise velocity of the bubbles, and the circulation in the wakes will be slowed down. Consequently, slight enhancements in viscosity could reduce the transport of particles in the wake. This may indeed be one explanation of why viscosifying additives have been frequently observed to reduce cell damage. Also, for a given volumetric aeration rate, use of larger bubbles reduces bubbling frequency; hence, the frequency of bubble rupture is reduced.

Based on the studies reviewed, several important observations can be made regarding freely suspended animal cells in sparged and agitated bioreactors: (*1*) the aeration rate should be kept as low as possible; (*2*) the mean bubble size should larger than 7 mm, preferably about 10–20 mm; (*3*) the location of the sparger should be such that the rising bubbles do not interact with any impellers; (*4*) with small airlift and bubble column reactors the aspect ratio should be about 14; however, in larger columns where the sparged portion of the cross section can be a small fraction of the total cross-sectional area, more realistic aspect ratios of about 6 or 7 are satisfactory; and (*5*) when an impeller is used, the average energy dissipation (input) rate should remain below about 1.0×10^3 W m^{-3}. Observations (*1–5*) are consistent with industrial practice (78). The sole purpose of the impeller should be to suspend the cells and mix the fluid gently so that the oxygen transferred from the bubbles is distributed throughout the vessel. Consistent with this purpose, the impeller should be of a kind that

does not produce excessively high local rates of energy dissipation. For example, relatively large axial flow hydrofoils are the preferred impellers (30,78). In addition, a suitably selected additive such as Pluronic F68 should be used whenever feasible.

Mitigation of Shear Damage Various approaches have been used to reduce bubble rupture–associated damage to cells. Some common approaches are the use of cell protective additives as noted here; compartmentalization of the culture into cell-free and cell-containing zones, with sparging confined to cell-free regions (80,81); use of bubble-free oxygenation through microporous or diffusion tubing made of silicone rubber or other polymer; use of liquid oxygen vectors such as perfluorocarbons; and surface aeration (see MASS TRANSFER). Alternatives to bubbling are suited typically only to specific cases; direct sparging remains the predominant method of aeration of cell cultures, and it is not likely to be displaced in the foreseeable future (76).

One adaptation of submerged aeration is the "bubble bed" bioreactor, which can substantially reduce surface rupture of bubbles in short-term batch culture (119). The bubble bed device (Fig. 11) is similar to a concentric draft-tube airlift bioreactor, but a downward pumping axial flow impeller located in the draft tube circulates the fluid. The downward liquid flow in the draft tube is sufficiently fast that gas bubbles injected into the draft tube cannot escape; hence, the bubbles do not rupture at the surface of the culture. Pure oxygen or oxygen-enriched gas is used to reduce the needed gas injection rate to very low values. The gas holdup in the downcomer increases during batch operation, and a noncirculating bed of bubbles develops. The cross-sectional area of the draft tube increases downward (Fig. 11) so that the superficial velocity of the liquid declines as it moves down; consequently, the downflowing liquid cannot drag the bubbles out of the draft tube and into the bubble-free annular zone. According to Sucker et al. (119), the cell growth and antibody production in bubble bed devices is comparable to values obtained in surface-aerated spinner flasks even when the sparged culture in the bubble bed units is not supplemented with serum, Pluronic F68, or other protective additives.

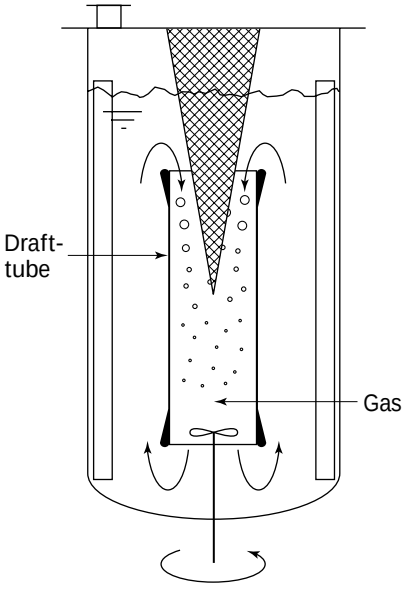

Figure 11. A bubble bed reactor.

Shear Protectants. Bubble-associated damage can be significantly reduced by adding shear-protective substances to the culture medium. Many additives have been examined for shear-protective function (120). Some of the protective additives are noted in Table 4. The protective effect depends on the properties of the specific additives, the concentration used, the type of cell, and the mechanism(s) of protection. Some common protective agents and their mechanisms of protection are treated next.

Serum. A concentration-dependent protective effect of fetal calf serum, horse serum, and others, has been widely observed in aerated and bubble-free suspension cultures of many types of animal cells (41,60,61,66,110,120–122). Typically, protection increases with increasing serum concentration until about 10% (vol/vol) serum. In one study reduction in fetal calf serum level from 2.5% to 0% substantially increased the death rate constant of a hybridoma in aerated culture (60). Investigations revealed that serum had no long-term biological effect, but only a direct nonspecific physical protective effect (60). Thus, cells growing in low-serum medium were immediately protected upon transfer to a medium with 2.5% serum. A physical protective effect of serum has been claimed to originate in its ability to reduce plasma membrane fluidity (41,121). According to Martens et al. (61), serum has an immediate physical protective effect, but also a physiological protective effect that takes longer to become effective. The latter finding concurs with the results of Michaels et al. (122). In bubble-free experiments in a Couette viscometer (shear rate = 5,000 s^{-1}, shear stress = 5 N m^{-2}), prolonged exposure of cells to fetal bovine serum (FBS) reduced their shear sensitivity in laminar flow studies (122); however, shorter (30–120 min) exposure to FBS did not affect shear tolerance of cells. Based on these results, the protective effect of FBS was claimed to have both physical and biological (biochemical) origins (122).

The precise nature of the physical protective effect of serum is not clear. Supplementation with serum enhances the viscosity of the culture medium, but the effect is small (92,123). Nevertheless, Croughan et al. (66) and others (67,104) have associated the observed protection to the turbulence-dampening effect of serum. In contrast, other evidence suggests a lack of relationship between the amount of protection afforded by the serum and enhance-

Table 4. Media Additives Associated with a Cell-Protective Effect

Serum	Pluronics
Proteins (e.g., serum albumin)	Polyvinyl alcohols
Derivatized celluloses (e.g., methyl cellulose)	Polyvinyl pyrrolidone
Derivatized starches (e.g., hydroxyethyl starch)	Polyethylene glycols
Dextrans	

ment of viscosity (124,125). In addition to dampening turbulence, the serum proteins may coat the cells so that the fluid eddies no longer penetrate to the vicinity of the cell membrane (66). In one study, increasing the concentration of fetal bovine serum over 0–10% (vol/vol) reduced plasma membrane fluidity of a hybridoma line, making the cells more resistant to shear damage (41,121).

Pluronic® F68. Another well-known shear protectant is the nonionic surfactant polyol Pluronic® F68, a block copolymer of poly(oxyethylene) and poly(oxypropylene). Highly pure Pluronic F68 is added to cell culture media, typically at 0.5–3 kg m^{-3} (92,109,110,112,120,122). The protective effect of the surfactant is concentration dependent, increasing with concentration but leveling off at ~0.5 g L^{-1} (Fig. 12).

The protective effect of Pluronic F68 is commonly associated with its ability to suppress attachment of cells to bubbles (110): in the presence of the surfactant, fewer cells are carried to the surface where much of the cell damage occurs in aerated culture. However, evidence exists for other protective mechanisms. For example, a cell-protective effect of Pluronic F68 has been observed even in unaerated culture (41,112). In one case this effect was observed in a strongly agitated culture sample (112). Although no bubbles were present, a deep vortex was drawn into the fluid by the marine impeller used. Extensive cell damage occurred, but the damage was significantly reduced when the culture was supplemented with Pluronic F68. Based on these observations, Jöbses et al. (112) concluded that the protective effect of Pluronic F68 was due to its direct influence on cells and to some effect of the surfactant on the gas–liquid interface. One possible explanation for the protection observed by Jöbses et al. (112) in the absence of the bubbles follows: the damage may have been occurring at the rapidly moving surface of the vortex (126), and supplementation of the culture with Pluronic F68 may have reduced the surface adherent tendency of the cells; hence, fewer cells may have attached to the surface during its formation at the periphery of the vessel.

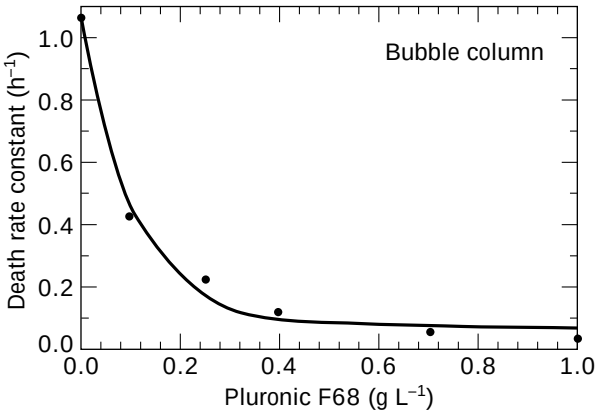

Figure 12. Cell protective effect of Pluronic® F68 in a bubble column. The specific first-order cell death rate constant is plotted as a function of the concentration of Pluronic F68 in the medium. All data were obtained at a constant specific power input of ~40 W m^{-3}. *Source*: Adapted from Ref. 112.

Using flow cytometry, Al-Rubeai et al. (86) showed that leakage of a positively charged dye, fluorescein diacetate, from murine hybridomas increased with rising intensity of agitation, suggesting a possible link between the permeability of the cell membrane and the shear rate. However, because intense agitation was accompanied by entrainment of gas bubbles into the culture (86), the observed leakage could not be conclusively associated with fluid turbulence. The authors noted that for otherwise fixed agitation conditions, the leakage of the dye reduced when the culture medium was formulated with 1% Pluronic F68. The protective effect of the surfactant was apparently linked at least partly with its biochemical association with the cell membrane. The agitation- and vortex-associated hydrodynamic forces were reported to also affect the antigen receptors embedded in the membrane of the hybridoma (86). The number of active surface receptors declined with increasing intensity of agitation and the accompanying increase in the size of the vortex; however, the viability of the cells was unaffected. Pluronic F68 had a protective effect on the receptors.

Pluronic F68 is known to reduce the plasma membrane fluidity (PMF) of cells, and this has been suggested as a possible mechanism of protection (41,121). Other additives that affect PMF also affect a cell's shear tolerance. For example, in one case cholesterol enrichment of the culture medium reduced membrane fluidity and enhanced the shear resistance of hybridomas, whereas supplementing the culture with benzyl alcohol increased PMF and made cells more shear sensitive relative to controls (41,121).

Other protective mechanisms speculated for Pluronic F68 include its stabilizing action on the gas–liquid interface and consequent slower film drainage during bubble rupture (110), improved nutritional transport because of a reduced cell–fluid interfacial tension, and incorporation of the surfactant into the cell membrane accompanied with membrane stabilization (127,128). Although the protective effect of Pluronic F68 is said to be solely due to physical factors (122), the surfactant is known to produce physiological and biochemical effects in at least some cases. Growth suppressing and stimulatory effects of Pluronic F68 have been seen even in some static cultures. Such effects are sometimes associated with impurities in Pluronic F68 samples. Pluronic F68 affects the permeability of some cells. Exposure of *Saccharomyces cerevisiae* to 0.2% (wt/vol) Pluronic F68 for 30 min at 20 °C made the cells more permeable, and they became susceptible to otherwise nonlethal doses of certain antibiotics (129). The mean activity of alcohol dehydrogenase in permeablized cells was more than 3.5-fold of that in normal cells. Although Pluronic F68 could permeablize the yeast cells, it did not inhibit growth or affect cell viability relative to controls when added to culture media at up to 1% (wt/vol), which was the highest concentration tested (129).

Other data suggest that the cell-protective effect of Pluronic F68 may not be quite general (43). For porcine erythrocytes suspended in isotonic buffer, Zhang et al. (43) noted that addition of Pluronic F68 actually increased cell lysis in agitated environments relative to results in the surfactant-free medium. Whether Pluronic F68 incorporates into an erythrocyte's membrane is not known; how-

ever, cholesterol enrichment or depletion of erythrocyte membrane is reported to not affect membrane viscosity and presumably, therefore, fluidity. In addition to Pluronic F68, several other pluronics are known to have a shear-protective capability.

Poly(ethylene glycol). Poly(ethylene glycol) (PEG) supplementation of the medium has a protective effect on some cells but not on others. In one study (129) that employed different PEGs with molecular weights of 400–35,000 Da in the concentration range of 0–2 kg m^{-3}, the polymer had a protective effect in sparged cultures when the molecular weight and the concentration exceeded 1,000 Da and 0.25 kg m^{-3}, respectively. The extent of protection afforded depended on the molecular weight and the concentration used. Under the best conditions, the PEG supplementation reduced the first-order cell death rate constant to 0.5% of the value in the PEG-free medium (130). The PEG additives affected the surface tension of the culture medium; however, in extreme cases the surface tension varied only between $\sim 60 \times 10^{-3}$ and 70×10^{-3} N m^{-1} (130). The pattern (but not the magnitude) of variation in surface tension with addition of PEG was similar to the pattern of change in the death rate constant. This led the authors to suggest that the presence of PEG at the gas–liquid interface was somehow related to the protective mechanism.

Michaels et al. (122) showed that, in sparged bioreactors, supplementing the culture medium with Pluronic F68, fetal bovine serum (FBS), or PEG (8,000 Da, 1 kg m^{-3}) protected cells irrespective of whether the CRL-8018 hybridomas were grown in the presence of the additive, or the additive was added after the damaging levels of agitation were imposed.

Composite Particles and Cell Aggregates

Microbial Biofilms on Suspended Particles. Gas–liquid–solid three-phase suspension reactors are increasingly being used in wastewater treatment (20,131). The suspended solid phase (usually sand, glass beads, or carbon particles) supports a biofilm of waste-degrading microorganisms (132). The hydrodynamic environment of such systems must be tailored to control the biofilm thickness without dislodging it altogether (20). Biofilm slurry reactors are conceptually similar to microcarrier-supported suspension culture of animal cells, but there the similarity ends. Unlike animal cell microcarrier suspensions, the biofilm reactors are much more turbulent, the solids loading is generally higher, the density difference between the solid and the liquid phase is much greater, and the biofilm is typically four or five times thicker than the monolayer of cells on microcarriers.

In studies of degradation of naphthalene-2-sulfonate by *Pseudomonads* immobilized as biofilms on sand particles suspended in an external-loop airlift bioreactor, Wagner and Hempel (133) noted that at solids loadings of 20–30 kg m^{-3}, only about 15–20% of the particles were covered with biofilm, but high solids loadings were necessary to control the film thickness at 75 ± 10 μm by providing a high-attrition environment (133). These observations were for particles about 200 μm in diameter, covered with a biofilm ~ 75 μm thick, suspended in the reactor under fairly turbulent conditions (230–440 W m^{-3} specific power inputs). Even when oxygen limitation is not an issue, diffusion of other substrates limits the useful thickness of microbial biofilm to less than 400 μm in most wastewater treatment operations (131).

The development of microbial biofilms on static surfaces and carriers suspended in airlift bioreactors has been investigated quite extensively (6,7,132,134–140). In one case, 21 carriers were tested at a constant carrier loading of 125 kg m^{-3} (132). The superficial gas velocity was constant at 0.038 m s^{-1}. The hydraulic retention time of wastewater was one or two hours. Based on the tests, carrier diameter and surface roughness were the major factors that influenced biofilm formation (132). Smaller particles, 0.1–0.3 mm in diameter, tended to show better biofilm development. This was said to be due to more frequent collisions among larger particles, causing biofilm detachment (132); however, with larger particles, a greater *severity* of collisions would have been a better explanation (20). For equal mass loadings of solids in two systems, the system with larger particles should have fewer particles per unit volume and, therefore, a lower frequency of particle–particle collisions. Cell disruption experiments in agitated slurries of glass beads confirm this (11). The explanation for the impact of surface roughness on biofilm formation lay in the fact that a rough surface provided many relatively protected, low-shear sites where microbial colonies could take hold in the process of gradually spreading over the whole surface. Based on the criteria of surface roughness, particle size, cost, and the requirement of a high-density carrier for ease of separation, basalt (ρ_S = 2,900 kg m^{-3}) was the best carrier (132).

Irrespective of carrier type, biofilm formation is favored at relatively high dilution rates when any detached cells are rapidly washed out (132,136). Tijhuis et al. (136) have shown that during start-up at high dilution rates, the concentration of bare carriers declines as an increasing number are covered with the biofilm. The total amount of the biomass in the reactor increases, but the amount per carrier remains constant until most of the carriers are covered. With few bare carriers remaining, the extent of abrasive loss of film declines, and the film thickness begins to increase until a stable thickness is reached (136). These observations suggest that varying the reactor operation to suit different stages of film development may be worthwhile (20).

In other similar work, detachment of biomass from nongrowing biofilms supported on carriers suspended in four configurations of draft-tube sparged internal-loop airlift reactors was examined (139). The superficial aeration velocity in the riser varied over the approximate range 0.03–0.09 m s^{-1}. The detachment of biomass from biofilm-covered carriers in the presence of bare solids was dominated by collisions between bare carriers and the covered particles (139,140). The concentration of bare solids and the particle roughness strongly influenced the detachment rate (139). For otherwise identical conditions, biofilm detachment due to bare carriers increased in the following order: glass, sand, basalt. The glass particles were the most round and smooth; the basalt carriers were the

roughest. Whereas biofilms develop more easily on rough surfaces (132), once developed, the film is readily damaged by biofilm-free rough carriers. Gjaltema et al. (139) observed that a "change in flow regime from bubbling to slug flow considerably increased the detachment rate." This change apparently occurred at a U_{Gr} value of $\sim$0.06 m s^{-1}. The "slug flow" regime noted by Gjaltema et al. (139) was more likely the highly chaotic churn turbulent regime in which particle-to-particle collisions are more frequent and severe than in the bubble flow regime. The bottom clearance of the draft tube had no effect on detachment rate (139), but only a small range of the A_d/A_b ratios was investigated. The volume fraction of carriers was 3.3–3.8%, and other properties were: basalt, d_p = 0.32 mm, ρ_S = 3,010 kg m^{-3}; sand, d_p = 0.31 mm, ρ_S = 2,606 kg m^{-3}; and glass, d_p = 0.28 mm, ρ_S = 2,887 kg m^{-3} (139). Another similar study focused on the effects of particle shape, structure, and concentration on biofilm detachment (140).

Strategies for development of biofilms with nitrification activity on carriers suspended in draft-tube sparged internal-loop airlift reactors were investigated by Tijhuis et al. (141) and van Benthum et al. (138). The development of the nitrifying films was similar to what had been reported for heterotrophic biofilms (134–137); however, the nitrifying films were more robust (141). This suggests that biofilms formed by different microorganisms can have markedly different physical properties and strength of attachment to substrate (20); hence, the operating regime of the reactor and, in extreme cases, the design peculiarities are likely to be affected.

In further studies of the dynamics of biofilm detachment from carriers suspended in airlift reactors, Tijhuis et al. (135,137) noted that the common assumptions of uniform growth and detachment of biomass over the surface of the film under fixed hydrodynamic conditions were inconsistent with observations. Instead, nonuniform local detachment of biofilm with formation of cracks and fissures on the surface and rapid filling of the spaces formed with new growing biomass was proposed as a more realistic picture of film dynamics (135).

During development of mixed bacterial biofilm on a static glass surface in a rectangular turbulent flow cell, Stoodley et al. (7) noted that parts of the biofilm sloughed off at a wall shear stress level of 1.32 N m^{-2}. In the region of detachment, pieces of the biofilm were still attached to the surface, suggesting that the glass-to-biofilm bond was stronger than the biofilm structure (7). Relative to the clean flow cell, the pressure drop through the channel was higher in presence of the biofilm (7), presumably because a patchy development of the film increased the effective surface roughness.

Flocs and Agglomerates. Microbial flocs are encountered in several commercially relevant processes, especially in wastewater treatment and beer fermentation with autoflocculating yeasts. Similarly, agglomerates of protein precipitates form during certain recovery operations. The size of flocs and agglomerates often needs to be preserved or increased during processing. Stable size of aggregates and flocs, and whether the flocculated mass further increases in size or breaks up, depends on the level of turbulence in the suspending fluid. Turbulent stress levels below about 0.75 N m^{-2} are generally too mild to break aggregates (142). Physical disruption of aggregates commences at stress levels of $\sim$2.6 N m^{-2}, and especially when the stress level exceeds about 5 N m^{-2} (142). In a turbulent field, aggregates may deform or breakup because of the influence of instantaneous velocity differences acting on different parts of the floc (143). Also, turbulent drag forces originating from the local motion of the fluid relative to the aggregate may contribute to fragmentation (142). The shear force across the aggregate due to instantaneous velocity difference is related to the energy dissipation rate in the fluid and the size of the aggregate (142); thus,

$$F_s = \frac{\pi}{4}(\rho_L \mu_L E)^{1/2} d_F^2 \tag{41}$$

The dynamic pressure fluctuations acting on opposite sides of the floc create a normal stress. Assuming that the eddy size is in the Kolmogoroff microscale range and that the particle dimensions are similar to those of the eddies, the normal force can be expressed as follows (142):

$$F_n \propto \left(\frac{E}{\mu_L}\right)\rho_L^2 d_F^2 \tag{42}$$

The turbulent drag force acting on an aggregate may be calculated using the expression (142)

$$F_D \propto \frac{C_D}{2}\left(\frac{d_F}{2}\right)^3 (\Delta u d_F)^2 \rho_L \tag{43}$$

where Δu is the difference in velocities of the particle and the fluid, and C_D is the drag coefficient. For low-density particles in the Stokes regime ($Re < 1$), the drag coefficient equals $24/Re$, where Re is the Reynolds number, or $(\rho_L \Delta u d_F)/\mu_L$. Reynolds shear stresses (i.e., turbulent stresses associated with the fluctuating component of the mean velocity) may be calculated using the equation (144)

$$\tau = 0.37\rho_L\left(\frac{E\rho_L}{\mu_L}\right)d_p^2 \tag{44}$$

which applies to stresses around a spherical particle. Reynolds stresses are independent of viscosity.

The maximum stable size of the aggregate in a turbulent field can be established by a force balance on a particle: at stable size the instantaneous turbulence force accelerating the particle just equals its mechanical strength (142). In the inertial subrange of turbulence when the eddy size is greater than the Kolmogoroff scale (l),

$$d_{F\ max} \propto \left(\frac{\rho_L \sigma_M}{\mu_L}\right)^{1/3} E^{-1} \tag{45}$$

whereas in the viscous subrange of turbulence when the eddy size is $\leq l$, we have

$$d_{F\ max} \propto \left(\frac{\sigma_M \mu_L}{\rho_L^2 E}\right)^{1/2} \quad (46)$$

where σ_M is the mechanical strength of the aggregate. In practice, the maximum stable floc size has correlated with the energy dissipation per unit mass of fluid,

$$d_{F\ max} \propto \Gamma E^{-m} \quad (47)$$

where the coefficient Γ depends on the nature of the particle, and m is usually between 0.2 and 0.4 (145).

In stirred tanks, the maximum floc size for particles of uniform composition has been theoretically and experimentally correlated with the rotational speed of the impeller (143); thus,

$$d_{F\ max} \propto N^{-1.5} \quad (48)$$

which applies to particles smaller than the microscale of turbulence. The dependence shown in equation 48 can be expressed in terms of the energy dissipation per unit mass; hence,

$$d_{F\ max} \propto E^{-0.5} \quad (49)$$

Expression 49 is consistent with that reported by Thomas (143), but the exponent on E is somewhat stronger than the values noted by Gregory (145) (see equation 47). In precipitation vessels, shear rate values of $\sim 80\ s^{-1}$ appear to be a damaging threshold for soya protein precipitate particles of 20–30 μm initial size (5). Particles exposed to approximate shear rates of $\geq 80\ s^{-1}$ over 10–12 min would be reduced to 5–8 μm. The shear rate numbers were calculated from the specific energy dissipation rates in the vessels, as follows:

$$\gamma = \left(\frac{\rho_L E}{\mu_L}\right)^{0.5} \quad (50)$$

Protein precipitates are easily damaged by pumping. Moyno screw pumps, centrifugal pumps, and gear pumps all damage precipitates to similar levels (5). Peristaltic pumps are apparently the only suitable ones.

Fragmentation of mycelial pellets of the molds *Lentinus edodes* and *Aspergillus niger* in a standard Rushton turbine stirred tank was examined by Taguchi et al. (145). Two types of pellet fragmentation patterns were noted: (*1*) decrease in diameter by erosion of surface, and (*2*) direct rupture of the spherical pellet. The rates of these processes were expressed as

$$-\frac{dd_p}{dt} = k_j (N d_i)^{5.5} d_p^{5.7} \quad (51)$$

for pellet surface erosion, and

$$-\frac{dN_p}{dt} = k' N_p = \alpha (d_p^{3.2} N^{6.65} d_i^{8.72})^{5.5} N_p \quad (52)$$

for rupture of the particle. In equations 51 and 52, d_p is the pellet diameter at time t, N is the rotational speed of the impeller, d_i is the impeller diameter, N_p is the concentration of unbroken pellets at time t, and k_j, k', and α are constants. Clearly, the rates of pellet erosion and rupture depend strongly the agitation intensity–associated factors (i.e., on N and d_i) and the dimensions of the pellet.

In submerged stirred-tank culture of the filamentous fungus *Aspergillus awamori*, Cui et al. (147) correlated the pellet size with the specific energy dissipation rate; thus,

$$d_p \propto E^{-0.16} \quad (53)$$

The E values varied over 0.2–5.7 W kg^{-1} (146), whereas the pellet diameter ranged roughly over 1–2 mm. The length of the "hairy" hyphal extensions from the well-defined surface of the denser pellet also correlated with the specific energy dissipation rate (147); thus,

$$L_h = 1.17 \times 10^{-4} E^{-0.25} \quad (54)$$

where L_h (m) is the length of the hairy extensions.

Bioactive Proteins

Enzymes are not generally susceptible to the shear rates that are commonly encountered during processing including high-shear operations such as cell disruption (1). Exceptions occur when shear stresses are applied in the presence of gas–liquid interfaces, at which proteins tend to unfold (1,8,148). Also, membrane-associated proteins are more prone to shear damage (1). In addition to processes such as high-pressure homogenization, high-shear processing of proteins occurs during liquid–liquid emulsification, which is used to produce microencapsulated proteins for drug delivery systems (149). Effects of extremely high shear rate levels ($>10^5\ s^{-1}$) on recombinant human growth hormone (rhGH) and recombinant human deoxyribonuclease (rhDNase) were examined by Maa and Hsu (149). The rhGH and rhDNase had respective molecular masses of 22.13 kDa and 32.74 kDa. The shearing was done at a controlled temperature of 20 °C. The aggregation and the bioactivity of the two proteins were not significantly affected at shear rates greater than $10^5\ s^{-1}$ applied over 60 min in the absence of gas–liquid interfaces (148,149). Thermodynamic properties of the proteins were determined before and after shearing using scanning microcalorimetery (SM). Alterations in secondary and tertiary structure of a protein are manifested in its scanning calorimetery data. The SM thermograms of rhDNase were not significantly affected by shearing; however, for rhGH, the SM indicated possible conformational changes (149). The silver-stained SDS-PAGE gels of rhGH showed no significant differences in the high molecular weight region, but low molecular weight fragments were observed in the sheared sample, which suggested some clipping of rhGH in the intense shear field. No significant changes were noted in the SDS-PAGE gels of sheared and unsheared rhDNase (148). If a globular protein's molecular weight is assumed to indicate it's size, the rhDNase molecule should be larger by a factor of approximately $(32.74/22.13)^{1/3}$, or 1.14, relative to the rhGH. It seems therefore that the molecular size is

not the sole determinant of a protein's susceptibility to damage; the specific structure or morphology also appear to play a role.

The damaging effect of shear in presence of gas–liquid and solid–liquid interfaces may be reduced by supplementing the protein solution with a surfactant. Added surfactants tend to reduce gas–liquid interface–induced aggregation and precipitation of rhGH (148). Proteins also adsorb on hydrophobic solid surfaces. Adsorption of insulin at hydrophobic surfaces, accompanied by denaturation, is well known. Similarly, tPA is known to adhere to solid surfaces (150), but the surface adherent tendency is reduced in presence of surfactants such as Tween-80 (polyoxyethylene sorbitane monooleate) added at 0.01% typical concentration (150). Shear susceptibility of proteins is further discussed elsewhere (5,151).

CONCLUDING REMARKS

Biocatalysts, especially molds, filamentous bacteria, certain microalgae, and plant and animal cells are susceptible to damage by hydrodynamic and mechanical forces encountered in bioprocessing. Typically, recombinant strains are more prone to shear damage than equivalent wild types. Extent of damage depends on the cell and the specific damaging mechanism operating. Often, the damage may be reduced by one or more of several approaches: adaptation of cells, supplementing culture media with shear-protectants, modification of processing operations and equipment, and other methods. In many cases, the mechanisms of protection and damage are not entirely clear, but multiple mechanisms seem to operate. As noted throughout this monograph, some sound guidance is available for engineering and operation of fragile culture processes; nevertheless, a priori quantitative prediction of culture behavior is not reliably possible. Empirical approaches must continue to be relied upon in engineering practice.

NOMENCLATURE

A_b	Cross-sectional area under the baffle or draft tube (m^2)
A_d	Cross-sectional area of the downcomer (m^2)
A_r	Cross-sectional area of the riser (m^2)
a	Parameter in equation 2
C_D	Drag coefficient
C_f	Fanning friction factor
d	Diameter or hydraulic diameter (m)
d_B	Bubble diameter (m)
d_c	Cell diameter (μm)
d_F	Floc diameter (m)
d_{Fmax}	Maximum stable diameter (m)
d_i	Impeller diameter (m)
d_L	Local diameter (m)
d_p	Microcarrier or particle diameter (m)
d_T	Tank or column diameter (m)
E	Energy dissipation rate per unit mass (W kg^{-1})
F_D	Turbulent drag force on a particle (N)
F_n	Normal force on a particle (N)
F_s	Shear force across the aggregate due to instantaneous velocity difference (N)
g	Gravitational acceleration (m s^{-2})
h	Channel height (m)
h_L	Height of liquid (m)
ICS	Impeller collision severity defined by equation 39 (kg m^{-2} s^{-3})
ISF	Integrated shear factor defined by equation 33 (s^{-1})
K	Consistency index (Pa s^n)
k	Parameter in equation 2 (m^{-1})
k'	Constant in equation 52 (s^{-1})
k_d	Death rate constant (s^{-1})
k_i	Constant in equation 9
k_j	Constant in equation 51 ($s^{4.5}$ $m^{-10.2}$)
L	Channel length (m)
L_h	Length of hairy extensions from pellet surface (m)
l	Mean microeddy length (m)
m	General exponent
N	Rotational speed (s^{-1}) or cell concentration (m^{-3})
N_o	Initial cell concentration (m^{-3})
N_p	Concentration of unbroken pellets at time t (m^{-3})
n	Flow behavior index
n_B	Number of impeller blades
Po	Power number
ΔP	Pressure drop (Pa)
Q	Volume flow rate of gas (m^3 s^{-1})
Re	Reynolds number
Re_i	Impeller Reynolds number defined by equation 36
Re_L	Local Reynolds number defined by equation 23
r_c	Radius of the vortex zone defined by equation 35 (m)
r_i	Impeller radius (m)
r_T	Tank radius (m)
S	Burst strength (N)
TCS	Turbulent collision severity for particle-to-particle collisions (kg m^{-2} s^{-3})
t	Time (s)
U_B	Bubble rise velocity (m s^{-1})
U_G	Superficial gas velocity (m s^{-1})
U_{Gr}	Superficial gas velocity in riser (m s^{-1})
U_L	Average liquid velocity (m s^{-1})
u	Mean velocity of the microeddies (m s^{-1})
Δu	Difference in velocities of the particle and the fluid (m s^{-1})
u_o	Jet velocity at orifice (m s^{-1})
V_k	Dimensionless hypothetical specific killing volume

V_L Volume of liquid (m^3)
W Width of the impeller blade (m)
x Parameter in equation 19

Greek Symbols

α Constant in equation 52 ($s^{35.575}\ m^{-65.56}$)
Γ Coefficient in equation 47
γ Shear rate (s^{-1})
γ_{av} Average shear rate (s^{-1})
$\gamma_{av\cdot T}$ Time averaged shear rate (s^{-1})
γ_i Isotropic turbulence shear rate defined by equation 24 (s^{-1})
γ_{max} Time averaged maximum shear rate (s^{-1})
γ_w Wall shear rate (s^{-1})
ϵ_S Volume fraction of microcarriers or solids (−)
μ_{ap} Effective or apparent viscosity (Pa s)
μ_L Viscosity of liquid (Pa s)
π Pi
ρ_L Density of liquid (kg m^{-3})
ρ_S Density of microcarriers or solid (kg m^{-3})
σ_M Mechanical strength of aggregate (N m^{-2})
τ Shear stress (N m^{-2})
τ_w Wall shear stress (N m^{-2})

BIBLIOGRAPHY

1. Y. Chisti and M. Moo-Young, *Enzyme Microb. Technol.* **8**, 194–204 (1986).
2. H.Y. Makagiansar, P.A. Shamlou, C.R. Thomas, and M.D. Lilly, *Bioprocess Eng.* **9**, 83–90 (1993).
3. E. Ujcová, Z. Fencl, M. Musi'lková, and L. Seichert, *Biotechnol. Bioeng.* **22**, 237–241 (1980).
4. M. Papadaki and S.G. Eskin, *Biotechnol. Prog.* **13**, 209–221 (1997).
5. C.R. Thomas, in M.R. Winkler ed., *Chemical Engineering Problems in Biotechnology*, Elsevier, London, 1990, pp. 23–93.
6. W.K. Kwok, C. Picioreanu, S.L. Ong, M.C.M. van Loosdrecht, W.J. Ng, and J.J. Heijnen, *Biotechnol. Bioeng.* **58**, 400–407 (1998).
7. P. Stoodley, Z. Lewandowski, J.D. Boyle, and H.M. Lappin-Scott, *Biotechnol. Bioeng.* **57**, 536–544 (1998).
8. Y. Chisti, in G. Subramanian ed., *Bioseparations and Bioprocessing: A Handbook*, vol. 2, Wiley-VCH, New York, 1998, pp. 3–30.
9. E. Dreveton, F. Monot, J. Lecourtier, D. Ballerini, and L. Choplin, *J. Ferment. Bioeng.* **82**, 272–276 (1996).
10. M. Moo-Young and Y. Chisti, *Biotechnology*, **6**(11), 1291–1296 (1988).
11. F. Garrido, U.C. Banerjee, Y. Chisti, and M. Moo-Young, *Bioseparation*, **4**, 319–328 (1994).
12. I.M. Tamer, M. Moo-Young, and Y. Chisti, *Ind. Eng. Chem. Res.* **37**, 1807–1814 (1998).
13. P.M. Doran, *Adv. Biochem. Eng. Biotechnol.* **48**, 115–168 (1993).
14. E. Molina Grima, Y. Chisti, and M. Moo-Young, *J. Biotechnol.* **54**, 195–210 (1997).
15. E.T. Papoutsakis, *Trends Biotechnol.* **9**, 427–437 (1991).
16. D.C. Augenstein, A.J. Sinskey, and D.I.C. Wang, *Biotechnol. Bioeng.* **13**, 409–418 (1971).
17. N. Shiragami, *Bioprocess Eng.* **10**, 47–51 (1994).
18. A. McQueen, E. Meilhoc, and J.E. Bailey, *Biotechnol. Lett.* **9**, 831–836 (1987).
19. Y. Chisti and M. Moo-Young, *Biotechnol. Bioeng.* **34**, 1391–1392 (1989).
20. Y. Chisti, *Appl. Mech. Rev.* **51**, 33–112 (1998).
21. Y. Chisti, *Airlift Bioreactors*, Elsevier, London, 1989.
22. L.K. Shi, J.P. Riba, and H. Angelino, *Chem. Eng. Commun.* **89**, 25–35 (1990).
23. L.A. Glasgow, J. Hua, T.-Y. Yiin, and L.E. Erickson, *Chem. Eng. Commun.* **113**, 155–181 (1992).
24. K. Okada, S. Shibano, and Y. Akagi, *J. Chem. Eng. Jpn.* **26**, 637–643 (1993).
25. A. Lübbert and B. Larson, *Chem. Eng. Sci.* **45**, 3047–3053 (1990).
26. A. Lübbert, B. Larson, L.W. Wan, and S. Bröring, *Inst. Chem. Eng. Symp. Ser.* **121**, 203–213 (1990).
27. R. Bowen, *Chem. Eng.* June 9, 55–63 (1986).
28. B. Robertson and J.J. Ulbrecht, in C.S. Ho and J.Y. Oldshue eds., *Biotechnology Processes: Scale-Up and Mixing*, American Institute of Chemical Engineers, New York, 1987, pp. 31–35.
29. P.H. Calderbank and M.B. Moo-Young, *Trans. Inst. Chem. Eng.* **37**, 26 (1959).
30. Y. Chisti and M. Moo-Young, in V. Moses and R.E. Cape eds., *Biotechnology: The Science and the Business*, Harwood Academic, New York, 1991, pp. 167–209.
31. D.C.-H. Jan, A.N. Emery, and M. Al-Rubeai, *Biotechnol. Techn.* **7**, 351–356 (1993).
32. Y. Chisti, B. Halard, and M. Moo-Young, *Chem. Eng. Sci.* **43**, 451–457 (1988).
33. Y. Chisti and M. Moo-Young, *J. Chem. Technol. Biotechnol.* **42**, 211–219 (1988).
34. V.N. Sokolov and V.P. Metkin, *Zh. Prikl. Khim.* **54**, 1321–1326 (1981): *J. Appl. Chem. USSR* **54**, 1103–1107 (1981).
35. V.P. Metkin and V.N. Sokolov, *J. Appl. Chem. USSR* **55**, 558–563 (1982).
36. K. Wichterle, V. Sobolík, M. Lutz, and V. Denk, *Chem. Eng. Sci.* **51**, 5227–5228 (1996).
37. A.W. Nienow, *Appl. Mech. Rev.* **51**, 3–32 (1998).
38. J.J. Meijer, H.J.G. ten Hoopen, Y.M. van Gameren, K.Ch.A.M. Luyben, and K.R. Libbenga, *Enzyme Microb. Technol.* **16**, 467–477 (1994).
39. M. Moo-Young, Y. Chisti, and D. Vlach, *Biotechnol. Lett.* **14**, 863–868 (1992).
40. M. Moo-Young, Y. Chisti, and D. Vlach, *Biotechnol. Adv.* **11**, 469–479 (1993).
41. O.T. Ramírez and R. Mutharasan, *Biotechnol. Bioeng.* **36**, 911–920 (1990).
42. E.H. Dunlop, P.K. Namdev, and M.Z. Rosenberg, *Chem. Eng. Sci.* **49**, 2263–2276 (1994).

43. Z. Zhang, Y. Chisti, and M. Moo-Young, *J. Biotechnol.* **43**, 33–40 (1995).
44. H. Märkl, R. Bronnenmeier, and B. Wittek, *Int. Chem. Eng.* **31**, 185–197 (1991).
45. J. Wu, G. King, A.J. Daugulis, P. Faulkner, D.H. Bone, and M.F.A. Goosen, *J. Ferment. Bioeng.* **70**, 90–93 (1990).
46. Y. Chisti and M. Moo-Young, *Trans. Inst. Chem. Eng.* **74**A, 575–583 (1996).
47. M. Moo-Young and Y. Chisti, in G. Durand, L. Bobichon, and J. Florent eds., *Proceedings, 8th International Biotechnology Symposium*, vol. 1, Société Française de Microbiologie, Paris, 1988, pp. 454–466.
48. M. Moo-Young, Y. Chisti, Z. Zhang, F. Garrido, U. Banerjee, and D. Vlach, *Ann. N. Y. Acad. Sci.* **782**, 391–401 (1996).
49. A. Converti, C. Sommariva, M.D. Borghi, and G. Ferraiolo, *Bioprocess Eng.* **9**, 183–189 (1993).
50. A. Converti, M.D. Borghi, G. Ferraiolo, and C. Sommariva, *Chem. Eng. J.* **62**, 155–167 (1996).
51. P.F. MacLoughlin, D.M. Malone, J.T. Murtagh, and P.M. Kieran, *Biotechnol. Bioeng.* **58**, 595–604 (1998).
52. C.R. Thomas, in P.A. Shamlou ed., *Processing of Solid–Liquid Suspensions*, Butterworth-Heinemann, Oxford, 1993, pp. 158–191.
53. A. Prokop and R.K. Bajpai, *Adv. Appl. Microbiol.* **37**, 165–232 (1992).
54. C. Gudin and D. Chaumont, *Bioresource Technol.* **38**, 145–151 (1991).
55. Y. Watanabe, J. de la Noüe, and D.O. Hall, *Biotechnol. Bioeng.* **47**, 261–269 (1995).
56. E. Molina Grima, J.A. Sánchez Pérez, F. García Camacho, J.L. García Sánchez, F.G. Acién Fernández, and D. López Alonso, *J. Biotechnol.* **37**, 159–166 (1994).
57. E. Molina Grima, J.A. Sánchez Pérez, F. García Camacho, J.M. Fernández Sevilla, F.G. Acién Fernández, and J. Urda Cardona, *Appl. Microbiol. Biotechnol.* **42**, 658–663 (1995).
58. H.J. Silva, T. Cortiñas, and R.J. Ertola, *J. Chem. Technol. Biotechnol.* **40**, 41–49 (1987).
59. T. Suzuki, T. Matsuo, K. Ohtaguchi, and K. Koide, *J. Chem. Technol. Biotechnol.* **62**, 351–358 (1995).
60. L. van der Pol, W.A.M. Bakker, and J. Tramper, *Biotechnol. Bioeng.* **40**, 179–182 (1992).
61. D.E. Martens, C.D. de Gooijer, E.C. Beuvery, and J. Tramper, *Biotechnol. Bioeng.* **39**, 891–897 (1992).
62. J. Tramper, D. Joustra, and J.M. Vlak, in C. Webb and F. Mavituna, eds., *Plant and Animal Cells: Process Possibilities*, Ellis Horwood, Chichester, 1987, pp. 125–136.
63. J. Tramper, D. Smit, J. Straatman, and J.M. Vlak, *Bioprocess Eng.* **2**, 37–41 (1987).
64. A.N. Emery, M. Lavery, B. Williams, and A. Handa, in C. Webb and F. Mavituna, eds., *Plant and Animal Cells: Process Possibilities*, Ellis Horwood, Chichester, 1987, pp. 137–146.
65. H.C.P. Matthijs, H. Balke, U.M. Van Hes, B.M.A. Kroon, L.R. Mur, and R.A. Binot, *Biotechnol. Bioeng.* **50**, 98–107 (1996).
66. M.S. Croughan, E.S. Sayre, and D.I.C. Wang, *Biotechnol. Bioeng.* **33**, 862–872 (1989).
67. A. McQueen and J.E. Bailey, *Biotechnol. Lett.* **11**, 531–536 (1989).
68. M. Midler and R.K. Finn, *Biotechnol. Bioeng.* **8**, 71–84 (1966).
69. P.M. Kieran, P.F. MacLoughlin, and D.M. Malone, *J. Biotechnol.* **59**, 39–52 (1997).
70. U. Fischer and A.W. Alfermann, *J. Biotechnol.* **41**, 19–28 (1995).
71. R. Ballica and D.D.Y. Ryu, *Biotechnol. Bioeng.* **42**, 1181–1189 (1993).
72. E. Reinhard, W. Kreis, U. Barthlen, and U. Helmbold, *Biotechnol. Bioeng.* **34**, 502–508 (1989).
73. H. Tanaka, *Biotechnol. Bioeng.* **23**, 1203–1218 (1981).
74. J.-J. Zhong, K. Fujiyama, T. Seki, and T. Yoshida, *Biotechnol. Bioeng.* **44**, 649–654 (1994).
75. P.M. Kieran, H.J. O'Donnell, D.M. Malone, and P.F. MacLoughlin, *Biotechnol. Bioeng.* **45**, 415–425 (1995).
76. J.J. Chalmers, *Appl. Mech. Rev.* **51**, 113–120 (1998).
77. W.R. Arathoon and J.R. Birch, *Science*, **232**, 1390–1395 (1986).
78. Y. Chisti, *Bioprocess Eng.* **9**, 191–196 (1993).
79. J.R. Birch, K. Lambert, P.W. Thompson, A.C. Kenney, and L.A. Wood, in B.K. Lydersen ed., *Large Scale Cell Culture Technology*, Hanser, New York, 1987, pp. 1–20.
80. Y. Chisti and M. Moo-Young, *Trans. Inst. Chem. Eng.* **71C**, 209–214 (1993).
81. Y. Chisti and M. Moo-Young, *Trans. Inst. Chem. Eng.* **72C**, 92–94 (1994).
82. B.-Y. Kim, A.J. Putnam, T.J. Kulik, and D.J. Mooney, *Biotechnol. Bioeng.* **57**, 46–54 (1998).
83. K.K. Chittur, L.V. McIntire, and R.R. Rich, *Biotechnol. Prog.* **4**(2), 89–96 (1988).
84. R.C. Ziegelstein, L. Cheng, and M.C. Capogrossi, *Science*, **258**, 656–659 (1992).
85. R.S. Cherry, *Biotechnol. Adv.* **11**, 279–299 (1993).
86. M. Al-Rubeai, A.N. Emery, S. Chalder, and M.H. Goldman, *J. Biotechnol.* **31**, 161–177 (1993).
87. P.L. Blackshear and G.L. Blackshear, in R. Skalak and S. Chien eds., *Handbook of Bioengineering*, McGraw-Hill, New York, 1987, pp. 15.1–15.19.
88. C. Born, Z. Zhang, M. Al-Rubeai, and C.R. Thomas, *Biotechnol. Bioeng.* **40**, 1004–1010 (1992).
89. N. Shiragami, *Bioprocess Eng.* **16**, 345–347 (1997).
90. C.G. Smith and P.F. Greenfield, *Biotechnol. Bioeng.* **40**, 1045–1055 (1992).
91. L.A. Olivier and G.A. Truskey, *Biotechnol. Bioeng.* **42**, 963–973 (1993).
92. J.G. Aunins and H.-J. Henzler, in H.-J. Rehm and G. Reed eds., *Biotechnology*, vol. 3, 2nd ed., VCH Weinheim, 1993, pp. 219–281.
93. N. Shiragami and H. Unno, *Bioprocess Eng.* **10**, 43–45 (1994).
94. T.L. LaPorte, J. Shevitz, Y. Kim, and S.S. Wang, *Bioprocess Eng.* **15**, 1–7 (1996).
95. R.M. Hochmuth, in R. Skalak and S. Chien eds., *Handbook of Bioengineering*, McGraw-Hill, New York, 1987, pp. 12.1–12.17.
96. G.W. Schmid-Schönbein, in R. Skalak and S. Chien eds., *Handbook of Bioengineering*, McGraw-Hill, New York, 1987, pp. 13.1–13.25.

97. X. Dai, F. Ouyang, and Y. Qi, in W.K. Teo, M.G.S. Yap, and S.K.W. Oh, eds., *Better Living through Biochemical Engineering*, University of Singapore, Singapore, 1994, pp. 408–410.
98. R.S. Cherry and E.T. Papoutsakis, *Bioprocess Eng.* **1**, 29–41 (1986).
99. Y. Chisti and M. Moo-Young, *Chimica Oggi*, **11**(3–4), 25–27 (1993).
100. Z. Zhang, M.A. Ferenczi, and C.R. Thomas, *Chem. Eng. Sci.* **47**, 1347–1354 (1992).
101. Z. Zhang, M.F. Ferenczi, A.C. Lush, and C.R. Thomas, *Appl. Microbiol. Biotechnol.* **36**, 208–210 (1991).
102. A.J. Sinskey, R.J. Fleishaker, M.A. Tyo, D.-J. Giard, and D.I.C. Wang, *Ann. N. Y. Acad. Sci.* **369**, 47–59 (1981).
103. M.S. Croughan, J.-F. Hamel, and D.I.C. Wang, *Biotechnol. Bioeng.* **29**, 130–141 (1987).
104. R.S. Cherry and E.T. Papoutsakis, *Biotechnol. Bioeng.* **32**, 1001–1014 (1988).
105. R.S. Cherry and E.T. Papoutsakis, *Bioprocess Eng.* **4**, 81–89 (1989).
106. K.J. Ganzeveld, Y. Chisti, and M. Moo-Young, *Bioprocess Eng.* **12**, 239–247 (1995).
107. S.K.W. Oh, A.W. Nienow, M. Al-Rubeai, and A.N. Emery, *J. Biotechnol.* **12**, 45–62 (1989).
108. S.K.W. Oh, A.W. Nienow, M. Al-Rubeai, and A.N. Emery, *J. Biotechnol.* **22**, 245–270 (1992).
109. A. Handa, A.N. Emery, and R.E. Spier, *Dev. Biol. Stand.* **66**, 241–253 (1987).
110. A. Handa-Corrigan, A.N. Emery, and R.E. Spier, *Enzyme Microb. Technol.* **11**, 230–235 (1989).
111. N.S. Wang, J.-D. Yang, R.V. Calabrese, and K.-C. Chang, *J. Biotechnol.* **33**, 107–122 (1994).
112. I. Jöbses, D. Martens, and J. Tramper, *Biotechnol. Bioeng.* **37**, 484–490 (1991).
113. J. Wu and F.A. Goosen, *Enzyme Microb. Technol.* **17**, 1036–1042 (1995).
114. J.M. Boulton-Stone and J.R. Blake, *J. Fluid Mech.* **254**, 473–466 (1993).
115. M.A. Garcia-Briones, R.S. Brodkey, and J.J. Chalmers, *Chem. Eng. Sci.* **49**, 2301–2320 (1994).
116. J.J. Chalmers and F. Bavarian, *Biotechnol. Prog.* **7**, 151–158 (1991).
117. R.S. Cherry and C.T. Hulle, *Biotechnol. Prog.* **8**, 11–18 (1992).
118. F. Bavarian, L. S. Fan, and J.J. Chalmers, *Biotechnol. Prog.* **7**, 140–150 (1991).
119. H.G. Sucker, M. Jordan, H.M. Eppenberger, and F. Widmer, *Biotechnol. Bioeng.* **44**, 1246–1254 (1994).
120. E.T. Papoutsakis, *Trends Biotechnol.* **9**, 316–324 (1991).
121. O.T. Ramirez and R. Mutharasan, *Biotechnol. Prog.* **8**, 40–50 (1992).
122. J.D. Michaels, J.F. Petersen, L.V. McIntire, and E.T. Papoutsakis, *Biotechnol. Bioeng.* **38**, 169–180 (1991).
123. M. Lavery and A.W. Nienow, *Biotechnol. Bioeng.* **30**, 368–373 (1987).
124. K.T. Kunas and E.T. Papoutsakis, *J. Biotechnol.* **15**, 57–70 (1990).
125. S. Goldblum, Y.-K. Bae, W.F. Hink, and J.J. Chalmers, *Biotechnol. Prog.* **6**, 383–390 (1990).
126. Y. Chisti and M. Moo-Young, *J. Chem. Technol. Biotechnol.* **58**, 331–336 (1993).
127. D.W. Murhammer and C.F. Goochee, *Biotechnology*, **6**, 1411–1418 (1988).
128. D.W. Murhammer and C.F. Goochee, *Biotechnol. Prog.* **6**, 142–148 (1990).
129. L. Laouar, K.C. Lowe, and B.J. Mulligan, *Enzyme Microb. Technol.* **18**, 433–438 (1996).
130. L.A. van der Pol, I. Beeksma, and J. Tramper, *Enzyme Microb. Technol.* **17**, 401–407 (1995).
131. M.C.M. van Loosdrecht and S.J. Heijnen, *Trends Biotechnol.* **11**, 117–121 (1993).
132. J.J. Heijnen, M.C.M. van Loosdrecht, A. Mulder, and L. Tijhuis, *Water Sci. Technol.* **26**, 647–654 (1992).
133. K. Wagner and D.C. Hempel, *Biotechnol. Bioeng.* **31**, 559–566 (1988).
134. L. Tijhuis, H. Zwols, K.-H. van Meekeren, M.C.M. van Loosdrecht, and J.J. Heijnen, L. Alberghina, L. Frontali, and P. Sensi eds., *Progress in Biotechnology*, vol. 9, *Proceedings of the 6th European Congress on Biotechnology*, Elsevier, Amsterdam, 1994, pp. 953–956.
135. L. Tijhuis, W.A.J. van Benthum, M.C.M. van Loosdrecht, and J.J. Heijnen, *Biotechnol. Bioeng.* **44**, 867–879 (1994).
136. L. Tijhuis, M.C.M. van Loosdrecht, and J.J. Heijnen, *Biotechnol. Bioeng.* **44**, 595–608 (1994).
137. L. Tijhuis, M.C.M. van Loosdrecht, and J.J. Heijnen, *Biotechnol. Bioeng.* **45**, 481–487 (1995).
138. W.A.J. van Benthum, J.M. Garrido-Fernández, L. Tijhuis, M.C.M. van Loosdrecht, and J.J. Heijnen, *Biotechnol. Prog.* **12**, 764–772 (1996).
139. A. Gjaltema, L. Tijhuis, M.C.M. van Loosdrecht, and J.J. Heijnen, *Biotechnol. Bioeng.* **46**, 258–269 (1995).
140. A. Gjaltema, J.L. Vinke, M.C.M. van Loosdrecht, and J.J. Heijnen, *Biotechnol. Bioeng.* **53**, 88–99 (1997).
141. L. Tijhuis, J.L. Huisman, H.D. Hekkelman, M.C.M. van Loosdrecht, and J.J. Heijnen, *Biotechnol. Bioeng.* **47**, 585–595 (1995).
142. P.A. Shamlou and N. Titchener-Hooker, in P.A. Shamlou ed., *Processing of Solid–Liquid Suspensions*, Butterworth-Heinemann, Oxford, 1993, pp. 1–25.
143. D.F. Bagster, in P.A. Shamlou ed., *Processing of Solid–Liquid Suspensions*, Butterworth-Heinemann, Oxford, 1993, pp. 26–58.
144. T. Matsuo and H. Unno, *J. Environ. Eng. Div. Am. Soc. Civ. Eng.* **107**, 527–545 (1981).
145. J. Gregory, in P.A. Shamlou ed., *Processing of Solid–Liquid Suspensions*, Butterworth-Heinemann, Oxford, 1993, pp. 59–92.
146. H. Taguchi, T. Yoshida, Y. Tomita, and S. Teramoto, *J. Ferment. Technol.* **46**, 814–822 (1968).
147. Y.Q. Cui, R.G.J.M. van der Lans, and K.Ch.A.M. Luyben, *Biotechnol. Bioeng.* **57**, 409–419 (1998).
148. Y.-F. Maa and C.C. Hsu, *Biotechnol. Bioeng.* **54**, 503–512 (1997).
149. Y.-F. Maa and C.C. Hsu, *Biotechnol. Bioeng.* **51**, 458–465 (1996).
150. S.A. Rouf, M. Moo-Young, and Y. Chisti, *Biotechnol. Adv.* **14**, 239–266 (1996).
151. D.J. Bell, M. Hoare, and P. Dunnill, *Adv. Biochem. Eng.* **26**, 1–72 (1983).